MASTER COPY

THEORETICAL AND EXPERIMENTAL STUDIES OF TURBINE FLOWMETERS

PHILIP AH KOW TAN

PRESENTED FOR THE DEGREE OF DOCTOR OF PHILOSOPHY 1973

UNIVERSITY OF SOUTHAMPTON

DEPARTMENT OF

MECHANICAL ENGINEERING

ABSTRACT

FACULTY OF ENGINEERING AND APPLIED SCIENCE

MECHANICAL ENGINEERING

Doctor of Philosophy

THEORETICAL AND EXPERIMENTAL STUDIES OF TURBINE FLOWMETER

by Philip Ah Kow Tan

A new theoretical model of the flow through the tip-clearance is presented to describe the behaviour of the calibration curves of turbine flowmeters. When constants in the theoretical equation are determined empirically the equation plotted agrees well with experimental results. Analysis using this leakage model shows that reducing the frictional torque on turbine meters to a minimum can increase the variation of the meter coefficient over the operating range rather than its intended purpose of decreasing it.

Velocity profiles within meter annuli of different hub-ratios were measured and the results show that they are quite different from those previously assumed. Empirical equations are developed to predict the profiles. Experiments carried out on different turbine meters show that the behaviour of their calibration curves depends not only on the tip-clearances and hub-ratios but also on the types of blades the rotors are having. The calibration curves are found to be susceptible to changes in upstream velocity profile and to upstream disturbances but by the proper choice of type of blades, hub-ratio and tip-clearance, their effects could be kept to a minimum. In general, constant blade angle meters are better in avoiding such effects.

Based mainly on the results of this research, a guide to the design of turbine meters is given.

ACKNOWLEDGEMENTS

The author wishes to express his sincere thanks to the following.

Prof. S.P. Hutton, supervisor of this project, for his invaluable and unfailing guidance, advice, ideas and encouragement.

Esso Ltd., for the research studentship.

E.F.M., Kent Instruments Ltd., Elliot Ltd., and Esso Ltd., for the loan of turbine meters.

Mr. M.A. Batey and his workshop staff.

Mr. J.D. Sewill and his electronic workshop staff.

Mr. A.C. Riddell for the loan of weights.

Mr. J. Stanton, Contract Assistant to this project.

Mrs. A. Lampard for typing this thesis.

LIST OF SYMBOLS

AR	blade aspect ratio
A_h	cross-section area of hub
A_o	cross-section area of meter
c	blade chord
C_D	coefficient of drag
C_{Di}	coefficient of induced drag
C_{Do}	coefficient of drag for $\alpha = 0$
C_f	coefficient of skin friction
C_L	coefficient of lift, $C_L = C_1.K.\sin\alpha = C_K \cdot \sin\alpha$
C_1	lift coefficient, $C_1 = \left(\frac{e}{1 + \frac{2.e}{AR}}\right) \cdot 2\pi$
dr	elemental radius at radius r
dD	elemental drag at radius r
dL	elemental lift at radius r
g	leakage ratio
k	leakage factor
K	Weinig lattice-effect coefficient
m	reciprocal of exponent of power law equation in pipe
M	reciprocal of exponent of power law equation within meter annulus
n	speed of rotation
N	number of rotor blades
P	helical pitch
Q	total volume flow through meter per second
Q_c	volume flow through tip-clearance per second
Q_r	volume flow through rotor blades per second

r_h	hub radius
r_o	radius of meter casing
r_p	radius of pipe
r_t	blade tip radius
s	blade spacing at radius r
t	blade thickness
T	retarding torque (excluding blade drag)
T_d	total driving torque
u	axial velocity
U	reference axial velocity
U_e	absolute outlet velocity
U_i	absolute inlet velocity
v	inlet swirl velocity (tangential component)
v_e	outlet swirl velocity (tangential component)
V_e	outlet velocity relative to blade
V_i	inlet velocity relative to blade
V_m	mean velocity relative to blade
W	axial width of blade
α	angle of attack $\alpha = \beta - \theta$
β	blade angle
β'	effective blade angle
γ	blade tip-ratio, $\gamma = r_t/r_o$
δ	boundary layer thickness in pipe
δ_m	boundary layer thickness in meter annulus
δ^*	outlet deviation angle with respect to blade
ϵ	blade aerofoil efficiency

θ	mean velocity angle with respective to axis
θ_e	outlet " " " " " "
θ_i	inlet " " " " " "
λ	boundary layer thickness ratio, $\lambda = \delta/r_p$
ρ	density of fluid
ϕ	hub-ratio, $\phi = r_h/r_o$
ψ	ratio of meter casing radius to pipe radius, $\psi = r_o/r_p$

LIST OF SYMBOLS USED IN APPENDIX V

Approx.	approximate
Cal.	calculate
max.	maximum
min.	minimum
Spec.	specification
tip-clear.	tip-clearance $r_o - r_t$
A_{dn}	Minimum flow area through meter for design
A_{min}	Minimum flow area through meter dictated by cativation at flow rate Q_{max}
D_m	Minimum number of pipe diameters downstream of disturbances
e_d	Disturbance effect:- error due to upstream disturbances
e_p	Profile effect: error due to developing velocity profile
k	leakage factor
MC	meter coefficient at any flow rate Q
MC_{dx}	meter coefficient at maximum flow rate Q_{max} with flow area A_{dn}
MC_{max}	meter coefficient at maximum flow rate Q_{max} with flow area A_{max} i.e. $\frac{n_{max}}{Q_{max}}$
MC_{min}	meter coefficient at minimum flow rate Q_{min}
N	number of blades
n	speed of rotation
n_{max}	maximum speed of rotation
P	helical pitch of blade
Q	flow rate
Q_{max}	specified maximum flow rate
Q_{min}	specified minimum flow rate

r_h	hub radius of rotor
r_o	radius of meter casing
r_p	radius of pipe
t	blade thickness
T	bearing torque
v_a	specified variation
W	axial width of blades
β	blade angle of constant blade angle rotor

C O N T E N T S

	PAGE
CHAPTER 1 INTRODUCTION	1
1.1 Working principle of turbine meter	1
1.2 Definition and comments on terms used for turbine meters	2
1.3 Existing theories on turbine meters and their limitations	4
1.4 Aims of research	9
CHAPTER 2 DESCRIPTION OF RIG AND EXPERIMENTAL PROCEDURE	11
2.1 Main pump	11
2.2 Line filter	12
2.3 10" dia. pipe line	12
2.4 Test length	12
2.5 Control valve	13
2.6 Fish-tail diverter	13
2.7 Sump tank	14
2.8 Transfer pump	14
2.9 Weigh tank	14
2.10 Weighing machine	15
2.11 Turbine meter pick-up system	16
2.12 Start-up and shut-down of rig	16
2.13 Procedure for meter calibration	17
2.14 Dynamic weighing versus static weighing	19
CHAPTER 3 THEORY	
3.1 Introduction	22
3.2 Derivation of rotor coefficient	24
3.3 Leakage model	34
3.3.1 Determination of g and k	38
3.3.2 Using the leakage model to describe the behaviour of calibration curves of different turbine meters	41

PAGE

CHAPTER 4 VELOCITY PROFILE IN METER ANNULUS

4.1 Introduction 42

4.2 Experiment 43

4.3 Discussion 45

4.3.1 Empirical velocity profile in fully developed flow 47

4.3.2 Empirical velocity profile in partially developed flow 50

CHAPTER 5 EFFECT OF TIP-CLEARANCE ON TURBINE METER CALIBRATION CURVES

5.1 Introduction 52

5.2 Experiment 53

5.3 Discussion 54

5.3.1 Change in meter coefficient 55

5.3.2 Shape of calibration curves 58

5.3.2.1 Upstream position 58

5.3.2.2 Downstream position 61

5.3.3 Variation of leakage factor 65

5.3.4 Theoretical verification of meter coefficient equation 68

CHAPTER 6 EFFECTS OF DEVELOPING VELOCITY PROFILE IN PIPE ON TURBINE METER CALIBRATION AND METHODS FOR REDUCING THEM

6.1 Introduction 72

6.2 Experiments 73

6.3. Discussions 74

6.3.1 Meter effect 76

6.3.2 Drag effect 80

6.3.3 Profile effect on helical-blade rotors 81

6.3.4 Profile effect on constant blade angle rotors 83

6.3.5 Comparison between theory and experiment 83

PAGE

CHAPTER 7 EFFECTS OF UPSTREAM DISTURBANCES AND METHODS OF REDUCING THEM

7.1 Introduction 85

7.2 Experiment 85

7.3 Discussion 87

7.3.1 Effect of upstream disturbances on 0.125 hub-ratio helical-blade rotor 87

7.3.2 0.125 hub-ratio constant blade angle rotor 89

7.3.3 0.375 hub-ratio helical-blade rotor and a commercial meter 91

7.3.4 Effect of using flow straighteners 92

CHAPTER 8 HEAD-LOSS ACROSS TURBINE METERS

8.1 Introduction 94

8.2 Experiment 95

8.3 Theory 96

8.3.1 Head-losses H_{u1} and H_{2d} (Hub-loss) 96

8.3.2 Head-losses H_{1x} and H_{y2} 98

8.3.3 Head-losses H_{xy} and H_{v} 99

8.3.4 Head-loss H_{ud} across turbine meter 100

8.4 Discussion 101

CHAPTER 9 REPEATABILITY TESTS AND THE EFFECT OF BEARING FRICTION INCREASE

9.1 Introduction 106

9.2 Experiment 106

9.3 Discussion 107

9.3.1 Repeatability tests on helical-blade rotors 107

9.3.2 Effect of bearing friction on meter calibration 110

9.3.3 Effect of variation of resisting torque 112

PAGE

CHAPTER 10 CONCLUSION

10.1 Introduction 113

10.2 The effects of tip-clearance, hub-ratio and type of blades on meter performance 114

10.2.1 Tip-clearance 115

10.2.2 Hub-ratio 116

10.2.3 Types of blades 117

10.3 Design considerations 118

10.3.1 Design equation 119

10.3.2 Variation 119

10.3.3 Range 121

10.4 Design method 122

REFERENCES 123

APPENDICES

APPENDIX

I Meter coefficient equation 127

II Derivation of empirical velocity profile in meter annulus 131

III Dimensions of research rotors 134

IV Head-loss across turbine meters 135

V Design procedure 151

FIGURES

FIG.

2.1 Schematic Diagram of Test Rig

2.2 Block Diagram of Control System

2.3 Difference between Static and Dynamic Weighing for Different Amount of Water Collected in Weigh Tank

2.4 Error in Dynamic Weighing (Water collected = 1300 lb)

2.5 Calibration Rig Showing the 10" dia. Pipe and the 2" dia. Test Length (Photograph)

2.6 Motor-operated Pressure Regulating Valve and Fish-tail Diverter (Photograph)

2.7 Weigh Tank End of Calibration Rig (Photograph)

2.8 Control Panel of Calibration Rig (Photograph)

2.9 Partly Dismantled View of Turbine Meter (Photograph)

3.1 Velocity Diagrams at Radius r and the Forces Acting on Elemental Blade dr.

3.2 Angle of Attack on Rotors with Different Types of Blades

3.3 Weinig Lattice-effect (Cascade) Coefficient

3.4 Section of Turbine Meter Blade

3.5 Lift-drag Polars for a Flat Plate

3.6 Calibration Curves for Deducing Tip-clearance Flow

3.7 Flow through Tip-clearance when Turbine Meter Placed in Fully Developed Flow

3.8 Tip-clearance Flow-ratio through 0.38 Hub-ratio Helical-blade Research Rotor

3.9 Calibration Curve in Fully Developed Flow using Method 1

3.10 Calibration Curve in Fully Developed Flow using Method 2

3.11 Calibration Curve in Fully Developed Flow using Method 3

3.12 Calibration Curves of Helical-blade Research Rotor with 0.125 Hub-ratio at Upstream Position (i.e. Almost Uniform Flow)

3.13 Calibration Curves of Constant Blade Angle Research Rotor with 0.125 Hub-ratio at Upstream Position

FIG.

3.14 Calibration Curve of a 'Converging' Commercial Turbine Meter

3.15 Calibration of a 2" (0.0308 m) Commercial Turbine Meter

4.1 Traversing Gear for Velocity Profile Measurement

4.2 Velocity Profile at the Upstream and the Downstream Positions of the 2" Test Pipe

4.3 Velocity Profile within Meter Annulus at Upstream Position for Different Hub Sizes

4.4 Velocity Profile within $\frac{3}{4}$" Hub Annulus at Upstream and Downstream Positions

4.5 and 4.6 Comparison between Experimental and Empirical Profiles in Meter Annulus for Fully Developed Flow

4.7 Velocity Profile in Meter Annulus at Downstream Position (96D)

4.8 Radial Position where the Linear Part of Annulus Velocity Profile Terminates

4.9 Gradient of Linear Part of Velocity Profile in Meter Annulus

4.10 Reciprocal of Exponent of Power Law that Fits the Non-linear Part of Annulus Velocity Profile

4.11 Comparison between the Two Assumed Profiles and Predicted Profile for 0.125 Hub-ratio

4.12 Comparison between Assumed Profiles and Predicted Profile for 0.375 Hub-ratio

4.13 Comparison between Assumed Profiles and Predicted Profile for 0.75 Hub-ratio

4.14 Error in Meter Coefficient using Assumed Profiles

4.15 Pitot Traversing Gear with Centering Plunger (Photograph)

4.16 $\frac{1}{4}$", $\frac{3}{4}$" and $1\frac{1}{2}$" Simulation Hubs (Photograph)

4.17 Combined Mercury and Water Manometer (Photograph)

5.1 Effect of Tip-clearance on the Upstream Calibration Curves of the 0.125 Hub-ratio Constant Blade Angle Research Rotor

5.2 Effect of Tip-clearance on the Downstream Calibration Curves of the 0.125 Hub-ratio Constant Blade Angle Research Rotor

5.3 Effect of Tip-clearance on the Upstream Calibration Curves of the 0.375 Hub-ratio Constant Blade Angle Research Rotor

FIG.

5.4 Effect of Tip-clearance on the Downstream Calibration Curves of the 0.375 Hub-ratio Constant Blade Angle Research Rotor

5.5 & 5.6 Effect of Tip-clearance on the Upstream Calibration Curves of the 0.381 Hub-ratio Helical-blade Research Rotor

5.7 Effect of Tip-clearance on the Downstream Calibration Curves of the 0.381 Hub-ratio Helical-blade Research Rotor

5.8 Effect of Tip-clearance on the Upstream Calibration Curves of the 0.753 Hub-ratio Helical-blade Research Rotor

5.9 Effect of Tip-clearance on the Downstream Calibration Curve of the 0.753 Hub-ratio Helical-blade Research Rotor

5.10 Variation of Meter Coefficient with Tip-clearance for Constant Blade Angle Rotors

5.11 Variation of Meter Coefficient with Tip-clearance for Helical-blade Rotors

5.12 Leakage Ratio of Helical-blade Rotors

5.13 Leakage Ratio of Research Rotors at Upstream Position

5.14 Variation of Leakage Factor with Tip-clearance Area-ratio for Helical-blade Rotors

5.15 Comparison of Meter Coefficient Equations using Different Sets of Assumptions

5.16 Meter Coefficient Equation using Effective Blade Angle β' and Blade Angle β

5.17 $\frac{1}{4}$", $\frac{3}{4}$" and $1\frac{1}{2}$" Hub dia. Research Rotors with Bearing Housings (Photograph)

5.18 Turbine Rotor Holder used when Machining Down Blade Tip Radius (Photograph)

6.1 Variation of Boundary Layer Thickness Downstream of Pipe Inlet

6.2 Variation of m with Distance Downstream of Pipe Inlet

6.3 & 6.4 Profile Effect on the 0.38 Hub-ratio Helical-blade Rotor Subdivided into its Constituent Effects

6.5 & 6.6 Profile Effect on the 0.375 Hub-ratio Constant Blade Angle Rotor Subdivided into its Constituent Effects

6.7 Profile Effect on Turbine Meters with Helical-blade Rotors

6.8 Profile Effect on Different Types of Turbine Meters with Different Tip-clearances

6.9 Profile Effect on Turbine Meters with Constant Blade Angle Rotors

FIG.

6.10 Comparison between Theoretical and Experimental Profile Effect on Helical-blade Rotors

6.11 Comparison between Theoretical and Experimental Profile Effect on Constant Blade Angle Rotors

7.1 Effect of Gate Valve on $\frac{1}{4}$" Hub dia. Helical-blade Rotor without Flow Straightener

7.2 Variation of Meter Coefficient with Different Positions of Valve Closure without Flow Straighteners

7.3 Steadiness of Rotor Rotation at Different Position of Valve Closure without Flow Straighteners

7.4 Effect of Valve on $\frac{1}{4}$" Hub dia. Helical-blade Rotor with and without Flow Straightener

7.5 Effect of Gate Valve on Turbine Meters without Flow Straightener

7.6 Effect of Gate Valve on $\frac{1}{4}$" Hub dia. Rotors with Different Types of Blades

7.7 Effect of Valve on Helical-blade Rotors with Flow Straighteners

8.1 Section of Turbine Meter Showing Positions of Pressure Tappings

8.2 Head-loss Across 2" Research Turbine Meters in Fully Developed Flow

8.3 Head-loss Across 2" Research Meters with $\frac{3}{4}$" Hub dia.

8.4 Comparison between the Head-loss of a 2" Commercial Meter and a 2" Research Meter both with $\frac{3}{4}$" Hub dia.

8.5 Comparison of Head-loss across Research Meters with Commercial Meters

8.6 Pressure Recovery in Flow Deceleration due to the Hub for 2" Turbine Meters

8.7 Comparison of Blade-losses across Research Meters with a Commercial Meter

8.8 Comparison of Different Types of Losses of Different Turbine Meters

8.9 Comparison between Theoretical and Experimental Head-loss of Helical-blade Rotor

8.10 Comparison between Theoretical and Experimental Head-loss of $\frac{3}{4}$" Hub dia. Rotor with Constant Blade Angles

8.11 Pressure Tapping Flanges with Pressure Averaging Chamber (Photograph)

FIG.

9.1 Repeatability Test for Full-diameter Rotor using Open Bearings at Downstream Position (84D)

9.2 Repeatability Test for Full-diameter Rotor using Shielded Bearings at Downstream Position (84D)

9.3 Repeatability Test for Turned-down Rotor using Shielded Bearings at Downstream Position

9.4 Experimental and Theoretical Calibrations for Turned-down Rotor with New and with 'Run-in' Bearings

9.5 Sensitivity of Meters to Increase in Friction Torque

9.6 Variation of Meter Calibration Curve with Resisting Torque for Full-diameter Rotor in a Uniform Velocity Profile

9.7 Variation of Meter Calibration Curve with Resisting Torque for Turned-down Rotor in a Uniform Velocity Profile

10.1 Factors affecting Characteristics of Turbine Meter

10.2 to 10.14 Design of Turbine Meter using Leakage Theory

TABLES

TABLE

7.1 Effect of Flow Straightener

9.1 Mean Meter Coefficient and Standard Deviation of Repeatability Test on Full-diameter Rotor using Open Bearings

9.2 Mean Meter Coefficient and Standard Deviation of Repeatability Test on Full-diameter Rotor using Shielded Bearings

9.3 Mean Meter Coefficient and Standard Deviation of Repeatability Test on Turned-down Rotor using Shielded Bearings

CHAPTER 1

INTRODUCTION

Turbine meters are being increasingly used in many industries where high accuracy flow measurement over a wide range is required. In particular they are used in the aero-space industry (13-15), custody transfer (16,17), petroleum industry (16,18 & 19), gas industry (20-22), milk industry, brewery and for measuring cryogenic fluids (23-29). Though many aspects of turbine meter behaviour, e.g. transient response (30-33), time constant measurement (34), pulsating flows (35-37) and viscosity effects (3,5,13,38 & 39), have been studied, the more fundamental aspects governing the behaviour of meter calibration curves have hardly been touched (more about this later).

1.1 Working Principle of Turbine Meter

The turbine meter is a volumetric instrument and consists essentially of a rotor which rotates at a rate proportional to the volumetric flow rate passing through the rotor. With a suitable sensor (in commercial turbine meters this is usually a magnetic type pick-up), the signal from a turbine meter is obtained as a continuous train of pulses; the rate of these pulses corresponds to the speed of rotation. Therefore by using a timer-counter either to count the total pulses or to integrate the pulses over a certain time interval, it is possible to display the output as totalized flow or as rate of flow. Before a turbine meter can be used for measuring flow, it is necessary to know beforehand the correct average value of its meter coefficient so that the output in pulses or pulses per second can be

converted to the total flow or rate of flow respectively. The meter coefficient is obtained either from the manufacturer's calibration or, in some cases where high accuracy is required, from calibration in situ using a meter prover (12).

1.2 Definition and Comments on Terms Used for Turbine Meters

The meter coefficient of a turbine meter at any flow rate is defined as the ratio of the speed of rotation of the rotor at that flow rate to the flow rate itself. Alternatively, it is the ratio of the number of revolutions the rotor had revolved within a certain time interval to the total flow going through the meter in that same time interval. Therefore it has the dimensions of revolutions per unit volume but since each revolution produces a fixed number of pulses, depending on the number of rotor blades and the number of sensors used, it is often expressed as pulses per unit volume. Besides meter coefficient a few other terms, expressing the same thing, have been used and among them are "K factor", "meter constant" and "meter calibration". However it is felt the "meter coefficient" is the most appropriate term and it is therefore used in this research but is defined slightly differently. Since only one liquid (i.e. water) was used and since temperature variation from experiment to experiment and during each experiment was sufficiently small to avoid any appreciable change in specific volume, the meter coefficient is therefore expressed as pulse per unit weight.

Ideally the meter coefficient should remain constant throughout the flow range but in practice it does so only if the flow is sufficiently large. Its value normally varies with decreasing flow rates until below a certain flow the rotor stops completely. The

upper flow range usually presents little problem but it is at the lower flow range that any interesting change in meter behaviour manifests itself. Theoretically there is no limit to the maximum flow at which a turbine meter can be used but in practice this is limited by the maximum speed the bearings can withstand so as to give a reasonable life. In liquid turbine meters, the maximum flow is also limited by cavitation within the meter.

From the above paragraph it is evident that not only does the meter coefficient change with flow rate but also there is an upper and a lower limit beyond which the meter cannot be used. Therefore in assessing the merits of each individual meter, these factors have to be taken into account and two terms normally used for such purposes are "variation" and "range". These two terms are interdependent and are usually used together. Just quoting the range itself is quite meaningless for one needs to know by what variation the range is valid. Variation is defined as the difference in meter coefficient between that of the flat portion of the calibration curve and that within the range that differs most from the flat portion. Range is commonly defined as the ratio of the lowest to the highest flow measurable for a given variation. As defined, range is too loose a term to have any real value in assessing turbine meters. In commercial turbine meters, the value quoted extends from 1:10 to 1:200 and this has been a source of some disbelief especially among users of other flow measuring devices. The fault really lies not in the claims of manufacturers but in the way the term range is defined. This can best be illustrated by an example. Suppose two meters both have the same maximum flow rate, say 30 kg/s, and the lowest flow rate for a variation of 1% is 1.5 kg/s for one and because of slightly greater bearing

friction it is 3.0 kg/s for the other. Then the range of the first meter is 1:20 and that for the second is 1:10. This creates an exaggerated superiority for the first meter. After all the difference between the lowest flow rates is only 5% of the maximum flow but there is a 100% difference in range. Perhaps a better way of assessing a turbine meter is to use "range factor" instead defined here as

$$\text{Range factor} = \frac{\text{max. flow rate} - \text{min. flow rate}}{\text{max. flow rate}}$$ for a specified variation.

Therefore using this new definition, the range factor for 1% variation is 0.95 for the first meter and 0.90 for the second.

1.3 Existing Theories on Turbine Meters and Their Limitations

Though the principle of the turbine meter itself is simple, the theory governing its behaviour is not fully understood and theories that exist not only differ widely in concept but are also unable to explain some important characteristics of certain meters. This will be apparent later in this chapter when each individual theory is discussed.

Deriving the meter coefficient of a turbine meter theoretically is a relatively simple matter if ideal conditions are assumed. Ideal conditions in this context are taken to mean not only that the flow is uniform but also the absence of any resisting torque whatsoever that might retard the motion of the rotor. Hochreiter (1), in his model, uses such assumptions and the equation for the meter coefficient so derived shows that the calibration curve is uniform throughout the flow range. A meter having such a calibration not only would have the same meter coefficient at all flow rates but also could

measure flow rate right down to zero and still maintain the same meter coefficient. Such a meter would indeed be the ideal meter.

Unfortunately in practice such ideal conditions are never realised. Resisting torques consisting of both viscous drag and mechanical bearing friction are always present. In some meters, it also includes that imposed by the pick-up system (e.g. magnetic pick-up). In order to arrive at a more realistic model, Ruben et al (2) include resisting torque in their derivation. When this is done, the meter calibration curve would decrease with decreasing flow and the rate of this decrease would depend on the magnitude of the resisting torque. From their model, Rubin et al concluded that in order to keep the calibration curve as flat as possible, it is necessary to reduce the resisting torque to as small as possible. In other words, trying to get as near to Hochreiter's model as possible. However, from the leakage model, to be proposed by the author in the next chapter, and supported by experimental evidence, this is not necessarily the case (See Chapter 9).

When turbine meters are actually calibrated, none exhibits a flat calibration curve as predicted by Hochreiter's model although some do have calibration curves that approach that predicted by the model of Rubin et al. However in most commercial liquid meters, the calibration curve exhibits a characteristic "hump" i.e. the calibration curve has almost a flat region at high flow rates but at the medium flow range it rises with decreasing flow until below a certain flow rate it falls rapidly. This contradicts the model of Rubin et al because when it predicts the meter coefficient to fall with decreasing flow it rises instead. Clearly more is involved than just resisting torque.

By assuming the bearing friction is negligible, Lee and Karlby(3)

derived a model to explain the presence of "humps" in meter calibration curves. According to this model, the behaviour of any meter calibration curve depends upon the state of the boundary layers on the turbine blades. It assumed that in the high flow range the boundary layers are turbulent and an equation is derived to show that the calibration is flat in this region. In the medium flow range, the boundary layers are assumed to be transitional and another equation is derived to show that the calibration rises with decreasing flow rate. In the lower flow range the boundary layers are assumed to be laminar and a third equation is derived to show that the calibration curve falls rapidly with decreasing flow rate. Therefore to calculate the meter coefficient throughout the flow range, each of the three regions must be considered separately. For each region, two experimental points from that region are required to define the equation and in all six experimental points are used for the whole range. When the calibration curve is plotted, the transitional and laminar regions meet at a cusp. In practice such cusps do not exist and to overcome this discontinuity, it is simply rounded off. Anyway, if Lee & Karlby's theory is correct then all turbine meters should exhibit the "hump". As may be evident from earlier discussion, this is not so. For example, when using turbine meters with a small hub-ratio in this research (see Fig. 3.12), the calibration curve for a rotor with small tip-clearance does not exhibit such a "hump". Instead the meter coefficient falls with decreasing flow rate. However when the tip-clearance ratio is increased from the original 0.008 to 0.044, the new calibration curve exhibits the "hump". If the "hump" arises because of the state of boundary layers on the blades, then surely the calibration curves for both rotors should show similar

shapes. Even if changing the tip-clearance can somehow upset the boundary layers, the "hump" should be present in both cases. Perhaps the region may be altered but it will certainly not disappear completely and exhibit an opposite effect instead. However, the leakage theory to be presented later suggests that the behaviour of the meter calibration depends upon the nature of the flow through the tip-clearance It can explain the "hump" in the calibration of the big tip-clearance rotor, and the absence of the "hump" in the small tip-clearance rotor. Moreover this new model makes use of only one equation to describe the whole flow range with no rounding off awkward cusps. If desired and knowing the resisting torque, only two experimental points, say one in the higher flow region and one in the medium flow region, need be taken for the calibration curve throughout the whole range to be calculated.

Also trying to explain the "hump", Menkyna (4) suggested that its presence is due to wakes formed by flow-straighteners or bearing supports in front of the rotor. Because of these wakes the blades sweep through regions of varying velocities. This gives rise to unsteady flow and thus overestimation. Some of the objections raised against Lee & Karlby's theory can equally be applied here. If the "hump" is due to wakes, then the calibration curves of the two rotors mentioned earlier should have the "hump" because the blades of both rotors sweep through the same wakes. As explained earlier, one did have a hump while the other did not. Therefore the "hump" could not be due to wakes formed in front of the rotors.

In order to explain the differences in behaviour between the calibration curves of the two rotors, Salami (5) developed a new model. Perhaps it should be explained that although Salami is the

author's predecessor working partly on turbine meter research, his model was developed after the author's leakage model. His model says that the behaviour of the calibration curve of a turbine meter depends on the effect of the inlet velocity profile on the rotor. The model would fail to explain the existence of the "hump" if the inlet velocity profile is assumed completely uniform. However he argued that no such profile exists in practice and however successfully a velocity profile is flattened, there still exists a small non-uniform region near the pipe wall. It is true that at the inlet (i.e. at about 5" from the conical entrance) of the test length of this research rig, there is a boundary layer thickness of 0.050" near the pipe wall. Nevertheless it is a paradox of Salami's model that, theoretically the meter calibration curve of the turned-down rotor (i.e. the rotor with the bigger tip-clearance) should fall with decreasing flow if the inlet velocity is assumed to be complete uniform, yet it rises instead when the profile is almost uniform and the rise is much steeper than when the flow is fully developed. He chose three flow rates and calculated the meter coefficients for both rotors in almost uniform and also fully developed flows. His calculation did not show what happened to the calibration curve at very low flows and if extrapolation is tried on his theoretical meter coefficient for almost uniform flow, the calibration should rise. This is contrary to what happens experimentally. Moreover his calculation showed that for the full-diameter rotor (i.e. the one with the smaller tip-clearance) at almost uniform flow, the meter coefficient should rise by 0.5% when the flow rate drops from 15 to 4 lb/sec. but experimentally there is a drop of 0.5% instead. Even for the turned-down rotor the calculated rise is 3% compared with 1.7% obtained experimentally. In order

to explain this discrepancy he suggested that because of the blockage effect due to the rotor hub, the flow that was uniform in the pipe is accelerated in such a way that the velocity near the hub is greater than that near the tip. He then arbitrarily suggested three different values of "blockage effect" for the three flow rates used and went on to show that the discrepancy is reduced. It should be noted that his hypothesis on blockage effect is not substantiated by experiment and this is clearly evident from Fig. 4.3 which shows the experimental velocity profiles within meter annuli when the velocity profile in the pipe is almost uniform.

1.4 Aims of Research

From the foregoing, one can see how the "hump" causes so much controversy among researchers. While they rage over the "hump", surprisingly little is known about the factors affecting the meter calibration and consequently the "hump" itself. This sad state of affairs is reflected in the very empirical way turbine meters are designed. The main aim, when designing a turbine meter, is to keep the variation of the calibration curve as small as possible and over as wide a range as possible. Also in certain instances when different or odd velocity profiles cannot be avoided, the meter must be so designed that the effects of such profiles are minimised. However, using available knowledge for turbine meter design, the overall meter coefficient can be determined only approximately at the design stage thus leaving the designer uncertain how the final meter calibration curve would look, let alone its ability to reduce the effects of unavoidable profiles. At best he can only rely on his intuition which can lead to very interesting results. One sometimes sees

peculiar design features, the reasons for which are known only to the designer himself. It is true that Jepson et al (9) and Salami (5) showed that the effect of inlet velocity profile on a helical blade meter with small hub-ratio could be reduced by increasing the tip-clearance but the extent of this knowledge is so limited that it can be dangerous to generalise. Whilst it is true that increasing the tip-clearance can reduce the profile effect on helical blade meters, calculations using the equation developed in the next chapter, and supported by experiments, show that a similar tip-clearance increase on a constant blade meter can increase the effect rather than reduce it. Therefore it is the primary aim of this research to study how the behaviour of turbine meters is affected by various factors and in particular how the "hump", the effect of velocity profiles both by axisymmetric and asymmetric, and the head-loss across the meter are affected by changes in tip-clearance, hub-ratio and the type of blades used. Also to be studied is the repeatability of a turbine meter with a small hub-ratio and the effect of changes in bearing friction on the meter calibration, with particular attention to its range and variation. It is hoped that with such studies a better understanding of turbine meters can be achieved so that a more scientific and systematic approach to their design can be developed.

CHAPTER 2

DESCRIPTION OF RIG AND EXPERIMENTAL PROCEDURE

This chapter briefly describes the calibration rig used in this research and the general procedure and technique employed in operating the rig. When certain aspects of the research required special techniques, they are described in their respective chapters. The rig description, under the heading of each component of the rig, outlines the functions of each component and the control associated with it.

The calibration rig was designed by Salami (5) and a detailed description is given in the reference. Fig. 2.1 gives a schematic diagram of the rig while Fig. 2.2 gives a block diagram of the control system. The main pump circulates water from the sump tank round the rig. On its way the flow passes through a filter, into a 40 foot length of 10" diameter pipe which also houses the flow straighteners, contracts through a conical section into the 26 foot test length where turbine meters can be situated, through a pressure regulating valve, through a fish-tail diverter and finally either back into the sump or the weigh tank depending upon the position of the diverter.

2.1 Main Pump

The main pump is driven by a 25 hp. motor through a Kopp variable speed drive. The flow rate can be altered by varying the drive until the required pump speed is obtained. The speed of the pump, measured by a rotating toothed-gear wheel and a magnetic pick-up, is displayed on a frequency counter and is capable of being adjusted to the nearest rev/min. The maximum and the minimum outputs of the variable speed drive are set at about 2600 and 320 rev/min respectively. By controll-

ing the line pressure the maximum and the minimum flow rates obtained are about 21 and 0.2 lb/sec. of water respectively (9.5 and 0.09 kg/s).

2.2 Line Filter

The filter is installed to remove suspended material that may be present in the water. It is self-cleaning and it can do so even while the rig is running. It can be isolated from the flow by operating the appropriate valves.

2.3 10" Dia. Pipe Line (See Fig 2.5)

This section of the pipe is 40 feet long and connects the pipe-work at floor level to the test length at head level through two right-angled bends. Two honeycomb flow-straighteners are situated after the second bend to remove any swirl created in the flow. Two priming valves are also situated after the second bend. These valves are shut only after all the air is expelled from the system during start-up. They are connected to the sump so that any water expelled during priming remains in the system.

2.4 Test Length

From the 10" pipe, the flow converges gradually through a conical section to either a 2" dia. or a $1\frac{1}{2}$" dia. test length. The size of test length used depends upon the size of the turbine meter under test. The purpose of this big contraction in area is to make the flow uniform immediately after the conical section. Except for a very small region near the pipe wall, this was found to be the case experimentally (See Fig. 4.2). The test length, 26 feet long, is made up of shorter pipes ranging from 6" to 96" in length. By suit-

ably combining these pipe sections, a turbine meter can be tested at any position downstream of the conical entrance.

2.5 Control Valve (See Fig 2.6)

The diaphragm-type control valve, situated after the test length is used for controlling the line pressure. The valve is operated by a two-way motor and is remotely controlled from the panel. During normal running, the line pressure is set at 10 psig.

2.6 Fish-tail Diverter (See Fig 2.6)

After the control valve, water flows through the fish-tail diverter and finally either into the sump or into the weigh tank depending on the position of the diverter. The two diverter's positions are set by two pull-type solenoids, one on each arm of the diverter. Only one solenoid can be energized at any time and depending on which one has been energized, the diverter thus guides the flow either into the sump or the weigh tank.

A metal strip, painted black, is attached to one arm of the diverter so that when the flow is directed into the sump, the strip completely blocks the path of a light source from shining into a photo-cell. As the diverter is triggered to the other position (i.e. diverting flow into the weigh tank), the strip uncovers the light to the photo-cell thus creating a signal which is converted electronically to trigger the necessary counters. When the diverter is triggered to guide the flow back into the sump, either manually from the control panel or automatically when the required amount of water is collected, the strip again blocks off the path of light thus creating another signal in the photo-cell to stop the counters. The

strip was so adjusted that triggering of the counters occurs when the diverter is half way between the two positions.

2.7 Sump Tank

The sump tank, with a capacity of 700 gallons, houses 3 sets of immersion heaters capable of heating the water and maintaining the temperature up to 60°C where required. The heaters are interlocked with the transfer pump so that the heaters can only be switched on when the transfer pump is running. This is to avoid local overheating. When water is heated, the temperature can be controlled through three Foster temperature controllers.

2.8 Transfer Pump

By means of a solenoid operated 3-way valve, the transfer pump can be used either for transferring water from the weigh tank or for circulating water in the sump so as to keep the temperature uniform when the heaters are in use. Unless the heaters in the sump are in use, the transfer pump is switched off during each run.

2.9 Weigh Tank (See Fig 2.7)

The weigh tank rests on a weighing machine and no part of the tank is in direct contact with 'earth'. Before weighing air is allowed to bleed into the syphon transfer pipe so that it is not supporting any column of water.

Before each run the weigh tank is emptied by the transfer pump until the water level has reached its lower limit. At this level, a low level water controller switches the 3-way solenoid operated valve to the other position so that the transfer pump is circulating

water in the sump instead. Thus the transfer pump is protected from running dry. During each run water is prevented from overflowing the weigh tank by a high level controller. When water reaches the limit set by the high level controller, the diverter is switched to the other position so that water flows into the sump instead. However, the high level controller would only be actuated if the photo-electric cell of the weighing machine (to be described later) fails to operate.

2.10 Weighing Machine

The weighing machine is capable of weighing up to 2,000 lb. to the nearest ounce. Because of the weight of the weigh tank itself and the water in it at the lower level, the maximum amount of water collected during each run is 1,300 lb. Before each run, the tank is weighed at its lower limit of water level. The scale of the weighing machine is increased by the approximate amount of water required. In this position the arm of the weighing machine blocks a light source from shining into a photo-electric cell. The flow is then diverted into the weigh tank until the required amount of water is collected. When this occurs, the arm of the weighing machine tilts anti-clockwise thus uncovering the light to the photo-cell. This creates a signal to trigger the diverter back to the other position when flow is diverted into the sump again. The tank is weighed again and after the necessary correction, the difference in the two readings gives the actual weight of water collected. The temperature of water in the tank is measured with an ordinary mercury-in-glass thermometer.

From time to time, the weighing machine is calibrated with standard weights. These weights consist of fifty 22.4 lb. weights and six 50 lb. weights. Each individual weight has been adjusted by the Weight and Measure Department to within + 10 grains. (i.e. 0.00637% in each 22.4 lb. weight).

2.11 Turbine Meter Pick-up System (See Fig. 2.9)

In commercial turbine meters, a magnetic pick-up is normally used for recording the speed of rotation. Other than for those commercial meters on loan to us, this type of pick-up is not used on meters in this research because it imposes an additional drag on the rotors. Instead a photo-electric pick-up is used. In this system, a light from a 6V bulb is directed at the blade tips and the reflected light is picked up by a photo-electric cell. The incident light to and reflected light from the blade tips pass through a small transparent window that forms part of the meter casing. The light bulb and the photo-electric cell are housed in a single unit and mounted at the window. Four of such pick-up units are used for research meters and each pick-up is placed at 90° to the other. However, two of them are normally switched off so that only two are in use. To get a better contrast from the reflected light, the rotor hub is painted black.

The signal from the pick-up system is amplified and converted to rectangular wave-form through a wave-shaper before being fed to the counters and to the monitoring oscilloscope.

2.12 Start-up and Shut-down of Rig

When not in use, the following parts of the rig are in the states indicated

i) the two priming valves and the control valve are completely opened.

ii) The Kopp variable speed drive is at its lower limit.

iii) The main pump is permanently filled with water because it is below the sump water-level.

After the pump is started, water slowly displaces the air in the pipe-work. When water starts to flow out through the diverter, the

control valve is then completely shut and any air still remaining in the pipes is forced through the priming valves. The priming valves are connected to the sump through a long transparent tube. When no air can be seen to flow through the tube, the control valve is opened again. Using the control valve, the line pressure is raised and lowered between 5 psig and 15 psig. This is done for two to three times so that any air still trapped in the 10 inch pipe can be ejected through the priming valves. The rig is allowed to run for about 5 minutes before closing the priming valves. Meanwhile, all the necessary electronics are switched on.

To shut down the rig, the Kopp variable drive is brought down to its lower limit and the control valve completely opened. The pump can then be switched off. If it is desired to alter the test length immediately after shut-down, water in it can be rapidly drained by opening the pump by-pass valve. However, when doing this, the valve must be shut off before the next start-up.

2.13 Procedure for Meter Calibration

When calibrating, the meter can be placed at any position along the test length. By adjusting the pump speed, the flow can approximately be set to any required flow rate. As it is proportional to the flow rate, the pump speed itself gives a good indication of the flow obtained.

Normally, the line pressure is set to 10 psig except at very low flows (below 0.7 lb/sec.) when it needs to be raised higher before the required flow rate can be obtained. The weigh tank is weighed with its water level at its lower limit. The scale of the weighing machine is then increased by the same amount as that of water to be

collected, to a maximum of 1300 pounds. At high flow (i.e. above 7 lb/sec.) the maximum amount is collected. Below 7 lb/sec., the amount is selected so that the time required for its collection is between 150 and 300 seconds; the lower limit is for flows near to 7 lb/sec. while the upper limit for flows below 1 lb/sec.

The measured flow rate is given by the rotational speed of the turbine meter. This speed can be recorded in three ways. The first method is to use a frequency counter to record continuously the frequency of the pulses generated. The counter used can be read to the nearest 0.1 Hz. but as the lowest frequency is about 3.0 pulses per second, this method is not good enough for the accuracy desired. The second method is to use a pulse counter to record the total number of pulses generated within the period of time the required amount of water has been collected. This is done by triggering a pulse counter and a timer-counter at the instant flow is diverted into the weigh tank and again when it is diverted back to the sump (see section 2.6). Normally, this method is not used because when the necessary solenoids are energized to move the diverter, electrical disturbances are created. Sometimes this may have caused the counter to record stray pulses originating from such disturbances. Electrical disturbances may also occur during the initial few seconds of filling the weigh tank. During this period the low level sensor is being covered with water which may result in "chattering" of electrical relays.

The third and best method is by timing, to the nearest microsecond, the time interval for 1000 pulses continuously sampled during the period the weigh tank is being filled. Because of the disturbances previously mentioned, the first and the last sample are discarded. Depending on the meter used, between 8 to 20 samples can be obtained.

The average value is taken. This is the method used in this research.

The time taken for collecting the required amount of water is recorded electronically to the nearest millisecond. This is done with a timer-counter in the same manner as described in the second method.

After the required amount of water has been collected, the weigh tank is weighed again and the difference from the initial weight gives the weight of water collected. The temperature of water in the weigh tank is measured before it is transferred to the sump.

2.14 Dynamic Weighing Versus Static Weighing

The calibration rig used in this research and described in the preceding sections was designed primarily for static weighing but it can also be used for dynamic weighing. Although dynamic weighing is much easier and faster to do, it is not used in this research because it is felt that it would not give the accuracy required. This section serves to investigate the magnitude of the error likely to arise when dynamic weighing is used and to see if this error is significant when calibrating meters for general use.

In static weighing, the weigh tank is weighed initially when its content is at a low level. During normal operation the lowest level obtainable is when the weigh tank and its contents weigh about 610 lb. The weighing machine setting is increased by a predetermined amount. Flow is then diverted into the weigh tank and when the load on the weighing machine reaches the value set, the balance arm rises. In so doing it energizes a photo-electric cell which in turn causes the flow to be diverted back to the sump. The operation of this automatic switching system is explained in Section 2.10. The weigh tank is then weighed at leisure and the difference between the final and initial

weighings gives the actual amount of water collected. The time taken for collecting this amount is recorded on a timer-counter. The timer is triggered to start electronically just when the diverter is at the mid-point of the flow outlet and is similarly triggered to stop when the diverter is on the same mid-point on its way back. This arrangement ensures that timing is done only when water is being collected.

In dynamic weighing, no actual weighing is done. When the weigh tank is at a low level, the weighing machine is set to a reading (usually a round figure) about 40 lb. greater than the load already on the platform. Flow is diverted into the weigh tank and the load on the weighing machine reaches the set value, the flow is automatically diverted back to the sump as explained before. However, in this first operation, the timer is not allowed to operate. The weighing machine setting is increased by a predetermined amount and the above operation is repeated but this time with the timing system operating. The difference between the final and initial settings of the weighing machine is the amount of water collected within the measured time interval. From the foregoing discussion on dynamic weighing, it is evident that if the rates of response of the weighing machine at the initial and the final settings are the same, then the difference in the two machine settings would give the correct weight of water collected. If the rates of response are different there would be an error.

To check the accuracy of dynamic weighing against static weighing, the operations described in the preceding paragraph are carried out at machine settings ranging from 600 lb. to 1,900 lb. in steps of 100 lb. After weighing dynamically at each setting, the corresponding static weighing is carried out at leisure before proceeding to the

next setting. Fig. 2.3 shows the difference between static and dynamic weighings at different machine setting for 3 different flow rates. If all the points for a particular flow lie on a horizontal line, then there is no difference whether static or dynamic weighings are used provided the final and the initial weighings are done in the same way. However, this was not so and from Fig. 2.3, it can be seen that not only does the difference between static and dynamic weighings change with different loading on the weighing machine but also with the rate at which the load is being added. Suppose it is desired to measure the exact flow rate of water flowing at approximately 15 lb/sec. by collecting 1,300 lb. in the weigh tank. If the initial and the final settings are set at 600 and 1,900 lb. respectively, then the error in dynamic weighing is 2.25 lb. (an error of 0.17%). However, it may not be necessary to collect the full 1,300 lb. because it may take too long. If, say, 400 lb. is required and if the initial and final settings are at 1,500 and 1,900 lb. respectively, then the error is 2 lb. (i.e. 0.5%). The overall error permissible in this research should be less than 0.1% and therefore dynamic weighing cannot be used.

Fig. 2.4 shows the scatter in the errors due to dynamic weighing when the amount of water is collected 42 times. The amount collected is 1,300 lb. and the flow rate set at 15.0 lb/sec. The initial and the final machine settings are 650 and 1,950 lb. respectively. From the figure it can be seen that even when an average correction is used, each individual reading can be cut by as much as 1.6 lb. (i.e. 0.12%). Therefore in view of the accuracy required, only static weighing is used in this research. However, if a meter for general use is to be calibrated with this rig, dynamic weighing may be acceptable.

CHAPTER 3

THEORY

3.1 Introduction

The theory given in this chapter consists of two parts. The first part deals with the derivation of the general rotor coefficient equation (and hence the meter coefficient equation) of turbine meters while the second part deals with the development of a new theoretical model.

The velocity profile in the pipe just upstream of a turbine meter can be at any stage of boundary layer development. It is desirable at the design stage to know theoretically or otherwise the effect of velocity profile because this would enable allowance to be made when necessary without having first to carry out a tedious profile effect test. Moreover not all calibration rigs can be used for carrying out such a test. Even if it could be done and if the effect were found unsatisfactory, much time and money would have been lost because the rotor had to be redesigned. This could be avoided if a theoretical check were possible and reliable. Checking the design theoretically for profile effect, the meter coefficients for different stages of velocity profile development need only be compared and therefore the ability to predict the meter coefficient accurately as an absolute value is not important. In any case the accuracy required of a turbine meter would necessitate its calibration before putting it into service.

Different assumptions have been used by various researchers to derive the meter coefficient equation. Lee and Karlby (3) and Rubin et al (2) assumed that the flow is uniform and therefore that theory

cannot be used for checking the effect of velocity profile. Also they, Jepson and Bean (9) and Grey (44) assumed that the blade drag is independent of the angle of attack. Salami (5), Lee and Karlby, Rubin et al, and Jepson and Bean (9) assumed isolated blade theory and therefore no blade interference (i.e. cascade effects). Further discussion on different assumptions is given in Chapter 5 where the theoretical meter coefficients using them are compared with experiment. In the derivations given in the above references, only turbine meters with helical-blade rotors were considered. Using similar assumptions it is found that whilst they could be used quite satisfactorily for helical-blade rotors, they are not as good when dealing with constant blade angle rotors. This is mainly because not only is the angle of attack on the latter much larger but it varies considerably from blade radius to blade radius. This makes the effect of drag on their meter coefficients very much greater than for helical-blade rotors and therefore any change in drag that accompanied any change in velocity profile, cannot be ignored. Some assumptions used in the derivation of the meter coefficient equation in this chapter have not been used before. Although they make the derivation and computation more tedious and complicated, the resulting equation expresses more accurately the meter coefficient for a constant blade angle rotor.

The second part deals with the presentation of a new theoretical model for describing the behaviour of turbine meter calibration curves. Perhaps it is appropriate at this point to describe the experimental evidence that prompted the development of this model.

The two research rotors designed and used by Jepson (9), and later also used by Salami (5) and the author, are identical in design except that one has a small tip-clearance while the other has a big

tip-clearance. The original intention of Jepson for making the big tip-clearance rotor was because he thought that if the tip-clearance ratio were increased to that value (i.e. 0.044) the meter would have no profile effect. Though this was found not to be true the profile effect was considerably reduced (see Fig. 6.7). When the two rotors were calibrated the resulting calibration curves were found to behave differently. The meter coefficient of the rotor with small tip-clearance decreased with decreasing flow rate while that of the big tip-clearance rotor increased instead (see Fig. 3.12). The author found that existing theories on the behaviour of turbine meter calibration curves as proposed by Lee and Karlby (3) and Menkyna (4), could not be used to explain the difference in the behaviour of the two rotors (see Chapter 1 for a discussion of this). Since the difference between the two rotors was only a difference in tip-clearance, it was felt that perhaps the behaviour of turbine meters might not be as suggested by existing theories but rather depended on the manner of flow through the tip-clearance. It is on this that the leakage theory to be proposed is based.

As will be shown later at the end of the chapter, this new theory expresses the behaviour of turbine meter calibration curves very well. This is done not only for both the rotors mentioned above and on research rotors subsequently designed, but also for several commercial meters.

3.2 Derivation of Rotor Coefficient

Fig. 3.1 shows the inlet, the outlet and the mean velocity diagrams for a cylindrical section of an elemental blade dr at radius r. The inlet and the outlet velocity diagrams are taken to be after the inlet and before the outlet of the blade respectively. The elemental

lift dL and drag dD acting on the elemental blade are respectively perpendicular and parallel to the vectorial mean velocity V_m of V_i and V_e. V_i and V_e are the velocities relative to the blade at the inlet and the outlet of the blade respectively. It is assumed that V_e leaves the trailing edge of the blade inclined at an angle δ^* to the blade. The value of δ^* can be calculated from Constant's deviation angle equation (45). For a turbine it is given by

$$\delta^* = 0.26\,\theta^* \,.\, (s/c) \qquad \ldots \quad 3.1$$

θ^* is the camber angle. As the blades of turbine meters are considered as flat plates, there is no camber angle and equation [3.1] needs to be modified. If the flow enters and leaves a blade at its inlet and outlet blade angles, then θ^* is equal to the turning angle. Therefore for turbine meter θ^* can be assumed to be

$$\theta^* = \theta_e - \theta_i$$

$$= \beta - \delta^* - \theta_i \qquad \ldots \quad 3.2$$

i.e.

$$\delta^* = 0.26(\theta_e - \theta_i).(s/c)$$

$$= \frac{0.26(\beta - \theta_i).(s/c)}{1 + 0.26(s/c)} \qquad \ldots \quad 3.3$$

Using θ^* as defined in equation [3.2] the outlet velocity angle θ_e as shown in Fig. 3.1 is given by

$$\theta_e = \beta - \delta^*$$

Sometimes the angle of attack varies along the blades from

positive to negative values (see Fig. 3.2). On such occasions, the lift along that portion of the blade with a positive angle of attack acts toward one side of the blade while that with negative angle of attack toward the other. The nett torque developed by the rotor is the sum of all the lift torque. The tangential component of the positive lift and the rotation are in the same direction. This means that the region of a blade with negative angle of attack does not contribute towards the rotation but instead behaves in a similar manner to an axial compressor and has to be driven along. It is therefore assumed that the deviation angle δ^* along the portion of the blade with negative angle of attack follows that for a compressor (45) and the modified version of the Constant deviation angle is given by

$$\delta^* = \frac{0.26(\beta - \theta_i)\sqrt{s/c}}{1 + 0.26\sqrt{s/c}} \quad \ldots \quad 3.4$$

By definition the forces acting on the elemental blade is given by

$$dL = \tfrac{1}{2} \cdot \rho \cdot V_m^2 \cdot C_L \cdot c \cdot dr$$

$$= \frac{\tfrac{1}{2} \cdot \rho \cdot W \cdot C_L \cdot u^2 \cdot dr}{\cos^2 \theta \cdot \cos \beta} \quad \ldots \quad 3.5$$

$$dD = \frac{\tfrac{1}{2} \cdot \rho \cdot W \cdot C_D \cdot u^2 \cdot dr}{\cos^2 \theta \cdot \cos \beta} \quad \ldots \quad 3.6$$

If isolated blade theory is to be used then, as shown by Durand (6) and quoted by Wislicenus (8), the theoretical equation for the lift coefficient C_L of a straight and infinitely thin aerofoil is given by

$$C_L = 2\pi \sin \alpha \quad \ldots \quad 3.7$$

In this equation the angle of attack α is always measured between the direction of V_i and the zero-lift direction of the aerofoil considered.

If the cascade effect is to be considered as well, the theoretical equation for the lift coefficient of a system of straight and parallel blades (i.e. flat-plate cascades), as derived by Weinig (7), can be used. Weinig expresses his results as

$$C_L = 2\pi K . \sin \alpha \qquad \ldots \quad 3.8$$

where α is the angle of attack measured, in this case, between the direction of the vectorial mean velocity V_m and the zero-lift direction. The factor K is the Weinig lattice-effect coefficient and it expresses the effects of the cascade arrangement, because when K = 1, equation [3.8] gives the theoretical lift coefficient of the flat plate single aerofoil. The value of K is determined (7) from the following three equations:-

$$K = \frac{4}{\pi} . \frac{s}{c} . \frac{R}{R^2+1} . \frac{\cos \alpha^*}{\cos \beta} \qquad \ldots \quad 3.9$$

$$\tan \alpha^* = \tan \beta . \frac{R^2-1}{R^2+1} \qquad \ldots \quad 3.10$$

$$\frac{c}{s} = \frac{1}{\pi} \left\{ \cos \beta . \ln\left(\frac{R^2+2R.\cos \alpha^*+1}{R^2-2R.\cos \alpha^*+1}\right) + 2 \sin \beta . \tan^{-1} \frac{2R \sin \alpha^*}{R^2-1} \right\}$$

$$\ldots \quad 3.11$$

α^* and R are parameters used in the conformal transofrmation for deriving the three equations. Other symbols are defined in Fig. 3.1. At any blade radius r of a rotor, the peripheral pitch s between blades, the chord c and the blade angle β can be obtained from the

rotor dimensions. The numerical solution of K at any radius can be found using the three equations. A computer program is developed for doing this and the results are shown in Fig. 3.3.

Equations [3.7] and [3.8] were derived from two dimensional considerations and can therefore be applied only to blades of infinite aspect ratio. To take into account finite aspect ratio and blade aerofoil efficiency, the lift coefficient of a blade in cascade is modified to

$$C_L = \left(\frac{\epsilon}{1 + \frac{2.\epsilon}{AR}} \right) 2\pi \,.\, K \,.\, \sin\alpha \quad . . \quad 3.12$$

where

$$AR = \text{aspect ratio} = \frac{(r_t - r_h)^2}{\text{blade area}}$$

and

$$\epsilon = \text{blade aerofoil efficiency.} \quad 0.9 < \epsilon < 1.0$$

Equation [3.12] can be expressed as

$$C_L = C_1 \,.\, K \,.\, \sin\alpha \quad . . . \quad 3.13$$

where

$$C_1 = \left(\frac{\epsilon}{1 + \frac{2.\epsilon}{AR}} \right) . \, 2\pi \quad . . . \quad 3.14$$

The coefficient of drag C_D varies with the angle of attack α and consequently it also varies with the coefficient of lift C_L. Experimental results as given in Betz (41) shows that there is a parabolic variation between C_L and C_D when the angle of attack on a flat plate is increased. The relationship between C_D and C_L can be

represented in the form

$$C_D = \frac{C_L^2}{J} + C_{Do} \qquad \ldots \quad 3.15$$

where J is a constant and C_{Do} is the coefficient of drag when the angle of attack is zero. C_{Do} can be taken to be

$$C_{Do} = 2\,C_f \qquad \ldots \quad 3.16$$

where C_f is the coefficient of skin friction on one side of a flat plate. Using the data given by Betz (41), J was found to be 8.26 for the flat plate used. The comparison between the experimental points and the fitted equation [3.15] is given in Fig. 3.5.

In equation [3.15] C_L^2/J is the coefficient of induced drag C_{Di} and as shown by Prandtl and Tietjens (42), the value of J for an elliptical lift distribution is given by

$$J = \pi \cdot AR$$

and as pointed out by them, it is the case for minimum induced drag. To get a more realistic value, a factor of 0.9 is included

i.e.

$$J = 0.9\pi \cdot AR \qquad \ldots \quad 3.17$$

Experiments done by Howell and Carter (43), on the variation of drag coefficient with angle of attack for turbine cascades, shows that C_D remains almost constant for positive angles of attack but varies rapidly when the angle of attack is negative. (Note that negative angle of attack as defined here is positive as defined by Howell and Carter). Therefore C_D can be taken to be

$$C_D = C_{Do} \qquad \text{for} \quad \alpha > 0^\circ \qquad \ldots \quad 3.18$$

Consider the forces acting on the elemental blade as shown in Fig. 3.1 and if the rotor has N blades, then the elemental torque dT_d driving the rotor is

$$dT_d = N \,.\, (dL \,.\, \cos\theta - dD \,.\, \sin\theta) \,.\, r$$

$$= \tfrac{1}{2}\rho \,.\, N \,.\, W \,.\, u^2 \,.\, r \,.\, dr \,.\, \left\{ \frac{C_1 \,.\, K \,.\, \sin\alpha}{\cos\beta \,.\, \cos\theta} - \frac{C_D \,.\, \tan\theta}{\cos\beta \,.\, \cos\theta} \right\}$$

$$\ldots \quad 3.19$$

Now

$$v_e = u \tan(\beta - \delta^*) - 2\pi rn$$

and

$$\tan\theta = \frac{2\pi rn + \frac{v_e - v}{2}}{u}$$

$$= \frac{\pi rn}{u} + \frac{\tan(\beta - \delta^*)}{2} - \frac{v}{2u} \qquad \ldots \quad 3.20$$

Therefore

$$\frac{\sin\alpha}{\cos\beta \, \cos\theta} = \tan\beta - \tan\theta$$

$$= \tan\beta - \frac{\pi rn}{u} - \frac{\tan(\beta - \delta^*)}{2} + \frac{v}{2u} \qquad \ldots \quad 3.21$$

Substituting equations [3.21] into [3.19], integrating from hub to tip (i.e. from h to t) and taking the total driving torque T_d to be equal to the total resisting torque T, we get

$$\frac{T}{\frac{1}{2}\rho.N.W} = \frac{U^2.r_o^2}{2}.C_1\int_h^t K.\{2\tan\beta - \tan(\theta-\delta^*)\}\left(\frac{u}{U}\right)^2\frac{rdr}{r_o^2}$$

$$- n.\pi.U^2.r_o^3.C_1.\int K.\left(\frac{u}{U}\right)\frac{r^2dr}{r_o^3} + \frac{U^2.r_o^2}{2}.C_1.\int_h^t K.\left(\frac{v}{u}\right)\left(\frac{u}{U}\right)^2\frac{rdr}{r_o^2}$$

$$- U^2.r_o^2.\int \frac{C_D.\tan\theta.\left(\frac{u}{U}\right)^2.rdr}{\cos\beta.\cos\theta.r_o^2}$$

$$= \frac{U^2.r_o^2}{2}.C_1.I(n) - \pi.n.U^2.r_o^3.C_1.B(n) + \frac{U^2.r_o^2}{2}C_1.V(n)$$

$$- U^2.r_o^2.Z(n)$$

Therefore

$$n = \frac{1}{\pi.r_o.B(n)}\left\{\frac{I(n)}{2} + \frac{V(n)}{2} - \frac{Z(n)}{C_1}\right\} - \frac{T}{\frac{1}{2}.\rho.C_1.N.W.\pi.U.r_o^3.B(n)} \quad \ldots \quad 3.22$$

Now the flow going through the rotor is

$$Q_r = \int_h^t (2\pi r - N.t)\,u\,dr$$

$$= \pi\, r_o^2.U.\int_h^t \left(2r - \frac{N.t}{\pi}\right)\left(\frac{u}{U}\right).\frac{dr}{r_o^2}$$

$$= \pi\, r_o^2.U.C(n) \quad \ldots \quad 3.23$$

and the flow going through the tip-clearance is

$$Q_c = \int_{r_t}^{r_o} 2\pi r u \, dr$$

$$= \pi r_o^2 . U . D(n) \qquad \ldots \quad 3.24$$

Now the total flow Q is

$$Q = Q_r + Q_c$$

$$= \pi r_o^2 . U . [C(n) + D(n)] \qquad \ldots \quad 3.25$$

Therefore from equations [3.22] , [3.23] and [3.25] , the rotor coefficient is

$$\frac{n}{Q_r} = \frac{I(n)}{2\pi^2 r_o^3 . B(n) . C(n)} + \frac{V(n)}{2\pi^2 r_o^3 . B(n) . C(n)} - \frac{Z(n)}{C_1 . \pi^2 r_o^3 . B(n) . C(n)}$$

$$- \frac{2 . T . [C(n)+D(n)]^2}{\rho . C_1 . N . W . r_o . B(n) . C(n) . Q^2} \qquad \ldots \quad 3.26$$

When there is no inlet swirl V(n) is zero.

Therefore,

$$\frac{n}{Q_r} = \frac{I(n)}{2\pi^2 r_o^3 . B(n) . C(n)} - \frac{Z(n)}{C_1 . \pi^2 . r_o^3 . B(n) . C(n)} - \frac{2 . T . [C(n)+D(n)]^2}{\rho . C_1 . N . W . r_o . B(n) . C(n) . Q^2}$$

$$\ldots \quad 3.27$$

For the case when there is no flow through the tip-clearance D(n) is zero.

Therefore

$$\left(\frac{n}{Q}\right)_{nl} = \frac{I(n)}{2\pi^2 r_o^3 . B(n) . C(n)} - \frac{Z(n)}{C_1 . \pi^2 . r_o^2 . B(n) . C(n)} - \frac{2 . T . C(n)}{\rho . C_1 . N . W . r_o . B(n) . Q^2}$$

. . . 3.28

The values of I(n), B(n), C(n), D(n), V(n) and Z(n) are as defined in Appendix I. The equations for the velocity profile u/U within the meter annulus are as empirically derived in Chapter 4.

Fig. 3.4 shows a cross-section of a turbine meter blade. The section is a ~~trapezium~~ parallelogram with the leading and trailing edges not perpendicular to the sides of the blade but to the axis of rotation instead. In the derivation of the meter coefficient equation the blade angle β is taken to be between one side of the blade and the axis. This would be the case when the blade is infinitely thin (i.e. $t \rightarrow o$) or when the leading and trailing edges are squared up with respect to the blade sides. The dotted line in Fig. 3.4 joins the mid-points of the blade thickness from the leading to the trailing edges. Throughout most of the blade section it is also inclined at an angle β to the axis. The exceptions are at the leading and the trailing edges where a small part of the dotted line is inclined at an angle $(90^o - \beta)/2$ to the adjacent blade side. It is likely that effective blade angle is not β but β plus a small proportion of $(90^o - \beta)/2$. The proportion would probably depend on the blade thickness t, the blade angle β and the axial width W. Referring to the enlarged section of the leading edge shown in Fig. 3.4, the line ab is perpendicular to the blade. If the leading edge and the trailing edge are trimmed to ab, the effective blade angle β' would be equal to β. The line cd is the axial distance from the midpoint of the leading edge to ab.

i.e.

$$cd = \frac{t}{2.\tan \beta}$$

The proportion contributed by $(90^\circ-\beta)/2$ can be taken such that the effective blade angle is given by

$$\beta' = \beta + \frac{cd}{W} \cdot \frac{(90^\circ-\beta)}{2}$$

$$= \beta + \frac{t.\tan \beta.(90^\circ-\beta)}{4.W} \qquad \ldots \quad 3.29$$

Further discussion about the effect of leading and trailing edges is given in Chapter 5 when the meter coefficients of turbine meters are calculated theoretically

3.3 Leakage Model

When analysing turbine meters there are actually two coefficients to be considered; namely, the meter coefficient n/Q and the rotor coefficient n/Q_r. The coefficient obtained when calibrating a turbine meter is the meter coefficient and the two experimental variables used to calculate its value are the speed of rotation n and the total flow rate Q. However not all of Q is responsible for producing the rotation. The rotor responds only to that part of the flow rate Q_r that goes through the rotor. What passes outside the sweep of the rotor blades, i.e. that part of the flow Q_c that goes through the clearance between the blade tips and the meter casing, is not registered. Rotor coefficient is therefore not a coefficient that can be measured experimentally but rather it is a theoretical concept expressing the ratio of the speed of the rotor n to the flow rate Q_r that is actually responsible for producing that speed. The two coefficients differ in value because of the flow going through the tip-clearance.

Tip-clearance flow consists of two parts. One part is due to the flow resulting from the presence of the gap between the blade tips and the meter casing. The other part is due to any interchange of flow between the volume enclosed by the sweep of the blades and that within the tip-clearance that results from any flow inequilibrium caused by the motion of the rotor blades.

It has been observed that when a turbine meter (especially with smaller hub-ratio) is calibrated with a small tip-clearance and again with the tip-clearance increased sufficiently, the shapes of the resulting calibration curves are completely different towards the lower range of flows. When the tip-clearance is small, the meter coefficient decreases with decreasing flow rate but when the tip-clearance is large, the meter coefficient rises with decreasing flow rate in the medium range of flows before falling rapidly at very low flow rates. Examples of such behaviour can be seen in Figs. 3.12 and 3.13. If the theories proposed by Lee and Karlby (3) and Mankyna (4) are correct, then both calibration curves should behave in the same way since the prerequisites in flow conditions required in their theories are the same in both cases. This has been argued in Chapter 1. Evidently the behaviour of turbine meter calibration curves must be affected by flow through the tip-clearance. This is the basis on which the leakage theory, to be proposed herewith, is based.

The relationship between the two coefficients and the different flow rates associated with turbine meters are as follows

$$Q = Q_r + Q_c$$

$$\frac{n}{Q} = \frac{n}{Q_r} \cdot \frac{Q_r}{Q}$$

$$= \frac{n}{Q_r}\left(1 - \frac{Q_c}{Q}\right) \qquad \ldots \quad 3.30$$

Equation [3.30] shows the relationship between the meter coefficient n/Q, the rotor coefficient n/Q_r and the tip-clearance flow ratio Q_c/Q. It is evident from the equation that the variation of the meter coefficient with flow rate depends not only on how the rotor coefficient would vary but also on how the tip-clearance flow-ratio would vary as well. If the flow-ratio remains constant at all flow rates, then the meter coefficient is governed solely by the rotor coefficient and the meter coefficient would decrease with decreasing flow rate towards the lower flow range. A plot of tip-clearance flow Q_c versus the total flow rate Q is a straight line passing through the origin as shown in Fig. 3.7.

If the tip-clearance flow-ratio varies with flow rate, then the meter coefficient would vary with it as well as that of the rotor coefficient. It will be shown later by semi-empirical deduction that the tip-clearance flow-ratio is of the form

$$\frac{Q_c}{Q} = g - \frac{k}{Q} \qquad \ldots \quad 3.31$$

where g and k are constants.

Combining equations [3.30] and [3.31], the meter coefficient equation becomes

$$\frac{n}{Q} = \frac{n}{Q_r}\left(1 - g + \frac{k}{Q}\right) \qquad \ldots \quad 3.32$$

The rotor coefficient equation is given in equation [3.27] and to save space it is shortened so that the meter coefficient becomes

$$\frac{n}{Q} = \left(T_1 - T_2 - \frac{T_3}{Q^2}\right)\left(1 - g + \frac{k}{Q}\right) \qquad \ldots \quad 3.33$$

where

$$T_1 = \frac{I(n)}{2.\pi^2.r_o^3.B(n).C(n)}$$

$$T_2 = \frac{Z(n)}{C_1.\pi^2.r_o^3.B(n).C(n)}$$

$$T_3 = \frac{2.T.\left[C(n)+D(n)\right]^2}{\rho.C_1.N.W.r_o.B(n).C(n)}$$

Note that T_2, T_3/Q^2 and k/Q are small compared to T_1 and therefore $(T_2.k)/Q$ and $(T_3.k)/Q^3$ are very small and can be neglected in the discussion on the behaviour of meter calibration curve.

From equation [3.33] it is therefore evident that three main interacting terms come into play when the flow varies, i.e.

1) $+ T_1.k/Q$

2) $- T_2.(1-g)$

3) $- \frac{T_3.(1-g)}{Q^2}$

The absolute values of the three main interacting terms increase with decreasing flow rate. As the flow rate decreases $+(T_1.k)/Q$ tries to pull the calibration curve up while the other two terms try to pull the calibration curve down. The direction which the curve would follow depends on the values of leakage factor k and T_3 (T_3 is a function of the resisting torque T). If the leakage factor is sufficiently large (e.g. in turbine meters with large tip-clearances) in comparison with the resisting torque, then at medium flow rates, $+(T_1.k)/Q$ predominates thus giving the rising section of the calibration curve. However below a certain flow rate $-T_2.(1-g)$ and $-T_3(1-g)/Q^2$

predominate and their values increase very rapidly with decreasing flow rate. As a result the calibration curve falls very rapidly at very low flow rates.

In the case of small leakage factor (e.g. in meters with small tip-clearance and hub-ratio) $-T_2.(1-g)$ and $-T_3(1-g)/Q^2$ predominate at all flow rates and no rising section of the calibration curve is obtained.

The values of all the three terms decrease with increasing flow rate and the meter coefficient tends to the value $T_1.(1-g)$. At sufficiently high flow rates the meter coefficient remains constant if other influences (e.g. cavitation) are absent.

3.3.1 Determination of g and k

Before equation [3.33] can be evaluated theoretically for plotting, the values of g and k need to be known. These values are constants relating the tip-clearance flow ratio to the flow rate and they can be evaluated in three ways.

Method 1 (semi-experimental deduction)

In this method, the theoretical calibration curves, when there is no tip-clearance flow and when the tip-clearance flow ratio is constant, are plotted using equations [3.30] and [3.28] respectively. The meter coefficient obtained experimentally is also plotted on the same graph. An example is given in Fig. 3.6 for a research rotor with helical-blades, having a hub-ratio of 0.38 and tip-clearance ratio of 0.030. The meter is in fully developed flow.

In Fig. 3.6 curve 1 has no tip-clearance flow, while curve 2 has a constant tip-clearance flow ratio of $D(n)/\{C(n)+D(n)\} = 0.0558$. Curve 3 is the experimental calibration curve. Then by using proportionally the actual tip-clearance flow ratio Q_c/Q and the tip-

clearance flow Q_c at any flow rate can be deduced as follows. At any flow rate, the proportion $\{(a-b)/(a-c)\}$ x 0.0558 gives the actual tip-clearance flow-ratio at that flow rate. The tip-clearance flow would then be $\{(a-b)/(a-c)\}$ x 0.0558 x Q. This is done for other flow rates. Graphs of tip-clearance flow-ratio and tip-clearance flow against the flow rate can be plotted as shown in Figs. 3.8.

From Fig. 3.7, it can be seen that the graph of Q_c against Q is a straight line with a gradient g and intercept -k. The equation of the line is

$$Q_c = gQ - k \qquad \ldots \quad 3.34$$

By this semi-experimental deduction, the tip-clearance flow-ratio is therefore shown to be in the form given in equation[3.31]. For this particular rotor used in the example the values of g and k so obtained are used in equation[3.32]so that the theoretical calibration curve throughout the flow range can be plotted. This is shown in Fig. 3.9 together with the experimental points.

Method 2 (Using two experimental points)

This method uses a few of the experimental points to evaluate the unknown constants in the meter coefficient equation and the number of points chosen depends on the number of unknowns. This method was used by Lee and Karlby (3) to evaluate the constants in each of the three equations they derived to describe the different sections of the calibration curve. In all they took six experimental points since each equation has two unknown constants.

However, using the leakage model as given in equation [3.32] , only one equation is required to describe the calibration throughout the whole range of flow. Hence only two experimental points need be

used to determine g and k. Preferably one point is taken towards the higher flow range and the other towards the lower flow range. Taking the same research rotor as that used in Method 1, the theoretical meter calibration curve is shown in Fig. 3.10 together with all the experimental points. The two experimental points used for determining g and k are marked with crosses.

Method 3 (method of least squares)

In method 2, the degree of agreement between the theoretical curve with the experimental points would depend on how well the two experimental points were chosen to evaluate g and k. If the two points chosen were among the worst of all the points, the agreement might not be as good as shown in Fig. 3.10. Therefore to get more accurate values of g and k more experimental points are used. Then g and k can be determined by the method of least squares as follows. Simplifying equation [3.33]

$$\frac{n}{Q} = T_1.(1-g) - T_2.(1-g) + \frac{T_1.k}{Q} - \frac{T_3.(1-g)}{Q^2} + \ldots$$

. . . 3.35

The rest of the terms are very small and can be neglected as stated before. At any flow rate Q the values of T_1, T_2 and T_3 can be calculated theoretically. Therefore using the meter coefficient n/Q and the flow rate Q from the experimental points, the values g and k can be calculated by the method of least squares. Note that T_3 includes the resisting torque T and if T is not known, then T_3 can be calculated along with g and k. As all other factors in T_3 are known, the resisting torque T can be determined. Therefore, using method 3, the resisting torque can also be estimated. In fact its values used in

For the research rotors shown in Figs. 3.11 to 3.13, the values of the various terms given in equation (3.35) are given in the table below.

		Values quoted in pulse/lb				
	Flow-rate lb/sec	Meter Coeff. n/Q	$T_1.(1-g)$	$T_2.(1-g)$	$T_1.k/Q$	$T_3.(1-g)/Q^2$
Helical blade at 96D	2.0511	10.6131	10.5481	0.2371	0.5142	0.2128
Hub-ratio = 0.381						
Tip-clearance = 0.030"	18.3943	10.4790	10.5481	0.1259	0.0573	0.0026
Constant blade angle at OD	2.0723	8.9134	9.0362	0.2588	0.2094	0.0801
Hub-ratio = 0.125						
Tip-clearance = 0.007"	18.7963	8.9028	9.0362	0.1622	0.0231	0.0010
Constant blade angle at OD	2.2033	9.4633	9.5013	0.2026	0.3048	0.1400
Hub-ratio = 0.125						
Tip-clearance = 0.050"	17.9747	9.3523	9.5013	0.1841	0.0374	0.0021
Helical blade at OD	2.2363	9.1280	8.9645	0.1879	0.5335	0.1833
Hub-ratio = 0.125						
Tip-clearance = 0.044"	17.4538	8.9370	8.9645	0.0940	0.0684	0.0030

CHAPTER 4

VELOCITY PROFILE IN METER ANNULUS

4.1 Introduction

In fully developed turbulent flow, the velocity distribution in a pipe can be taken to follow approximately the power law velocity profile. In the past, except for Jepson (9) and Salami (5), analysis of the forces acting on the blades of a turbine meter was done by assuming that the flow is uniform across the pipe section. This assumption simplifies the analysis enormously but in practice, the meter is never situated in a region of uniform flow. The importance of the effect of inlet velocity profile on the calibration of a turbine meter had been demonstrated by Jepson (9); an error of $2\frac{1}{2}\%$ could arise when a meter calibrated in fully developed flow is used in a region with uniform flow.

From the above paragraph, it is important therefore to consider velocity distribution when analysing forces acting on turbine meter blading. When doing so, it is also important to differentiate between distribution in the pipe itself and that in the annulus formed by the rotor hub and the meter wall. Although Jepson and Salami did consider velocity profile in their analysis, they assumed that the distribution in the meter annulus is the same as that in the region of the pipe cross-section formed between the imaginary hub radius and the pipe wall i.e. the velocity distribution in the pipe core having a radius the same as the hub is ignored. This assumption may be acceptable for meters with small hubs (as in their cases) but it is not satisfactory in general since commercial turbine meters have much larger hubs. A more realistic approximation would be to assume that the velocity in the pipe is proportionally contracted

within the annulus so that the whole profile is still being retained. In fact this assumption was used in the paper by Tan and Hutton (46).

On further consideration, it was felt that when fluid flows from the pipe into the meter annulus, the resulting area contraction would not only alter the value of the exponent of the power law velocity profile but also tend to flatten part of the profile as well. This part of the research was therefore conceived to study experimentally the actual velocity profile in the meter annulus and how it would vary with different hub sizes. From the experimental results it is hoped that a general empirical equation can be formulated to predict the velocity profile in the meter annulus when the hub size is known. With this new equation, errors that arise from the above two assumptions are then determined for different hub sizes.

When studying the effect of inlet velocity profile on turbine meter calibration, the meter was placed at different positions downstream of the conical entrance of the test length. It was assumed that immediately after the conical entrance, the flow is uniform. Whether this is so is to be verified experimentally in this part of the research program.

4.2 Experiment

A pitot-static traversing gear shown ~~diagrammatically~~ in Figs 4.14 & 4.15 was used for determining any velocity profile required. The internal diameter of the traversing gear is the same as that of the test length so that it forms a continuous section with the pipe when placed at any position along it. The pitot tube is held on a micrometer device capable not only of moving the pitot head diametrically across the pipe but also rotating it to any angular position with respect to the pipe axis.

For any velocity measurement the total head is taken from the external end of the pitot tube. The static head is taken from three pressure taps in the wall of the traversing gear. The taps, located on the same plane as the pitot head entrance, are connected to an averaging chamber from which the average static head is taken. The total and the static heads are connected to each limb of an inverted water manometer whose inclination to the horizontal can be adjusted to any desired degree. The water level in the manometer is adjusted by pumping air into the air column above it (See Fig 4.17)

Before the traversing gear is fitted in the test length the inlet of the pitot head is aligned using a centering plunger. (See Fig. 4.1). The plunger, with a needle at the centre, fits exactly into the bore of the gear. The pitot head is adjusted so that it exactly coincides with the needle thus establishing the radial coordinate of the pitot head and also ensuring the pitot head is parallel to the pipe axis. The micrometer reading is noted and the plunger withdrawn.

For measuring the velocity profile within the annulus formed by the rotor hub and the turbine meter wall, three simulation hubs (see Fig. 4.16) were made and each of them can be slid coaxially into the traversing gear. The hubs were made dimensionally similar to the research rotors so that they simulate the upstream and the downstream bearing supports with the rotor hub in between. When each hub is inserted into the traversing gear, it would correspond to the research meter of the same hub size but with the blades removed. The hub is kept in position by a $\frac{1}{8}$" (3.175×10^{-3} m) diameter rod that connects the downstream end of the hub and a thin cross-piece retainer at the outlet of the gear. The rod's length can be adjusted axially so that

the pitot head can be at the mid-length of the hub. For measuring the velocity profile within the annulus, the pitot head can be traversed radially within it. As the outer diameter of the pitot head is 0.042" (1.067×10^{-3} m), it is not possible to measure point velocity nearer than 0.021" (0.533×10^{-3} m) to the hub or to the wall.

4.3 Discussion

In this research the velocity profile immediately after the conical entrance to the test length (referred to as the upstream position) is considered uniform. Except for a small region near the pipe wall, this was found to be so when the velocity profile at this position was measured experimentally (see Fig. 4.2). For a 2" (50.8×10^{-3} m) diameter pipe, the boundary layer thickness is only about 0.06" (1.5×10^{-3} m) at this position. The boundary layer thickness δ is defined as the distance from the pipe wall to the point at which the velocity is 99% of the 'free stream' value i.e. velocity of the uniform core. When a turbine meter is located at the upstream position the boundary layer thickness would be further reduced because of the contraction in flow area by the rotor hub. This is evident from Fig. 4.3, where the velocity profiles within the annuli formed by the pipe wall and a $\frac{3}{4}$" (19.05×10^{-3} m) and a $1\frac{1}{2}$" (38.1×10^{-3}m) simulation hub are compared with that without using any hub. When using the $\frac{3}{4}$" (19.05×10^{-3} m) simulation hub, the thickness is reduced to 0.05" (1.27×10^{-3} m) , while with $1\frac{1}{2}$" (38.1×10^{-3} m) one, it is reduced to 0.03" (0.76×10^{-3} m). However, from Fig. 4.4, there is no noticeable change in the boundary layer thickness within the annulus for a particular simulation hub when the flow rate is altered.

As the flow moves away from the conical entrance, there is a

progressive change in boundary layer thickness until a fully developed velocity profile occurs at some distance downstream. Jepson (9) and Salami (5) found that a fully developed profile occurs after about 50 diameters downstream. The velocity profile at 96 diameters is shown in Fig. 4.2 and it is compared with the profile at the upstream position. It can be seen that the velocity profile is radically altered between the two positions.

When a turbine meter is used in a region with fully developed profile, the shape of the profile can be expected to change when the flow enters the meter annulus. Figs. 4.5 and 4.6 show how such a change in the profile would occur for meters with different hub sizes. In this experiment, three simulation hubs of different sizes were used and the flow rates in all cases were set to 14.0 lb/sec. (6.35 kg/s). From the profiles obtained, it is evident that when flow enters a turbine meter, the general shape of the profile within the meter annulus no longer resembles that in the pipe. Part of the new profile near the hub is linear while the remaining part near the wall is not. Also, not only does the gradient of the linear part change with hub size, but so does the radial position where the linear part terminates. As the axial length of the hub is short, no development of boundary layer on the hub is detectable at a distance from the surface further than half the pitot head diameter (the pitot head diameter is 0.042" (1.067×10^{-3} m)). It can therefore be assumed that the linear part of the profile extends right up to the hub.

When the experimental profiles in Figs. 4.5 and 4.6 are plotted on log-log scale (see Fig. 4.7) the non-linear parts of the profiles can now be approximated by straight lines. Without using any simulation hub, the profile is a straight line throughout the radial positions

on this plot. The gradient of the line is 0.1306. Therefore it is justified to assume that the velocity profile in the pipe obeys the power law equation. From the gradient obtained, the reciprocal of the exponent of the power law equation, m, is 7.66 at this flow rate. When simulation hubs are used, the gradient of the straight line part of the profile on this new plot, varies with the hub size. This part of the annulus can therefore be represented by the power law equation but since the gradient varies with hub size, the value of m in the equation must also vary.

4.3.1 Empirical Velocity Profile in Fully Developed Flow

From the foregoing, it is evident that the velocity profile in a meter annulus can be represented by a linear part near the hub and a non-linear one that follows the power law equation. The radial position where the linear part terminates (hence where the non-linear part begins), the gradient of the linear part, and the reciprocal of the exponent of the power law equation describing the non-linear part, all depend on the hub size of the meter. Therefore before an empirical equation can be formulated to predict the velocity profile in a meter annulus, the relationships between the three variables and the hub size must first be determined. How each of the variables varies with hub size is given in Figs. 4.8, 4.9 and 4.10. The expressions relating them are derived in Appendix II and given in their final form below.

The equation for the linear part of the annulus profile is

$$\frac{u}{U} = -z.\left(\frac{r - r_h}{r_o}\right) + 1 \qquad \ldots \quad 4.1$$

where z is the gradient of the linear part and it is related to the hub ratio $\left(\frac{A_h}{A_o}\right)$ by the equation

$$z = -\frac{\left[0.00013645 - 0.3119\left(\frac{A_h}{A_o}\right)\right]}{\left[\left(\frac{A_h}{A_o}\right) + 0.0063696\right]} \qquad \ldots \quad 4.2$$

The radial position r_c where the linear part of the annulus profile terminates is related to the hub area ratio by the equation

$$\frac{r_c}{r_o} = 1.0283 \cdot \left(\frac{A_h}{A_o}\right)^{0.15476} \qquad \ldots \quad 4.3$$

The equation of the non-linear part of the annulus profile is

$$\frac{u}{U} = Y \cdot \left(1 - \frac{r}{r_o}\right)^{1/M} \qquad \ldots \quad 4.4$$

where M is the reciprocal of the exponent of the power law which the non-linear part of the profile follows. It is related to the hub area ratio by

$$M = 21.752 \cdot \left(\frac{A_h}{A_o}\right) + m \qquad \ldots \quad 4.5$$

where m is the value of the reciprocal of the exponent power law when there is no hub (i.e. the value in the pipe).

The value of Y in equation [4.4] is given by

$$Y = \frac{-z \cdot \left(\frac{r_c - r_h}{r_o}\right) + 1}{\left(1 - \frac{r_c}{r_o}\right)^{1/M}} \qquad \ldots \quad 4.6$$

Thus the velocity profile in a meter annulus can be predicted by equations [4.1] and [4.4] . For a flow rate of 14.0 lb/sec. of water (at 20°C) the value of m, obtained from the gradient of the plot in Fig. 4.7, is 7.66. Using this value of m, the predicted velocity profiles in the meter annuli for different hub sizes are given in

Figs. 4.5 and 4.6. From the figures, it can be seen that the predicted velocity profiles are in good agreement with the measured profiles.

The velocity profile assumed by the author in part of this research is

$$\frac{u}{U} = \left(\frac{r_o}{r_o - r_h}\right)^{1/m} \cdot \left(1 - \frac{r}{r_o}\right)^{1/m} \quad \ldots \quad 4.7$$

whereas that by Jepson (9) and Salami (5) is

$$\frac{u}{U} = \left(1 - \frac{r}{r_o}\right)^{1/m} \quad \ldots \quad 4.8$$

Figs. 4.11, 4.12 and 4.13 show how the two assumed profiles differ from the empirical profiles for hub sizes of $\frac{1}{4}$", $\frac{3}{4}$" and $1\frac{1}{2}$" (6.35, 19.05 and 38.10, x 10^{-3}m) diameter respectively. Since the empirical profiles agree well with the measured profiles, they can be taken to be the correct profiles. For small hub sizes, there may be not much difference between the two assumed profiles and the actual one but for big hub sizes, the difference can be quite substantial. Fig. 4.14 shows how error in the meter coefficient calculated using the two assumed profiles varies with hub-ratio. For meters with 0.125 hub-ratio, the effect is negligible but for meters with 0.75 hub-ratio, the error is 1.02% for helical blade rotor and 1.95% for constant blade angle rotor. It may appear paradoxical the meter coefficient calculated using any of the two assumed profiles (i.e. equations [4.7] or [4.8]) gave rise to the same magnitude of error. This is because the difference between the two equations is a difference in the reference velocity. The reference velocity U in equation [4.7]

is the maximum velocity within the meter annulus (i.e. at the hub) while that for equation [4.8] is the maximum velocity in the pipe (i.e. at the pipe centre before flow enters the annulus). No matter which equation is used, the absolute velocity at any point within the meter annulus is the same.

4.3.2 Empirical Velocity Profile in Partially Developed Flow

The empirical equations developed for approximating the velocity profile within a meter annulus are only for fully developed flow. When the flow is partially developed, the equations need to be modified and it is done under the following assumptions.

If the boundary layer thickness in a pipe of radius r_p is δ, it is assumed to be contracted proportionally to δ_m

where

$$\delta_m = \frac{\delta \cdot (r_o - r_h)}{r_p} \qquad \ldots \quad 4.9$$

The value of m in the pipe is altered to M on entering the meter annulus according to equation [4.5].

The value of r_c is calculated according to equation [4.3].

Now for $r_c \leq (r_o - \delta_m)$

then

$$\frac{u}{U} = 1.0 \qquad \ldots \quad 4.10$$

for $r_h \leq r \leq (r_o - \delta_m)$

and

$$\frac{u}{U} = Y \cdot \left(1 - \frac{r}{r_o}\right)^{1/M} \qquad \ldots \quad 4.11$$

for $r > (r_o - \delta_m)$

where

$$Y = \frac{1}{\left(1 - \frac{r_o - \delta_m}{r_o}\right)^{1/M}} \qquad \ldots \quad 4.12$$

For $r_c > (r_o - \delta_m)$

then

$$\frac{u}{U} = 1.0 \qquad \ldots \quad 4.13$$

for $r \leqslant (r_o - \delta_m)$,

$$\frac{u}{U} = z \cdot \left(\frac{r - r_o + \delta_m}{r_o}\right) + 1 \qquad \ldots \quad 4.14$$

for $r_o - \delta_m < r \leqslant r_c$

and

$$\frac{u}{U} = Y\left(1 - \frac{r}{r_o}\right)^{1/M} \qquad \ldots \quad 4.15$$

for $r > r_c$

where z is as given in equation [4.2]

and

$$Y = \frac{z \cdot (r_c - r_o + \delta_m) + 1}{\left(1 - \frac{r_c}{r_o}\right)^{1/M}} \qquad \ldots \quad 4.16$$

When calculating the profile effect on turbine meters in Chapter 6, the boundary layer thickness δ_m within the meter annulus is taken to be as given by equation [4.9] and the velocity profile as given by equations [4.10] to [4.16].

CHAPTER 5

EFFECT OF TIP-CLEARANCE ON TURBINE METER CALIBRATION CURVES

5.1 Introduction

The calibration curve of a turbine meter should ideally be as flat as possible (i.e. as small a variation as possible) over as wide a range as possible. This is not always found in commercial turbine meters and variations of as much as 2 to 3% have been observed in some. It is true that modern electronics can be employed to correct automatically any variation in meter calibration but it is felt that if a simple meter can be designed to achieve the same order of accuracy, the more expensive electronic solution is unnecessary. Moreover most users may want the extra accuracy without having to go to auxiliary equipment.

Existing theories on turbine meter behaviour tends to suggest that nothing much can be done with the rotor dimensions to improve the variation other than to add extra components to the meter. For example, Lee and Karlby (3) suggested a revolving drum while Menkyna (4) suggested increasing the wakes formed by the flow straightening vanes. These suggestions were based on their respective theories. It has been shown in Chapter 1 and 3 why their theories could not be used to explain the behaviour of all turbine meters. According to the leakage theory proposed in Chapter 3 and supported by initial experimental results (see Fig. 3.12) the variation of turbine meter calibration curves can be altered by changing the tip-clearance. Fig. 3.12 shows how a calibration curve with a negative variation is altered to one with a positive variation when the tip-clearance of the

rotor is increased.

In this chapter the effect of tip-clearance on the meter calibration is studied to see if the variation can be minimised by choosing the correct tip-clearance, for both helical and constant blade angle rotors of different hub-ratios.

5.2 Experiment

Four research rotors were used in this part of the research. (See Fig. 5.17) Full particulars of these rotors are given in Appendix III. Briefly the hub-ratios of the rotors are:-

	Type of blade	Designed hub-ratio	Measured hub-ratio
i)	constant blade angle	0.125	0.125
ii)	constant blade angle	0.375	0.375
iii)	helical blade	0.375	0.381
iv)	helical blade	0.75	0.753

The experiments required the tip-clearance of each rotor to be progressively increased. At each tip-clearance, the rotor was calibrated in the upstream position (OD) and in the downstream position (96D).

Each rotor was initially made to have the blade tip radius corresponding to the smallest tip-clearance required. As the tip-radius is the radius of the cylindrical rod from which the rotor is made, the rod was first machined to the necessary diameter before cutting the blades. However once the blades had been cut, it was not possible to clamp the rotor on a lathe again and then trim the blade to the next tip-clearance. If this was done, the cutter could easily

distort the blades thus changing their blade angles. As all the blades on each rotor had to be trimmed evenly filing the blade tips by hand would not be practical because not only would it be difficult to measure the tip-radius accurately, but also it would be difficult to judge the correct amount of blade tip that has been removed. Finally a special clamping tool as shown in Fig. 5.18 was designed. Any of the rotors used could be clamped centrally inside the tool. The blade tip could then be reduced by machining the clamping tool on a lathe until the required blade tip diameter had been obtained. The blade tip diameter would then be the diameter of the clamping tool which could be easily measured with a micrometer. (See Fig. 5.18)

To prevent distortion of the blades during machining, all empty spaces between the blades and the clamping tool body were filled with plaster of paris and allowed to harden. The rotor has been previously coated with a layer of wax so that the plaster could be easily removed after machining. Before plaster of paris was thought of, molten wax was first tried. However, it was found that for a 0.125 hub-ratio rotor wax was not stiff enough to prevent the blade from distorting.

5.3 Discussion

When the tip-clearance of a turbine meter is increased, two main effects can be observed on the meter calibration curves. Firstly there is a change in the meter calibration and secondly there is a change in the shape of the calibration curve especially towards the lower range of flow. These changes in the meter behaviour can be used advantageously in turbine meter design. The term 'meter calibration' is taken to mean the average meter coefficient over the flow range which the meter is designed to operate.

5.3.1 Change in Meter Coefficient

In general it can be said that at given flow rate increasing the tip-clearance of a turbine meter increases the speed of rotation of the rotor and consequently increases the meter coefficient. At first sight this may seem surprising because it is equivalent to an increase in the turbine 'efficiency'. However, one must not confuse the turbine meter with other axial turbo-machines. This is because it has a comparatively smaller hub-ratio and the velocity diagrams at the hub are quite different from those at the tip especially if the flow in the meter annulus is fully developed. When the blades are not twisted to take radial changes in velocity diagrams into account, the angle of attack will vary from radius to radius.

Fig. 3.2 shows the angles of attack for meters with both helical and constant blade angle rotors placed in fully developed, and almost uniform flow. The lift distribution is related to the distribution of the angle of attack. As will be fully explained in Section 6.3.1 in Chapter 6, any change in the meter calibration of a turbine meter when its tip-clearance is altered is due to the change in the total lift developed by the rotor blades. An increase in the meter calibration is the result of a reduction in the negative lift. This effect can be seen from the calibration curves of the two constant blade angle rotors shown in Figs. 5.1 to 5.4 for both upstream and downstream positions. The calibration curves in Figs. 5.1 and 5.2 are for the constant blade angle research rotor with a hub-ratio of 0.125 and with its tip-clearance ratio progressively increased from 0.007 to 0.050. The curves in Fig. 5.3 and 5.4 are for the other constant blade angle research rotor (i.e. 0.375 hub-ratio) with the tip-clearance similarly increased. The effect of tip-clearance on

the meter calibrations for both rotors can again be seen from Fig. 5.10 where the meter coefficients at a flow rate of 15 lb/sec. (6.8 kg/s) were plotted against the tip-clearances. It can be seen that the meter coefficient increases with tip-clearance and the increase is greater in fully developed flow than in uniform flow. This greater increase in fully developed flow is because any reduction in blade tip is accompanied by a greater reduction in negative lift.

The calibration curves of the helical-blade rotor with 0.381 hub-ratio in fully developed flow are shown in Fig. 5.7. Again there is an increase in the meter calibration with tip-clearance. However, the rate of increase is much smaller than in the equivalent and constant blade angle rotor. This can be seen by comparing Figs. 5.4 and 5.7. The reason for the smaller increase is because of the smaller reduction in negative lift.

In all the cases considered so far, the effect of increasing the tip-clearance is to increase the meter calibration. The exception to this is when helical-blade rotor is placed in uniform flow. In a helical-blade rotor, the blade angle increases with radius. When the flow is uniform the changes in blade angle with radii nullify any corresponding changes in velocity diagrams with radii so as to maintain the angle of attack positive, small and almost constant. Therefore increasing the tip-clearance would remove part of the positive lift. As the positive lift is small, the effect is slightly to reduce the meter calibration. This would be the case if the flow were uniform. However, when a turbine meter is placed at the upstream position in the research rig, there is a small boundary layer near the pipe wall and the flow is uniform for only 95% of the diameter (see Fig. 4.3 for the velocity profile at this position). Figs.

5.5, 5.6 and 5.11 show the effect of increasing the tip-clearance on the helical-blade rotor with 0.38 in such a flow. At a flow rate of 15 lb/sec. (6.8 kg/s) the meter coefficient remains essentially constant. The small initial rise is due to the small boundary layer near the pipe wall.

The rotors discussed so far have comparatively small hub-ratios (i.e. < 0.4) and consequently comparatively long blades. A change in tip-clearance does not alter the blade height as significantly as when the hub-ratio is large. For example, when the tip-clearance ratio for a 0.375 hub-ratio is increased from 0.010 to 0.050, the blade height is altered by 6.5%. The same increase on a 0.75 hub-ratio rotor alters the blade height by 16.7%. Figs. 5.8 and 5.9 show the calibration curves for the helical-blade rotor with 0.75 hub-ratio at the upstream and the downstream positions. At both positions, the meter coefficient increases initially with tip-clearance by a small amount but falls with further increase. This can be explained as follows.

When the tip-clearance of a rotor is increased, there are two other possible effects that can be significant when the hub-ratio is large. Firstly, since the blade height is small, increasing the tip-clearance can affect the blade aspect ratio to a considerable extent. The result is an increase in the blade drag which in turn reduces the meter coefficient. Secondly there may be a greater increase in the proportion of flow going through the tip-clearance than expected. In theory the proportion of the total flow going through the tip-clearance is assumed to be proportional to the tip-clearance part of the velocity profile used to describe the flow within the meter annulus. In practice, the proportion may be greater

than calculated as the tip-clearance offers an easier flow passage, particularly when the tip-clearance is large. Since the tip-clearance area of a large hub-ratio rotor occupies a large proportion of the flow area through the meter annulus, the extra flow going through the tip-clearance cannot be ignored and the extra flow increases with tip-clearance. Since any flow not going through the rotor blades does not contribute to the rotation, the meter coefficient would be reduced. Hence increasing the tip-clearance of large hub-ratio rotors can reduce the meter coefficient when the two effects described are larger than the reduction of the negative lift that accompanies the tip-clearance increase. Note also that the negative lift is much smaller in a large hub-ratio rotor since the velocity profile is much flatter.

5.3.2 Shape of Calibration Curves

The following discussion is made under three separate headings namely (i) the calibration curves in uniform flow, (ii) the calibration curves in fully developed flow and (iii) the variation with tip-clearance of leakage factor k, as determined from their calibration curves.

5.3.2.1 Upstream Position

At the upstream position of the calibration rig, the flow is essentially uniform (see Fig. 4.3) and the velocity profile, within the sweep of the rotor blades of a turbine meter placed there, can be assumed to remain the same at all flow rates. Therefore the behaviour of calibration curves can be explained simply by the leakage theory without being complicated by the effects of velocity profile changes that could occur if the flow were fully developed

(i.e. at the downstream position).

The calibration curves at the upstream position for the two constant blade angle rotors with hub-ratio of 0.125 and 0.375 are shown in Figs. 5.1 to 5.4 respectively. Each rotor was calibrated six times at this position; each time with a different tip-clearance. When the flow rate is sufficiently large (i.e. > 2.5 kg/s) the calibration curves remain essentially constant thus indicating that the effects of leakage factor and resisting torque are not significant above this flow rate. When the tip-clearance ratio is small (e.g. 0.007) the meter coefficient below 2.5 kg/s decreases with decreasing flow rate. As explained in Section 3.3 this is because the leakage factor is small compared with the resisting torque and the effect of the latter predominates at all flow rates. However, when the tip-clearance is increased, so also does the leakage factor. This is reflected by the calibration curves, towards the lower flow range, becoming progressively flatter as the tip-clearance is increased i.e. an improvement in the variation. At the same time the lowest flow rate the rotor can measure within a given variation has also improved. When the tip-clearance ratio is sufficiently large (e.g. > 0.030) the meter coefficient, instead of decreasing with decreasing flow rate, increases. Only when the flow rate has dropped below a certain value does the meter coefficient fall rapidly. Any further increase in tip-clearance, though it continues to reduce the minimum flow that the rotor can measure, no longer improves the variation but increases it instead.

From the previous paragraph, it is evident that for the best results, the turbine rotor should have neither too large nor too small a tip-clearance. Taking the rotor with 0.125 hub-ratio as an example

(see Fig. 5.1), when the tip-clearance ratio is 0.007, the meter coefficient decreases with decreasing flow rate and the variation at 1 lb/sec (0.45 kg/s) is -3.5%. When the tip-clearance ratio is increased to 0.050, the meter coefficient increases with decreasing flow and the variation at the same flow rate is +2.0%. Therefore there must be an intermediate tip-clearance where the meter coefficient would remain essentially constant. From Fig. 5.1 it can be seen that at a tip-clearance ratio of 0.022, the calibration curve comes closer to this description. At the flow rate quoted, the variation is only -0.5%. Note that, for a variation of $\pm$ 2%, the minimum flow rate the rotor can measure has improved from 2.0 lb/sec. (0.91 kg/s) when the tip-clearance ratio is 0.007 to 0.4 lb/sec. (0.18 kg/s) when the tip-clearance ratio is increased to 0.050.

A question that immediately arises is what then is the optimum tip-clearance. The answer is that it depends on the magnitude of the resisting torque used in each design. For the example taken above, a tip-clearance ratio of 0.022 is about the best. However, as will be shown in Chapter 9, if the resisting torque on a rotor is increased, the calibration curve can be greatly altered so that the variation that was good at one resisting torque is no longer acceptable at another. For each turbine meter design, the tip-clearance must be chosen to suit and the proper way is to select a tip-clearance whose leakage factor is such that its effect is sufficient to counteract that of the resisting torque so that the required variation and minimum flow rate are obtained. This can be done using equation [3.33] and the design procedure is given in Appendix V.

In Chapter 3 it was observed that the calibration curve of the helical-blade rotor with 0.125 hub-ratio changed completely when the tip-clearance ratio was increased from 0.008 to 0.044 (see Fig. 3.12).

The behaviour is similar to that observed on the two constant blade angle rotors. Figs. 5.5 and 5.6 show the calibration curves for another helical-blade rotor but with a bigger hub-ratio (i.e. 0.381). Again the calibration curves are for six different tip-clearances but this time, to prevent overcrowding, the curves are shown on two separate figures. It can be seen that even for the smallest tip-clearance ratio used (i.e. 0.008), the leakage factor is sufficiently large and the meter coefficient increases with decreasing flow rate in the medium range of flow. Like the constant blade angle rotors, the leakage factor increases with tip-clearance. This is indicated by the greater variation in the calibration curves. As will be shown later in sub-section 5.3.3 where the leakage factors are evaluated for comparison, those for helical-blade rotors are greater than those of the corresponding constant blade angle rotors. As will be pointed out later, evidence from all the research rotors tends to suggest that the leakage factor depends not only on the tip-clearance and hub-ratio but also on the angle of attack. The smaller the angle of attack, the larger the leakage factor. In uniform flow, the angle of attack on helical-blade rotors is very much smaller than for the corresponding constant blade angle rotor (see Fig. 3.2) and hence the leakage factor for the former is very much greater.

5.3.2.2 Downstream Position

The calibration curves discussed so far are those for the meter in the upstream position where the flow is uniform. Therefore any change in the flow rate does not alter the velocity profile across the sweep of the rotor blades and the angles of attack along the blades maintain about the same order of magnitude throughout the

working range of the meter. The induced drag, which depends on the angles of attack, remains essentially constant and there is no noticeable influence on the behaviour of the calibration curves. Though there is no change in induced drag at the upstream position, there is nevertheless a change of skin friction drag with flow rate but this is taken into account in the meter coefficient equation.

When the flow is partially or fully developed, then the behaviour of turbine meter calibration curves can become more complicated due to the fact that there is, in addition, a change in the velocity profile with flow rate. The change is such that as the flow rate decreases, the gradient of the velocity profile becomes greater (i.e. tending more and more towards the laminar parabolic profile). Any change in velocity profile would also increase the angles of attack along the blades which are greatest near the blade tips. Consequently, the increase in induced drag that accompanies the increase in angles of attack, can be sufficiently large to affect the meter coefficient.

As the angles of attack along the rotor blades of constant blade angle rotors are comparatively large (see Fig. 3.2), the viscous drag has a considerable effect on the meter coefficient. For example, at a flow rate of 15 lb/sec. (6.8 kg/s) the part played by the viscous drag in fully developed flow is 7.6% of the meter coefficient in the case of the constant blade angle rotor with 0.125 hub-ratio, and 2.1% in the case of the corresponding helical-blade rotor. The difference arises from the very much greater induced drag on the former. From equation [3.15] it can be seen that the coefficient of induced drag depends on the square of the coefficient of lift C_L and from equation [3.12] , C_L in turn depends on the angle of attack. For the same change in the angle of attack, the rotor that has the greater

initial value would undergo a greater change in induced drag. Therefore the effect of any change in velocity profile would affect a constant blade angle rotor to a greater extent than on a corresponding helical-blade rotor.

Figs. 5.2 and 5.4 show the calibration curves at the downstream position (i.e. at 96D) for the two constant blade angle rotors. Though the general trend of the calibration curves shows that the leakage factor of the rotors also increases with tip-clearance, the behaviour of the calibration curves is more complicated than that in uniform flow. When the tip-clearance ratio is large (.e.g. > 0.030) the meter coefficient seems to be prevented from rising with decreasing flow rate. Only when the flow rate has dropped to 3.0 lb/sec. (1.36 kg/s) does the meter coefficient rise and does so quite rapidly. This is probably because, above this flow rate, changes in induced drag, as described above are sufficiently large to counteract any potential increase in meter coefficient due to leakage factor.

An interesting phenomenon is observed for the downstream position calibration curves of the constant blade angle rotor with 0.125 hub-ratio. As the flow rate is decreased, the calibration curve of the 0.007 tip-clearance ratio shows a sudden drop in value of about 1½% at a flow rate of about 2.7 lb/sec. (1.2 kg/s). When the tip-clearance ratio is increased to 0.015, the drop occurs at a lower flow rate. As the tip-clearance ratio is further increased the drop tends to become less prominent until at 0.030, it disappears altogether. A drop of this nature was also observed by Salami (5) but in his case it was on a helical-blade rotor of 0.125 hub-ratio and 0.008 tip-clearance ratio and calibrated in a liquid mixture whose viscosity was very much greater than that of water. He attributed

this drop to the change from turbulent pipe velocity profile to the laminar parabolic profile and the increase in drag that accompanies this change. Perhaps it should be pointed out that theoretical calculation using only the profile change from turbulent to laminar (i.e. without considering any change in drag) shows that the meter coefficient should jump up instead of the sudden drop as observed. Although Salami discounted stalling as the cause in his case, the drop in the calibration curves of the constant blade angle rotor shown in Fig. 5.2 is probably due to stalling near the blade tips when the angles of attack there exceed a critical value. This probably occurs when the flow in the pipe is still turbulent. At the flow rate when the drop occurs, the pipe Reynolds number is 30,500. This big Reynolds number suggests that the flow is not laminar and therefore the drop most probably could not be the result of the velocity profile changing from turbulent to laminar. Moreover the fact that the flow rate at which the drop occurs can be shifted by increasing the tip-clearance and can be made to disappear when the tip-clearance is made sufficiently large suggests that stalling near the blade tips is responsible for the drop.

The drop in meter coefficient can also be observed on the constant blade angle rotor with 0.375 hub-ratio but it occurs only at a tip-clearance ratio of 0.007 (see Fig. 5.4). No drop can be observed for tip-clearance ratios equal to and greater than 0.015. This rotor is less susceptible to stalling because its bigger hub tends to flatten more of the pipe velocity profile when the flow enters the meter annulus.

Fig. 5.7 shows the calibration curves for the helical-blade rotor with 0.381 hub-ratio. It can be seen that the changes in velocity profile with flow rate that affected constant blade angle rotors, are

not noticeable here. This is because of the smaller angle of attack. In fact, using the leakage theory, the behaviour of the calibration curves for this helical-blade rotor can be expressed throughout its flow range by simply keeping the velocity profile constant at all flow rates. This was done in Chapter 3 for this rotor (see Figs 3.9 to 3.11).

The calibration curves shown in Fig. 5.7 are for 6 different tip-clearances. Changes in the shapes of the calibration curves with tip-clearance suggest that the leakage factor increases with the tip-clearance but the rate of increase is smaller than when the flow is uniform (compare with Figs. 5.5 and 5.6). This is discussed further in sub-section 5.3.3 where the leakage factors are evaluated.

5.3.3 Variation of Leakage Factor

According to the leakage theory the shape of the calibration curve of a turbine meter depends on the tip-clearance between the tips of its rotor blades and the meter casing. The experiments described in this chapter were specifically designed to check whether this is generally true for rotors of different design. In the preceding sections, the behaviour of the calibration curves were qualitatively described and they suggest that the leakage factor, on which the shape of the calibration curves is dependent, does vary with tip-clearance. To see the variation quantitatively, the leakage factors for the calibration curves of all the helical-blade research rotors used were calculated using 'Method 3' as described in Chapter 3. The leakage factors for the two constant blade angle rotors at the upstream position were also calculated.

Figs 5.12 and 5.13 show how the leakage factor of each rotor

varies with tip-clearance. Though the helical-blade rotors of 0.125 hub-ratio and tip-clearance ratio of 0.008 and 0.044 used by Jepson (9) and Salami (5) were not used in the experiments, their leakage factors were calculated and included in the figures for comparison. From the figures, the clear conclusion can be drawn that the leakage factor does vary with tip-clearance as suggested by the leakage theory but there are other factors affecting the leakage factor.

In all the rotors used, there is generally an initial increase in leakage factor with tip-clearance and the rate of the initial increase is large when compared with the subsequent increase. However, the variation of leakage factor with tip-clearance also depends on the hub-ratio. For the 0.125 hub-ratio rotors, the leakage factor increases for all tip-clearance ratios between 0.007 and 0.050 though the rate of increase is smaller towards the later stage. For the medium hub-ratio rotors (i.e. 0.375 and 0.38) there is a comparatively rapid increase in leakage factor between 0.007 and 0.030 tip-clearance ratio. Beyond this there is hardly any further increase. For the large hub-ratio rotor used (i.e. 0.75) there is actually a fall in leakage factor beyond 0.030 tip-clearance ratio. These observations tend to suggest that the leakage factor varies not with tip-clearance ratio as such but with the tip-clearance area ratio. The tip-clearance area ratio is defined as the ratio of the area occupied by the tip-clearance to the flow area through the meter annulus. The leakage factor increases with tip-clearance area ratio up to a point. Any further increase results in a fall in leakage factor. For the same tip-clearance, the tip-clearance area ratio is larger the bigger the hub-ratio and consequently the drop in leakage factor that accompanies excessive tip-clearance increase occurs first with the larger hub-

ratio rotors.

The foregoing discussion on the variation of leakage factor with tip-clearance area ratio was a very general observation based on the trend of all the rotors. However, the actual behaviour is more complicated. For example, the leakage factor of helical-blade rotors calibrated in the upstream position increases initially with hub-ratio but decreases again with further increase in hub-ratio (the leakage factors of the 0.38 hub-ratio rotor are greater than for the 0.125 and 0.75 hub-ratio rotors). Though this ties up with the observation (i.e. variation of leakage factor with tip-clearance area ratio), a plot of leakage factor with tip-clearance area ratio (see Fig. 5.14) suggests that no simple relationship is possible. Moreover in the case of the constant blade angle rotors there is no distinguishable difference in leakage factor between the 0.125 and 0.375 hub-ratio rotors except that while the latter rotor shows a slight decrease in leakage factor at the later stage of tip-clearance increase, there is still an increase on the 0.125 hub-ratio rotor. Also the leakage factors for the two rotors are lower than for the corresponding helical-blade rotors and when the flow is fully developed, the leakage factor of the helical-blade rotors are lower than in uniform flow. These observations tend to suggest that the leakage factor also depends on the angle of attack i.e. the smaller the angle of attack, the larger the leakage factor. For helical-blade rotors in uniform flow the angle of attack is small whilst that for the constant blade angle rotor is very large (see Fig. 3.2). Hence the leakage factor is larger for helical-blade rotors. Comparing the angle of attack on helical-blade rotors in uniform flow and in fully developed flow (see Fig. 3.2) that of the latter is much larger. Hence the leakage factor in fully developed flow is smaller.

5.3.4 Theoretical Verification of Meter Coefficient Equation

As had been pointed out in Chapter 3, the meter coefficient equation has been derived by various researchers using different sets of assumptions. The simplest set of assumptions that had been used is to consider the rotor blades as isolated aerofoils which are straight, infinitely thin, with infinite aspect ratio and placed in a flow that is uniform. The drag on the blades is assumed to arise from skin friction drag only. These assumptions were used by Rubin et al (2) and by Lee and Karlby (3). In the case of the latter, forces acting on the rotor blades were obtained using the momentum approach rather than the aerofoil approach. The equation so derived is alright if only a very rough estimate of meter coefficient is required. However, since the flow was assumed to be uniform, the equation does not give any indication of the effect of changes in velocity profile on the meter calibration and hence cannot be used when designing a meter for minimal profile effect.

Jepson (9) used similar assumptions but in his case, changes in velocity profile were also considered. The velocity profile within the meter annulus was taken to be that in the pipe and capable of being approximated by the power law equation. This assumption in velocity profile is satisfactory only if the hub of the rotor is small but as shown in Chapter 4, it can lead to a wrong estimate of profile effect when the hub is large. Using similar assumptions mentioned above, the meter coefficients and profile effects on two research rotors, with similar hub-ratios but different types of blades, are calculated and shown in Fig. 5.15. Instead of using the velocity profile equation suggested by Jepson, that given in Chapter 4 is used instead. This should give better results since it approximates the

actual velocity profile much better. It can be seen from the Fig. 5.15 that whilst the assumptions are satisfactory for the helical-blade rotor, they are not so for dealing with the constant blade angle rotor. In the latter rotor, the experimental profile effect at a tip-clearance ratio of 0.050 is -1.5% as compared with -3.3% in theory.

Improvement in these assumptions was made by Salami (5). Though he still assumed the same velocity profile equation as Jepson (9), he took into account that the drag on the rotor blades consists not only of skin friction drag but induced drag as well. Also he included blade aspect ratio in his assumption of the coefficient of lift (i.e. he did not assume the blades to have infinite aspect ratio). Using similar assumptions but again with velocity profile equations given in Chapter 3, the absolute meter coefficient and profile effects on the two rotors are again calculated. The results are shown in Fig. 5.15. As before the assumptions are satisfactory for the helical-blade rotor. Though there is some improvement in the predicted profile effect on the constant blade angle rotor, it is still not satisfactory for design purposes. For the same tip-clearance ratio quoted (i.e. 0.050) the profile effect predicted has improved to -2.2% (as compared to -1.5% in experiment) while the absolute meter coefficient differs from experiment by 0.9 pulse/lb. (0.33 rev/kg or -8.0%).

Neglecting any induced drag on the rotor blades, Thompson and Grey (44) however took cascade effects between adjacent blades into account when expressing the lift coefficient of the blades. They assumed the velocity profile within the meter annulus to be that in fully developed flow between two concentric pipes. In practice, the rotor hubs of turbine meters are too short for this type of profile

to occur which was shown experimentally to be so in Chapter 4. Using similar assumptions to Thompson and Grey but the velocity profile given in Chapter 4, the meter coefficients and profile effects on the two research rotors are calculated and shown in Fig. 5.15. It can be seen that for the constant blade angle rotor, the differences between theoretical and experimental values are worse than that when using Salami's assumptions.

The assumptions used in this thesis for deriving the meter coefficient equation were explained in Chapter 3. Briefly they are:-

(i) cascade effects between adjacent blades using Weinig lattice-effect coefficient.

(ii) blade aspect ratios are not infinite.

(iii) induced drag for negative angle of attack.

and (iv) flow leaves the blade inclined at an angle to the blade i.e. using Constant deviation equation.

Using the induced drag for the case of elliptical lift distribution (i.e. for the case of minimum induced drag) the meter coefficients and the profile effects for the two research rotors are calculated and shown in Fig. 5.16. To take into account that induced drag is not at the minimum, a factor of 0.9 is introduced to the coefficient of induced drag as given in equation [3.17]. Calculations using this additional assumption are also given in Fig. 5.16. Again this assumption is satisfactory for the helical-blade rotor and for the constant blade angle rotor, the profile effect predicted is nearer to that obtained experimentally. It has improved to -1.7% as compared with -1.5% in the experiment (i.e. at tip-clearance of 0.050). However, the predicted meter coefficient for the constant blade angle rotor is 10.31 pulse/lb. (3.79 rev/kg) as compared to 11.31 pulse/lb. (4.16

rev/kg), a difference of -8.8%. However, if the effective blade angle β' is used instead of the blade angle β, as suggested in equation [3.29], the meter coefficient predicted has improved to 10.81 pulse/lb. (3.97 rev/kg), a difference of -4.4% with experiment. The profile effect remains the same as when the blade angle β is used but the predicted meter coefficient for the helical-blade rotor has been made worse (from -1.5% to +4.6%). Therefore a possible solution is to use blade angle for helical-blade rotor and effective blade angle for constant blade angle rotor. For calculating the profile effect, it does not matter which angle is used.

Fig. 5.15 shows the comparison with experiment of predicted meter coefficients and profile effects under the different sets of assumptions discussed. It can be seen from the figure that the set of assumptions used in this thesis is generally best for design purposes especially when the profile effect is to be calculated theoretically for constant blade angle rotors.

CHAPTER 6

EFFECTS OF DEVELOPING VELOCITY PROFILE IN PIPE ON TURBINE METER CALIBRATION AND METHODS FOR REDUCING THEM

6.1 Introduction

Though the turbine meter is considered as a volumetric instrument, strictly speaking the rotor responds only to velocity. Since the velocity integrated over the flow area of a turbine meter is related to the volumetric flow rate, it is therefore perhaps justifiable to call it a volumetric instrument.

In uniform flow, the velocity anywhere in the cross-section of a pipe is the same and is equal to the average velocity. This type of velocity distribution can be expected at the inlet of a pipe. However, as the flow moves away from the pipe entrance, there is a progressive change in the distribution until a fully developed profile occurs at some distance downstream. Therefore if a turbine meter is calibrated in a fully developed flow region of a pipe and then used where the velocity profile is different, one can expect an error to arise in the reading. Ideally, it is best to calibrate a meter in fully developed flow and then to use it in or downstream of the region of the pipe where fully developed flow has occurred. In practice this is not always possible and the meter may have to be located in a position where partially developed or even distorted flow occurs. Therefore it is part of the aim when designing a meter to arrive at one that is not affected to any appreciable extent by changes in velocity profile.

The effects of developing velocity profile on a helical-blade

rotor with a hub-ratio of 0.125 have been studied by Jepson (9) and Salami (5). They found that by increasing the tip-clearance of the rotor, profile effects could be reduced. However it is dangerous to generalise on the evidence of this rotor alone because as will be shown later in this chapter, increasing the tip-clearance of other meters can have the opposite effect. Also, with such a small hub-ratio, the presence of the hub hardly alters the shape of the velocity profile when the flow enters the meter annulus (see Chapter 4). In practice turbine meters have much larger hub-ratios and some have constant blade angle rotors instead of helical-blade rotors. In this chapter the effects of developing velocity profile on meter calibration are studied with rotors not only with different hub-ratios but also with different types of blades and with different tip-clearances. It is hoped that a method or methods for reducing profile effects can be generalised for use in design.

6.2 Experiments

Four research rotors and one commercial meter were used in this part of the research. All meters were for use in 2" (0.0508 m) nominal pipe diameter. The commercial meter was tested as manufactured but each of the research rotors was tested with two different tip-clearances. Two of the research rotors have helical-blades while the other two have constant blade angle blades. For complete dimensional details of all research rotors, refer to Appendix III. Relevant particulars of the rotors are as follows:-

	Type of blade	Hub-ratio	Tip-clearance ratio
1)	Helical	0.125	0.010 and 0.050
2)	Helical	0.381	0.008 and 0.050
3)	Constant blade angle	0.125	0.007 and 0.050
4)	Constant blade angle	0.375	0.007 and 0.050

To study the effects of developing velocity profile, each meter was tested in turn by placing it at varying distances downstream of the conical entrance of the test length. The test length was made up of pipe sections of different lengths varying from 3D (i.e. three pipe diameter) to 48D. By using different sections or combinations of sections, the desired length in front of the meter can be installed. When the meter is said to be xD downstream, it means that between the meter and the conical entrance, there are pipe sections of total length equal to x times the diameter of the pipe. When a meter is placed immediately after the conical entrance (i.e. at 0D) the mid-length of the meter is actually 2D downstream of the position where the tapering part of the conical section ends.

At each position three readings were taken with the flow rate set at 14.95 $\pm$ 0.05 lb/sec. (6.78 $\pm$ 0.023 kg/s).

6.3 Discussion

In this discussion, the phrases 'profile effect' and 'effect of velocity profile' are taken to mean the effect of developing velocity profile in a pipe upon the meter coefficient of a turbine meter.

Before attempting to explain the mechanism of profile effect it is best to examine how the velocity profile in a pipe develops. Jepson (9) and Salami (5) found that not only does the boundary layer thickness increase with increasing distance from the pipe inlet but there is also a progressive change in the velocity gradient within the boundary layer thickness. This is reflected in the value m of the reciprocal of the exponent of the power law equation used in approximating the velocity profile. The greater the value of m, the flatter is the velocity profile. They found that m decreases as the boundary layer increases (i.e. with increasing distance from the pipe inlet) until a position is reached when the boundary layer thickness covers the whole section of the pipe. However, beyond this point, m continues to change but this time it increases in value instead until at a further distance downstream, the flow is fully developed and the velocity profile remains constant subsequently. How the boundary layer thickness δ and the value of m vary with distance downstream of the pipe inlet are shown in Figs 6.1 and 6.2.

The profile effect on a turbine meter is actually a combination of two separate effects both arising from the change in velocity distribution across the meter annulus as the boundary layer thickness grows progressively with distance from the pipe inlet. The extent to which each individual effect contributes, depends not only on the type of blades the meter has but also where along the developing flow the meter has been placed. For lack of better names, the two effects are to be referred to as (1) meter effect and (2) drag effect. Meter effect can further be subdivided into rotor flow effect and tip-clearance flow effect. Figs 6.3 to 6.6 show the part each individual effect contributes to the profile effect on two rotors having the same

The meter coefficient of any turbine meter is given by equation (3.33) and how it changes with different stages of boundary layer development in the pipe is termed as the profile effect on the meter. Profile effect can be divided into meter effect and drag effect. Meter effect itself can be further divided into rotor flow effect and tip-clearance flow effect. Their equations are:-

Profile effect = PE = $(T_1 - T_2 - T_3/Q^2)(1 - Q_c/Q)$

Meter effect = ME = $T_1.(1 - Q_c/Q)$

Rotor flow effect = RFE = T_1

Tip-clearance flow effect = TFE = $- T_1 Q_c/Q$

Drag effect = DE = $- (T_2 + T_3/Q^2)(1 - Q_c/Q)$

Their upstream and downstream values (in pulse/lb) at 15 lb/sec for the rotors shown in Figs 6.3 to 6.6 are as follows:-

Rotor	Position	PE	ME	RFE	TFE	DE
Helical blade	Upstream U	10.305	10.459	10.632	-0.173	-0.154
Hub-ratio = 0.38	Downstream D	10.159	10.399	10.539	-0.140	-0.240
Tip-clearance = 0.008"	Ratio U:D	1.014	1.006	1.009	1.237	0.642
Helical blade	Upstream U	10.329	10.482	11.802	-1.320	-0.153
Hub-ratio = 0.38	Downstream D	10.386	10.577	11.684	-1.107	-0.191
Tip-clearance = 0.050"	Ratio U:D	0.995	0.991	1.010	1.192	0.801
Constant blade angle	Upstream U	10.220	10.720	10.871	-0.151	-0.500
Hub-ratio = 0.375	Downstream D	10.235	11.136	11.263	-0.127	-0.902
Tip-clearance = 0.007"	Ratio U:D	0.999	0.963	0.965	1.189	0.554
Constant blade angle	Upstream U	10.627	11.128	12.507	-1.379	-0.501
Hub-ratio = 0.275	Downstream D	10.809	11.638	12.834	-1.196	-0.828
Tip-clearance = 0.050"	Ratio U:D	0.983	0.956	0.975	1.153	0.605

hub-ratio but of different types of blades. Also shown are how these effects would alter when the tip-clearances are increased. They are plotted using equations [3.30] and [3.27] and will be more comprehensible as each effect is explained qualitatively.

6.3.1 Meter Effect

The meter effect arises from changes in the nett lift torque on the rotor blades when the velocity profile within the meter annulus changes. This effect acts differently depending upon whether it is on a helical-blade rotor or on a constant blade angle rotor. The reason behind this is best explained with the aid of Fig. 3.2 which shows the angle of attack along the blades of both rotors when the flow is uniform and when fully developed.

In the case of helical-blade rotor in uniform flow, the angle of attack on the blades is always positive and therefore the lift along any blade is directed to one side of the blade only. The total torque developed by the blades is the sum of the lift torque along the blades. If the flow is not uniform (e.g. in fully developed flow) the velocity and consequently the angle of attack along the blades varies from hub to tip. The angle of attack changes from positive around the hub to negative around the tip. Though the lift along any blade is considerably greater, it does not act on one side of the blade alone. That with positive angle of attack acts on one side and that with negative angle of attack on the other. Not only are the positive angles of attack generally smaller than the negative one but the lift resulting from the former also acts at smaller radii. Therefore the additional torque created by the positive lift is less than that imposed by the negative lift and the resultant torque developed by

the blades is lower than when placed in uniform flow. Consequently for a helical-blade rotor, the meter coefficient would be lower when the meter is placed in more developed flow.

When compared with the helical-blade rotor, not only is the angle of attack along the blades of a constant blade angle rotor in uniform flow very much larger but also it varies from positive near the hub to negative near the tip. When the meter is moved to fully developed flow both the negative and the positive lifts are increased but the additional positive torque created is greater than the additional negative torque imposed on the blades. Therefore, unlike the helical-blade rotor, the net torque developed by a constant blade angle rotor is greater in fully developed flow. Consequently the more developed the velocity profile in the pipe, the greater would be the meter coefficient.

From the foregoing it is evident that increasing the tip-clearance would have different effects not only on rotors with different types of blades but also on where the meter is placed. In the case of a helical-blade rotor in uniform flow when the lift distribution along the blades is small and positive, increasing the tip-clearance only removes a small part of the lift at the blade tips. The nett effect is a negligible decrease in the meter coefficient (see Fig. 6.3). However when the flow is fully developed increasing the tip-clearance results in the removal of a substantial part of the negative lift near the blade tips. The reduction in negative lift results in the increase of nett torque developed by the rotor and consequently an increase in the meter coefficient. As the meter coefficient in fully developed flow is smaller than in uniform flow, increasing the tip-clearance would reduce their difference and hence the meter effect.

In the case of a constant blade angle rotor, increasing the tip-clearance results in the removal of a substantial part of the negative lift, and consequently increasing the meter coefficient, no matter whether the flow is uniform or fully developed (see Fig. 6.5). However the more developed the flow the greater is the negative lift removed.As the meter coefficient in fully developed flow is greater in fully developed flow than in uniform flow, increasing the tip-clearance would further increase their difference and hence the meter effect.

Figs 6.3 and 6.5 show the meter effect on different rotors and with different tip-clearances. It can be seen that when tip-clearance is increased on a helical-blade rotor, there is a hump near the pipe inlet. To understand this hump and also to look at the meter effect from a different angle, it is best to divide the meter effect further into rotor flow effect and tip-clearance flow effect.

Rotor flow effect is analogous to rotor coefficient described in Chapter 3. The behaviour of rotor coefficient in different flow profiles corresponds to that of meter coefficient described earlier and any change in its value with different flow profiles depends not only on the profile itself but on the type of blades used. However rotor coefficient is concerned only with flow within the sweep of the rotor blades and the increase in nett torque brought about by the increase in tip-clearance, also at the same time decreases the flow through the rotor blades. Increasing the tip-clearance therefore increases the rotor coefficient as can be seen from Figs. 6.4 and 6.6. However rotor flow effect is concerned only with changes in rotor coefficient with changing velocity profiles and as can be seen from the figures, increasing the tip-clearance has a negligible

influence on the rotor flow effect. Though increasing the tip-clearance increases the nett torque in fully developed flow by a greater amount than in uniform flow, the corresponding decrease in flow going through the rotor blades is less thus compensating for the difference in the nett torque increase.

The magnitude of the meter coefficient of a turbine meter depends, among other things, on the proportion of the total flow going through the tip-clearance. The tip-clearance flow effect arises therefore, from changes in this proportion when the velocity profile within the meter annulus changes. The greater the proportion going through the tip-clearance, the smaller would be that going through the blades and therefore the lower would be the speed of rotation and consequently the meter coefficient. If the boundary layer thickness is smaller than the tip-clearance, the velocity distribution within the sweep of the rotor blades is uniform. As the flow is going through an enclosed area any change in boundary layer thickness within the tip-clearance would affect the proportion of flow going through the blades. The proportion would also vary when there is any change in velocity gradient within the tip-clearance. When the boundary thickness grows beyond the tip-clearance, any change in tip-clearance flow results only from changes in velocity gradient within it. As the change in flow near the pipe wall is greatest at the initial stages of boundary layer development, the tip-clearance flow effect is most profound near the pipe inlet (see Figs 6.4 and 6.6). This effect is greater the greater the tip-clearance.

The presence of the hump in the meter effect (and consequently the profile effect) of helical-blade rotors with big tip-clearance is the result of the interaction between the rotor flow effect and the

tip-clearance flow effect. As the meter is moved away from the pipe inlet the rotor flow effect would decrease the meter coefficient but the tip-clearance would increase it instead. As the latter is greatest near the pipe inlet and when the tip-clearance is sufficiently large, the nett effect is to decrease the meter coefficient more than if the meter is further away from the inlet. However when the meter is sufficiently far away, the rotor flow effect predominates and the meter coefficient decreases with increasing development of velocity profile. Therefore the greatest profile effect on a helical-blade is not felt directly at the pipe inlet but a short distance downstream. The distance depends on the tip-clearance the rotor has.

6.3.2 Drag Effect

Drag effect arises from changes in the total drag on the rotor blades when the velocity profile within the meter annulus changes. As stated in Chapter 3 drag on the rotor blades can be assumed to consist of skin friction drag and induced drag. While the skin friction drag remains essentially the same, the induced drag varies with the angle of attack along the blades. Unlike the lift, it does not change direction when the angle of attack changes from positive to negative (i.e. it always opposes the motion of the blade irrespective of the angle of attack).

Along the blades of a helical-blade rotor placed in uniform flow, the angle of attack is small and therefore the induced drag is negligible. In fully developed flow the induced drag along the blades is greater but even so is smaller than that in a constant blade angle rotor. In both rotors, the drag effect is greater in fully developed flow than in uniform flow. This tends to reduce the meter coefficient

in fully developed flow more. See Figs 6.3 and 6.6 for this effect.

As explained in Section 6.3.2 the meter effect on helical-blade rotor is such as to make the meter coefficient in fully developed flow less than in uniform flow. Therefore the addition of a drag effect would increase their difference even more. The opposite is true for the meter coefficient of constant blade angle rotor and the addition of the drag effect would instead reduce the difference in meter coefficients.

As the angle of attack is greatest at the blade tips and since the drag torque is greater in fully developed flow, increasing the tip-clearance would reduce the drag effect. However because of the different way the profile effect acts on various types of blade, the reduction in drag effect reduces the profile effect for the helical-blade rotor only whereas for constant blade angle rotor, the profile effect is increased (see Figs 6.3 and 6.6).

6.3.3 Profile Effect on Helical-blade Rotors

All the conclusions resulting from the discussion in Section 6.3.1 and 6.3.2 can clearly be seen to be true from the experimental results shown in Figs 6.7 and 6.8. The figures show the profile effect on helical-blade rotors not only of different hub-ratios but also with different tip-clearances. For the rotor with 0.125 hub-ratio and with a tip-clearance ratio of 0.010, the profile effect is 2.5% but when the tip-clearance ratio is increased to 0.050, the effect is reduced to 0.6% at the crest of the hump. If the tip-clearance ratio remains about the same (i.e. 0.008), increasing the hub-ratio to 0.38 decreases the profile effect 1.2%. If the tip-clearance ratio of this rotor is increased to 0.050 as well, the profile effect is reduced to 0.35% at the crest of the hump and -0.8%

at OD (zero diameter i.e. no pipe section between the meter and the conical entrance). Perhaps it should be pointed out that when a meter is placed at OD, the axial centre of the rotor is approximately 2D away from the point where the conical contraction ends. At this meter position the boundary layer thickness ratio (δ/r_o) is about 0.05.

There are therefore two methods of reducing the profile effect on helical-blade rotors. One method is to increase the hub-ratio and the other is to increase the tip-clearance. If the profile effect is to be reduced by increasing the tip-clearance and if the tip-clearance is increased sufficiently, there is a small section immediately after the pipe inlet where the profile effect is negative (i.e. the meter coefficient is less than that for fully developed flow). This can be seen for the rotor with 0.38 hub-ratio and a tip-clearance ratio of 0.050 in Fig. 6.7. This is acceptable if the negative effect is not too large. What then is the maximum tip-clearance? As will be pointed out in Chapter 10 this would depend on what characteristics the meter is required to have. If profile effect is the sole criterion then the limit to which tip-clearance can be increased depends on how far from the pipe inlet the meter is expected to be placed. If it is placed sufficiently far away, the crest of the hump can be considerably reduced before the negative profile effect is reached at the minimum distance specified. This can best be illustrated by looking at the two helical-blade research rotors having a tip-clearance ratio of 0.050. If the rotor with 0.125 hub-ratio is to be placed any where after the pipe inlet, then the hump can further be reduced by increasing the tip-clearance ratio beyond 0.050. For the rotor with 0.38 hub-ratio, a tip-clearance ratio of 0.050 is already too large as the negative profile effect is already greater than that at the crest.

However if the meter is expected to be placed not nearer than 6D from the conical entrance, then the tip-clearance ratio can still be decreased. Therefore the extent to which the tip-clearance ratio can be increased depends on each design and upon each requirement.

6.3.4 Profile Effect on Constant Blade Angle Rotor

The conclusions that can be drawn from the discussion on the effect of velocity profile on constant blade angle rotors are quite different from that on helical-blade rotors. When the tip-clearance is small, the profile effect is such that the meter coefficient would increase with increasing distance from the pipe inlet. When the tip-clearance is large the profile effect is increased, unlike the helical-blade rotor. However the effect is reduced when the hub-ratio is increased. Also all these conclusions can be seen to be true from the experimental results shown in Fig. 6.9, for two research rotors having constant blade angle and with different tip-clearances. For the rotor with 0.125 hub-ratio and with a tip-clearance ratio of 0.007, the profile effect is -0.6% but when the tip-clearance ratio is increased to 0.050, the effect is increased to -2.0%. If the tip-clearance ratio remains at 0.007, increasing the hub-ratio to 0.375 decreases the profile effect to -0.2%. If the ratio is increased to 0.050, the profile effect is increased to -1.5%.

Unlike helical-blade rotors, the profile effect on a constant blade angle rotor is least when the tip-clearance is kept to a minimum. When this is done, as can be seen from Fig. 6.8, the constant blade angle rotor is more suitable for eliminating profile effect.

6.3.5 Comparison between Theory and Experiment

In Chapter 5, the profile effect predicted by the meter coefficient

equation derived in Chapter 3, was compared with that obtained experimentally for the upstream position only. In this chapter, experiments were carried to determine the profile effect for four research rotors placed at varying distances from the inlet of the test length. The results have been discussed but before they can be compared with theory, the boundary layer thickness δ and the reciprocal of the exponent m of the power law equation, used to approximate the velocity profile in the boundary layer, are required. These values of δ and m are taken from the measurements carried out by Salami (5) and are shown in Figs 6.1 and 6.2. As the velocity profiles measured by Salami are for flow in the pipe, the velocity profile when the flow enters the meter annulus could be altered as was shown in Chapter 4. The values of δ and m in the meter annulus are modified for calculations in this chapter according to the equations suggested in Chapter 4.

Figs 6.10 and 6.11 show the comparison between the experimental and theoretical profile effects for the four research rotors used. For each rotor the profile effect for two tip-clearance are given. The agreement between theory and experiment is satisfactory for both constant blade angle and helical-blade rotors. Though it is not as good as hoped for, it is generally better than the meter coefficient equations using other sets of assumptions, as had been pointed out in Chapter 5. This is especially so for constant blade angle rotors. For example, the experimental profile effect at the upstream position for the constant blade angle rotor with 0.375 hub-ratio and 0.050 tip-clearance ratio is -1.5%. Using similar sets of assumptions by Jepson (9), Salami (5) and Thompson & Grey (44), the predicted profile effects are -3.8%, -2.2% and -3.3% respectively. The profile effect predicted here is -1.7% and therefore is in better agreement with experiment than when using other sets of assumptions.

CHAPTER 7

EFFECTS OF UPSTREAM DISTURBANCES AND METHODS OF REDUCING THEM

7.1 Introduction

When installing a turbine meter, ideally it is best to do so in a region where the flow conditions very nearly approximate to those during calibration. The effect of inlet velocity profile on turbine meters has been studied in Chapter 6, together with methods of reducing it. In practice, this may not be the only effect encountered. Very often the flow profile may be asymmetric and on top of that swirl may also be encountered when a turbine meter is placed downstream of either a valve, a bend, or a pump. When such meter location cannot be avoided, then it is important either to eliminate such disturbances wherever possible, or to design a meter that can keep errors due to such flow disturbances to a minimum.

This part of the research is concerned with studies of the effect of upstream disturbances on turbine meters having different design features. From these results it is hoped to arrive at the design that is best suited to cope with such disturbances.

7.2 Experiment.

A 2" (50.8×10^{-3} m) diameter gate valve was used to create upstream disturbances in the flow. The valve is placed at 48 diameters downstream from the conical entrance and at this position fully developed flow has already occurred. The valve can be shut completely with 8 complete turns of its wheel. Therefore by closing the valve by different numbers of turns, different degrees of disturbances can

be created.

To study the effect of disturbances created by the gate valve on a turbine meter, the meter is placed at various distances downstream of the valve. In this series of experiments, meters were placed in positions ranging from 3 diameters to 81 diameters downstream. At each position, the valve is partially closed to four different degrees of closure, namely, when the valve is completely opened, when the valve is closed by 2 turns, 4 turns and 6 turns. The flow rate is set to 14.9 lb/sec. (6.75 kg/s) of water and is determined from another turbine meter situated at about 100 diameters. This reference meter is protected from the effect of swirl by an effective flow straightener and at this position, as will be evident later, the effect of flow asymmetry is no longer felt. In any case the reference meter is used only for setting the flow rate to within $\pm$ 0.05 lb/sec. (0.023 kg/s). The actual flow rate is determined in the usual manner with the weigh tank. When the valve is partially closed, the flow rate can be altered slightly. When this happens, the pump speed is altered until the reference meter indicates its original reading.

The following 2 inch (0.0508 m) diameter meters were used for this investigation.

1) $\frac{1}{4}$" (6.35×10^{-3} m) hub helical-blade rotor with 0.008 tip-clearance ratio.
2) $\frac{1}{4}$" (6.35×10^{-3} m) hub constant blade angle rotor with 0.007 tip-clearance ratio.
3) $\frac{3}{4}$" (19.05×10^{-3} m) hub helical-blade rotor with 0.008 tip-clearance ratio.
4) a commercial meter.

Particulars of these meters are given in Appendix III. Except for the commercial meter, all the other meters were tested both with and without flow straightener. The flow straightener used was an 8 vane straightener 1 diameter in length. Salami (10) found that this particular straightener is effective in eliminating strong swirls. The commercial meter has its own flow straightener.

7.3 Discussion

7.3.1 Effect of Upstream Disturbances on 0.125 Hub-Ratio Helical-Blade Rotor

This rotor is sometimes referred to as the full-diameter rotor. The first test was made without using any flow straightener and the results for two flow rates are shown in Fig. 7.1. When the gate valve was closed by 2 and by 4 turns, its effect was to cause the meter to overestimate. The velocity profile that was symmetrical upstream of the valve, becomes asymmetric on passing through the partially closed valve. In an asymmetric profile, the rotor blades sweep through regions of varying velocity and this angular fluctuation of velocity causes the rotor to rotate faster than it would have done in a symmetrical velocity profile. This effect decreases as the meter is placed further and further away from the valve. As will be demonstrated later, there is no swirl generated by the valve at these two stages of valve closing.

When the valve is closed by 2 turns, both the magnitude of its effect as well as the distance downstream at which the meter needs to be placed, are less than when the valve is closed by 4 turns. At 2 turns, the overestimation at 5 diameters was 0.6% and the distance before no valve effect was 20 diameters. For the case of 4 turns,

the overestimate at 5 diameters was 1.7% and the meter needed to be 55 diameters downstream before no valve effect was felt. The importance of this observation is that even when a meter is installed downstream near a valve and calibrated in situ with a meter prover, one cannot be certain that the meter is giving the correct reading because its reading will depend on how much the valve is closed.

Because of the asymmetric profile, the rotor rotation tends to be unsteady. Fig. 7.3 can be used to give an indication of the unsteadiness of its rotation for different degrees of asymmetric profile. Throughout the period of each measurement, the speed of the rotor was measured by continually taking the time required for counting 100 pulses from the meter pick-up system. In this way, about 22 readings were taken for each measurement. The standard deviation of the reading in each measurement was taken and plotted against the valve opening. Fig. 7.3 shows that the standard deviation increases as the valve is closed thus indicating a greater degree of unsteadiness of the rotor speed.

So far no mention has been made of the valve effect when it is almost completely shut, i.e. at 6 turns. As will be apparent later, its effect at this position is more than just due to asymmetric profile. The variations of meter coefficient with different positions of valve opening for two meter positions are shown in Fig. 7.2. The figure shows that overestimation of the meter increases at first as the valve is closed but if the valve is closed further beyond 4 turns, overestimation of the meter decreases and underestimating can occur instead. The underestimation is better illustrated by Fig. 7.1, where the meter coefficient at 6 turns of the valve is plotted against the meter position. Whereas the overestimation at 2 and at 4 turns dies out at about

55 diameters the underestimation at 6 turns persists even up to 78 diameters. As one would expect a meter to overestimate in an asymmetric profile, this underestimation may be due to other disturbances created by the valve. One hypothesis is that at this stage of valve closure, swirl may also be generated in addition to asymmetric profile. While the asymmetric profile causes a positive error, the swirl generated is of such direction as to give a negative error. If this swirl is of sufficient magnitude, the resultant effect on the meter can be underestimation.

This hypothesis can be verified in two ways. For the first way, the use of an effective flow straightener should eliminate any swirl created by the valve. Thus the meter should overestimate instead at 6 turns. Salami (10) found that an eight-vane straightener, one diameter in length, is very effective even for strong swirl. This straightener was used and Fig. 7.4 shows the results of using such a straightener compared with not using it. While the overestimation at 2 and 4 turns remains essentially the same with or without straightener, thus showing that no swirl is present at these two positions of valve closing, this is not so at 6 turns. The underestimation without the straightener has become overestimation when a straightener is used. In fact the overestimation is about the same order of magnitude as in the case of 4 turns.

7.3.2 0.125 Hub-Ratio, Constant Blade Angle Rotor

The second way of verifying whether the flow disturbance created by the valve contains swirl or not, is to make another rotor but with blade angles in the opposite sense. If there is swirl, its effect on this new rotor should be in the same sense as that of the asymmetric

profile, i.e. the new rotor should overestimate not only because of the profile but also because of the swirl.

The dimensions of this new rotor were made the same as the previous helical-blade rotor except for two differences. Firstly, it is a constant blade angle rotor but the angle was so chosen that its meter coefficient in a flat velocity profile is the same as the helical rotor. (The angle is $32^{\circ}37'$ against a helical pitch of 6.28" (0.1595 m)). Secondly, the blade is left-handed instead of right-handed as in the previous rotor.

With this new rotor, the experiment on the effect of the valve was repeated first without using a flow straightener. The results are shown in Fig. 7.5 together with those of other meters. Unlike the right-handed helical-blade rotor, this left-handed rotor overestimates throughout all positions of the meter. Also, downstream of the position where the asymmetric profile is no longer felt (i.e. after about 40D), the magnitude of the overestimation of this rotor is about the same as that of the underestimation of the right-handed blade rotor. This proves that swirl is generated by the valve when it is closed by 6 turns.

To demonstrate this further and to see the effect of an asymmetric profile on the constant blade angle rotor, the experiment was repeated with a flow straightener. The results are shown in Fig. 7.6 to compare with those of the equivalent helical-blade rotor. The overestimation, that was present when not using flow straightener, is effectively eliminated after 15D. This again confirms that swirl is generated by the valve at 6 turns. From the figure, it is evident that asymmetry of the flow profile affects a constant blade angle rotor less. Not only is the magnitude of the effect less but also

the distance the meter needs to be placed before the effect is no longer felt. For the helical-blade rotor, the distance is 35D as compared with 10D for this rotor.

7.3.3 0.375 Hub-Ratio Helical-Blade Rotor and a Commercial Meter

The foregoing experiments, besides showing the effects of a gate valve on turbine meters of small hub diameter, also show that a constant blade angle rotor is better suited for measuring asymmetric flows. The object of the next part of this series of experiments is to see whether it is possible to reduce the effect of asymmetric flow by increasing the hub diameter (i.e. decreasing the flow area). For this, two $\frac{3}{4}$" hub diameter rotors with helical-blades were used. The first meter, made in the Department, has a helical pitch of 6.28" (0.1595 m) and the meter wall casing diameter is 2.0" (0.0508 m). That of the second meter, a commercial one, has 3.960" (0.1006 m) pitch and 1.82" (0.0925 m) respectively. This means that the commercial meter has a smaller flow area than that made in the Department. As the commercial meter itself is provided with a flow straightener, the effect of the gate valve on this meter was investigated without using another straightener. For the other meter, the experiment was done both with and without the straightener.

Fig. 7.5 shows the effect of the valve at 6 turns shut on this $\frac{3}{4}$" hub meter and its comparison with the two $\frac{1}{4}$" hub meters, all without flow straighteners. Since this rotor has right-handed blades (i.e. the same as $\frac{1}{4}$" hub helical-blade rotor) the swirl generated by the valve causes it to underestimate. To compare the sensitivity of different meters to swirl, only results at distances greater than 40D should be considered. This is because the asymmetric profile is

still felt at distance less than this. Take the case when all the meters are placed at 78D downstream of the valve. While the effect of the swirl affects the two $\frac{1}{4}$" hub rotors by about the same amount, it affects the $\frac{3}{4}$" hub less. In fact at 78D the ratio of the error caused by the swirl on the $\frac{3}{4}$" hub to that of the $\frac{1}{4}$" hub is 0.667.

To compare the effect of asymmetry on meters having different flow areas, the results for the commercial meter, the $\frac{1}{4}$" hub and the $\frac{3}{4}$" hub rotors are plotted in Fig. 7.7. The figure shows that the smaller the flow area (i.e. the bigger the blockage area) the more effective is the meter in eliminating error due to asymmetry of flow. For the $\frac{1}{4}$" hub, the asymmetry is felt some 35D downstream, this distance is reduced to about 15D for the two $\frac{3}{4}$" hub meters. In fact for the commercial meter, which has a smaller flow area, the distance is slightly less (10D). However, if one is to look again at Fig. 7.6, the constant blade angle rotor is as effective as the commercial meter in eliminating error due to asymmetric profile even though it has a much bigger flow area.

7.3.4 Effect of Using Flow Straighteners

When a flow straightener is placed directly in front of a turbine meter, its presence may alter the overall meter coefficient. This is because it is difficult to make the vanes of the straightener completely axial and therefore swirl may be created by the straightener itself to offset the meter coefficient. Also wakes created by the vanes may affect the meter coefficient.

Table 7.1 shows how the use of the same flow straightener affects two rotors of different design. Both rotors have the same hub-ratio

of 0.125 but the first is a right-handed helical-blade rotor while the other is a left-handed constant blade angle rotor. When using the flow straightener, the meter coefficient of the right-handed blade rotor is decreased while that for the left-handed blade rotor is increased. Since the same flow straightener was used, the reason for this change is probably because the vanes were not completely axial. Whatever the reason may be, it is best to calibrate any turbine meter together with its flow straightener. Otherwise the calibration may be altered when using the straightener.

CHAPTER 8

HEAD-LOSS ACROSS TURBINE METERS

8.1 Introduction

One of the criteria sometimes used for comparing the relative merits of flow measuring devices is the magnitude of the head-loss caused by them, because the greater the losses the greater would be the cost of conveying the metered fluid. Using the specification of commercially available turbine meters, Scott (11) found that the head-loss caused by them falls between 0.6 and 1.5 pipe velocity heads. In this respect the turbine meter is superior to many other flow measuring devices (e.g. differential pressure meters). Perhaps it is because of this that the head-loss of turbine meters is very often neglected in design considerations and the resulting meter may have a head-loss far larger than necessary. For a turbine meter, the head-loss can be divided into two types; namely:-

i) Rotational losses:- these losses are actually the energy required to keep the rotor in motion.

ii) Contraction and expansion losses:- these losses result from the changes in flow areas as the fluid goes through the meter.

Though it is desirable, at the design stage, to keep the rotational loss in mind, nothing much can be done once the bearings, pick-up system and the blades have been fixed. As the second type of losses result mainly from the expansion of flow, it is best to keep the flow area through the meter as near to that of the pipe as possible and any changes should be as gradual as possible so that the maximum pressure recovery can be achieved.

This chapter describes how the head-losses across three research meters of different design were investigated experimentally and compared with that of a commercial meter. Also the rotational losses are studied theoretically.

8.2 Experiment

Three 2" research meters and one 2" commercial meter, all with about the same tip-clearance, were used in the experiments. The research rotors are

i) $\frac{3}{4}$" hub helical-blade rotor with 0.008 tip-clearance ratio

ii) $\frac{3}{4}$" hub constant blade angle rotor with 0.007 tip-clearance ratio

iii) $\frac{1}{4}$" hub constant blade angle rotor with 0.007 tip-clearance ratio.

The commercial meter is a $\frac{3}{4}$" hub helical-blade rotor with 0.010 tip-clearance ratio. The head-losses for all the meters were measured in fully developed flow. The head-loss across each meter was determined by measuring the pressure drop across it using two adaptor flanges as shown in Fig. 8.1. Each flange has three static pressure tappings located circumferentially on the same plane at 120° to each other. Pressure from the three tappings are connected to a pressure averaging chamber and the averaged pressure is connected to one limb of a mercury manometer or an inverted water mamometer or both. Pressure from the other flange is similarly connected to the other limb of the manometer. Using this arrangement the head-loss across each meter was measured at different flow rates. To measure the head-loss due to the contraction and expansion of flow because of the hub, the rotor of each meter was removed and replaced with another hub

of the same diameter but without any blade. The pressure drop across the meter was again measured at different flow rates. The difference gives the losses due to rotation and to the change in flow area as the flow enters and leaves the blades.

8.3 Theory

Fig. 8.1 shows the cross-section of a turbine meter fitted with two adaptor flanges, one at each end. Head-loss across the meter is taken to be between planes (u) and (d) where the upstream and the downstream pressure tappings are respectively located. For flow going through the rotor blades, plane (1) refers to the plane just before the blade inlet, plane (x) just after, plane (y) just before the blade outlet and plane (2) just after the outlet. The convention used here to denote the pressure, velocity and velocity distribution at plane (x) is p_x, u_x and $(u/U)_x$ respectively. The head-loss between two planes (x) and (y) is denoted by H_{xy}. The axial velocity distribution at each of the following two planes are assumed to be similar to each other.

(i) planes (u) and (d)

(ii) planes (1) and (2)

(iii) planes (x) and (y)

8.3.1 Head-losses H_{u1} and H_{2d} (Hub Loss)

When fluid enters and leaves the annulus formed by the rotor hub and the meter casing, there is an acceleration and a deceleration in the flow due to the change in flow area. H_{u1} is the head-loss resulting from the acceleration and H_{2d} is that due to the deceleration.

Applying Bernoulli equation between planes (u) and (1)

$$H_{u1}\int_{o}^{r_p} \rho g \cdot 2\pi r.u_u.dr = (p_u-p_1).\int_{o}^{r_p} \rho g.2\pi r.u_u.dr + \frac{\rho g}{2g}\{\int_{o}^{r_p} 2\pi r.u_u^3.dr - \int_{r_h}^{r_o} 2\pi r.u_1^3.dr\} \quad \ldots \quad 8.1$$

Similarly applying Bernoulli equation between planes (2) and (d)

$$H_{2d}\int_{o}^{r_p} \rho g.2\pi r.u_d.dr = (p_2-p_d).\int_{o}^{r_p} \rho g.2\pi r.u_d.dr + \frac{\rho g}{2g}\{\int_{r_h}^{r_o} 2\pi r.u_2^3.dr - \int_{o}^{r_p} 2\pi r.u_d^3.dr\} \quad \ldots \quad 8.2$$

If the rotor has no blade and assuming the viscous losses between plane (1) and (2) are negligible, then

$$p_1 = p_2$$

Also it can be assumed that $u_u = u_d$ and $u_1 = u_2$.

∴ adding eqns. [8.1] and [8.2] gives

$$H_{u1} + H_{2d} = (p_u - p_d)_{nb} \quad \ldots \quad 8.3$$

where $(p_u-p_d)_{nb}$ is the pressure drop across planes (u) and (d) when there is no blade on the rotor. In practice $H_{u1} << H_{2d}$ and can be neglected.

If there is no pressure recovery when flow leaves the annulus, then the head-loss H'_{2d} is

$$H'_{2d}.\int_{r_h}^{r_o} \rho g.2\pi r.u_2.dr = \frac{\rho g}{2g}\{\int_{r_h}^{r_o} 2\pi r.u_2^3.dr - \int_{o}^{r_p} 2\pi r.u_d^3.dr\}$$

As shown in Appendix IV

$$H'_{2d} = \frac{[G(n) - J(n)^3.H(n)]}{2g.\pi^2.r_o^4.F(n)^3} . Q^2 \quad \ldots \quad 8.4$$

∴ the ratio of the pressure recovery is $1 - \frac{H_{u1} + H_{2d}}{H'_{2d}}$

8.3.2 Head-losses H_{1x} and H_{y2}

H_{1x} and H_{y2} are also the losses resulting from acceleration and deceleration in the flow but in this case changes in flow area are due to the rotor blades. If there is no pressure recovery when the flow leaves the blades then, as shown in Appendix IV, the head-loss H'_{y2} is

$$H'_{y2} = \frac{\{K(n)^3.[L(n) + M(n)] - G(n)\}}{2g.\pi^2.r_o^4.F(n)^3} . Q^2 \quad \ldots \quad 8.5$$

If the percentage pressure recovery is assumed to be the same as that for the hub (see Section 8.3.1), then

$$\frac{H'_{2d} - (H_{u1} + H_{2d})}{H'_{2d}} = \frac{H'_{y2} - (H_{1x} + H_{y2})}{H'_{y2}}$$

Rearranging and substituting equations [8.4] and [8.5],

$$H_{1x} + H_{y2} = (H_{u1} + H_{2d}) \frac{\{K(n)^3.[L(n) + M(n)] - G(n)\}}{G(n) - J(n)^3.H(n)} \quad . \quad 8.6$$

$(H_{u1} + H_{2d})$ is the hub loss and is the measured head-loss when the blades of the rotor are removed.

8.3.3 Head-losses H_{xy} and H_v

H_{x_y} is the loss between planes (x) and (y) and it is due to energy being extracted from the flow to keep the rotor spinning. Referring to the inlet and outlet velocity diagrams in Fig. 3.1 and applying the Bernoulli equation between planes (x) and (y) for an elemental radius dr,

$$H_{xy}.\rho g.\left\{\int_{r_h}^{r_t}(2\pi.r-N.t).u.dr+\int_{r_t}^{r_o}2\pi.r.u.dr\right\}$$

$$=\rho g.\int_{r_h}^{r_t}\frac{(p_x-p_y)}{\rho g}(2\pi.r-N.t).u.dr-\rho g.\int_{r_h}^{r_t}\frac{v_e^2}{2g}.(2\pi r-N.t).u.dr$$

. . . 8.7

Equating the axial forces acting on the elemental radius dr,

$$(p_x-p_y).(2\pi.r-N.t).dr=\tfrac{1}{2}\rho\,NW\left\{\frac{C_L.\sin\theta}{\cos^2\theta.\cos\beta}+\frac{C_D.\cos\theta}{\cos^2\theta.\cos\beta}\right\}u^2.dr$$

. . . 8.8

From equations [8.7] and [8.8] and as shown in Appendix IV

$$H_{xy}=\frac{C_1.N.W.N(n).Q^2}{2g.\pi^3.r_o^5.[C(n)+D(n)]}-\frac{P(n).Q^2}{2g.\pi^3.r_o^4.[C(n)+D(n)]}\quad..\quad 8.9$$

If it is assumed that the tangential velocity at the blade outlet is dissipated as head-loss H_v before reaching plane (d) without any pressure redovery, then H_v is equal to the second term on the right hand side of equation [8.9]

i.e. $$H_v = \frac{P(n) \cdot Q^2}{2g.\pi^3.r_o^4.[C(n)+D(n)]} \quad \ldots \quad 8.10$$

8.3.4 Head-loss H_{ud} across Turbine Meter

The total head-loss H_{ud} across the meter is the sum of each individual loss.

$$H_{ud} = H_{u1} + H_{1x} + H_{xy} + H_{y2} + H_{2d} + H_v$$

$$= (H_{11} + H_{2d}) + (H_{1x} + H_{y2}) + H_{xy} + H_v$$

$$= (H_{u1} + H_{2d}).\{1 + \frac{K(n)^3.[L(n)+M(n)]-G(n)}{G(n) - J(n)^3.H(n)}\} + \frac{C_1.N.W.N(n).Q^2}{2g.\pi^3.r_o^5.[C(n)+D(n)]}$$

$$\ldots \quad 8.11$$

$(H_{u1} + H_{2d})$ is the measured pressure drop across planes (u) and (d) when the rotor blades are removed and is a function of the flow rate Q.

In the discussion of the next section three types of losses are referred to; namely, meter-loss, hub-loss and blade-loss. Meter-loss H_m is defined as the total head-loss across the meter when the rotor is working normally, i.e.

$$H_m = H_{u1} + H_{1x} + H_{xy} + H_{y2} + H_{2d} + H_v \quad 8.12$$

The hub-loss H_h is defined as the head-loss across the meter when the rotor blades are removed i.e. the rotor replaced by a hub of the same diameter but with blades.

$$\therefore \quad H_h = H_{u1} + H_{2d} \quad \ldots \quad 8.13$$

The blade-loss H_b is the sum of the rotational loss H_{xy} and the

losses, H_{1x} and H_{y2} , due to flow acceleration and deceleration as the fluid goes into and out of the rotor blades, i.e.

$$H_b = H_{1x} + H_{xy} + H_{y2} \quad \ldots \quad 8.14$$

The pressure recovery P_r due to flow deceleration as fluid leaves the rotor hub is defined as

$$P_r = 1 - \frac{H_{u1} + H_{2d}}{H'_{2d}} \quad \ldots \quad 8.15$$

8.4 Discussion

All losses and pressure measurements in this chapter are expressed in centimetres of water. Fig. 8.2 shows the meter-losses across three 2" research meters, all of which have about the same tip-clearances but with rotors of different designs. However the shapes of the 'flow guiding' sections, i.e. the sections to enable gradual area change as fluid enters and leaves the meter annulus, are designed geometrically similar and each section formed part of the bearing housing (see Fig. 5.17). As can be seen from Fig. 8.2 the meter-loss across the turbine meter with constant blade angle rotor of $\frac{3}{4}$" diameter is larger than that of the equivalent meter with a helical-blade rotor. Even for the constant blade angle rotor with a smaller hub diameter ($\frac{1}{4}$" instead of $\frac{3}{4}$") the meter-loss is still larger. This is because the angle of attack along the blade is large. Consequently the outlet velocity has large tangential swirl and because of the swirl, the head-loss across the meter would be larger. Therefore from the point of view of head-loss, helical-blade

rotors are superior but it needs to be added that for certain type of application, e.g. to reduce the effects of poor velocity profiles (see Chapters 6 and 7), the advantage of using a constant blade angle rotor may outweigh the disadvantage of greater head-loss.

As the bearing supports for the two $\frac{3}{4}$" diameter rotors are the same, the greater loss for the constant blade angle rotor must be due to greater blade-loss. This can be seen from Fig. 8.3 which shows the head-losses across the meters both when their rotors are running normally and when the rotor blades are removed (i.e. rotor replaced by a hub of the same diameter). The difference in the two losses gives the blade-loss. The greater blade-loss for the constant blade angle rotor is more clearly shown in Fig. 8.7 where it is expressed as a ratio of the pipe velocity head. More about this figure later.

To compare the different types of losses of the research meters with those of the commercial meter, the same measurements were carried out on a 2" commercial meter with a helical-blade rotor of $\frac{3}{4}$" hub diameter. Fig. 8.4 shows losses across the meter both with rotor running normally and with the blades removed. For comparison, the meter-loss across the 2" research meter with helical-blade rotor is also plotted. Though both meters have the same type of blade and the same hub diameter, the meter loss for the commercial meter is very much larger. At 15 lb/sec. (6.8 kg/s), the meter-loss is 0.84 m. of water as compared to 0.125 m. for the research meter. From the figures quoted, the commercial meter has a head-loss 6.7 times greater.

For a better comparison the meter-losses are plotted as a ratio of the pipe velocity head. This is shown in Fig. 8.5 and differences between different meters are clearly brought out. In his survey on

commercial turbine meters available in U.K., Scott (11) found that their meter-losses to be between 0.6 to 1.5 pipe velocity heads. This range is also indicated on the figure for comparison. For the commercial meter tested, the meter-loss lies near the upper value quoted (about 1.4 pipe velocity heads). On the other hand those for the research meters are less than half that quoted for the lower limit for commercial meters. This suggests that in general the head-losses across commercial meters can be reduced substantially.

To investigate the reasons behind the greater loss suffered by the commercial meter tested and to see in general which of the losses formed the major part of the total head-loss, the two types of losses are investigated separately. The hub-loss for the commercial meter is also plotted in Fig. 8.4 and as can be seen that even this loss by itself is greater than the meter-loss of the research meters. This indicates that its hub-loss is rather excessive. To show this more clearly, the pressure recovery for both meters at different flow rates are calculated using equation[8.15] and shown in Fig. 8.6. While the pressure recovery at 15 lb/sec. (6.8 kg/s) is about 51% for the research meter, that for the commercial meter is only 13%; a difference by a factor of 4. When the meter was examined, it was found that not only are the changes in area section rather abrupt but also the vanes supporting the bearing housings rather excessively thick. Therefore the head-loss across the meter can be greater reduced if its pressure recovery process is improved e.g. by having thinner supporting vanes and more gradual area change.

The other losses, i.e. blade-losses, of the meters are shown in Fig. 8.7 and are expressed as a ratio of the pipe velocity head. For the research meter the blade-loss is only 3.5% of the pipe velocity

head while it is 38% for the commercial meter. Even for the research meter with constant blade angle rotor, the blade-loss is only 9.5%. It is true nothing much can be done about blade-loss once the type of bearings, the pick-up system and the rotor dimensions are fixed. However, it is good design practice to ascertain whether any modification or alternative design can be made that can equally achieve the same objectives but with a smaller blade-loss. This can best be illustrated by examining the design of the commercial meter. The meter uses journal bearings while the same manufacturer's $1\frac{1}{2}$" meter, which also has the same hub diameter (i.e. $\frac{3}{4}$"), uses ball bearings instead. Judging from the dimensions given and substantiated by its calibration curve (see Fig. 3.15), the meter would have a large 'hump' and therefore a larger variation on its calibration curve if the resisting torque is reduced (see Chapter 9 about this phenomenon). It is probable that journal bearings were chosen so that their values of friction torque could offset the large variation in meter coefficient. However, the use of journal bearings not only itself increases the head-loss but also triggers a chain of design changes resulting in greater losses i.e. more blades, smaller flow area, smaller helical pitch, etc. A better way of reducing the variation is by reducing the tip-clearance or hub-ratio or both (see the design procedure proposed in Appendix V). Actually it is rather unfair to criticize any design because many factors governing the behaviour of calibration curves and related data are not known or available. Therefore design is carried out rather empirically by trial and error. However it is hoped that the proposed design procedure, which uses the leakage theory and information from this research, may enable a more systematic design.

The meter, the hub and the blade-losses for the commercial and the research meters are shown on the same graph in Fig. 8.8 so that the proportion of the meter-loss contributed by the hub and the blades can be assessed readily. It can be seen that in all cases, the hub-loss forms the major part of the meter-loss and it is therefore important to have gradual flow area change so that maximum pressure recovery can be achieved. The blade-loss contributes the smaller proportion but this also depends not only on the type of blades used but also on the design of the rotor. In general rotors having a greater number of blades, bigger bearing torque, larger hub-ratio and smaller helical pitch (or bigger blade angle) have greater blade-losses.

The meter-loss can be calculated using equation [8.11] but before this can be done the resisting torque opposing the motion of the rotor has to be determined first. In these calculations here, the resisting torque of each meter is determined from its calibration curve by using 'Method 2' as explained in Section 3.3.1 of Chapter 3. For gas turbine meters the 'spin' test as proposed by Lee and Evans (40) can be used. The comparison between the experimental meter loss and that obtained theoretically using equation [8.11] for different meters are shown in Figs. 8.9 and 8.10. There is good agreement between theory and experiment thus indicating that the assumptions used in deriving the equation is valid.

CHAPTER 9

REPEATABILITY TESTS AND THE EFFECT OF BEARING FRICTION INCREASE

9.1 Introduction

One of the criteria for a good flow measuring device is its ability to repeat its meter coefficient over a long period of time under the same flow conditions. In this part of the research, repeatability tests over a period up to 100 hours were carried out on a helical-blade rotor of 0.125 hub-ratio. This rotor can be considered as an extreme case of design because the hub-ratio, the number of blades and the bearing friction normally encountered in commercial meters are very much larger. Therefore the results from these tests can be considered to be among the worst possible cases and in general, it is safe to expect commercial meters to perform much better.

Any change in the bearing friction of a turbine rotor can alter the shape of the meter calibration curve especially at lower flows. This effect is demonstrated both experimentally and theoretically. Again it needs to be emphasised that commercial meters would not exhibit as great a change. This is illustrated theoretically by increasing the number of blades and the hub-ratio.

9.2 Experiment

Two helical-blade rotors, both of the same design and the same hub-ratio of 0.125, were used in this series of repeatability tests. The two rotors are referred to as the full-diameter rotor and the

turned-down rotor; the tip-clearance of the former is 0.008" (2.03×10^{-4} m) while that of the latter is 0.044" (11.18×10^{-4} m). Full particulars of these and other rotors are given in Appendix III.

In all, three tests were carried out. Two of the tests were with the full-diameter rotor; one using shielded bearings and the other using open bearings. By open bearings, it is meant that the shields of the bearings were removed and the lubricant in the bearing washed off with acetone. The third test was with the turned-down rotor and using shielded bearings only.

In each test, three flow rates were used i.e. at approximately 15.0, 8.8 and 3.7 lb/sec. (6.8 , 4.0 and 1.68 kg/s). These flow rates were achieved by setting the pump speed at 2000, 1350 and 750 r.p.m. respectively. The meter coefficients at the 3 flow rates were determined experimentally one after the other in a cycle. Each cycle took about 1 hour while the test itself lasted between 70 to 95 hours.

To see how the calibration curve of a turbine meter is affected by the increase of bearing friction, the turned-down rotor was calibrated when the bearings were new and again after 75 hours of running.

9.3 Discussion

9.3.1 Repeatability Tests on Helical-Blade Rotors

Figs. 9.1, 9.2 and 9.3 are the results for the three repeatability tests. Each figure shows the meter coefficient plotted against running time at three different flow rates.

Fig. 9.1 is for the full-diameter rotor using open bearings. At the low flow rate (2.6 lb/sec.) the meter coefficient dropped sharply from 8.65 to 8.45 pulse/lb (3.18 to 3.10 rev/kg) in 5 hours. After this there was a gradual drop to 8.37 pulse/lb (3.08 rev/kg) for

50 hours of running time.

Fig. 9.2 is for the same rotor but this time with shielded bearings. Unlike the open bearings, the meter coefficient at low flow rates remained constant for about 8 hours and then dropped to 8.45 pulse/lb (3.10 rev/kg). This drop is less sharp when compared with the open bearings. The difference in the two cases is probably because the lubricant in the shielded bearings takes time to be washed away by the metered fluid while that of the open bearings was washed away with acetone before being used. Therefore increasing bearing friction for the shielded bearings takes a longer time to manifest itself.

Tables 9.1 and 9.2 give the arithmetic mean and the standard deviation of the meter coefficient for flow rates of 15 and 8.8 lb/sec. (6.8 and 4.0 kg/s) for both shielded and open bearings. Comparing the two, the shielded bearings seem to give better repeatability. For a flow rate of 15 lb/sec. (6.8 kg/s) the standard deviation after 50 hours of running is 0.0048 for open bearings as compared with 0.0044 for shielded bearings, while for a flow rate of 8.8 lb/sec. (4.0 kg/s) it is 0.0128 for open bearings and 0.0082 for shielded bearings. In both cases the open bearings had bigger standard deviation. Between 60 hours and 70 hours of running time, the standard deviation of open bearings jumped from 0.048 to 0.084 at the higher flow rate. This change in meter coefficient may be due to dirt getting into the bearings.

From the foregoing, it is not possible to conclude that, in general, shielded bearings are better just because the meter coefficient was more repeatable. In this particular meter design, there is no flow through the bearings and therefore shielded bearings are

better in preventing dirt from getting into them. However, in certain designs where there is a small flow going through the bearings, it is probably better to use open bearings instead because shields are not enough to prevent dirt from getting in. With open bearings, dirt that got inside the bearings could get out again more easily.

Fig. 9.3 gives the results of the repeatability test on the turned-down rotor using shielded bearings. As for the full-diameter rotor, the meter coefficient at 2.7 lb/sec. (1.22 kg/s) again dropped to a mean value but this time it happened after 35 hours. For the full-diameter rotor the mean value dropped to 8.396 lb/sec. (3.09 rev/kg). Taking the first reading at the same flow rate as a reference, this represents a drop in meter coefficient of 0.236 pulse/lb. (0.0867 rev/kg). If the bearing friction causing the drop was the same for the turned-down rotor, the equivalent drop by calculation should be 0.257 pulse/lb. This represents a drop to 8.685 pulse/lb. (3.191 rev/kg), again taking the first reading as reference. The actual drop after 35 hours was to a mean value of 8.668 pulse/lb. (3.185 rev/kg) which is quite close to that calculated.

By balancing both the rotors on two knife edges it was found that the full-diameter rotor was slightly more unbalanced. This may be the reason why the turned-down rotor took a longer time for its meter coefficient to drop at the lower flow rate (2.7 lb/sec.)

Table 9.3 gives the mean and standard deviation of the turned-down rotor's meter coefficient after every 10 hours of running at the two higher flow rates. Comparing this with Table 9.1, it appears that at both flow rates the full-diameter rotor is more repeatable. At 15 lb/sec. (6.8 kg/s), the standard deviation after 80 hours of running for the turned-down rotor is 0.01023 pulse/lb. (0.00376 rev/kg)

as compared with that of the full-diameter rotor which is 0.00906 pulse/lb. (0.00333 rev/kg) for open bearings and 0.00544 for shielded bearings. Similarly, at 8.8 lb/sec. (4.0 kg/s), the standard deviation of the turned-down rotor is again bigger. This is probably because it has a bigger tip-clearance area ratio, which is defined as the ratio of the area within the tip-clearance to the total flow area of the meter. The value of its tip-clearance ratio os 0.09080 compared with 0.01702 of the full-diameter rotor. Because of the greater flow through the tip-clearance of the turned-down rotor, any fluctuation or change in the flow within this region would result in a bigger change in meter coefficient.

9.3.2 Effect of Bearing Friction on Meter Calibration

The experimental points plotted in Fig. 9.4 show the calibration curves of the turned-down rotor when the bearings were new and after running for 75 hours. Though the meter coefficients at the high flow rates are not much affected, those at the low flow rates show a considerable change. This change is approximately inversely proportional to the flow rate. This alteration in the calibration curve is due to the increase in bearing friction. In practice therefore, calibration on such a rotor needs to be done after the bearings have been "run-in".

Using the leakage theory proposed in Chapter 3, the calculated friction torque for the new bearings is 4.19×10^{-4} lb. in (4.73×10^{-5} Nm) and after 75 hours of running its value is 14.0×10^{-4} lb.in. (15.82×10^{-5} Nm). Using these two values of frictional torque, the theoretical calibration curves for the rotor both with new bearings and after 75 hours of running are also shown in Fig. 9.4 to compare with those obtained experimentally.

As stated in the introduction, the rotor used in this part of the research is an extreme case of design. Generally, commercial meters have a much larger hub-ratio and more blades. Therefore a corresponding increase in bearing friction would not result in such large change in meter calibration. This can be demonstrated theoretically. Using the same leakage factor (k = 2.2567 cu.in/sec.) throughout, the changes of the meter coefficient due to the increase of bearing torque from 0.00042 to 0.0014 lb.inch for three different designs are shown in Fig. 9.5. Fig. 9.5.a is for a 2" meter with a rotor of helical pitch of 6.28" (0.160 m), hub-ratio 0.125 and with three blades. With the given increase in bearing torque, the meter coefficient is reduced by 2.44% at a flow rate of 3 lb/sec. (1.36 kg/s). If the number of blades of this rotor is increased from three to six, the drop in meter coefficient is reduced to about 1.3%. The calibration curves for this six bladed rotor are shown in Fig. 9.5.b. However if the helical pitch is reduced to 2.5" (0.0635 m) and the hub-ratio increased to 0.5, still with six blades, the effect of the increase in frictional torque is reduced considerably as can be seen from Fig. 9.5.c. The drop in meter coefficient at 3 lb/sec. (1.36 kg/s) is only about 0.26%. This new rotor is thus better suited if there are any changes in bearing friction. What actually has been done is to raise the meter coefficient as well as increasing the driving torque. The penalty for doing this is the reduction of the maximum flow rate. If the maximum speed of rotation is limited to 8000 r.p.m., the maximum flow rate of the rotor in Fig. 9.5.a is 89.7 lb/sec. (40.7 kg/s) and that for Fig. 9.5.c is only 26.7 lb/sec. (12.1 kg/s).

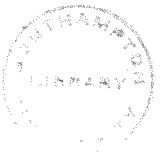

9.3.3 Effect of Variation of Resisting Torque

It has sometimes been thought that by decreasing the resisting torque, it is possible to reduce the variation in the meter coefficient over the operating range. However, analysis, on the assumption that the leakage ratio g and the leakage factor k remain constant, shows that this may not necessarily be the case. Analysis for the full-diameter and the turned-down rotor are shown in Fig. 9.6 and 9.7 respectively. For the full-diameter rotor where there is no rising section of the calibration curve, the decrease in resisting torque does reduce the variation. On the other hand for the turned-down rotor, increasing the resisting torque can reduce the variation of the meter instead of increasing it. There is then an optimum resisting torque where this variation is minimal. Any further increase in resisting torque will increase the variation. For both the rotors, decreasing the resisting torque does decrease the minimum flow that the meter can measure but does not necessarily improve the uniformity of the calibration curve.

CHAPTER 10

CONCLUSION

10.1 Introduction

In the preceding chapters, the effects of different parameters affecting the characteristics of turbine meters have been studied experimentally and also, in some cases, theoretically. In each chapter, the effects of these parameters on a certain aspect of the meter performance were studied quite independently from their effects on other aspects. However when all chapters have been compared, it is evident that although changing a parameter can improve certain aspects of meter performance, the same change can, at the same time, adversely affect other aspects. For example, if the meter has a constant blade angle rotor, increasing the tip-clearance generally reduces the lower range of the turbine meter, but increases the effect of velocity profile. As always, therefore, design must be a compromise.

Further, while changing a parameter to improve a certain aspect of the performance of a particular type of meter, the same change could have an adverse effect on the same aspect of meter performance if the meter were of a different type. For example, whereas increasing the tip-clearance can reduce the effect of velocity profile for a helical-blade rotor, the same increase has the opposite effect for a constant blade angle rotor. Therefore the first purpose of this chapter is to condense the results of all the previous chapters so that the effects of different parameters on particular aspects of meter performance for various types of meter can clearly be brought out. The interconnection between these various factors is summarised in Fig. 10.1 which will become clearer with the description given

later in the chapter.

One of the main aims of this research is to evolve a systematic procedure for designing turbine meters. If designing means just producing a turbine meter that can be used up to a given maximum flow rate, then the design is very easy and can be completed very quickly but the designer would not know how the calibration curve would look until the meter had been constructed and actually calibrated. If the meter is required to behave within certain specification, it is not possible to produce a meter and say at the design stage whether the meter can meet the specification. At best, the designer can rely on his experience and intuition to guide him in his design. At worst, he has to make a model, calibrate it and if not satisfied, change certain features and hope that it may improve the performance. Clearly this type of design is unsatisfactory because it is not only costly but time consuming. Because of the lack of knowledge about the behaviour of turbine meters, this has been the general method employed when designing a turbine meter. An alternative method is to design the meter within a given specification but this is only possible if there is information available on the effects of various parameters upon the meter performance. Therefore the second purpose of this chapter is to use the results of this research and the leakage theory proposed to evolve a systematic procedure for turbine meter design such that the designer would know, without having actually to test it, whether the resulting meter could meet the required specification.

10.2 The Effects of Tip-clearance, Hub-ratio, and Type of Blades on Meter Performance.

The effects of parameters like tip-clearance, hub-ratio and the

type of blades upon different aspects of turbine meter performance have been studied separately. For a detailed discussion on each aspect, the relevant chapter should be consulted. This section discusses how changes of each parameter affect different aspects of meter performance and the likely consequences that may arise from such changes. The interconnections between the different parameters and various aspects of meter performance are summarised as a block diagram in Fig. 10.1

10.2.1 Tip-clearance

From Chapter 5, it can be seen that one of the effects of changing the tip-clearance is the alteration of the value of leakage factor k. This is reflected in the change in shape of the meter calibration curve especially towards the lower range of flow. Increasing the tip-clearance increases the leakage factor but this does not go on indefinitely. There is a critical tip-clearance beyond which any further increase would result in a decrease of leakage factor (see Fig. 5.12). In general the tip-clearance of commercial turbine meters seldom reaches this critical value. One of the practical consequences of increasing the leakage factor is that it can be used advantageously, within limits, to offset the effects of the retarding torque opposing the motion of the rotor. For example, if a meter has a calibration curve that decreases with flow rate, then increasing the leakage factor would not only decrease the minimum flow the meter can measure but would also decrease the variation throughout most of the range as well (see Fig. 5.1). However, if the "hump" is present in the calibration curve, increasing the leakage factor would again reduce the minimum flow rate but it would, on the other hand, increase the variation as well (see Fig. 5.5).

As can be seen in Chapter 6, changing the tip-clearance can also be used advantageously to reduce the effect of velocity profile. However, care must be exercised because the same change affects various types of meter differently. Whilst increasing the tip-clearance of helical-blade rotors can reduce the effect of velocity profile, the same increase on constant blade angle rotors has the opposite effect (see Fig. 6.9). Therefore if it is required to reduce the "hump" of the calibration curve of a meter and if the meter has a constant blade angle rotor, it would best be done by decreasing the tip-clearance because it would decrease the effect of velocity profile as well. For a helical-blade rotor, the same double advantages cannot be achieved. However changing the tip-clearance can give another type of double advantage to the helical-blade rotor provided the meter has a calibration curve that decreases with decreasing flow rate. In this case increasing the tip-clearance would not only decrease the variation and the minimum flow rate the meter can measure but also reduce the effect of velocity profile.

10.2.2 Hub-ratio

The flow area through a turbine meter is primarily determined by the hub-ratio. As the presence of the hub in the path of the metered fluid tends to flatten the velocity profile in the rotor annulus, a meter having a larger hub-ratio would be affected less by the effect of inlet velocity profiles due either to partially developed profiles or to poor profiles caused by upstream disturbances. The effect of developing velocity profile can be seen from Fig. 6.8 and that due to upstream disturbance from Fig. 7.7 . A further advantage of having a flattened inlet velocity profile is the reduction of the angle of

attack on the blades (especially for a constant blade angle rotor) which thus reduces the likelihood of stalling on the blades. When stalling occurs there is a sudden change in meter coefficient (see Fig. 5.1). However it must be pointed out that one consequence of increasing the hub-ratio is to increase the head-loss across the meter (see Fig. 8.2) and the danger of cavitation.

If the tip-clearance is kept the same, increasing the hub-ratio also increases the ratio of the flow between that through the tip-clearance and that through the rotor itself. This means that increasing the hub-ratio would also increase the leakage factor k. This can be seen from Fig. 5.12. The practical significance of increasing the leakage factor was given in Section 10.2.1. In trying to get a bigger value of leakage factor, there is a big difference between increasing the tip-clearance and increasing the hub-ratio. While the former has hardly any effect on the bearing torque, the latter not only increases it significantly, because of the extra load caused by the heavier rotor, but also increases the surface area of the hub. Therefore the total resisting torque is increased. Since the main purpose of increasing the leakage factor is to offset the effect of resisting torque, this method of doing so is rather self-defeating. One way of overcoming this problem is to have a "converging" meter where the meter casing is made smaller than the pipe diameter. In this way most of the objectives of increasing the hub-ratio can be achieved equally well if not better.

10.2.3 Types of Blades

For turbine meters, there are generally two types of blade that can be chosen; namely, helical and constant angle. Selecting the

type of blade depends very much on the objectives of the design. If a meter is to be designed so that the effects of partially developed and poor velocity profiles on the meter calibrations are to be minimised, then the constant blade angle rotor is more suitable (see Fig. 6.8 and 7.6). However, care must be exercised if the tip-clearance has to be increased as well because when this is done, the profile effect is increased (see Fig. 6.9). If the meter has to measure very low flows, then a tip-clearance increase may be unavoidable. In such a case, sometimes it may be better to choose a helical-blade rotor instead since any increase in tip-clearance would decrease the profile effect (see Fig. 6.7). Because the constant blade angle rotor has a much larger angle of attack, the exit tangential velocity is also greater. Thus there is a greater head-loss on a meter with a constant blade angle rotor (see Fig. 8.2).

10.3 Design Considerations

From this research into the behaviour of meter calibration curves, it is evident that there is not a universal turbine meter design that can achieve all the desirable characteristics within one design. A design that is excellent in reducing the effect of developing velocity profile may not have the least variation in meter coefficient. Usually some sacrifice is necessary and it is up to the designer to assess the order of priorities he requires the meter to achieve. The design can then be optimised according to the priorities and to within the values specified. Therefore in any recommendations given in Appendix V, no values are quoted because they would depend on the priority of each specification and the specification itself. For each aspect of meter characteristic required, the direction which the values should take is given together with the consequences for doing so.

10.3.1 Design Equation

For the purpose of design, the Weinig lattice effect coefficient K and the coefficient of drag C_D can be assumed to be constant along the blade radius and the value K is taken as unity. Also for ease in computation uniform velocity can be assumed. Therefore, basing on the leakage theory, the equation of the meter coefficient for design is

$$\frac{n}{Q} = \left[\frac{n}{Q_r}\right]\left[1 - g + \frac{k}{Q}\right] \qquad \ldots \quad 10.1$$

where

$$\frac{n}{Q_r} = \frac{I(1)}{2\pi^2 . r_o^3 . B(1) . C(1)} - \frac{V(1)}{C_1 . \pi^2 . r_o^3 . B(1) . C(1)} - \frac{2 . T . [C(1)+D(1)]^2}{\rho . C_f . \pi . r_o . N . W . B(1) . C(1) . Q^2}$$

$$\ldots \quad 10.2$$

$$= \text{Term 1} - \text{Term 2} - \text{Term 3}$$

At high flow rates term 3 and $\frac{k}{Q}$ tend to zero while term 2 tends to a value that is small in comparison with term 1. Therefore the magnitude of the meter coefficient is determined by term 1 (or more accurately (term 1).(1-g)) and its value remains essentially the same throughout the flow rate.

10.3.2 Variation

When designing a turbine meter one of the aims is to reduce the variation of the meter calibration curve and at the same time to be able to use the meter to as low a flow as possible. In general the lowest flow rate a meter can measure is closely related to the varia-

tion required because both depend on the magnitude of the resisting torque T and the leakage factor k. Very often it is not possible to achieve a gain in one without sacrificing something for the other.

Suppose the design requirement is such that the meter must be able to measure exceptionally high flows in a certain system. In such a case the meter should be designed to have very small hub-ratio so as to reduce the average velocity going through the meter. Otherwise either cavitation may occur in the meter or the rotor may rotate too fast for the bearings to last for any reasonable period of time. If such a meter is to have a small tip-clearance ratio (e.g. < 0.015) the resulting calibration curve would decrease with decreasing flow rate (for an example of this type of calibration curve see Fig. 9.6). The rate at which the meter coefficient decreases (and hence the variation increases) with flow rate depends upon the magnitude of the resisting torque. Sometimes the variation within the flow range required is not acceptable and the design has to be improved. One method of doing this is to reduce the magnitude of term 3 in equation [10.2]. In practice this can be done in the following manner.

1) Reduce the bearing friction. The effect of this is shown in Fig. 9.6.
2) Increase the number of blades. This is shown in Fig. 9.5 where the number of blades is increased from 3 to 6. There is a limit to the number of blades a rotor can have because not only does the cost per unit go up with the number of blades required but also the difficulty of machining increases.
3) Increase the axial length of blades. The overall effect of this is not great and it is normally used for small adjustment only.

The other method of reducing the variation is to increase the leakage factor wither by changing the tip-clearance (see Section 10.2.1) or increasing the hub-ratio (see Section 10.2.2). In this particular design requirement where the meter has to measure exceptionally high flows, increasing the hub-ratio is not practicable as it also reduces the maximum flow rate the meter can measure.

Perhaps it should be pointed out that for a calibration curve that decreases with flow rate, as in the case described in the preceding paragraphs, reducing the variation also reduces the minimum flow the meter can measure. In most turbine meters the hub-ratio is comparatively large and 'humps' are usually present on the calibration curves. If the variation is found to be unacceptable, then the remedies opposite to those suggested previously can be applied. However, reducing the variation in this case would increase the minimum flow rate instead.

10.3.3 Range

The range of a meter is the ratio of the lowest flow rate to the maximum flow rate within a specified variation. The close relationship between the lowest flow rate and the variation has already been outlined in Section 10.3.2.

The maximum flow rate is governed by the maximum speed of rotation permissible which in turn depends on the stress allowable on the rotor blades, and on the bearings used. Two of the main variables manipulated in turbine meter design that can affect the range are the hub-ratio and the helical pitch (or blade angle). Increasing the hub-ratio or decreasing the helical pitch increases the speed of rotation. This of course lowers the maximum flow rate. Therefore, if a large

meter coefficient is desired, one can either increase the hub-ratio or decrease the pitch. However, there is a major difference in the two. In addition to the consequences mentioned in Section 10.2.2, increasing the hub-ratio is essentially decreasing the flow area through the meter and thus increasing the likelihood of cavitation. Therefore, the maximum speed of rotation is not only the governing factor on the range but cavitation in the meter is also a factor. On the other hand, decreasing the helical pitch does not appreciably increase the likelihood of cavitation.

10.4 Design Method

In the preceding sections, the effects of different parameters on particular aspects of meter performance for various types of meter were discussed. Recommendations for improving each aspect are given in Appendix V together with the consequences for employing them. A comprehensive design procedure, based on the leakage theory, is also given in the same appendix.

REFERENCES

1. HOCHREITER, H.M. — 'Dimensionless correlation of coefficients of turbine type flow meter'. Trans A.S.M.E. vol. 80, 1958 pages 1363-1368.

2. RUBIN, M., MILLER, R.W. and FOX, W.G. — 'Driving torque in a theoretical model of a turbine meter'. Trans A.S.M.E., Journal of Basic Engineering, vol.87, June 1965, pages 413-420.

3. LEE, W.F.Z. and KARLBY, H. — 'A study of viscosity effects and its compensation on turbine-type flowmeter'. Trans A.S.M.E., Journal of Basic Engineering, vol.82, Sept. 1960, pages 717-728.

4. MENKYNA, V. — 'Correction of the error curve of axial turbine liquid flow meters'. Proceedings of Third Conference on Fluid Mechanics and Fluid Machinery, 1969, Akademai Kiado, Budapest, pages 373-379.

5. SALAMI, L.A. — 'Scale and Reynold's number effects on some axial flow turbomachines'. Ph.D. Thesis 1971, Mech. Eng. Dept., University College, Cardiff. Chapter 4.

6. DURAND, W.F. — 'Aerodynamic Theory'. Vol.1, Div. B, Vertag Julius Springer, 1935, Durand Reprinting Committee, California Institute of Technology, Pasadena, California.

7. WEINIG, F. — 'Die Stromung um die Schaufeln von Turbomaschinen'. Johann Ambrosius Barth, Munich, 1935.

8. WISLICENUS, G.F. — 'Fluid Mechanics of Turbomachinery'. McGraw-Hill Book Company, Inc., New York, 1947.

9. JEPSON, P. and BEAN, P.G. — 'Effect of upstream velocity profiles on turbine flowmeter registration'. Journal of Mechanical Engineering Science, Vol.11, No.50. Oct. 1969, pages 503-510.

10. SALAMI, L.A. — 'Swirl effects on turbine type flowmeters and effectiveness of different types of flow straighteners'. Dept. of Mech. Eng., Southampton University, Report No. ME/72/3.

11. SCOTT, R.W.W. 'Turbine flowmeters'. Instruments, Electronics, Automation Year Book and Buyers Guide, 1967. pages 688-691.

12. IVES, G.O. 'Proving liquid meters'. Pipeline Gas Journal, Vol.197, August 1970. pages 56-61.

13. SUNLEY, H.L.G., SIMPKIN, A.J. and TOWNSEND, W.G. 'The effect of viscosity upon the performance of turbine type flowmeters'. Spaceflight, Vol.8, No.8, August 1966 page 283.

14. BOWERS, K., GALLEY, R.L. and VINCELETT, P.S. 'Flow measurement in rocketry'. Instrument Control System, Vol.34, 1961 pages 638-640.

15. GRANT, D.J. 'Precision flow measurement techniques for low thrust auxiliary propulsion liquid rockets'. NASA-TM-X-55967, 1967.

16. DUNLOP, A.R. and McCUTCHEON, C.A. 'New turbine-type meters for custody transfer of crude petroleum and petroleum products'. Oil Gas Journal, Sept. 1958 pages 83-85.

17. STRINGER, J.A. and BROTHERS, M.P. 'UK pipeline turbine meters are used for custody transfer'. Oil Gas Journal, Vol.65, pages 145-146.

18. KARLBY, H. and LEE, W.F.Z. 'Metering crude oil with a turbine'. ASME Paper No.59-PET-7.

19. MOBIL OIL CO. 'Mobil Oil Co. installs large in-line gasoline blenders'. Oil Gas Journal, 1964 Vol.62, page 195.

20. CALDWELL, B.J. 'Flow measurement Part 4: the fuel gas industry'. Mechanical Engineering, 1967 Vol. 89 pages 28-32.

21. CROSSCOMBE, A.T. 'The turbo-meter: new measuring device for gas'. Canada Gas Journal, 1966, Vol.59 pages 6-8.

22. STUBBS, P.S. 'Flow measurement in gas pipelines'. Gas World, 1970, Vol.172 pages 331-333.

23. ALSPACH, W.J. and FLYNN, T.M. 'Considerations when using turbine-type flowmeters in cryogenic service'. Advance in Cryogenic Engineering, Vol.10, Sec. F-3, page 246-252.

24. ALSPACH, W.J., MILLER, C.E. and FLYNN, T.M. 'Flow measurement Part 2: meas flow-meters in cryogenics'. Mechanical Engineering, 1967, Vol.89 pages 105-113.

25. BUCKNELL, R.L. 'Calibration systems and turbine type flow transducers for cryogenic flow measurement'. Advances in Cryogenic Engineering, 1963 Vol.8, Sec.F-5, pages 360-369.

26. GREY, J. 'Calibration of turbine flowmeters for cryogenic operation'. American Rocket Society Journal, 1960, Vol.30 page 192-193.

27. JEFFS, A.T. 'Comparative tests of turbine flow-meters with cryogenic fluids'. RPE Technical Note No.229, March 1964.

28. MINKIN, H.L., HOBART, H.F. and WARSHOWSKY, I. 'Performance of turbine type flowmeters in liquid hydrogen'. NASA TN-D-3770, December 1966.

29. SHAMP, F.F. 'Metering cryogenic liquids'. Oil Gas Journal, 1970, Vol.68, page 112-114.

30. DIJSTELBERGEN, H.H. 'Dynamic response of turbine flowmeters'. Instrument Revue, 1966 pages 241-244.

31. HIGSON, D.J. 'Transient performance of turbine flow-meter in water' Journal of Scientific Instruments, 1964, Vol.41, page 317-320.

32. GREY, J. 'Transient response of turbine flowmeter'. Jet Propulsion, 1956 Vol.57 page 61-63.

33. JEPSON, P. 'Transient response of a helical flow-meter'. Journal of Mechanical Engineer-ing Science, 1964, Vol.6 pages 337-342.

34. JEPSON, P. 'Method of measuring the time constants of current meters and turbine type flowmeters'. Journal Scientific Instrument, 1967, Vol.44 pages 17-20.

35. DIJSTELBERGEN, H.H. 'Rotameters and turbine flowmeters in pulsating flow measurement'. Paper presented at a symposium on the measure-ment of pulsating flow. University of Surrey, Guildford, 2-3 April, 1970.

36. HAALMAN, A. 'Pulsation errors in turbine flowmeters'. Control Engineering, 1965, Vol.5, pages 89-91.

37. DOWDELL, R.B. and LIDDLE, A.H. Jr. 'Measurement of pulsating flow with propeller and turbine type meters'. Transaction of ASME, 1953, Vol.75 page 961.

38. LEE, W.F.Z. and EVANS, H.J. 'Density effect and Reynold number effect on gas turbine flowmeters'. Journal of Basic Engineering, 1965, Vol.87, page 1043-1057.

39. WITHERS, V.R., INKLEY, F.A. and CHESTERS, D.A. 'Flow characteristics of turbine flowmeters'. Proceedings of International Conference on Modern Developments in Flow Measurement, Sept., 1971. Edited by C.G. Clayton. Published by Peter Peregrinus Ltd.

40. LEE, W.F.Z. and EVANS, H.J. 'A field method of determining gas turbine meter performance'. Trans. ASME. Journal of Basic Engineering, 1970, Vol.92, pages 724-731.

41. BETZ, A. 'Introduction to the theory of flow machines'. Pergamon Press London, 1st Edition. Page 250.

42. PRANDTL, L. and TIETJENS, O.G. 'Applied Hydro- and Aeromechanics'. Dover Publication, New York. Pages 201 and 207.

43. HOWELL, A.R., and CARTER, A.D.S. 'Fluid flow through cascades of aerofoils'. Sixth International Congress of Applied Mechanics, Paris, 1946.

44. THOMPSON, R.E. and GREY, J. 'Turbine Flowmeter Performance Model'. Trans A.S.M.E., Journal of Basic Engineering, 1970, Vol.92, pages 712-723.

45. HOWELL, A.R. 'Flow in cascades'. Aerodynamics of Turbines and Compressor, High Speed Aerodynamics and Jet Propulsion Vol X. Edited by HAWTHORNE, W.R.

46. TAN, P.A.K. and HUTTON, S.P. 'Experimental, analytical and tip clearance loss studies in turbine-type flowmeter'. Proceedings of the international conference on modern developments in flow measurement held at Harwell, 21st-23rd Sept. 1971. edited by C.G. Clayton. Published by Peter Peregrinus Ltd.

APPENDIX I

METER COEFFICIENT EQUATION

The values of I(n), Z(n) etc.in equation [3.26] are dimensionless values and given by the following equations

$$I(n) = \int_h^t K.\{2\tan\beta - \tan(\beta - \delta^*)\} \cdot \left(\frac{u}{U}\right)^2 \cdot \frac{r dr}{r_o^2} \qquad \text{I.1}$$

$$B(n) = \int_h^t K \cdot \left(\frac{u}{U}\right) \frac{r^2 dr}{r_o^3} \qquad \ldots \quad \text{I.2}$$

$$C(n) = \int_h^t \left(2r - \frac{N.t}{\pi}\right).\left(\frac{u}{U}\right) \cdot \frac{dr}{r_o^2} \qquad \ldots \quad \text{I.3}$$

$$D(n) = \int_t^{r_o} 2 \cdot \left(\frac{u}{U}\right) \frac{r.dr}{r_o^2} \qquad \ldots \quad \text{I.4}$$

$$V(n) = \int_h^t K.\left(\frac{v}{u}\right).\left(\frac{u}{U}\right)^2 \cdot \frac{r.dr}{r_o^2} \qquad \ldots \quad \text{I.5}$$

$$Z(n) = \int_h^t \frac{C_D.\tan\theta\left(\frac{u}{U}\right)^2 \cdot r.dr}{\cos\beta.\cos\theta.r_o^2} \qquad \ldots \quad \text{I.6}$$

Except for D(n) where integration is taken from the blade tip r_t to the meter casing r_o, the integrations for the rest are taken from the blade hub r_h to the blade tip r_t (i.e. from h to t). The n in I(n), Z(n) etc. must not be confused with the rotational speed but it is to denote whether the boundary layer thickness δ_m within the

meter annulus is greater or less than the tip-clearance.

When δ_m is less than the tip-clearance

i.e. $\delta_m \leqslant r_o - r_t$

then $n = 1$

In such a case the velocity profile of the flow within the rotor blades is uniform

i.e. $\frac{u}{U} = 1.0$ . . . I.7

The boundary layer thickness δ_m in the meter annulus is related to that in the pipe (i.e. δ). When the flow enters the meter annulus, it is assumed that δ is contracted proportionally to δ_m and the expression is given by equation [4.9].

When integrating, D(1) must be carried in two parts i.e. from r_t to $(r_o - \delta_m)$ and from $(r_o - \delta_m)$ to r_o.

$$\text{i.e.} \quad D(1) = \int_{r_t}^{r_o} 2.\left(\frac{u}{U}\right) \frac{rdr}{r_o^2}$$

$$= \int_{r_t}^{r_o-\delta_m} 2.\frac{rdr}{r_o^2} + \int_{r_o-\delta_m}^{r_o} 2.\left(\frac{u}{U}\right).\frac{rdr}{r_o^2}$$

When the boundary layer thickness δ_m is greater than the tip-clearance

i.e. $\delta_m > (r_o - r_t)$

then $n = 2.$

Except for D(2), integration for all other terms must be done in two

parts, i.e. from r_h to $(r_o - \delta_m)$ and from $(r_o - \delta_m)$ to r_t

e.g.

$$B(2) = \int_h^t K.(\frac{u}{U}) \frac{r^2 dr}{r_o^3}$$

$$= \int_{r_h}^{r_o-\delta_m} K . \frac{r^2 dr}{r_o^3} + \int_{r_o-\delta_m}^{r_t} K . (\frac{u}{U}) . \frac{r^2 dr}{r_o^3}$$

The empirical equations for the velocity profile, $(\frac{u}{U})$, within the meter annulus are given by equations [4.9] to [4.15] in Chapter 4.

For constant blade angle rotor tan β is a constant. For helical blade rotor

$$\tan \beta = \frac{2\pi r}{P} \qquad \ldots \quad I.8$$

where P is the helical pitch of the blades.

K, C_D and δ* are all functions of r. The Weinig lattice-effect coefficient K is solved numerically from equation [3.9], [3.10] and [3.11]. It is a function of r because the space-chord ratio (s/c) and the blade angle β (in the case of helical-blade rotors) are function of r.

The coefficient of drag C_D is given by equations [3.18] or [3.15] depending on whether the angle of attack is positive or negative. The deviation angle δ* is given by equations [3.3] or [3.4] depending also on whether the angle of attack is positive or negative. θ_i in equations [3.3] and [3.4] is the inlet velocity angle and it is given by

$$\tan \theta_i = \frac{2.\pi.r.n}{u}$$

$$= \frac{2.\pi^2.r_o^2.r}{(\frac{u}{U}).C(n)} (\frac{n}{Q_r}) \quad \ldots \quad I.9$$

The angle of attack α is given by

$$\alpha = \beta - \theta \quad \ldots \quad I.10$$

The value of θ is given in equation [3.20]

i.e. $$\tan \theta = \frac{\pi.r.n}{u} + \frac{\tan(\beta - \delta^*)}{2}$$

$$= \frac{\pi^2.r_o^2.r}{(\frac{u}{U}).C(n)} (\frac{n}{Q_r}) + \frac{\tan(\beta - \delta^*)}{2} \quad \ldots \quad I.11$$

It can be seen that the rotor coefficient equation [3.26] has to be solved numerically and this can be done by successive approximation. As all the other terms on the right hand side of the equation are small compared to the first term, the first approximation can be taken to be

$$\frac{n}{Q_r} = \frac{I(n)}{2.\pi^2.r_o^3.B(n).C(n)} \quad \ldots \quad I.12$$

The next approximation of (n/Q_r) can be calculated from equations [3.26] or [3.27], depending whether there is inlet swirl or not, by using the previous approximation. This is carried out until two consecutive approximations differ by not more than the accuracy desired.

The values of I(n), Z(n) etc. can be integrated numerically.

APPENDIX II

DERIVATION OF EMPIRICAL VELOCITY PROFILE IN METER ANNULUS

Radial Position (r_c) where the Linear Part of Velocity Profile Terminates

The three points in Fig. 4.8 are the plots of $\frac{r_c}{r_o}$ against the hub area ratio $(\frac{A_h}{A_o})$ where r_o is the pipe radius, A_h the hub area and A_o the pipe area. The values for r_c are obtained from the experimental plots in Fig. 4.5 and 4.6. When these points are plotted on a log-log scale, they fall into a straight line. By the method of least squares, the equation of the straight line was found to be

$$\log (\frac{r_c}{r_o}) = 0.15476 \log(\frac{A_h}{A_o}) + \log 1.0283$$

$$\frac{r_c}{r_o} = 1.0283 (\frac{A_h}{A_o})^{0.15476} \quad \ldots \quad 4.3$$

Gradient (z) of the Linear Part of Velocity Profile

The four points in Fig. 4.9 are the plot of gradient z against the hub area ratio. The values for z are the gradients of the linear part of the experimental velocity profiles in Fig. 4.5 and 4.6. The four points appear to form a rectangular hyperbola of the form

$$xy + ax + by + c = 0$$

Using the method of least squares, the equation obtained is

$$(\frac{A_h}{A_o}) . z - 0.3119 (\frac{A_h}{A_o}) + 0.0063696.z + 0.00013645 = 0$$

$$\therefore \quad z = - \frac{\left[0.00013645 - 0.3119 \left(\frac{A_h}{A_o}\right)\right]}{\left[\left(\frac{A_h}{A_o}\right) + 0.0063696\right]} \qquad \ldots \quad 4.2$$

Variation of the Reciprocal of Exponent of Power Law M

The values of M are obtained from the gradients of the straight line parts of the log-log plot in Fig. 4.7. These parts are actually the non-linear parts of the velocity profiles in Figs. 4.5 and 4.6. Fig. 4.10 shows the plot of M against the hub area ratio. Except for the 1½" diameter hub, they lie on a straight line. Using the method of least squares for the first three points, the equation of the line is

$$M = 21.752 \cdot \left(\frac{A_h}{A_o}\right) + 7.66$$

Since the value m of the power law equation for a pipe change with flow rate, the value 7.66 can be taken as m for the flow rate used in Fig. 4.10. Therefore, in general, the equation is

$$M = 21.752 \left(\frac{A_h}{A_o}\right) + m \qquad \ldots \quad 4.5$$

Empirical Velocity Profile in Meter Annulus

From the foregoing the linear part of the velocity profile in meter annulus is

$$\frac{u}{U} = - z \cdot \left(\frac{r - r_h}{r_o}\right) + 1 \qquad \ldots \quad 4.1$$

for $r_h < r < r_c$

and that for the non-linear part is

$$\frac{u}{U} = \left(1 - \frac{r}{r_o}\right)^{1/M}$$

for $r_c < r < r_o$

To make the two equations meet at r_c, the latter one must be modified to

$$\frac{u}{U} = Y \cdot \left(1 - \frac{r}{r_o}\right)^{1/M} \qquad \ldots \quad 4.4$$

where

$$Y = \frac{-z \cdot \left(\frac{r_c - r_h}{r_o}\right) + 1}{\left(1 - \frac{r_c}{r_o}\right)^{1/M}} \qquad \ldots \quad 4.5$$

APPENDIX III

DIMENSIONS OF RESEARCH ROTORS

Dimensions of all research rotors used.

Rotor Number	Type of blade	Hub-ratio (r_h/r_o)	Blade thickness t inches/metres	Tip-clearance ratios $(r_o-r_t)/r_o$
1 *	Helical	0.125	$0.050/1.27\times10^{-3}$	0.008,0.010
2 *	Helical	0.125	$0.046/1.17\times10^{-3}$	0.044,0.050
3	Helical	0.381	$0.073/1.85\times10^{-3}$	0.008,0.0155,0.022, 0.030,0.040,0.050.
4	Helical	0.753	$0.093/2.36\times10^{-3}$	0.0075,0.015,0.022, 0.030,0.040,0.050.
5	Constant angle $\beta = 32.644^{o}$	0.125	$0.060/1.52\times10^{-3}$	0.007,0.015,0.022, 0.030,0.040,0.050.
6	Constant angle $\beta = 35.716^{o}$	0.375	$0.062/1.57\times10^{-3}$	0.007,0.015,0.022, 0.030,0.040,0.050.

All rotors have the same following dimensions:-

i) Meter casing radius r_o = 1.000" (25.4×10^{-3} m)

ii) Helical pitch of rotors 1 to 4 only = 6.28" (159.5×10^{-3} m)

iii) Axial width W = 0.437" (11.1×10^{-3} m)

Rotor 1 is sometimes referred to as full-diameter rotor and rotor 2 as turned-down rotor.

* Rotors used by Jepson (9) and Salami (5).

APPENDIX IV

HEAD-LOSS ACROSS TURBINE METERS

IV.1 Head-loss H'_{2d} without Pressure Recovery

If there is no pressure recovery when fluid moves from planes (2) to (d), (see Figs. 8.1 and 3.1), then the head-loss H'_{2d} due to the hub is given by:-

$$H'_{2d} \int_{r_h}^{r_o} \rho.g.2\pi r.u_2.dr = \frac{\rho g}{2g} \{ \int_{r_h}^{r_o} 2\pi r.u_2^3.dr - \int_{o}^{r_p} 2\pi r.u_d^3.dr \}$$

$$H'_{2d} .U_2 . \int_{r_h}^{r_o} 2.(\frac{u}{U})_2 . \frac{r.dr}{r_o^2} = \frac{U_2^3}{2g} \{ \int_{r_h}^{r_o} 2 (\frac{u}{U})_2^3 . \frac{r.dr}{r_o^2} - (\frac{U_d}{U_2})^3 . \int_{o}^{r_p} 2.(\frac{u}{U})_2^3 . \frac{r.dr}{r_o^2}$$

$$\therefore \quad H'_{2d} .F(n) = \frac{U_2^2}{2g} \left[G(n) - (\frac{U_d}{U_2})^3 . H(n) \right] \qquad \ldots \quad IV.1$$

where F(n), G(n), H(n) are derived and given in Section IV.

The volume flow Q through the meter annulus is

$$Q = \int_{r_h}^{r_o} 2\pi r.u_2.dr$$

$$= \pi.r_o^2.U_2.F(n)$$

i.e. $$U_2 = \frac{Q}{\pi.r_o^2.F(n)} \qquad \ldots \quad IV.2$$

Applying the continuity equation between plane (2) and (d)

$$\int_{r_h}^{r_o} 2\pi r.u_2.dr = \int_{o}^{r_p} 2\pi r.u_d.dr$$

$$U_2.\pi.r_o^2.\int_{r_h}^{r_o} 2.\left(\frac{u}{U}\right)_2.\frac{r.dr}{r_o^2} = U_d.\pi.r_o^2.\int_{o}^{r_p} 2.\left(\frac{u}{U}\right)_d.\frac{r.dr}{r_o^2}$$

$$U_2.F(n) = U_d.I(n)$$

$$\therefore \quad \frac{U_d}{U_2} = \frac{F(n)}{I(n)} = J(n) \qquad \ldots \quad IV.3$$

Substituting equations IV.2 and IV.3 into IV.1

$$H'_{2d} = \frac{\left[G(n) - J(n)^3.H(n)\right].Q^2}{2g.\pi^2.r_o^4.F(n)^3} \qquad \ldots \quad IV.4$$

IV.2 Head-loss H'_{y2} without Pressure Recovery.

If there is no pressure recovery when fluid moves from planes (y) to (2), then the head-loss H'_{y2} due to the rotor blades is given by

$$H'_{y2}\int_{r_h}^{r_o} \rho g.2\pi.r.u_2.dr = \frac{\rho g}{2g}\left\{\int_{r_h}^{r_t}(2\pi r - N.t).u_y^3.dr + \int_{r_t}^{r_o} 2\pi r.u_y^3.dr - \int_{r_h}^{r_o} 2\pi r.u_2^3.dr\right.$$

$$\therefore \quad H'_{y2}.U_2.\int_{r_h}^{r_o} 2.\left(\frac{u}{U}\right)_2.\frac{r.dr}{r_o^2} = \frac{U_2^3}{2g}\left\{\left(\frac{U_y}{U_2}\right)^3.\left[\int_{r_h}^{r_t}\left(2r - \frac{N.t}{\pi}\right).\left(\frac{u}{U}\right)_y^3.\frac{dr}{r_o^2}\right.\right.$$

$$\left.\left. + \int_{r_t}^{r_o} 2.\left(\frac{u}{U}\right)_y^3.\frac{r.dr}{r_o^2}\right] - \int_{r_h}^{r_o} 2.\left(\frac{u}{U}\right)^3\frac{r.dr}{r_o^2}\right.$$

$$\therefore \quad H'_{y2} \cdot F(n) = \frac{U_2^2}{2g} \left\{ \left(\frac{U_y}{U_2}\right)^3 \cdot \left[L(n) + M(n) \right] - G(n) \right\} \qquad \text{IV.5}$$

Applying the continuity equation between planes (y) and (2)

$$\int_{r_h}^{r_t} (2\pi r - N.t).u_y.dr + \int_{r_t}^{r_o} 2\pi r.u_y.dr = \int_{r_h}^{r_o} 2\pi.r.u_2.dr$$

$$\therefore \quad U_y \left[C(n) + D(n) \right] = U_2.F(n)$$

$$\therefore \quad \frac{U_y}{U_2} = \frac{F(n)}{C(n)+D(n)} = K(n) \qquad \ldots \qquad \text{IV.6}$$

Substituting equations IV.2 and IV.6 into IV.5

$$H'_{y2} = \frac{\{K(n)^3 . [L(n) + M(n)] - G(n)\} . Q^2}{2g.\pi^2.r_o^4.F(n)^3} \qquad \ldots \qquad \text{IV.7}$$

IV.3 Head-losses H_{xy} and H_v

Referring to Fig. 3.1, H_{xy} is the head-loss between planes (x) and (y). Applying the Bernoulli equation between the two planes for an elemental radius dr,

$$H_{xy}\,\rho g\left\{\int_{r_h}^{r_t}(2\pi r-N.t).u.dr+\int_{r_t}^{r_o}2\pi.r.u.dr\right\}$$

$$=\rho g.\int_{r_h}^{r_t}\frac{(p_x-p_y)}{\rho.g}.(2\pi r-N.t).u.dr-\rho g.\int_{r_h}^{r_t}\frac{v_e^2}{2g}.(2\pi r-N.t).u.dr$$

. . . IV.8

Equating the axial forces acting on the elemental radius dr,

$$(p_x-p_y).(2\pi r-N.t).dr=\tfrac{1}{2}.\rho.N.W\left\{\frac{C_L\sin\theta}{\cos^2\theta.\cos\beta}+\frac{C_D.\cos\theta}{\cos^2\theta.\cos\beta}\right\}u^2\,dr$$

$$=\tfrac{1}{2}\rho\,N.W\left\{\frac{C_K\sin\alpha.\tan\theta}{\cos\theta.\cos\beta}+\frac{C_D}{\cos\theta.\cos\beta}\right\}u^2\,dr$$

. . . IV.9

Assuming the relative velocity at the blade outlet leaves the blade at the outlet blade angle, then $\delta^* = 0$

$$\therefore\quad\tan\theta=\frac{\pi rn}{u}+\frac{\tan\beta}{2}$$

$$\frac{\sin\alpha\tan\theta}{\cos\theta\cos\beta}=(\tan\beta-\tan\theta).\tan\theta$$

$$=\tan\beta.\tan\theta-\tan^2\theta$$

$$=\left(\frac{\pi rn}{u}\right).\tan\beta+\frac{\tan^2\beta}{2}-\left(\frac{\pi rn}{u}\right)^2-\left(\frac{\pi rn}{u}\right)\tan\beta-\frac{\tan^2\beta}{4}$$

$$=\frac{\tan^2\beta}{4}-\left(\frac{\pi rn}{u}\right)^2\qquad\text{. . . IV.10}$$

The total flow Q through the meter is

$$Q = \int_{r_h}^{r_t} (2\pi r - N.t)\, u.dr + \int_{r_t}^{r_o} 2\pi r.u.dr$$

$$= \pi . r_o^{\,2} . U . \left[C(n) + D(n) \right]$$

$$\therefore \quad U = \frac{Q}{\pi\, r_o^{\,2} . \left[C(n) + D(n) \right]} \qquad \ldots \quad \text{IV.11}$$

$$\therefore \quad \frac{n}{U} = \left(\frac{n}{Q}\right) . \pi\, r_o^{\,2} . \left[C(n) + D(n) \right] \qquad \ldots \quad \text{IV.12}$$

The coefficient of drag C_D is assumed to be constant along the blade.

Using equations [IV.9], [IV.10], [IV.11] and [IV.12]

$$\int_{r_h}^{r_t} (p_x - p_y).(2\pi r - N.t).u.dr = \tfrac{1}{2}\rho . N . W . \left[\int_{r_h}^{r_t} C_K . \frac{\tan^2\beta}{4} . u^3 . dr \right.$$

$$\left. - \int_{r_h}^{r_t} C_K . \pi^2 . n^2 . u . r^2 . dr + \int_{r_h}^{r_t} \frac{C_D . u^3 . dr}{\cos\theta . \cos\beta} \right]$$

$$\therefore \quad \int_{r_h}^{r_t} (p_x - p_y).(2\pi r - N.t).\left(\frac{u}{U}\right) . dr$$

$$= \tfrac{1}{2}\rho . N . W . U^2 . r_o \left[\int_{r_h}^{r_t} \frac{C_K \tan^2\beta}{4} \left(\frac{u}{U}\right)^3 . \frac{dr}{r_o} - \int_{r_h}^{r_t} C_K\, \pi^2 . \left(\frac{n}{U}\right)^2 . \left(\frac{u}{U}\right) \frac{r^2 dr}{r_o} \right.$$

$$\left. - \int_{r_h}^{r_t} \frac{C_D . \left(\frac{u}{U}\right)^3 . \frac{dr}{r_o}}{\cos\theta . \cos\beta} \right]$$

$$= \frac{\rho . C_1 . N . W . Q^2}{2\pi^2 . r_o^3 . [C(n)+D(n)]^2} \left[\int_{r_h}^{r_t} K . \frac{\tan^2\beta}{4} . \left(\frac{u}{U}\right)^3 . \frac{dr}{r_o} \right.$$

$$\left. - \left(\frac{n}{Q}\right)^2 . \pi^4 . r_o^6 . [C(n)+D(n)]^2 . \int_{r_h}^{r_t} K . \left(\frac{u}{U}\right) \frac{r^2 dr}{r_o^3} + C_D \int_{r_h}^{r_t} \frac{\left(\frac{u}{U}\right)^3 . \frac{dr}{r_o}}{\cos\theta . \cos\beta} \right]$$

$$= \frac{\rho . C_1 . N . W . Q^2}{2\pi^2 . r_o^3 . [C(n)+D(n)]^2} . \left[R(n) - \left(\frac{n}{Q}\right)^2 . \pi^4 . r_o^6 . [C(n)+D(n)]^2 . B(n) + \frac{C_D}{C_1} . T(n) \right]$$

$$= \frac{\rho . C_1 . N . W . Q^2}{2\pi^2 . r_o^3} . N(n) \qquad \ldots \quad \text{IV.13}$$

From the velocity diagrams in Fig. 3.1 for $\delta^* = 0$

$$v_e = u \tan\beta - 2\pi r n$$

$$\therefore \int_{r_h}^{r_t} \frac{v_e^2}{2g} (2\pi r - N.t) . \left(\frac{u}{U}\right) . dr$$

$$= \frac{1}{2g} \int_{r_h}^{r_t} \left[u \tan\beta - 2\pi r n \right]^2 . (2\pi r - N.t) . \left(\frac{u}{U}\right) . dr$$

$$= \frac{Q^2}{2g . \pi^2 . r_o^2 . [C(n)+D(n)]^2} \int_{r_h}^{r_t} \left[\left(\frac{u}{U}\right) . \tan\beta - 2\pi^2 . r_o^3 . \left(\frac{n}{Q}\right) . [C(n)+D(n)] . \frac{r}{r_o} \right]^2 (2\pi r - N.t) . \left(\frac{u}{U}\right) \frac{dr}{r_o^2}$$

$$= \frac{Q^2}{2g.\pi^2.r_o^2.[C(n)+D(n)]^2} \cdot U(n)$$

$$= \frac{Q^2}{2g\,\pi^2\,r_o^2} \cdot P(n) \qquad \ldots \quad IV.14$$

Substituting [IV.13] and [IV.14] into [IV.8]

$$H_{xy}.\pi.r_o^2.[C(n)+D(n)] = \frac{\rho.C_1.N.W.Q^2.N(n)}{\rho.g.2\pi^2.r_o^3} - \frac{P(n).Q^2}{2g.\pi^2.r_o^2}$$

$$H_{xy} = \frac{C_1.N.W.N(n).Q^2}{2g.\pi^3.r_o^3.[C(n)+D(n)]} - \frac{P(n).Q^2}{2g.\pi^3.r_o^4.[C(n)+D(n)]} \qquad IV.15$$

If the tangential velocity at the blade outlet is dissipated as head-loss H_v, then H_v is equal to the second term on the right hand side of equation [IV.15]

$$\therefore \qquad H_v = \frac{P(n) \cdot Q^2}{2g.\pi^2.r_o^4.[C(n)+D(n)]} \qquad \ldots \quad IV.16$$

IV.4 Evaluation of Integrals

If the boundary layer thickness in the pipe is δ, it is assumed that it contracts to $\delta \cdot \left[\frac{r_o-r_h}{r_p}\right]$ on entering the meter annulus. Thus the boundary layer thickness in the meter annulus can be in two conditions

$$(1) \qquad \delta \cdot \left[\frac{r_o-r_h}{r_p}\right] < (r_o - r_t)$$

(2) $\delta \cdot \left[\frac{r_o - r_h}{r_p}\right] \geqslant (r_o - r_t)$ where $(r_o - r_t)$ is the tip-clearance.

When integrating a function connected to flow in the meter annulus, the result of integration is represented by a dimensionless term, e.g. X(n), where n can be either (1) or (2) depending whether it is condition (1) or (2). When no blade is involved, e.g. planes (u), (1),(2) and (d), the value of n is always (2).

When integrating a function connected to flow in the pipe, e.g. planes (u) and (d), the substitution used is:-

$$\mu = 1 - \frac{r}{r_p}$$

$$\text{i.e. } \frac{r}{r_o} = (1 - \mu) \cdot \frac{r_p}{r_o}$$

$$= \frac{(1 - \mu)}{\psi} \quad , \quad \text{where } \psi = \frac{r_o}{r_p}$$

$$\therefore \frac{dr}{r_o} = -\frac{d\mu}{\psi}$$

when $r = 0$, $\mu = 1$

when $r = r_p - \delta$, $\mu = \frac{\delta}{r_p} = \lambda$

when $r = r_p$, $\mu = 0$

When integrating a function $\int_o^{r_p} f(r).dr$, the integration must be carried out in two parts,

$$\text{i.e. } \int_o^{r_p} f(r).dr = \int_o^{r_p - \delta} f(r).dr + \int_{r_p - \delta}^{r_p} f(r).dr$$

$$= \int_1^{\lambda} f(\mu).d\mu + \int_{\lambda}^{o} f(\mu).d\mu$$

The velocity profile in the pipe can be approximated by the power law equation, i.e.

$$\frac{u}{U} = \left(\frac{r_p - r}{\delta}\right)^{1/m} = \left(\frac{\mu}{\lambda}\right)^{1/m} \quad \ldots \quad \text{IV.17}$$

In fully developed flow $\delta = r_p$ and therefore $\lambda = 1$. The velocity profiles in planes (u) and (d) are $\left(\frac{u}{U}\right)_u$ and $\left(\frac{u}{U}\right)_d$ respectively and they are assumed to be as given in equation [IV.17]

$$\text{i.e.} \quad \left(\frac{u}{U}\right)_u = \left(\frac{u}{U}\right)_d = \left(\frac{r_p - r}{\delta}\right)^{1/m} = \left(\frac{\mu}{\lambda}\right)^{1/m} \quad \ldots \quad \text{IV.18}$$

For $r < (r_p - \delta)$, $\frac{u}{U} = 1$

When integrating a function connected to flow in the meter annulus, i.e planes (1), (x), (y) and (2), the substitution used is:-

$$\eta = 1 - \frac{r}{r_o}$$

$$\text{i.e.} \quad \frac{r}{r_o} = 1 - \eta$$

$$\therefore \quad \frac{dr}{r_o} = -d\eta$$

when $r = r_h$, $\eta = 1 - \frac{r_h}{r_o} = 1 - \phi$

when $r = r_o - \delta \cdot \frac{(r_o - r_h)}{r_p}$, $\eta = \frac{\delta}{r_p}\left(1 - \frac{r_h}{r_o}\right) = \lambda(1 - \phi)$

when $r = r_t$, $\eta = 1 - \frac{r_t}{r_o} = 1 - \gamma$

when $r = r_o$, $\eta = 1 - \frac{r_o}{r_o} = 0$

When integrating a function $\int_{r_h}^{r_o} f(r).dr$, the integration must be carried out in two parts,

i.e. $$\int_{r_h}^{r_o} f(r).dr = \int_{r_h}^{r_o-\delta\frac{(r_o-r_h)}{r_p}} f(r).dr + \int_{r_o-\delta\frac{(r_o-r_h)}{r_p}}^{r_o} f(r).dr$$

$$= \int_{1-\phi}^{\lambda(1-\phi)} f(\eta).d\eta + \int_{\lambda(1-\phi)}^{o} f(\eta).d\eta$$

The velocity profile on entering the meter annulus is assumed to be contracted proportionally between the rotor hub and the meter casing. The new velocity profile is:-

$$\frac{u}{U} = \left(\frac{r_o-r}{\delta} \cdot \frac{r_p}{r_o-r_h}\right)^{1/M}$$

$$= \left(\frac{r_p}{\delta} \cdot \frac{r_o}{r_o-r_h}\right)^{1/M} \cdot \left(\frac{r_o-r}{r_o}\right)^{1/M}$$

$$= \left[\frac{1}{\lambda(1-\phi)}\right]^{1/M} \cdot \eta^{1/M}$$

$$= \quad \cdot \eta^{1/M} \qquad \ldots \qquad \text{IV.19}$$

where M is assumed to follow equation [4.5]

i.e. $$M = 21.752\left(\frac{A_h}{A_o}\right) + m \qquad \ldots \qquad \text{IV.20}$$

and $$= \left[\frac{1}{\lambda(1-\phi)}\right]^{1/M}$$

The velocity profiles in planes (1),(x),(y) and (2) are $\left(\frac{u}{U}\right)_1$,

$(\frac{u}{U})_x$, $(\frac{u}{U})_u$ and $(\frac{u}{U})_2$ respectively and they are assumed to be the same as equation [IV.19]

i.e. $$\frac{u}{U} = (\frac{u}{U})_1 = (\frac{u}{U})_x = (\frac{u}{U})_y = (\frac{u}{U})_2 = \zeta \cdot (1 - \frac{r}{r_o})^{1/M}$$

$$= \zeta \cdot \eta^{1/M} \quad \ldots \quad \text{IV.21}$$

If a more accurate velocity profile in the meter annulus is required for fully developed flow, the empirical equations developed in Chapter 4 can be used instead of equation [IV.21] . In this case, it is more convenient to use numerical integration instead.

Note that for $r < r_p - \delta\frac{(r_o - r_h)}{r_p}$, $\frac{u}{U} = 1$.

To show that $\int_o^{r_p} 2 \cdot (\frac{u}{U})_d^3 \cdot \frac{r\,dr}{r_o^2} = H(2) = H(n)$

$$\int_o^{r_p} 2 (\frac{u}{U})_d^3 \cdot \frac{r\,dr}{r_o^2}$$

$$= \int_o^{r_p-\delta} 2r \cdot \frac{dr}{r_o^2} + \int_{r_p-\delta}^{r_p} 2 \cdot (\frac{u}{U})^3 \cdot \frac{r.dr}{r_o^2}$$

$$= \int_1^{\lambda} \frac{2(1-\mu)}{\psi} (\frac{-d\psi}{\psi}) + \int_{\lambda}^{o} \frac{2(1-\mu)}{\psi} (\frac{\mu}{\psi})^{3/m} \cdot (\frac{-du}{\psi})$$

$$= \int_1^{\lambda} \frac{2(1-\mu)}{\psi^2} \cdot (-d\mu) + \int_o^{\lambda} \frac{2}{\psi^2 . \lambda^{3/m}} \cdot \sum_{n=o}^{n=1} (-1)^n \binom{1}{n} \cdot \mu^{n+3/m} \cdot du$$

$$= \left[\left(\frac{1-\mu}{\psi} \right)^2 \right]_{\mu=1}^{\mu=\lambda} + \left[\frac{2}{\psi^2 . \lambda^{3/m}} \sum_{n=o}^{n=1} \frac{(-1)^n . \binom{1}{n} . \mu^{n+1+3/m}}{n + 1 + 3/m} \right]_{\mu=o}^{\mu=\lambda}$$

$$= H(2)$$

To show that $\int_{r_h}^{r_t} (2.r - \frac{N.t}{\pi}) . (\frac{u}{U})_y^3 . \frac{dr}{r_o^2} = L(n)$

For condition (1) i.e. $\delta . \left[\frac{r_o - r_h}{r_p} \right] < (r_o - r_t)$

$$\int_{r_h}^{r_t} (2r - \frac{Nt}{\pi}) (\frac{u}{U})_y^3 . \frac{dr}{r_o^2}$$

$$= \int_{r_h}^{r_t} (2r - \frac{Nt}{\pi}) \frac{dr}{r_o^2}$$

$$= \int_{1=\phi}^{1-\gamma} \{ 2(1-\eta) - \frac{Nt}{\pi . r_o} \} (-d\eta)$$

$$= \left[(1-\eta)^2 + \frac{Nt.\eta}{\pi . r_o} \right]_{\eta = 1-\phi}^{\eta = 1-\gamma}$$

$$= L(1)$$

For condition (2) i.e. $\delta \left[\frac{r_o - r_h}{r_p} \right] \geq (r_o - r_t)$

$$\int_{r_h}^{r_t} (2r - \frac{Nt}{\pi}) \cdot (\frac{u}{U})^3 \cdot \frac{dr}{r_o^2}$$

$$= \int_{1-\phi}^{\lambda(1-\phi)} \{2(1-\eta) - \frac{Nt}{\pi . r_o}\}(-d\eta) + \int_{\lambda(1-\phi)}^{1-\gamma} \zeta^3 \{2(1-\eta)\eta^{3/M} - \frac{N.t.\eta^{3/M}}{\pi . r_o}\}(-d\eta)$$

$$= \left[(1-\eta)^2 + \frac{N.t.\eta}{\pi . r_o}\right]_{\eta=1-\phi}^{\eta=\lambda(1-\phi)} + \left[2.\zeta^3 . \sum_{n=o}^{n=1} \frac{(-1)^n \binom{1}{n} \eta^{n+1+3/M}}{n+1+3/M} - \frac{N.t.\eta^{3/M+1}}{(3/M+1).\pi . r_o}\right]_{\eta=(1-\gamma)}^{\eta=\lambda(1-\phi)}$$

$$= L(2)$$

In general $\int_{r_h}^{r_t} (2r - \frac{N.t}{\pi}) \cdot (\frac{u}{U})_y^3 \cdot \frac{dr}{r_o^2} = L(n)$

Integration connected to planes (u) and (d)

$$I(n) = I(2) = \left[(\frac{1-\mu}{\psi})^2\right]_{\mu=1}^{\mu=\lambda} + \left[\frac{2}{\psi^2 . \lambda^{1/m}} \sum_{n=o}^{n=1} \frac{(-1)^n \binom{1}{n} \mu^{n+1+1/m}}{n+1+1/m}\right]_{\mu=o}^{\mu=\lambda}$$

$$H(n) = H(2) = \text{"} + \left[\frac{2}{\psi^2 . \lambda^{3/m}} \sum_{n=o}^{n=1} \frac{(-1)^n \binom{1}{n} . \mu^{n+1+3/m}}{n+1+3/m}\right]_{\mu=o}^{\mu=\lambda}$$

Integration connected to planes (1) and (2)

$$F(n) = F(2) = \left[(1-\eta)^2\right]_{\eta=1-\phi}^{\eta=\lambda(1-\phi)} + \left[2.\zeta \sum_{n=o}^{n=1} \frac{(-1)^n.\binom{1}{n}.\eta^{n+1+1/M}}{n+1+1/M}\right]_{\eta=o}^{\eta=\lambda(1-\phi)}$$

$$G(n) = G(2) = \text{"} + \left[2.\zeta^3 \sum_{n=o}^{n=1} \frac{(-1)^n.\binom{1}{n}.\eta^{n+1+3/M}}{n+1+3/M}\right]_{\eta=o}^{\eta=\lambda(1-\phi)}$$

$$J(n) = \frac{F(n)}{I(n)}$$

Integration connected to planes (x) and (y)

$C(n) = C(1)$ or $C(2)$

$$C(1) = \left[(1-\eta)^2 + \frac{N.t.\eta}{\pi.r_o}\right]_{\eta=1-\phi}^{\eta=1-\gamma}$$

$$C(2) = \left[\text{"} + \text{"}\right]_{\eta=(1-\phi)}^{\eta=\lambda(1-\phi)} + \left[2.\zeta \sum_{n=o}^{n=1} \frac{(-1)^n.\binom{1}{n}.\eta^{n+1+1/M}}{n+1+1/M} - \frac{N.t.\eta^{1/M+1}}{(1/M+1).\pi.r_o}\right]_{\eta=(1-\gamma)}^{\eta=\lambda(1-\phi)}$$

$$D(n) = \left[(1-\eta)^2\right]_{(1-\gamma)}^{\lambda(1-\phi)} + \left[2.\zeta \sum_{n=o}^{n=1} \frac{(-1)^n.\binom{1}{n}.\eta^{n+1+1/M}}{n+1+1/M}\right]_{o}^{\lambda(1-\phi)}$$

$$D(2) = \left[\text{"}\right]_{o}^{(1-\gamma)}$$

$$L(n) = L(1) \text{ or } L(2)$$

$$L(1) = \left[(1-\eta)^2 + \frac{N.t.\eta}{\pi . r_o} \right]_{(1-\phi)}^{(1-\gamma)} = C(1)$$

$$L(2) = \left[\text{"} + \text{"} \right]_{(1-\phi)}^{\lambda(1-\phi)} + \left[2.\zeta^3 \sum_{n=o}^{n=1} \frac{(-1)^n.\binom{1}{n}.\eta^{n+1+3/M}}{n+1+3/M} - \frac{N.t.\eta^{1/M+1}}{(1/M+1).\pi.r_o} \right]_{(1-\gamma)}^{\lambda(1-\phi)}$$

$$M(n) = M(1) \text{ or } M(2)$$

$$M(1) = \left[(1-\eta)^2 \right]_{(1-\gamma)}^{\lambda(1-\phi)} + \left[2.\zeta^3 \sum_{n=o}^{n=1} \frac{(-1)^n.\binom{1}{n}.\eta^{n+1+3/M}}{n+1+3/M} \right]_{o}^{\lambda(1-\phi)}$$

$$M(2) = \left[\text{"} \right]_{o}^{1-\gamma}$$

$$K(n) = \frac{F(n)}{C(n)+D(n)}$$

The following integrals have to be integrated numerically. Note that K is determined from equations [3.9] to [3.11] .

$$R(n) = \int_{r_h}^{r_t} \frac{K.\tan^2\theta}{4} . \left(\frac{u}{U}\right)^3 . \frac{dr}{r_o}$$

$$B(n) = \int_{r_h}^{r_t} K. \left(\frac{u}{U}\right) \frac{r^2 dr}{r_o^3}$$

$$T(n) = \int_{r_h}^{r_t} \frac{\left(\frac{u}{U}\right)^3 . \frac{dr}{r_o}}{\cos\theta . \cos\beta}$$

$$N(n) = R(n) - \left(\frac{n}{Q}\right)^2 . \pi^4 . r_o^6 . \left[C(n) + D(n)\right]^2 . B(n) + \frac{C_D}{C_1} . T(n)$$

$$= R(n) - \left(\frac{n}{Q_r}\right)^2 . \pi^4 . r_o^6 . C(n)^2 . B(n) + \frac{C_D}{C_1} . T(n)$$

APPENDIX V

DESIGN PROCEDURE

V.1 Design Recommendations

The following recommendations are for improving each individual aspect of turbine meter performance. When improving one aspect, the consequences on other aspects are given in the comment column. The symbols used and their meanings are as follows:-

(+) represents an improvement

(-) represents a deterioration

Improvements required	Comments
1. To reduce variation	See Section 10.3.2
1.1 For calibration curves with a 'hump'	
a) Increase term 3 of eqn. [10.2]	Min. flow rate (-)
by (i) reducing number of blades	Head-loss (+)
(ii) reducing axial width of blades	Head-loss (+)
(iii) increasing bearing torque	Head-loss (-)
b) Decrease leakage factor by	
(i) decreasing tip-clearance	Profile effect (- for helical-blade; + for constant blade angle).
	Min. flow rate (-)
(ii) decreasing hub-ratio	Head-loss (+)
	Profile effect (-)
	Disturbance effect (-)
	Max. flow rate (+)

1.2 For calibration curve that decreases with decreasing flow rate. Remedies opposite to those given in 1.1	See Section 10.3.2
2. <u>To reduce minimum flow rate measurable</u>	See Section 10.3.2
a) Reduce term 3 of eqn. [10.2] by	
(i) increasing number of blades	Head-loss (-)
(ii) increasing axial width of blades	Head-loss (-)
(iii) reducing bearing torque	Head-loss (+)
b) Increase leakage factor	Variation (- for calibration with 'hump'; + for calibration that decreases with flow rate)
by (i) increasing tip-clearance	Profile effect (+ for helical-blade; - for constant blade angle)
(ii) increasing hub-ratio	Head-loss (-) Profile effect (+) Disturbance effect (+) Max. flow rate (-)
3. <u>To increase maximum flow rate</u>	See Section 10.3.3. Head-loss (+) Min. flow rate (-) Variation (+ for calibration with hump; - for calibraction decreasing with decreasing flow).

(i) decreasing hub-ratio	Profile effect (-) Disturbance effect (-).
(ii) increasing helical pitch (or blade angle in constant angle blade)	
4. <u>To reduce profile effects</u>	See Chapter 6.
by (i) increasing hub-ratio	Head-loss (-) Disturbance effect (+) Min. flow rate (+) Variation (- for calibration with hump; + for calibration decreasing with flow) Max. flow rate (-)
(ii) using constant blade angle rotor instead of helical-blade	Head-loss (-)
(iii) for helical-blade rotor, increase tip-clearance	Variation (- for calibration with hump; + for calibration decreasing with decreasing flow) Min. flow rate (+)
(iv) for constant blade angle rotor,	Variation (+ for calibration with hump; - for calibration decreasing with decreasing flow) Min. flow rate (-)

5. <u>To reduce upstream disturbance effect</u>	See Chapter 7.
Use flow straightener.	Head-loss (-)
In addition	
(i) Increase hub-ratio	Head-loss (-) Profile effect (+) Min. flow rate (+) Max. flow rate (-) Variation (- for calibration with hump; + for calibration decreasing with flow rate)
(ii) Use constant blade angle rotor	Head-loss (-)
6. <u>To reduce effect of change in bearing torque</u>	See Chapter 9.
by (i) increasing number of blades	Head-loss (-) Variation (- for calibration with 'hump'; + for calibration decreasing with decreasing flow) Min. flow rate (+)
(ii) increasing hub-ratio	Head-loss (-) Variation (- for calibration with 'hump'; + for calibration decreasing with decreasing flow) Min. flow rate (+) Max. flow rate (-) Profile and disturbance effect (+)

V.2 Design Procedure

Because so many parameters are involved in turbine meter design and because varying one parameter to achieve a certain effect can at the same time adversely affect other aspects of meter performance, systematic design is not as straight forward as one would like. If the meter dimensions are to be determined by manipulating the design equation alone, the number of unknown variables involved would prevent any further computation. In the design procedure proposed in this section, only those dimensions that can be calculated using the specification given are tentatively determined and the rest of the dimensions are estimated in the light of the priorities of the design objectives and the values of the specification given. Each aspect of meter performance is quantified and then checked systematically to see if it falls within the specified value. If not, the necessary modifications are carried out. Sometimes it may be well within the specification and if the head-loss across the turbine meter is to be kept as low as possible, then modifications in the opposite direction are carried out. Therefore the initial estimates need not be correct. However the greater the accuracy of the initial estimates, the faster would the design be completed.

V.2.1 Flow Chart of Design Procedure

The proposed design procedure is based on the leakage theory and is given in the form of a flow chart as shown in Figs 10.2 to 10.14. At various stages of the design rough sketches are given at the side of the flow chart to show how the meter is behaving. Sometimes it is not possible to meet all the design specifications and some compromise is therefore necessary. This is up to the designer to decide for himself depending on the priorities of each specification. For example,

if the effect of upstream disturbance is more important, then it is better to make some sacrifices on the minimum flow rate measurable or on the variation of meter coefficient.

Each step of the flow chart is given a code by its side. The flow chart is complete by itself and the reasons behind each step will be clear if Section 10.3 is consulted. Some of the steps that need further expansion are described in the following paragraphs.

M2 & M3 If the metered fluid is a liquid, the minimum flow area A_{min} is calculated using as a criterion, cavitation at the specified maximum flow rate Q_{max} at circuit pressure. In the case of gas, the criterion is when choking occurs at sonic velocity. The flow area A_{dn} for design must therefore be chosen greater than A_{min}.

M4 Two types of meter casing can be selected

i) 'Straight-through' meter where $r_o = r_p$

ii) 'converging' meter where $r_o < r_p$

The 'Straight-through' meter is easier to manufacture and it is generally selected. However if the influence of profile is to be kept to the absolute minimum and the rotor is required to be as light as possible, then it is better to select a 'converging' meter right away.

M5,A,B & C Here the blade tip radius r_t, the blade thickness t, the number of blades N and the axial width W of the blades are approximated. Good starting values are as follows.

$$r_t = 0.98\ r_o$$

$$t = 0.05\ r_o$$

$$N = 5 \text{ to } 8$$

$$W = 0.5 r_o.$$

M6 The hub radius can now be calculated.

$$A_{dn} = \pi(r_o^2 - r_h^2) - N.t(r_t - r_h)$$

M7 The type of bearings is now selected. Knowing the bearings, the maximum speed of rotation n_{max} and the bearing torque can be obtained from the specification. It is good policy to keep the bearing torque as low as possible at this stage.

The maximum coefficient the meter can have is calculated i.e. $MC_{max} = \frac{n_{max}}{Q_{max}}$. The design meter coefficient MC_{dx} will be less than MC_{max}.

M8 Two types of blade can be selected i.e.

i) helical-blade

ii) constant angle blade.

As the case may be, the helical pitch P or the blade angle β can be calculated.

For a helical-blade rotor

$$MC_{max} = \frac{1}{P.A_{dx}}$$

For a constant blade angle rotor

$$MC_{max} = \frac{3.\tan\beta.(r_t^2 - r_h^2)}{4.\pi.(r_t^3 - r_h^3).A_{dx}}$$

M9 This is the first of a series of tests to see if the meter conforms to the design specifications. Here it is to test the effect of upstream disturbances e_d at distance D_m from the disturbance. For a partially closed gate valve, the effect can be read off or interpolated from Fig. 7.7.

M10 The effect of developing velocity profile (i.e. profile effect) can be read or interpolated from Fig. 6.8 or calculated theoretically using the meter coefficient equation.

M11 & M12 As all the relevant parameters are known, the leakage factor k can be read or interpolated from Figs 5.12 and 5.13. Hence the meter coefficients, MC_{dx} and MC_{min}, at maximum flow rate Q_{max} and minimum flow rate Q_{min} can respectively be calculated using equation [10.1]. It is better at this stage to calculate the meter coefficient MC at a number of other flow rates so that a rough calibration curve can be sketched. This will make the checking of the variation in the subsequent steps easier.

M13 to M18 The remaining steps are self-explanatory. They are concerned with ascertaining the shape of the calibration curve and checking whether the variation v_a and the minimum flow rate Q_{min} are within the values specified. If not appropriate remedies are taken as shown.

M19 This step is to check if the meter coefficient MC_{dx} at the maximum flow rate is below the maximum permissible meter coefficient MC_{max}. This sometimes happens because of modifications to suit certain design specifications. If MC_{dx} is much greater than MC_{max} and therefore not acceptable, the design has to be modified by increasing the flow area. When this is done, sometimes it conflicts with other specifications being met and thus a compromise has to be made.

M20 The necessary specifications have been met. Sometimes the variation and the minimum flow rate are smaller than required. If head-loss is important, the design can be improved to reduce the loss by bringing v_a and Q_{max} nearer to the specified values.

The rest of the flow chart is concerned with improving the meter design to meet the necessary specifications. The reasons behind each step will be apparent if the recommendations given in Section V.1 are consulted.

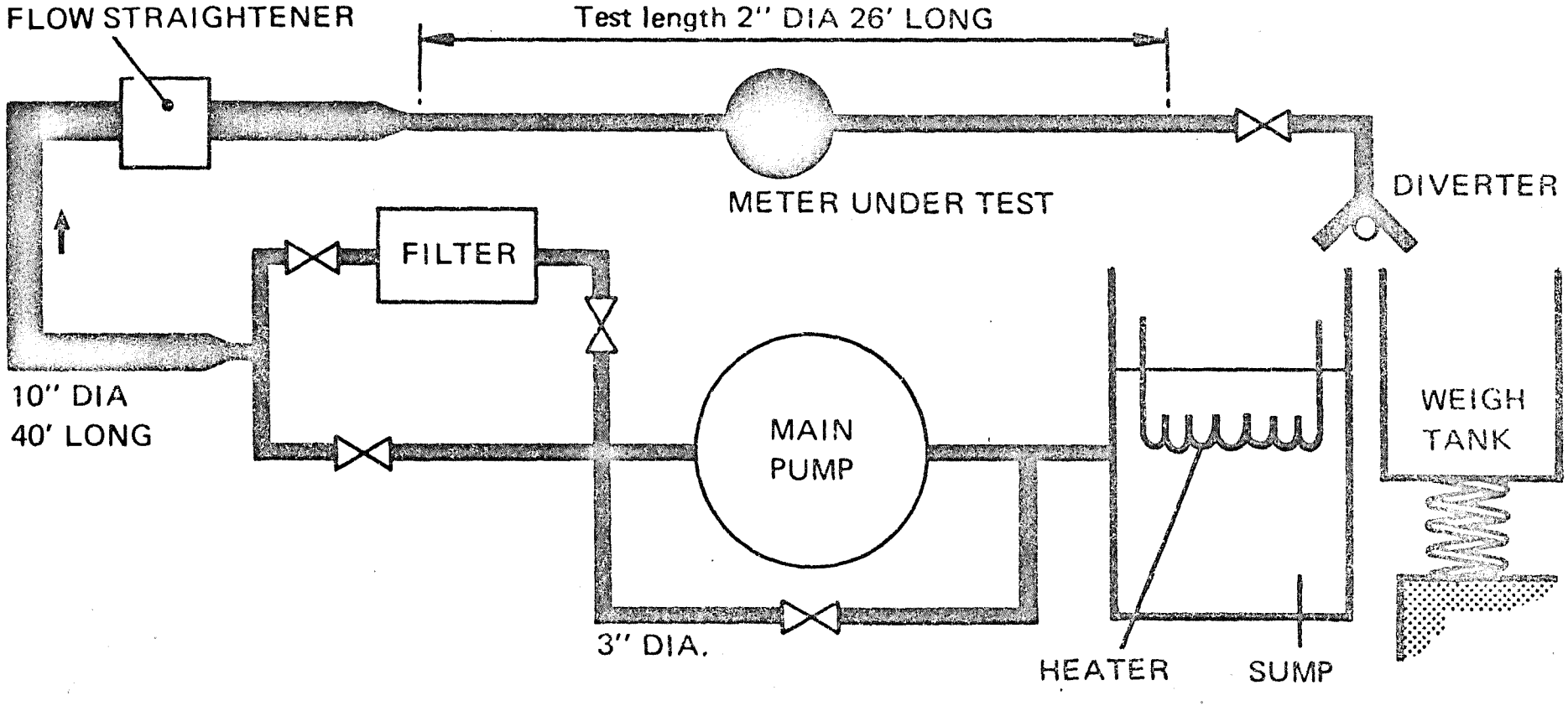

Fig. 2.1 Schematic Diagram of Test Rig

Fig. 2.2 Block Diagram of Control System

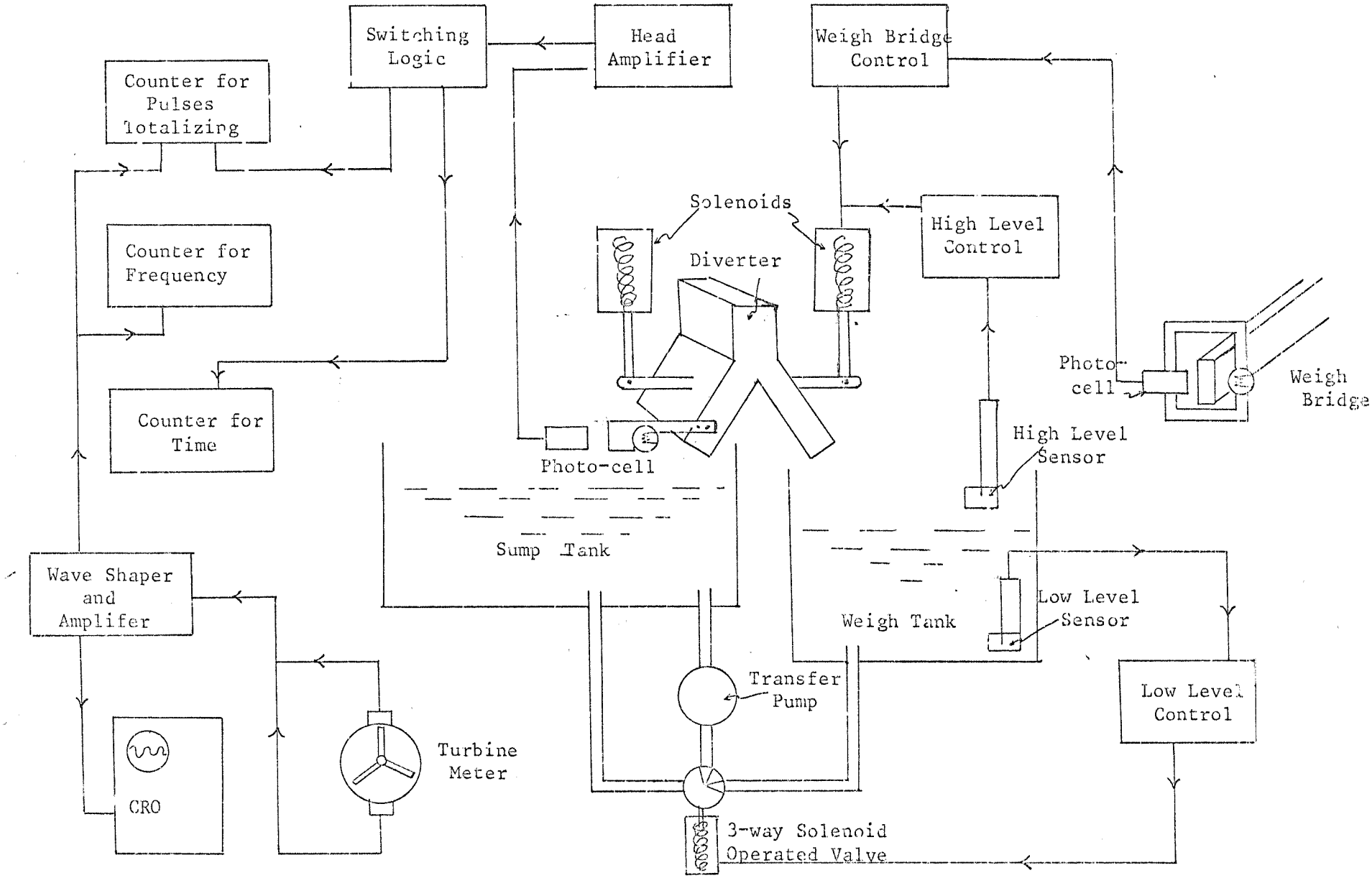

Fig. 2.3 Difference between Static and Dynamic Weighing for Different amount of Water collected in Weigh Tank

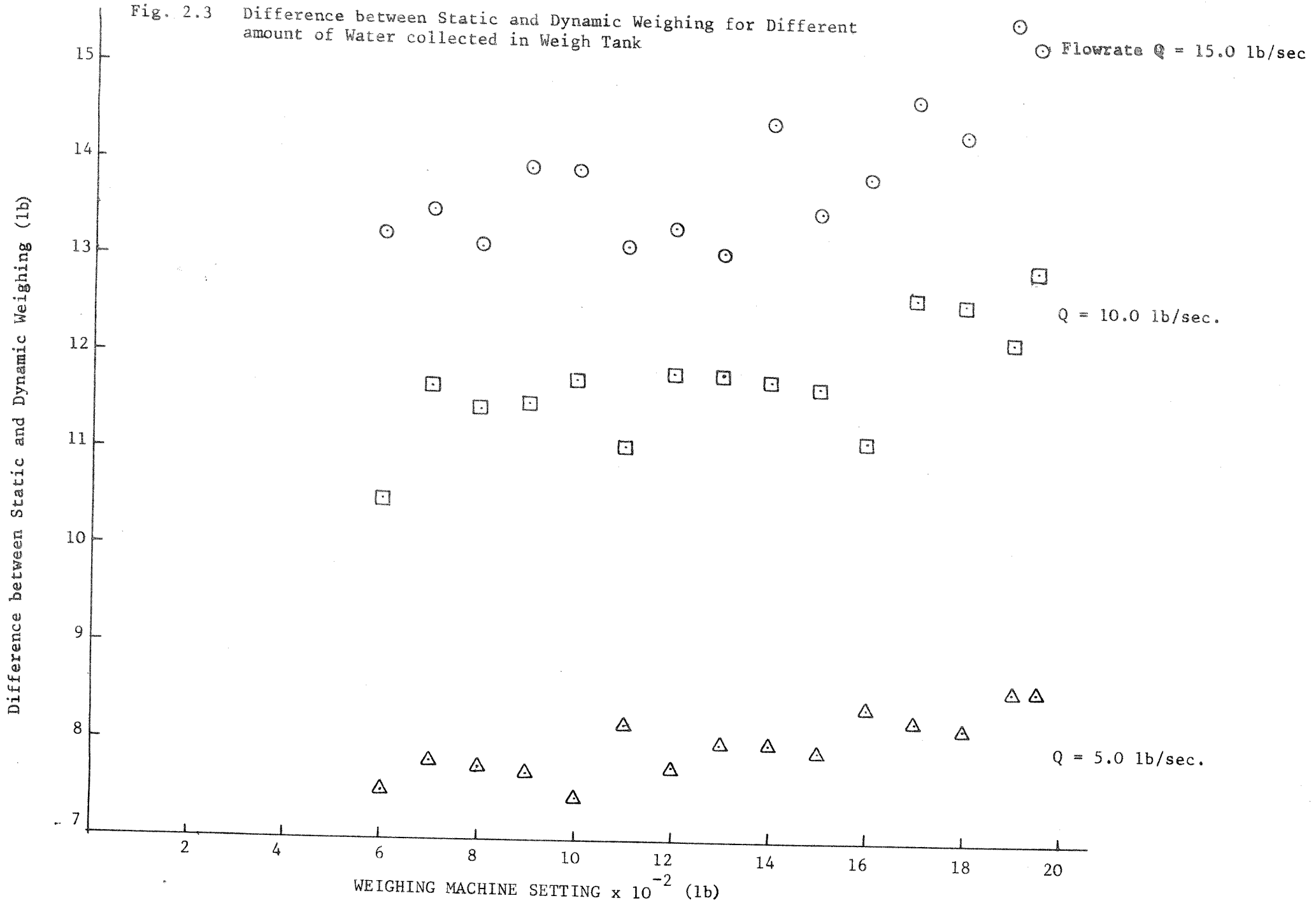

Fig. 2.4 Error in Dynamic Weighing (Water collected = 1300 lb).

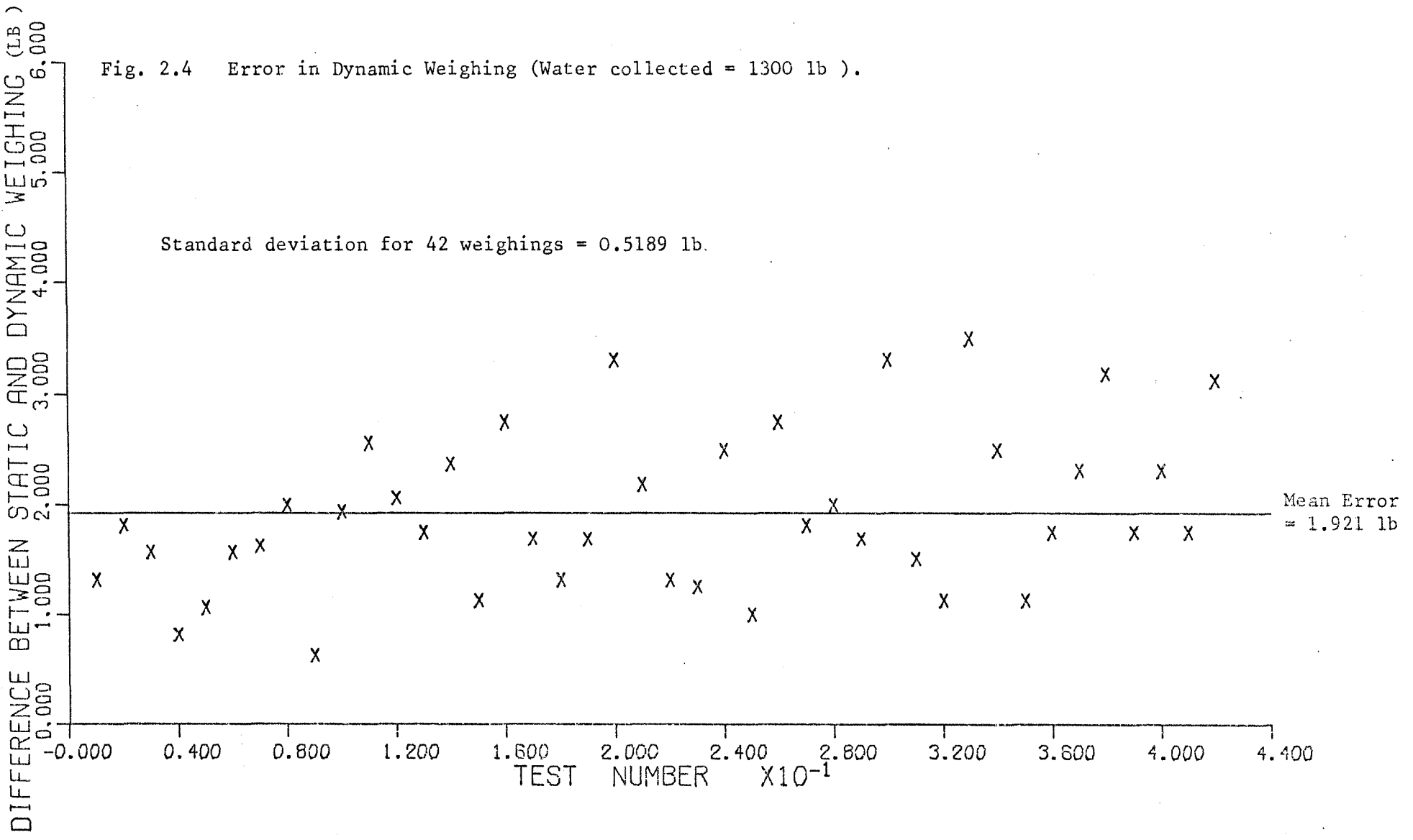

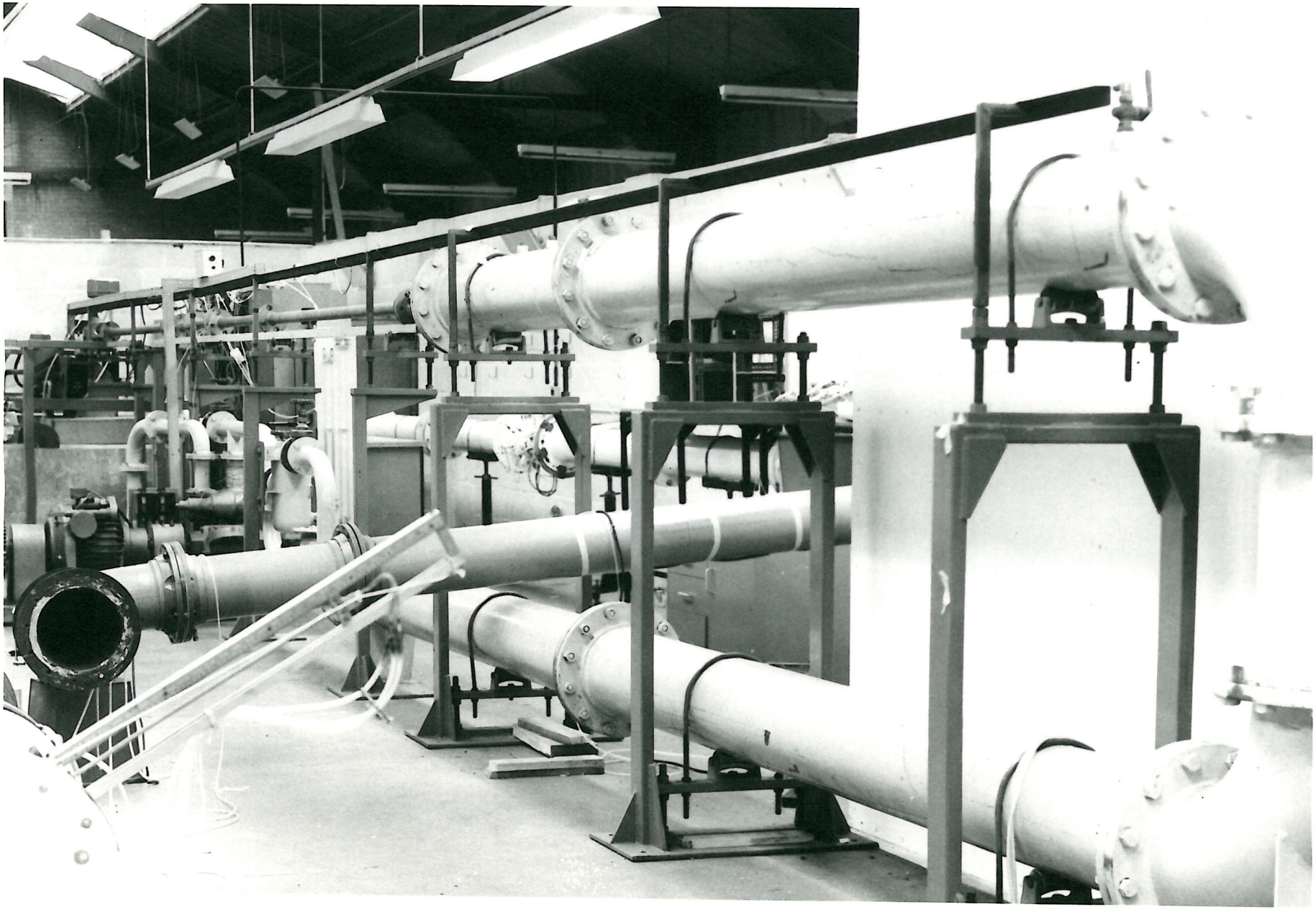

Fig. 2.5 Calibration Rig Showing the 10" dia. Pipe and the 2" dia. Test Length

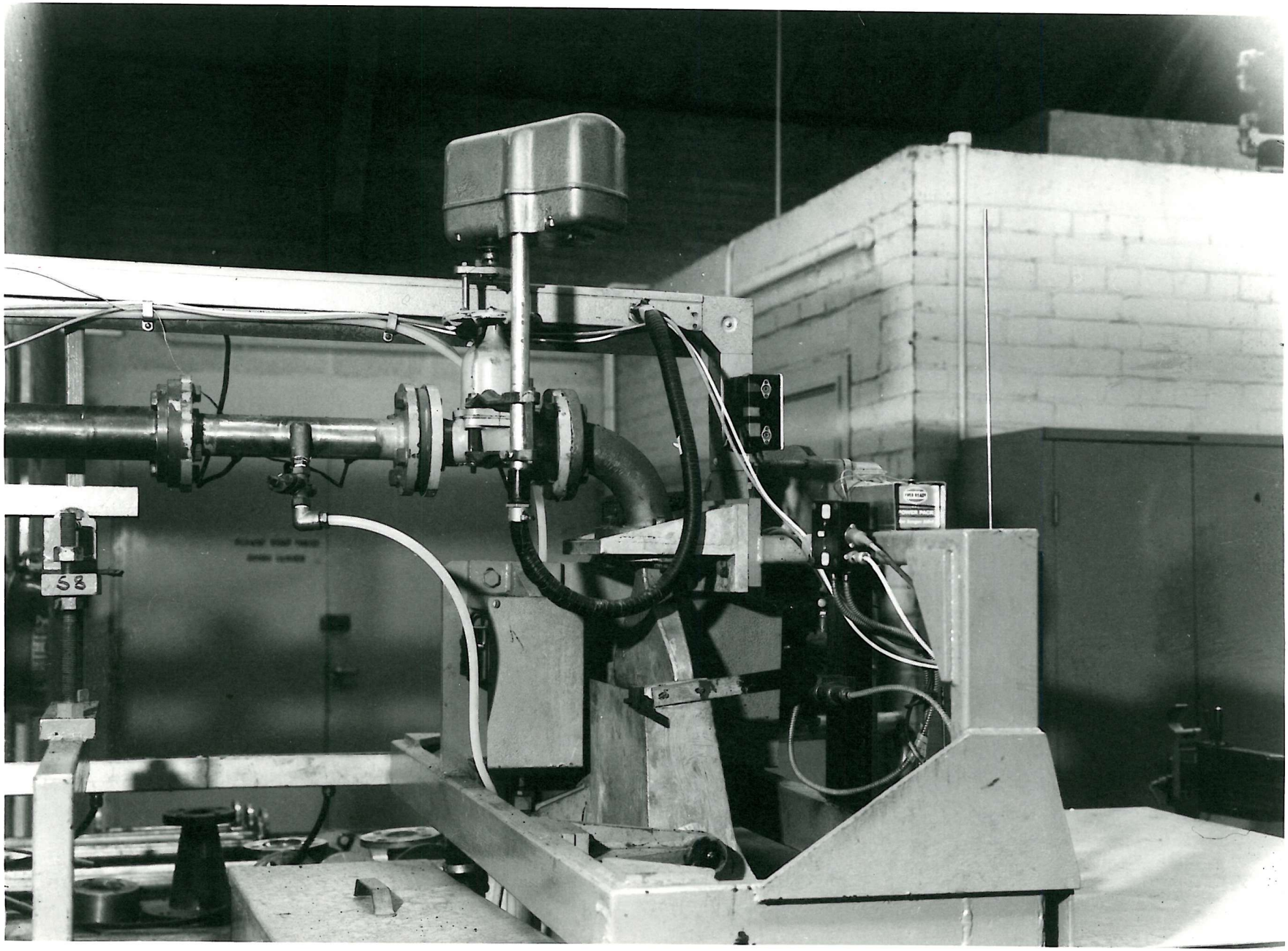

Fig. 2.6 Motor-Operated Pressure Regulating Valve and Fish-Tail Diverter

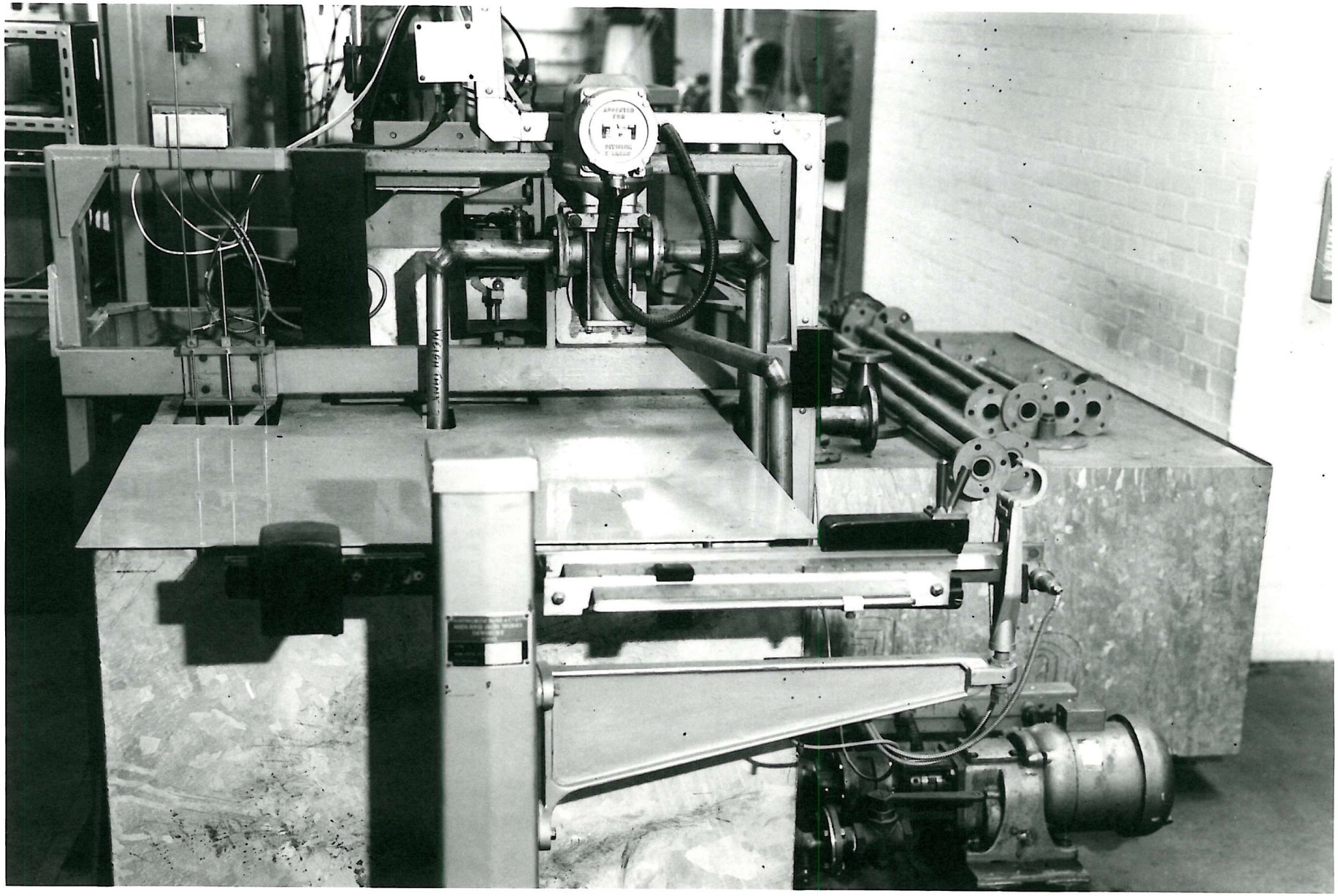

Fig. 2.7 Weigh Tank End of Calibration Rig

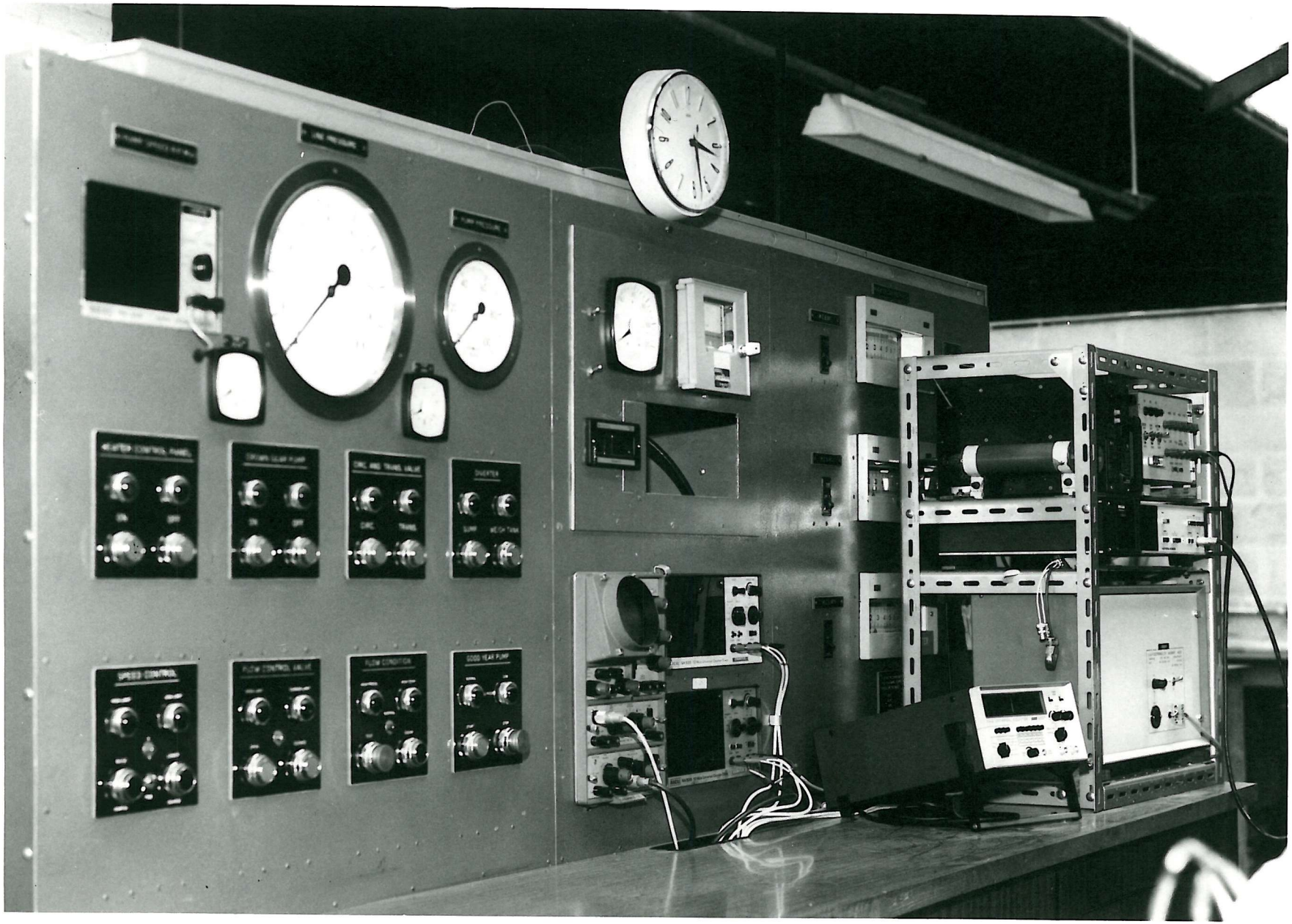

Fig. 2.8 Control Panel of Calibration Rig

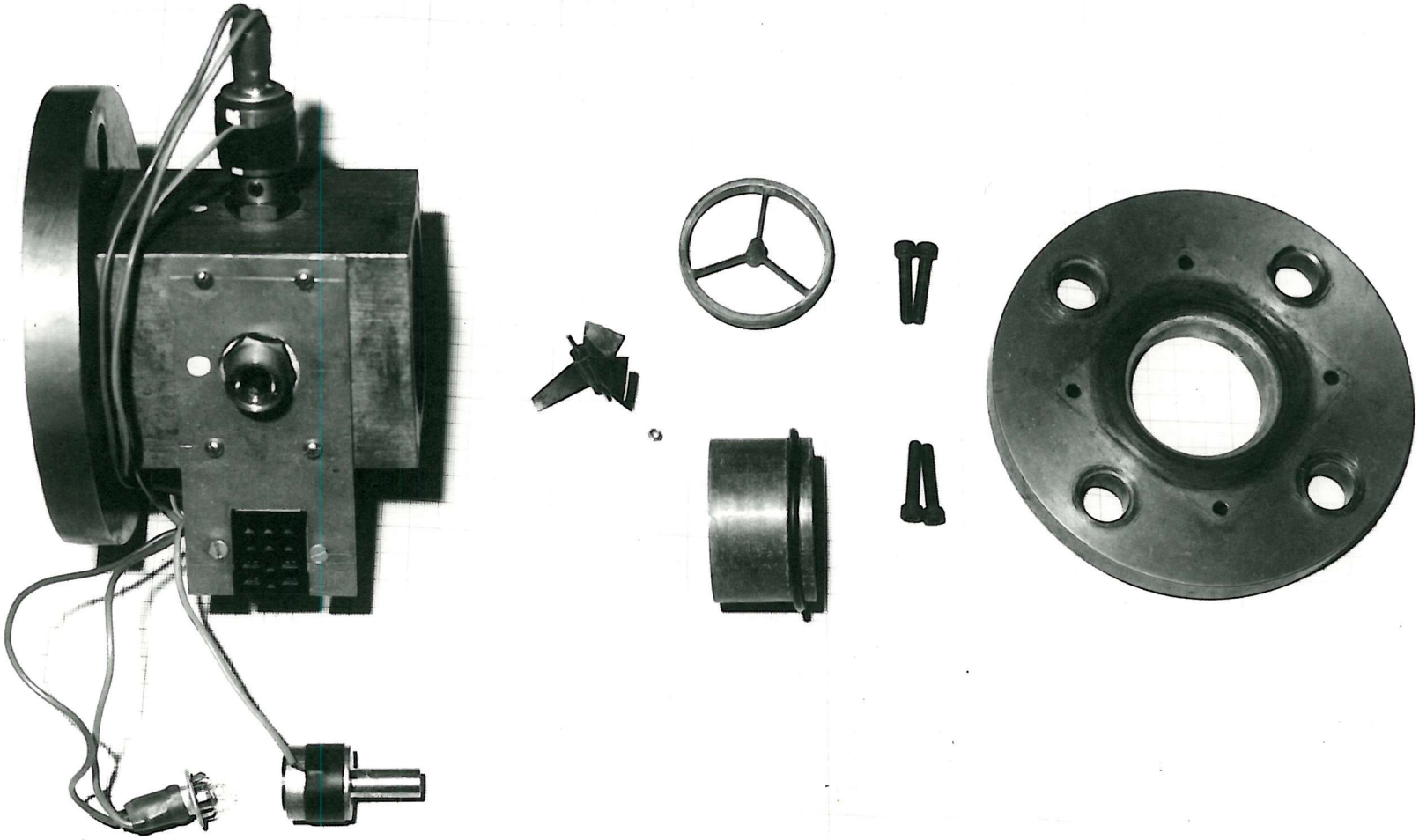

Fig. 2.9 Partly Dismantled View of Turbine Meter

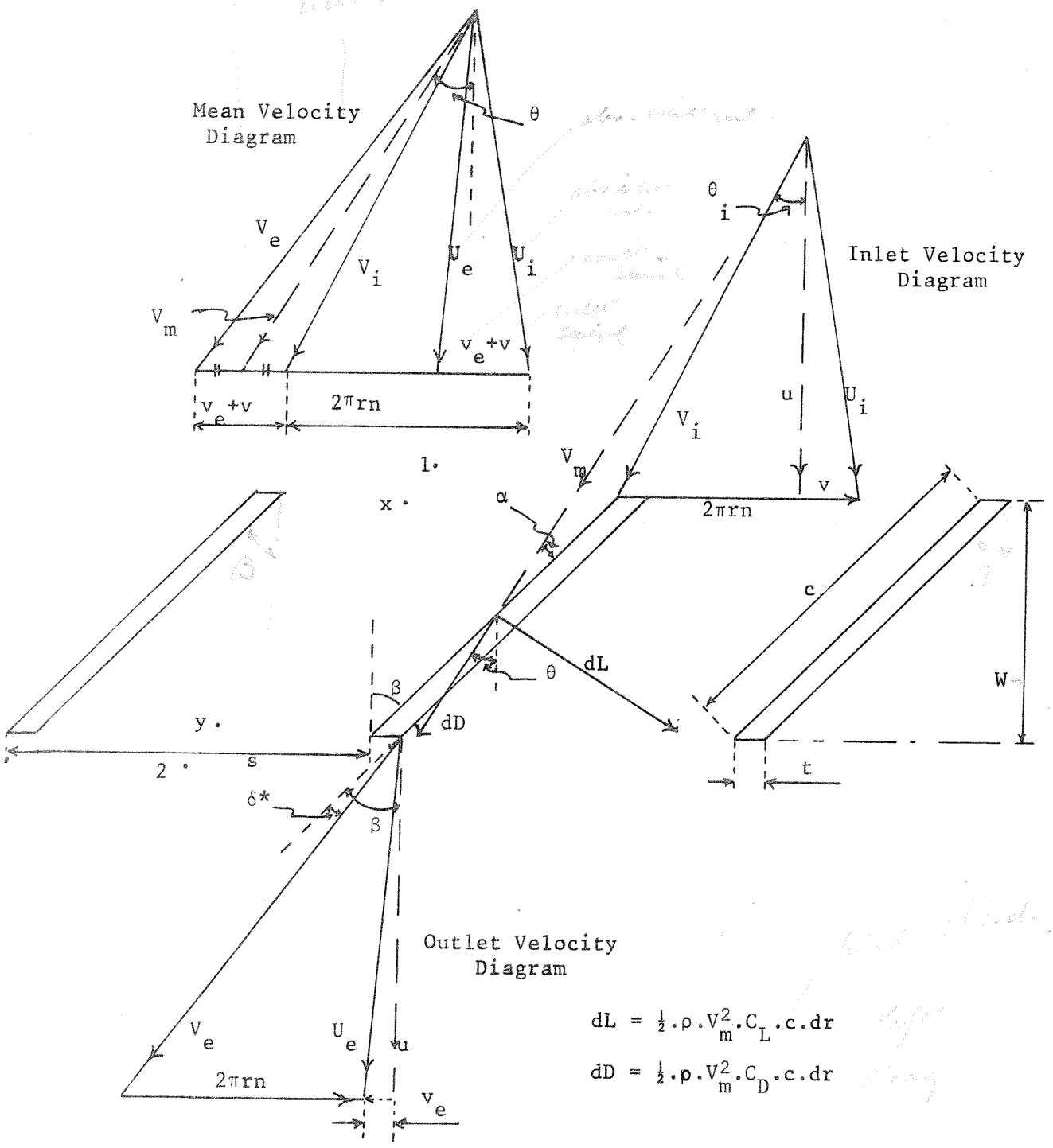

Fig. 3.1 VELOCITY DIAGRAMS AT RADIUS r AND THE FORCES ACTING ON ELEMENTAL BLADE dr

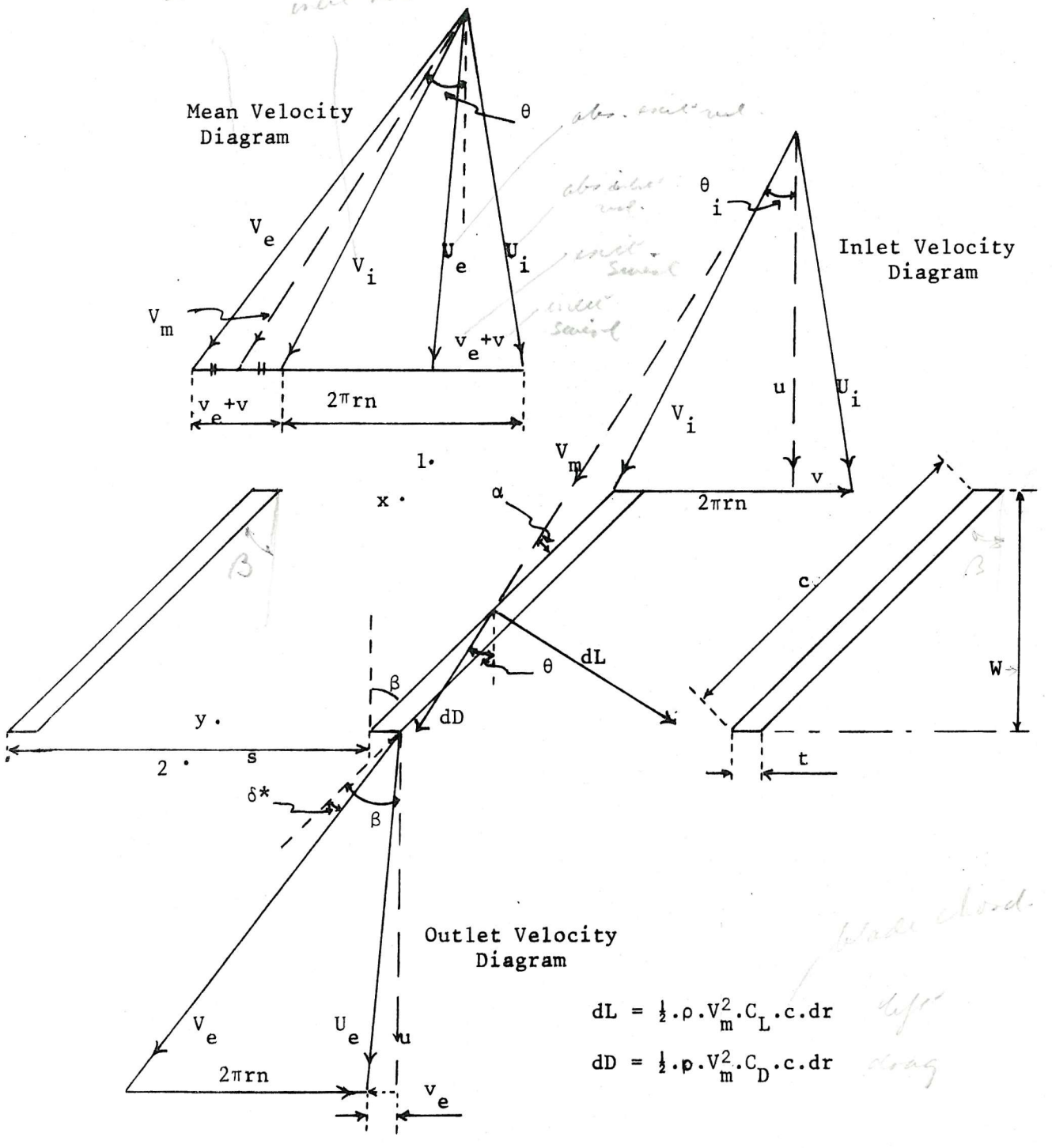

Fig. 3.1 VELOCITY DIAGRAMS AT RADIUS r AND THE FORCES ACTING ON ELEMENTAL BLADE dr

Fig. 3.2 Angle of Attack on Rotors with Different Types of Blade

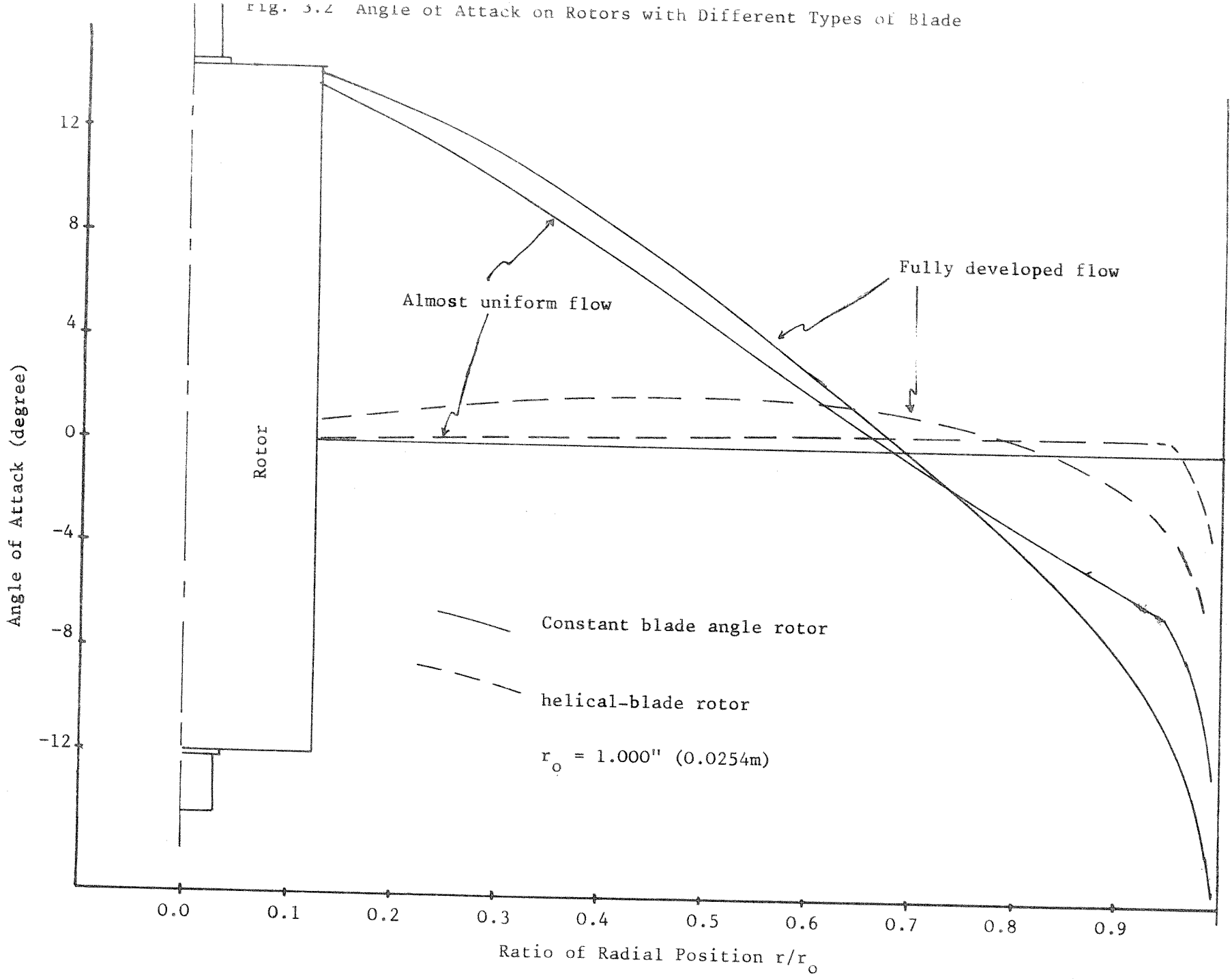

Fig. 3.3 Weinig Lattice-effect (cascade) Coefficient

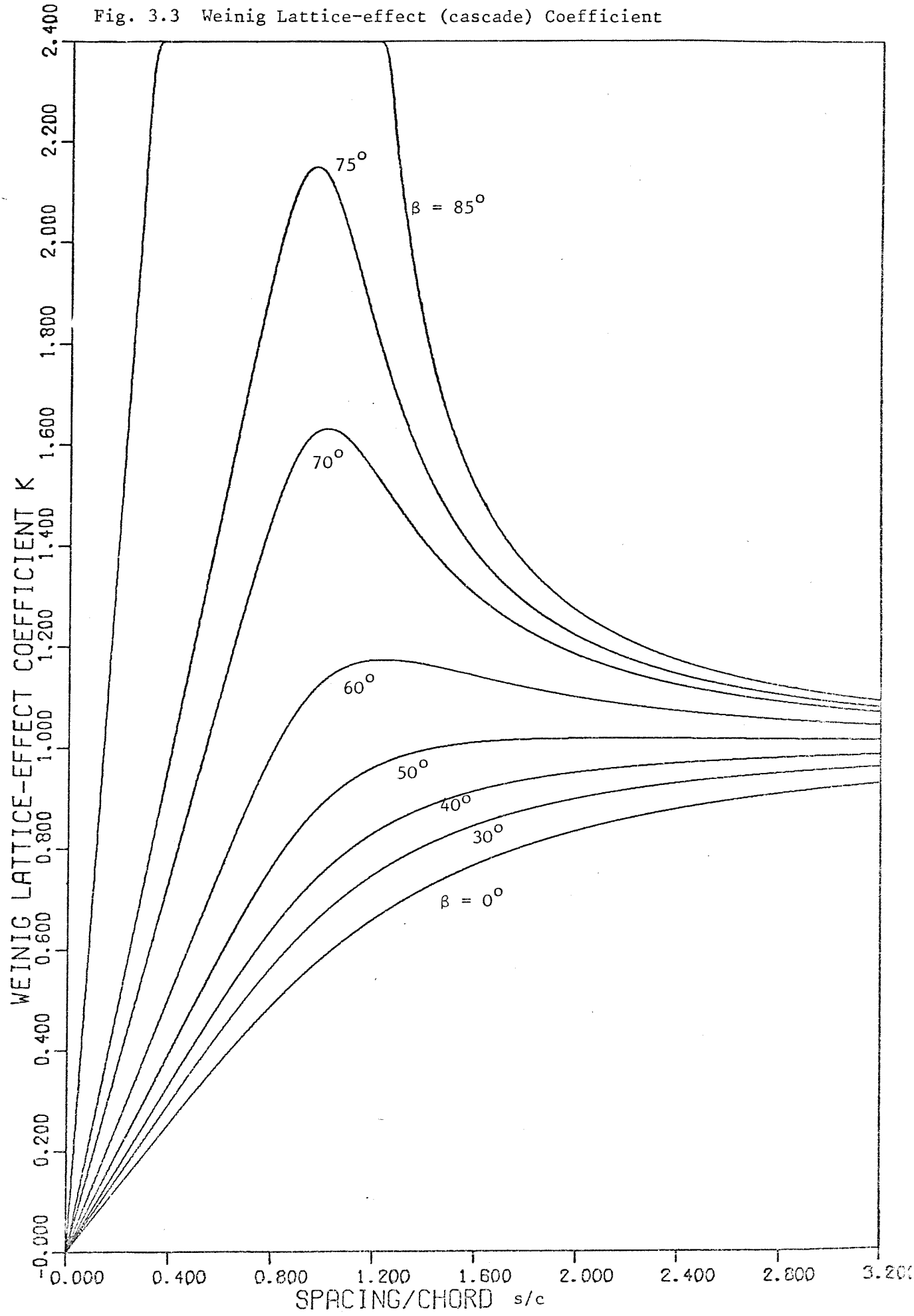

Fig. 3.4 Section of Turbine Meter Blade

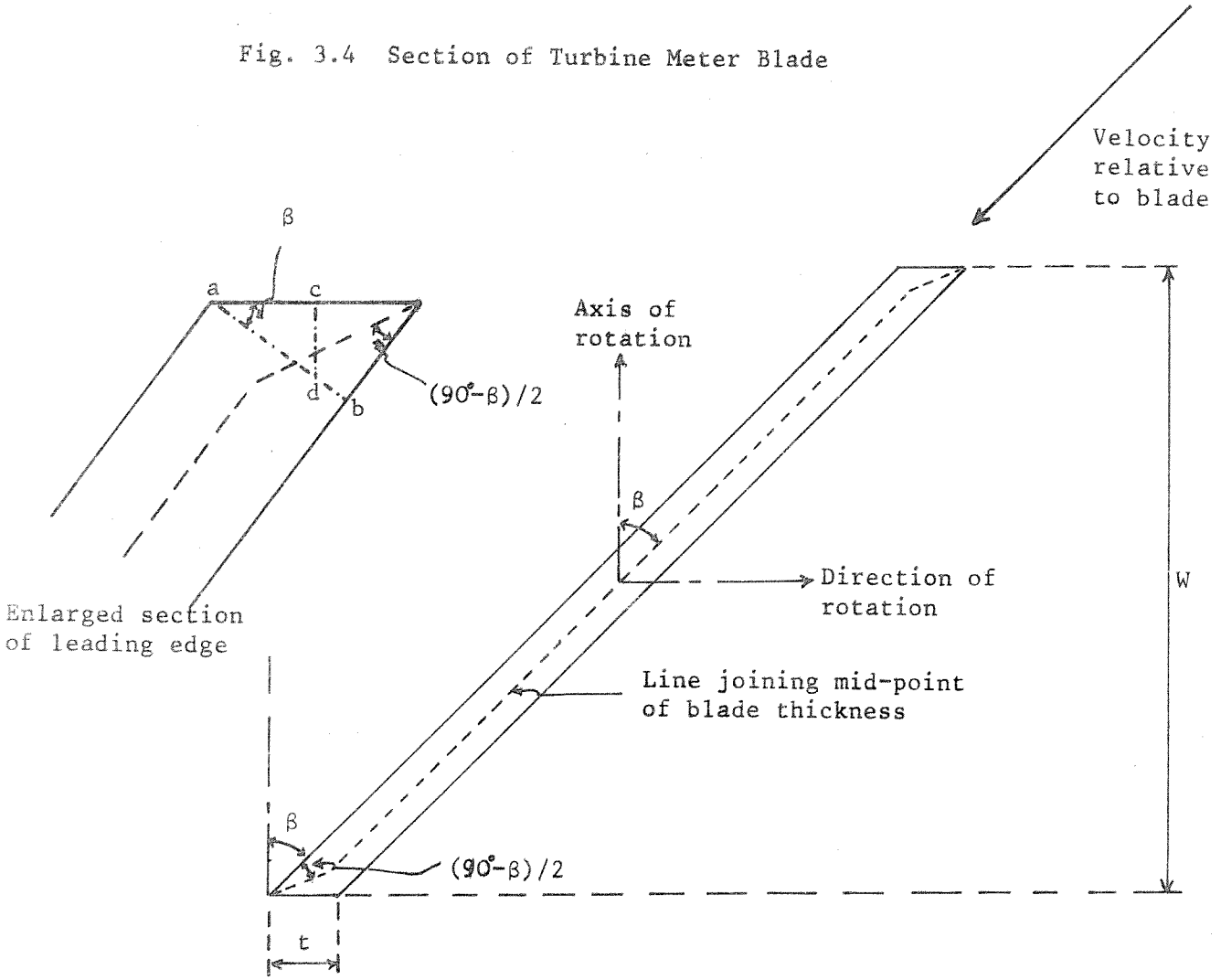

Fig. 3.5 Lift-drag Polars for a Flat Plate

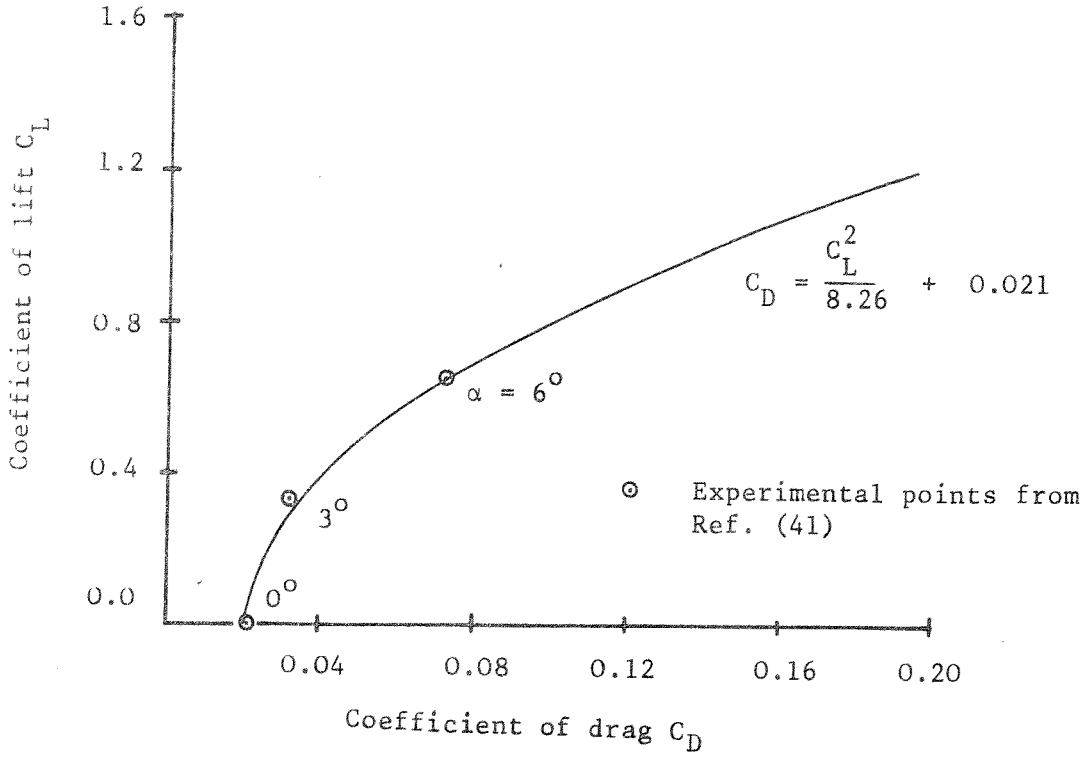

Fig. 3.6 Calibration curves for deducing tip-clearance flow

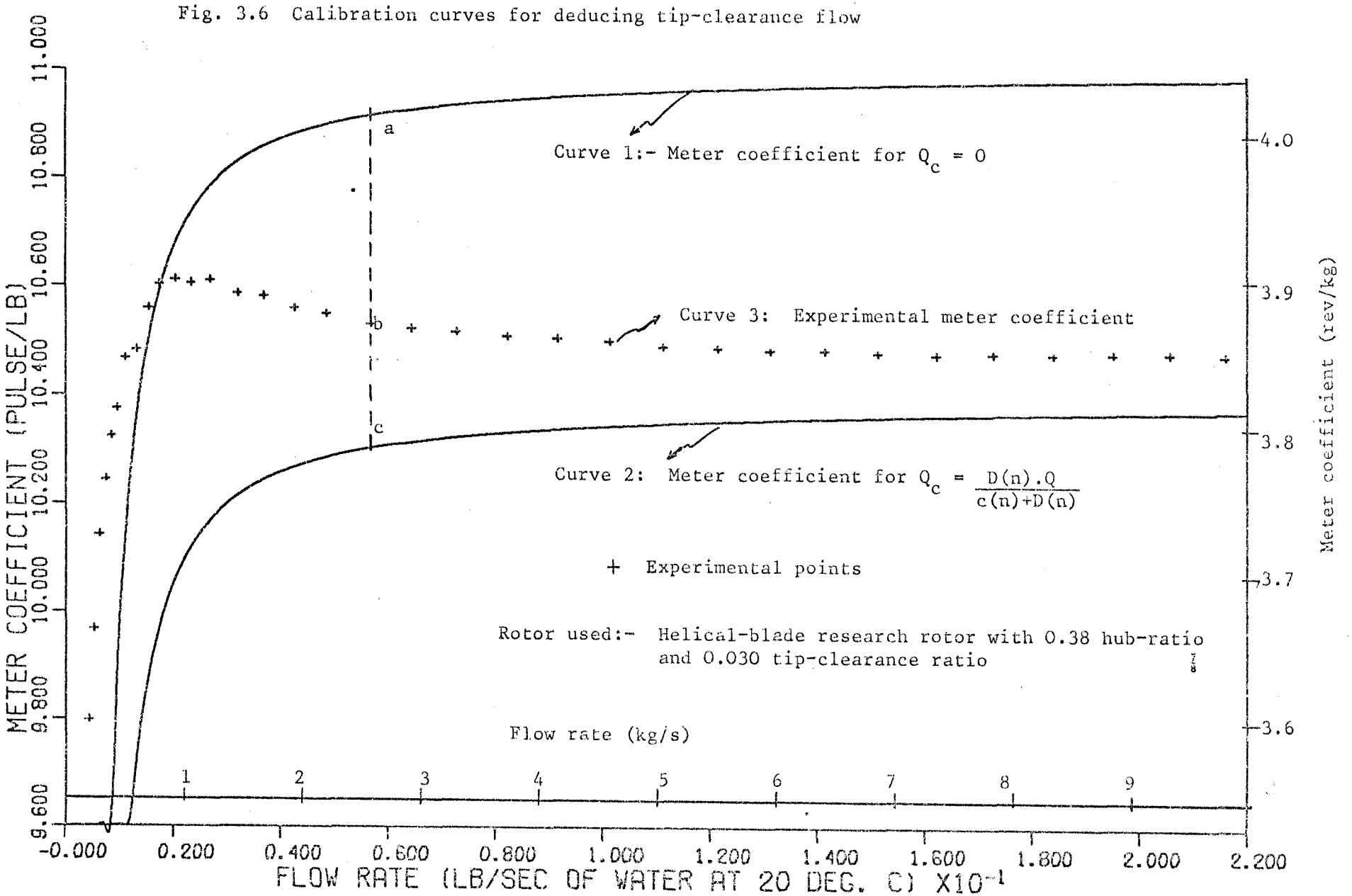

Fig. 3.7 Flow through tip-clearance when turbine meter placed in fully developed flow

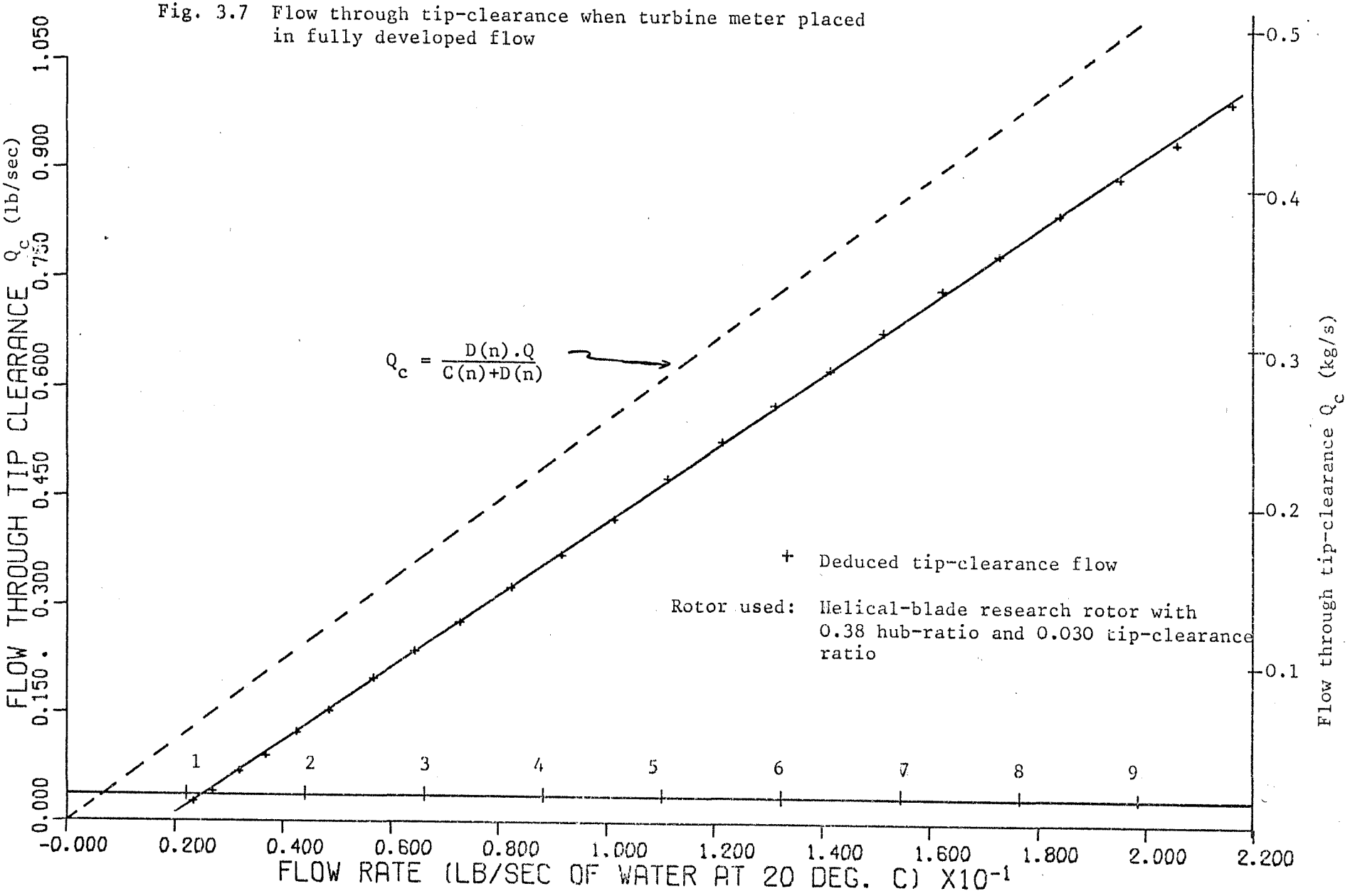

Fig. 3.8 Tip-clearance flow-ratio through 0.38 hub-ratio helical-blade research rotor

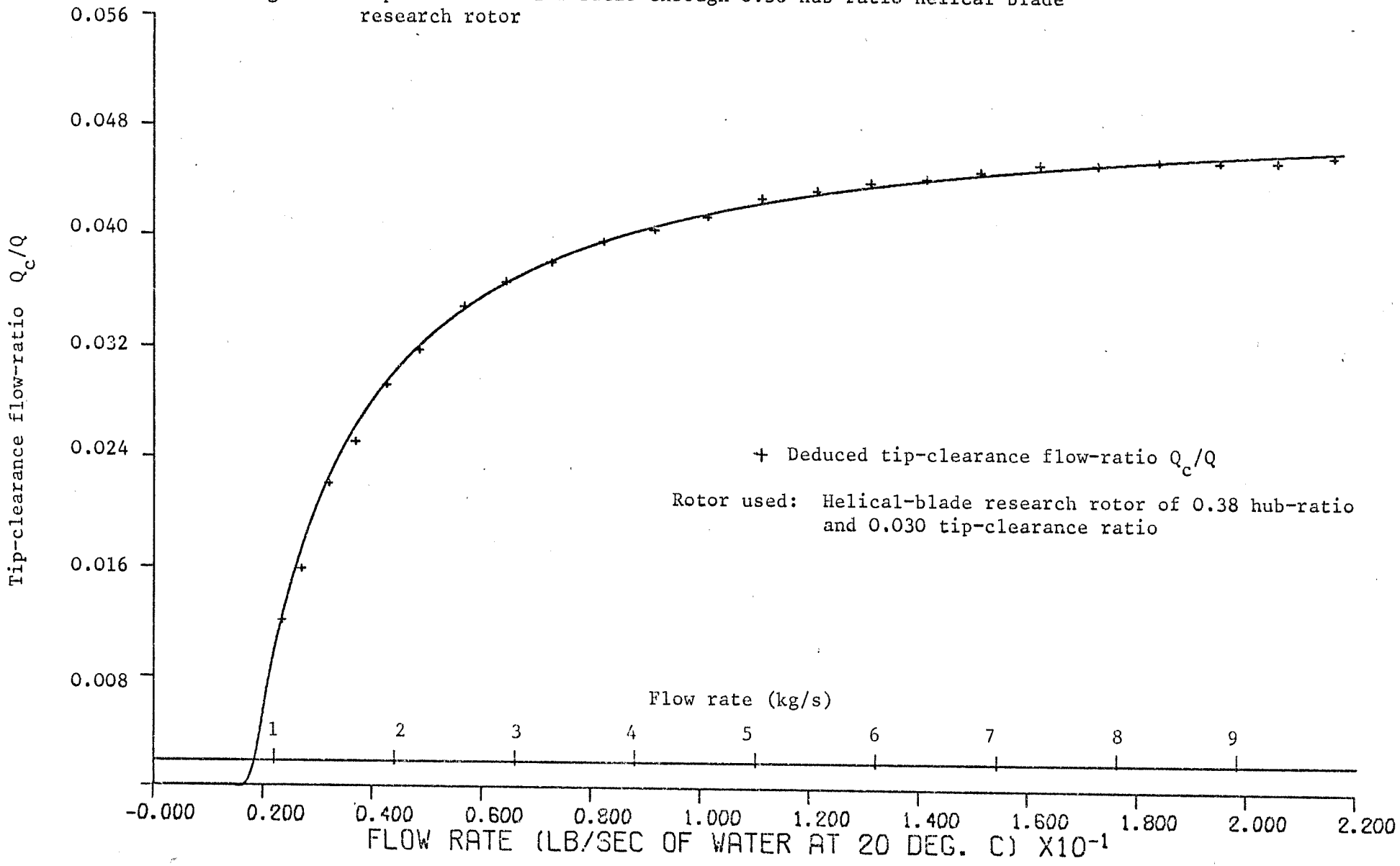

Fig. 3.9 Calibration curve in fully developed flow using Method 1

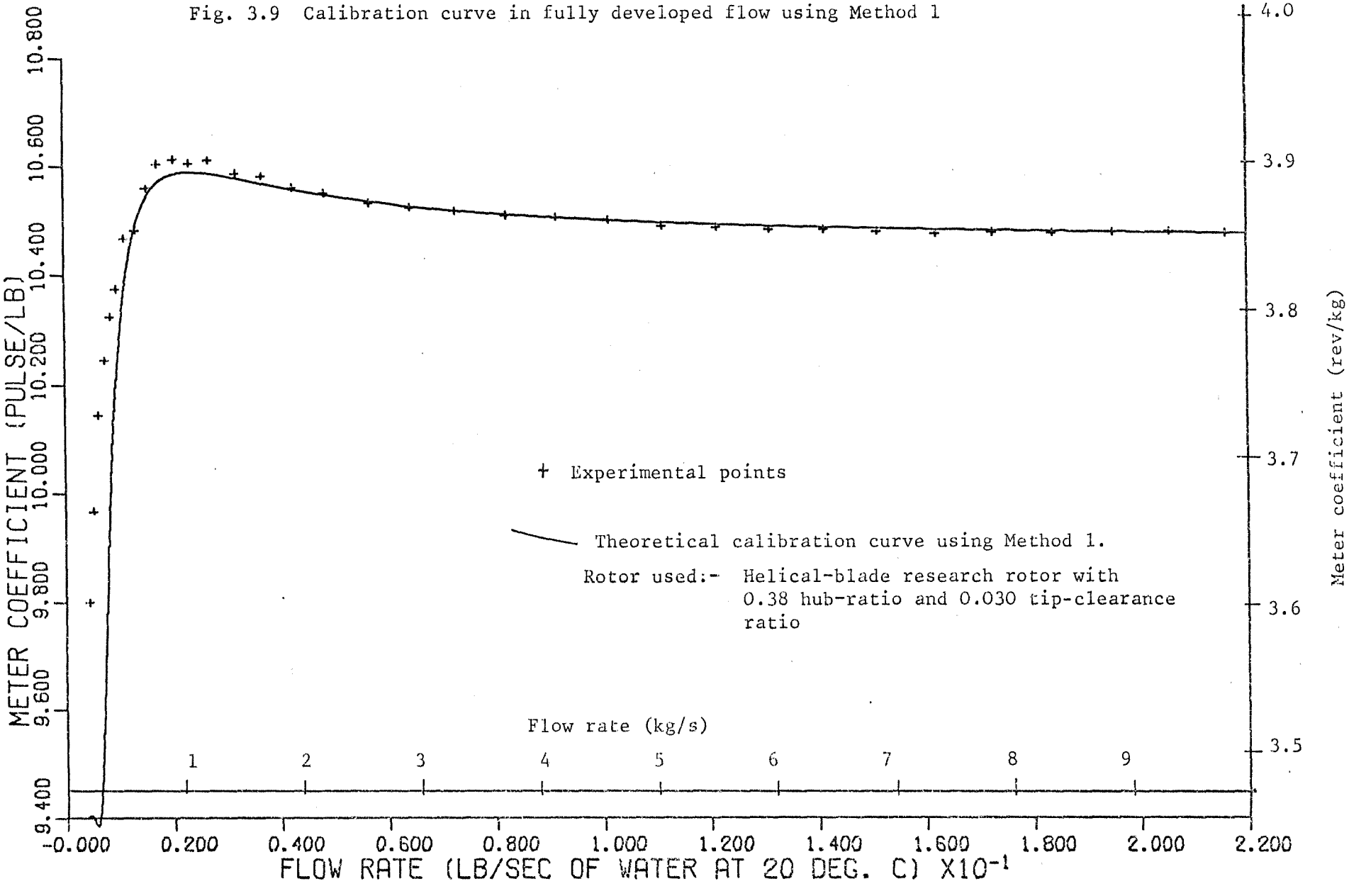

Fig. 3.10 Calibration curve in fully developed flow using Method 2

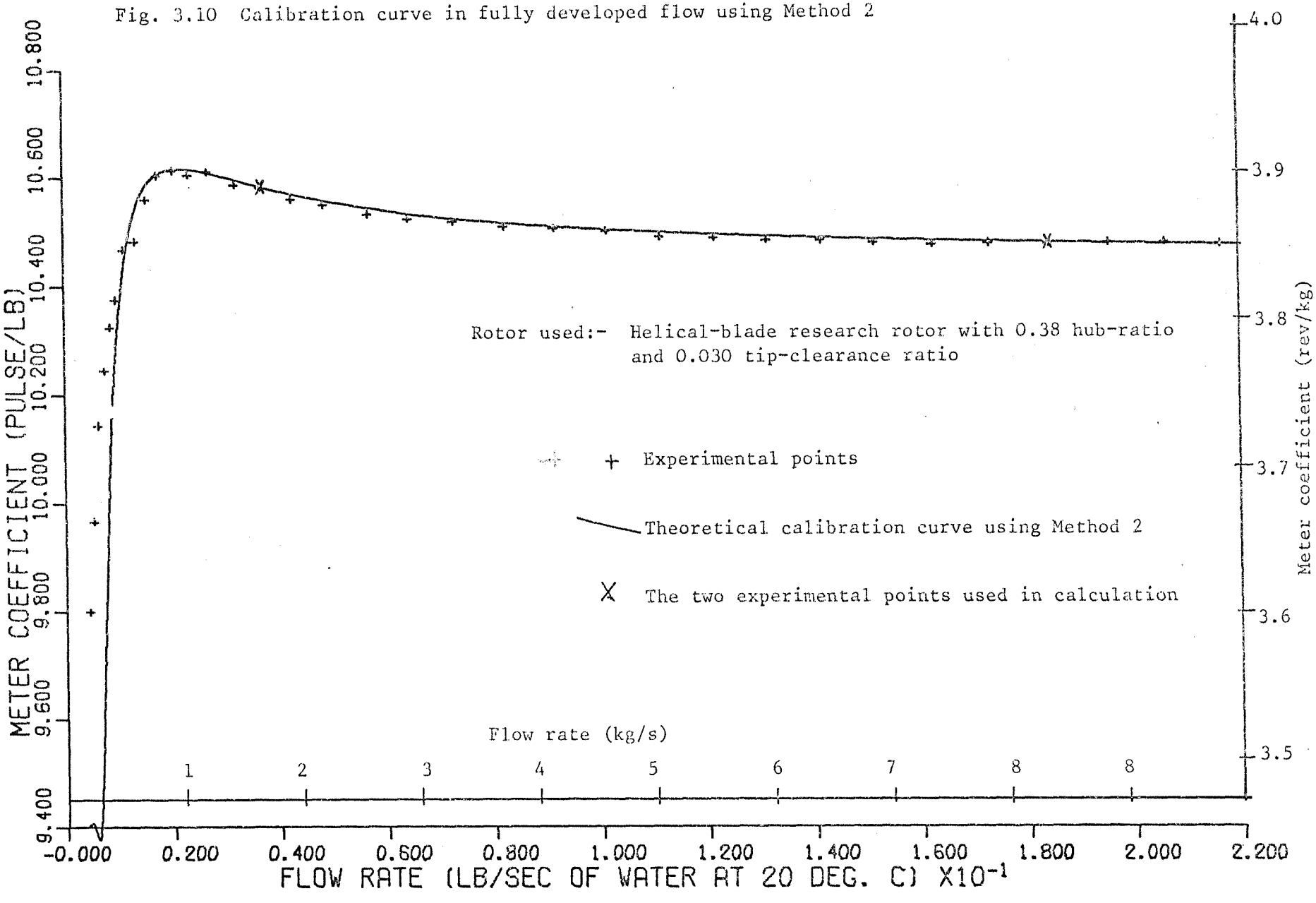

Fig. 3.11 Calibration curve in fully developed flow using Method 3

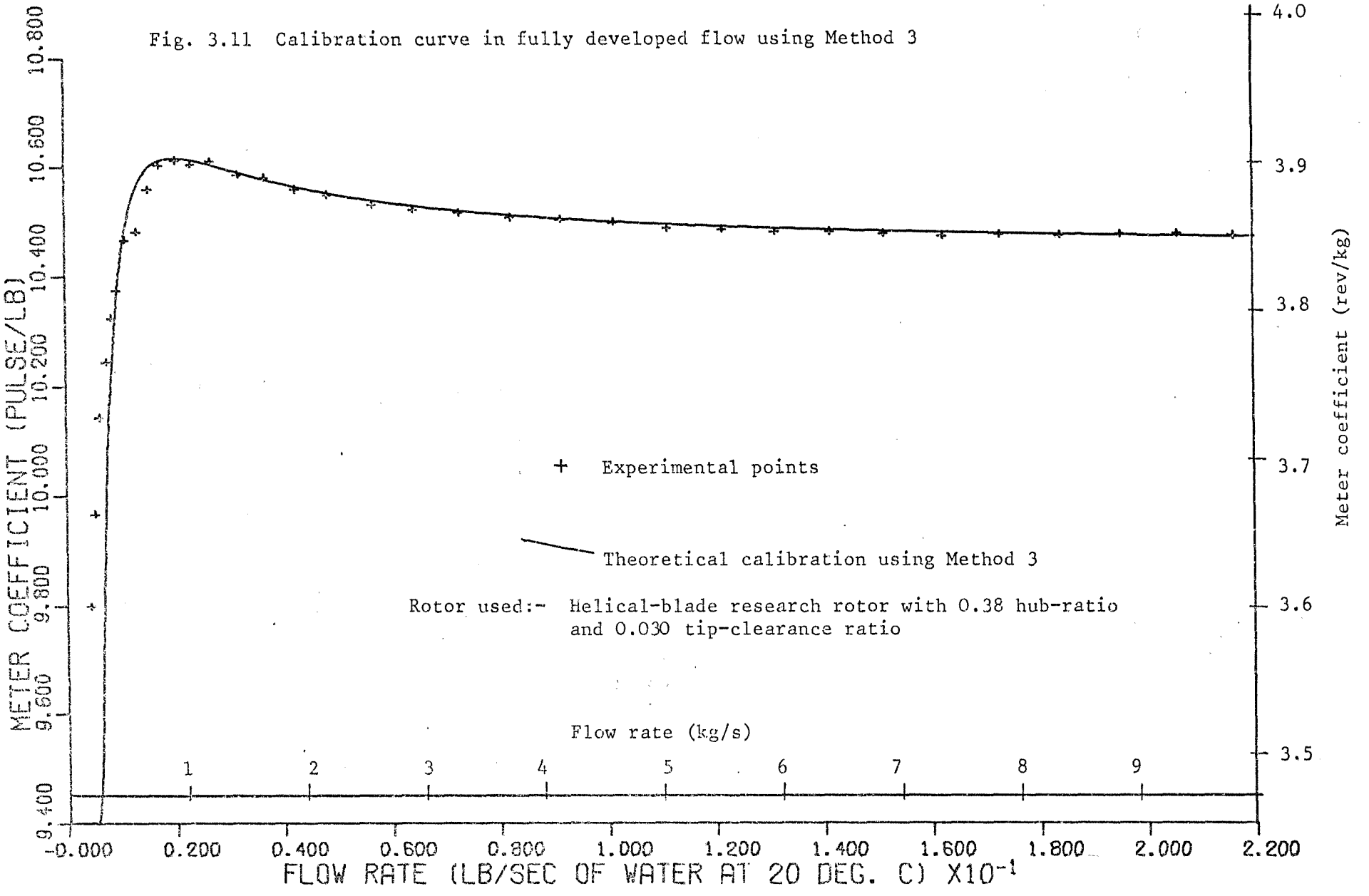

Fig. 3.12 Calibration curves of helical-blade research rotor with 0.125 hub-ratio at upstream position (i.e. almost uniform flow)

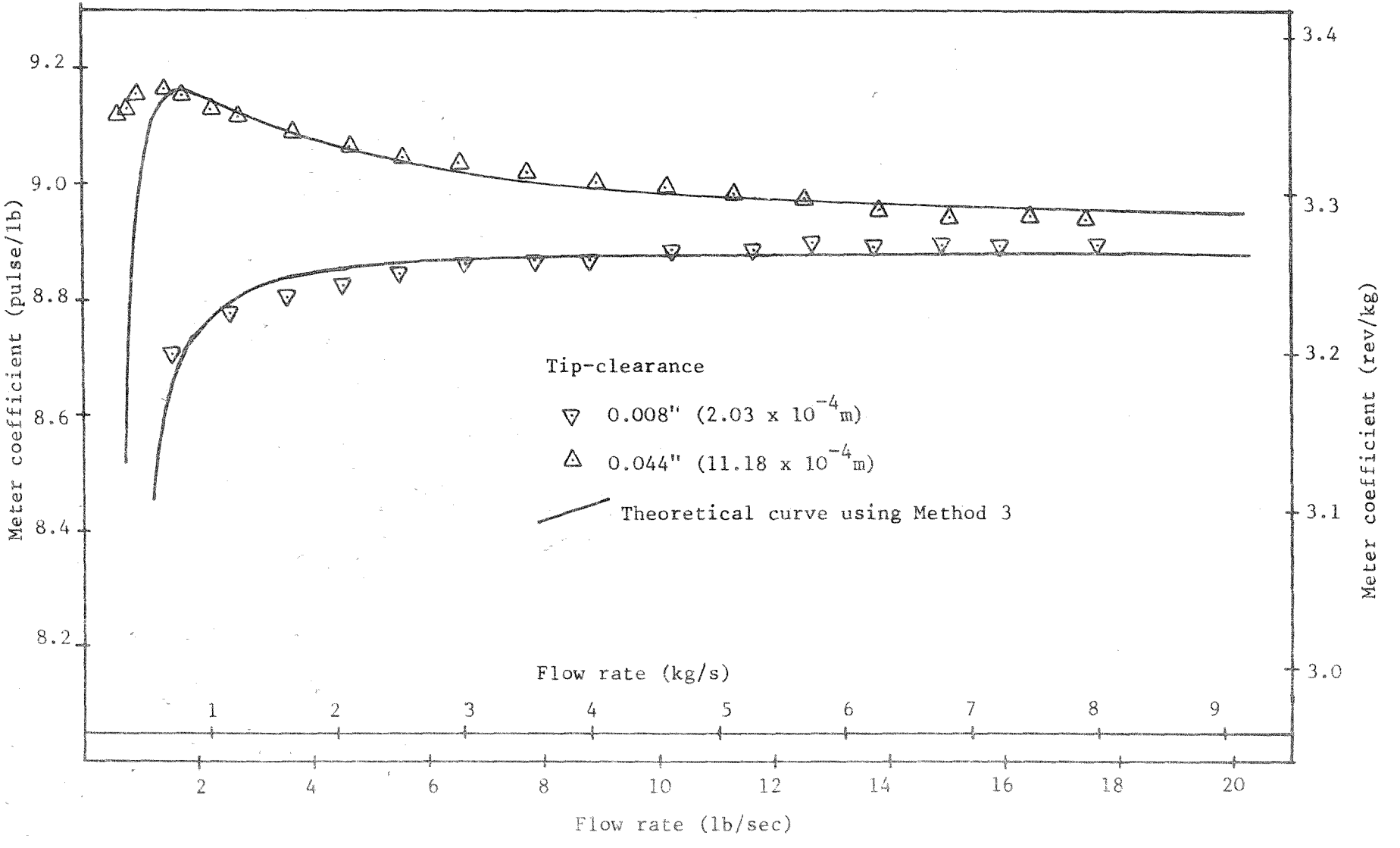

Fig. 3.13 Calibration curves of constant blade angle research rotor with 0.125 hub-ratio at upstream position (i.e. almost uniform flow)

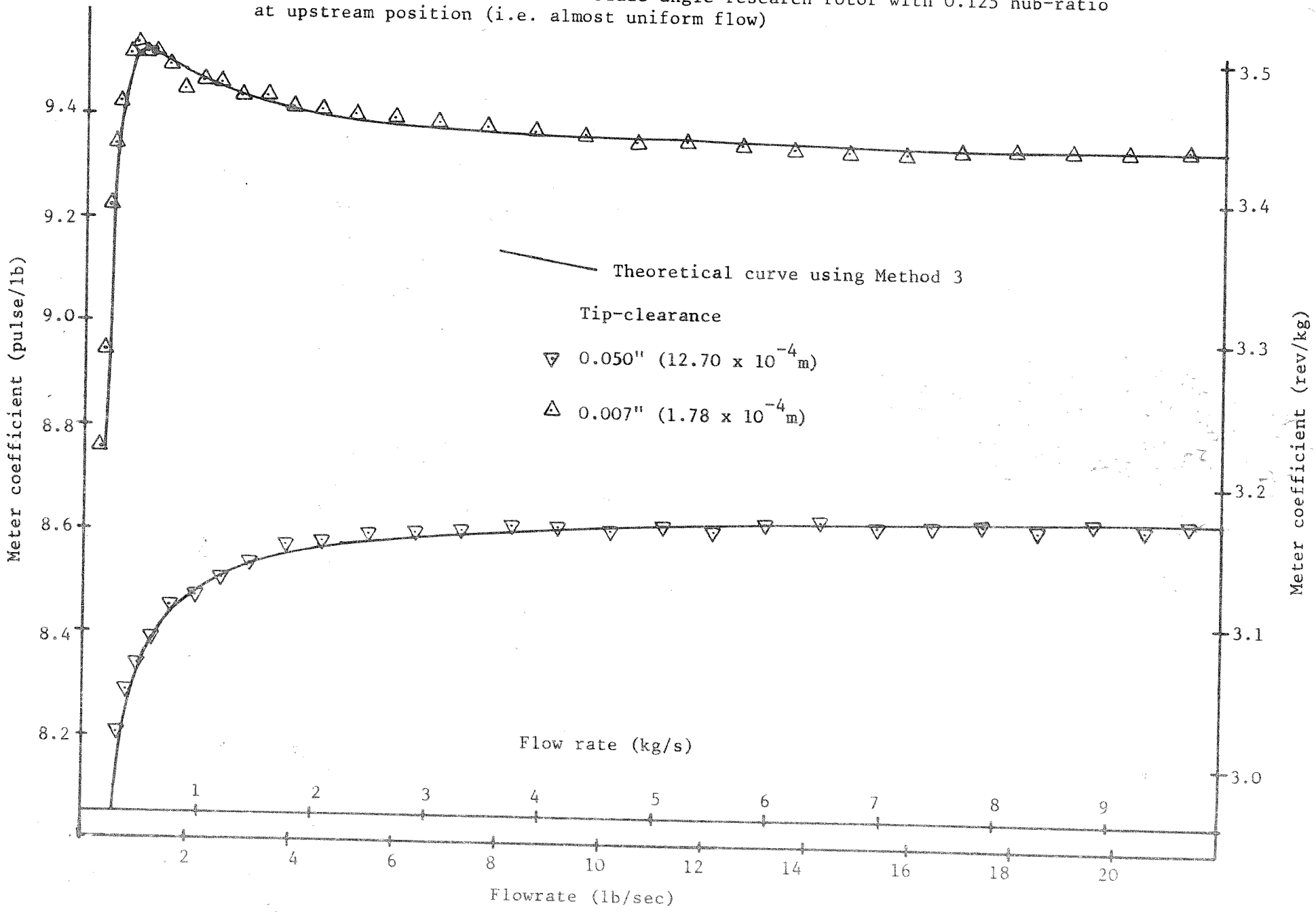

Fig. 3.14 Calibration curve of a 'converging' commercial turbine meter

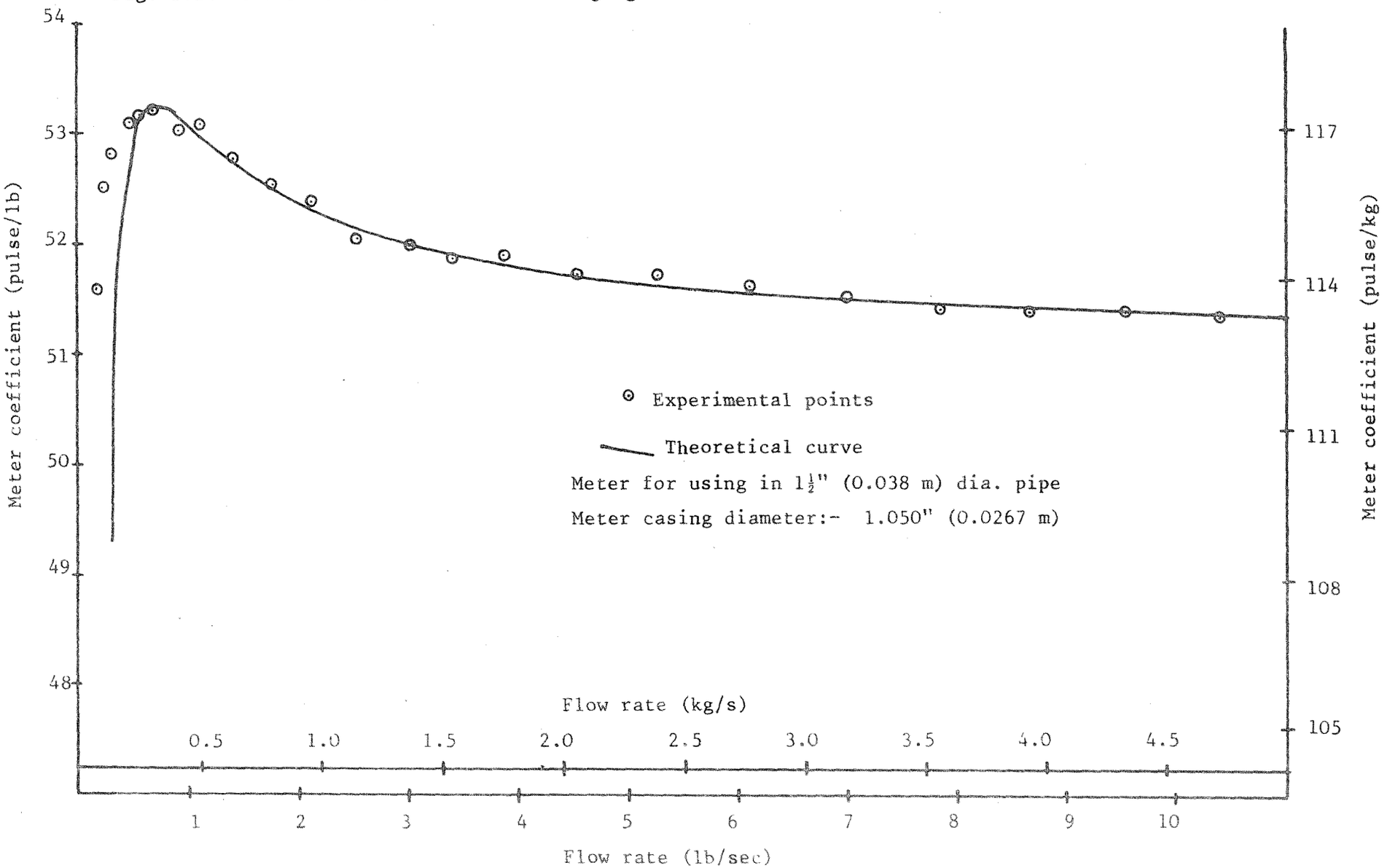

Fig. 3.15 Calibration of a 2" (0.0508 m) commercial turbine meter

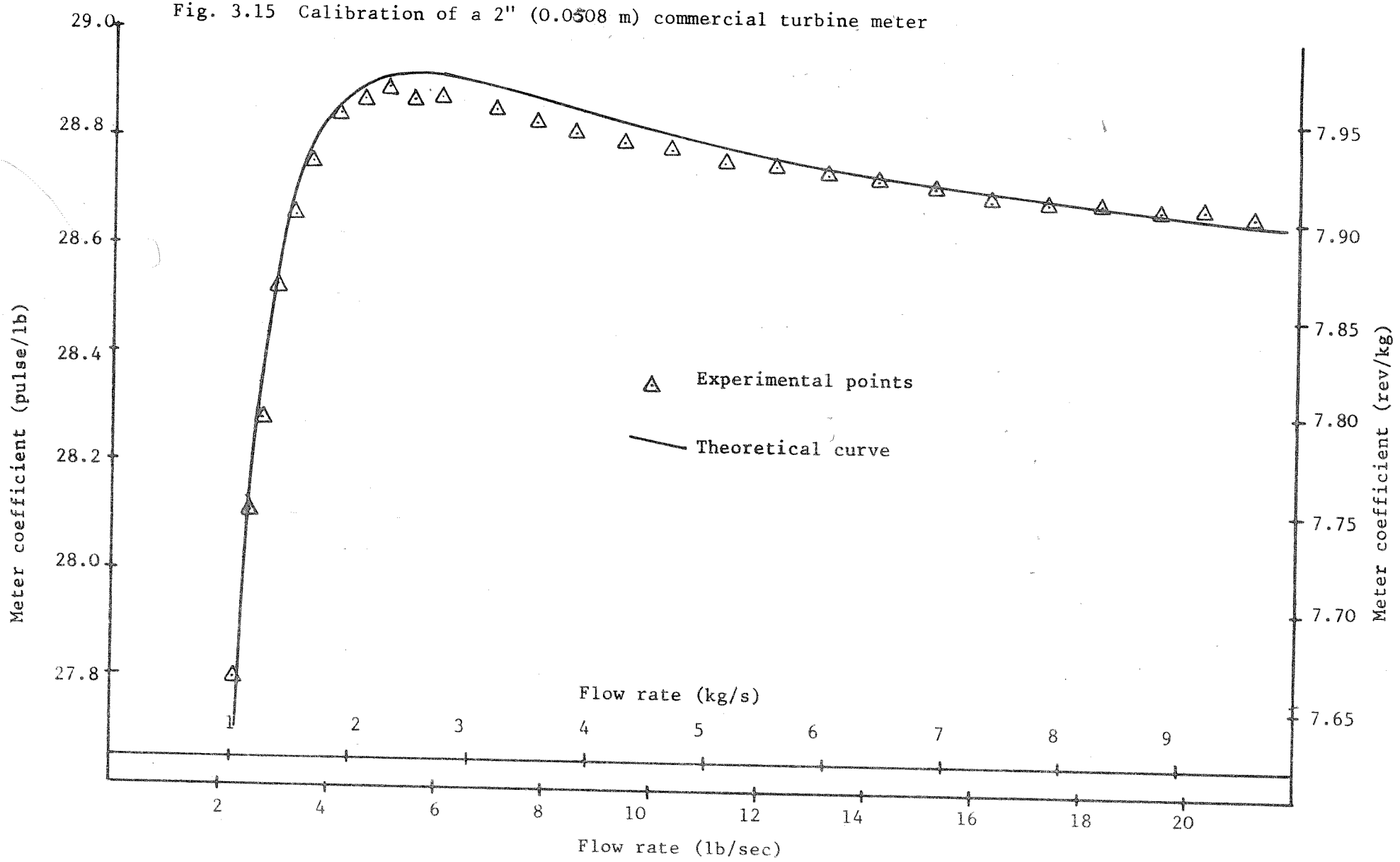

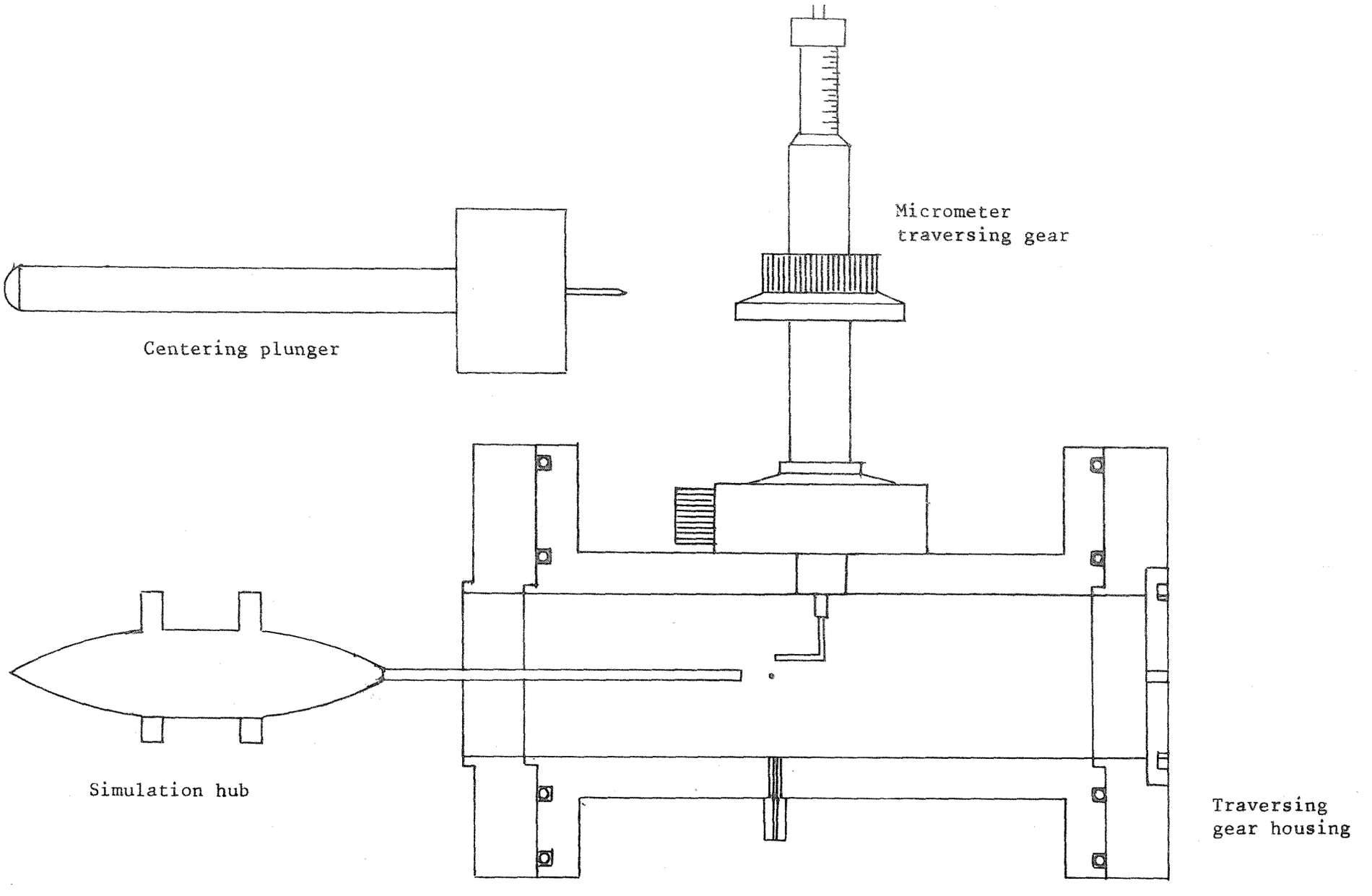

Fig. 4.1 TRAVERSING GEAR FOR VELOCITY PROFILE MEASUREMENT

Fig. 4.2 Velocity Profile at the Upstream and the Downstream Positions of the 2" Test Pipe

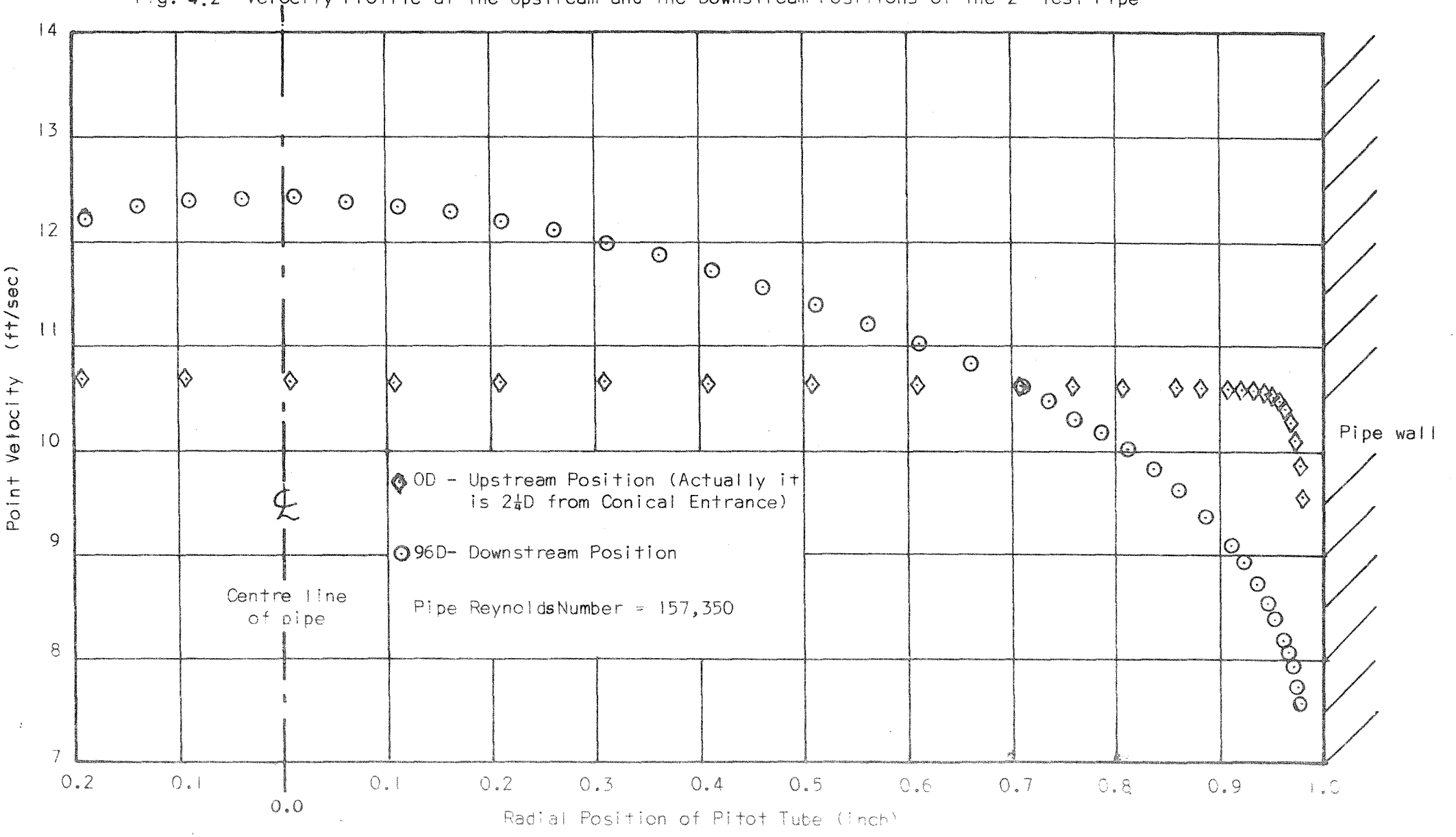

Fig. 4.3 VELOCITY PROFILE WITHIN METER ANNULUS AT UPSTREAM POSITION (0×dia.)
FOR DIFFERENT HUB SIZES

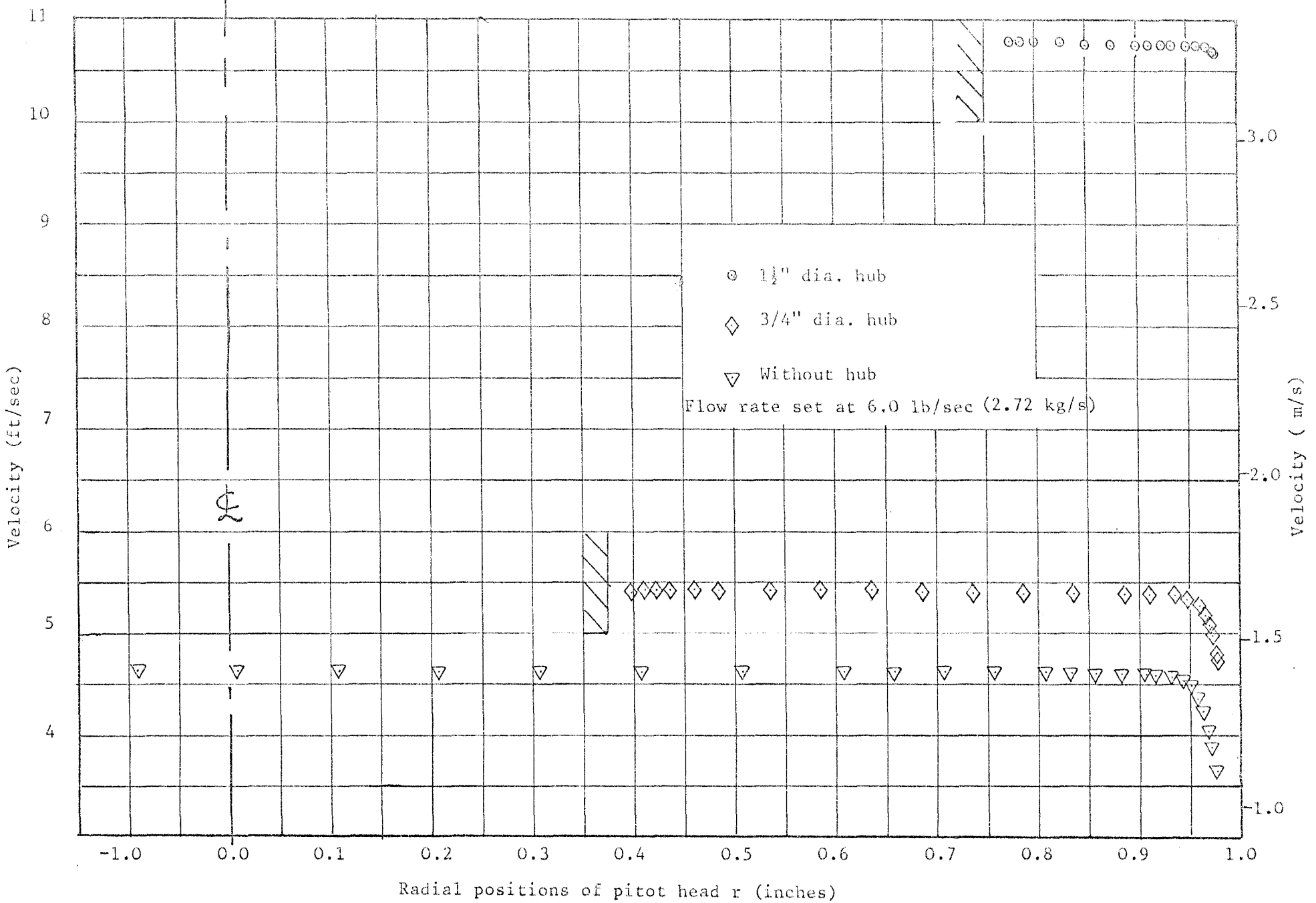

Fig. 4.4 VELOCITY PROFILE WITHIN 3/4" HUB ANNULUS AT UPSTREAM AND DOWNSTREAM POSITIONS

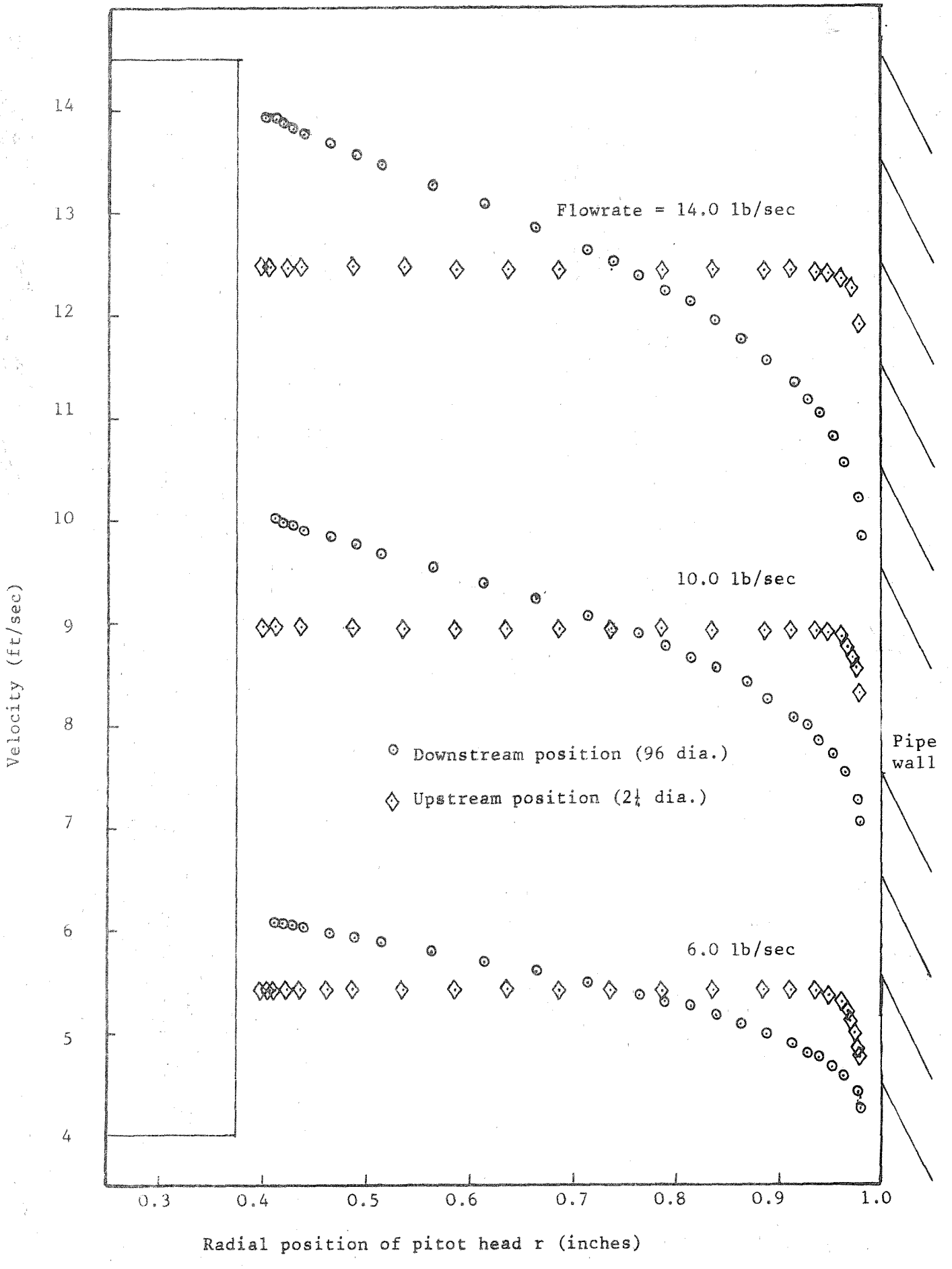

Fig. 4.5 COMPARISON BETWEEN EXPERIMENTAL AND EMPIRICAL PROFILES IN METER ANNULUS FOR FULLY DEVELOPED FLOW

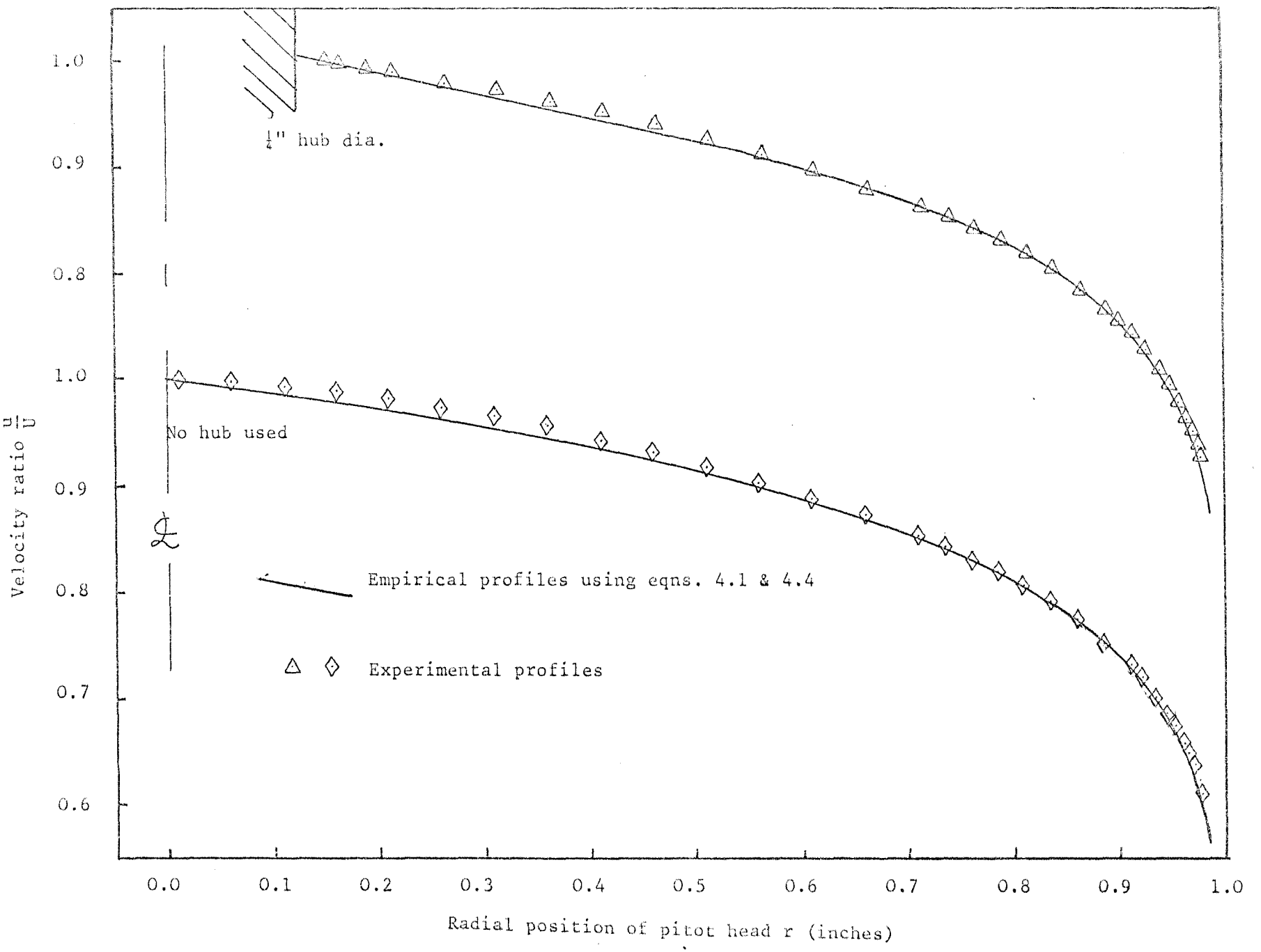

Fig. 4.6 COMPARISON BETWEEN EXPERIMENTAL AND EMPIRICAL PROFILES IN METER ANNULUS FOR FULLY DEVELOPED FLOW

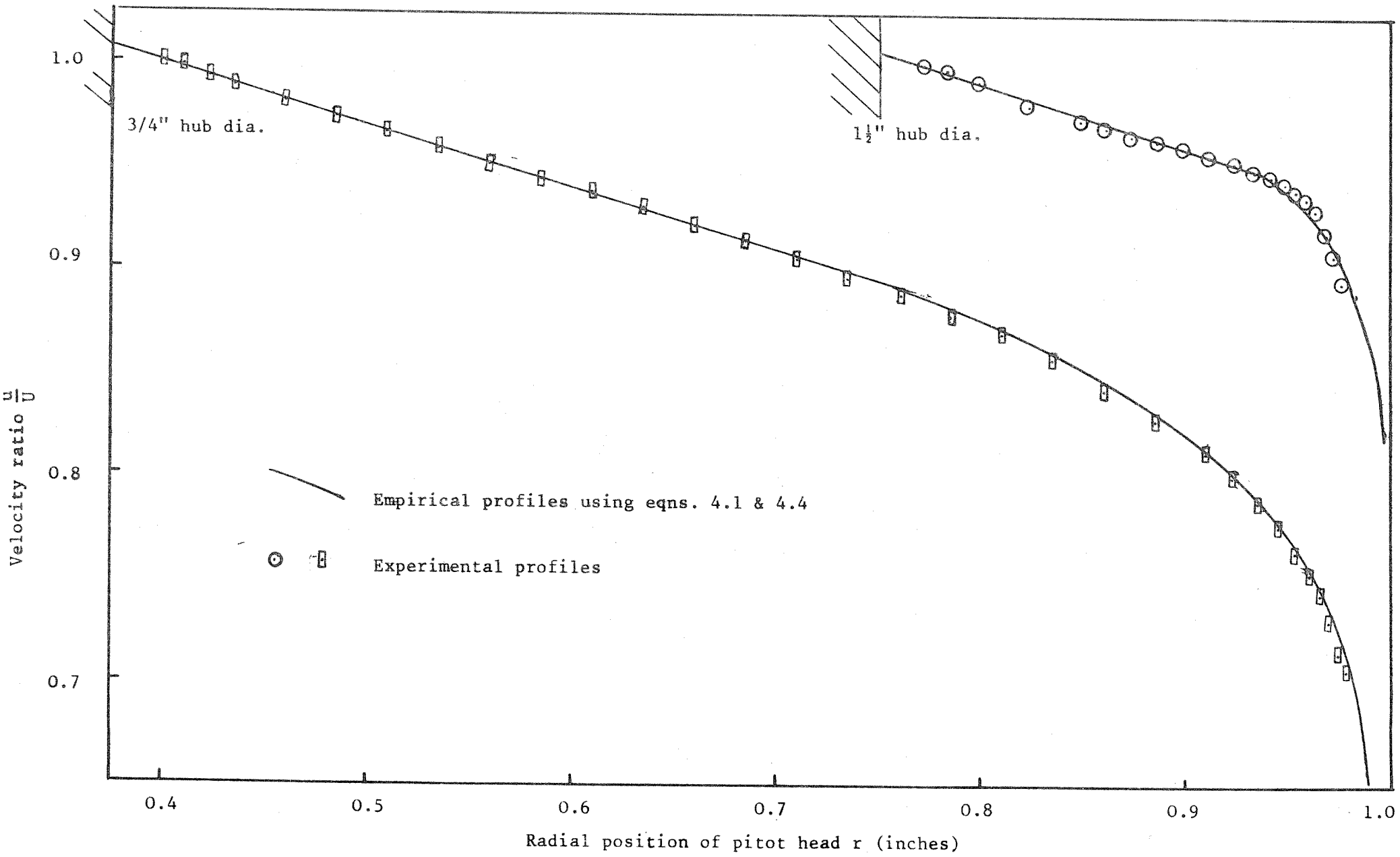

Fig. 4.7 VELOCITY PROFILE IN METER ANNULUS AT DOWNSTREAM POSITION (96D)

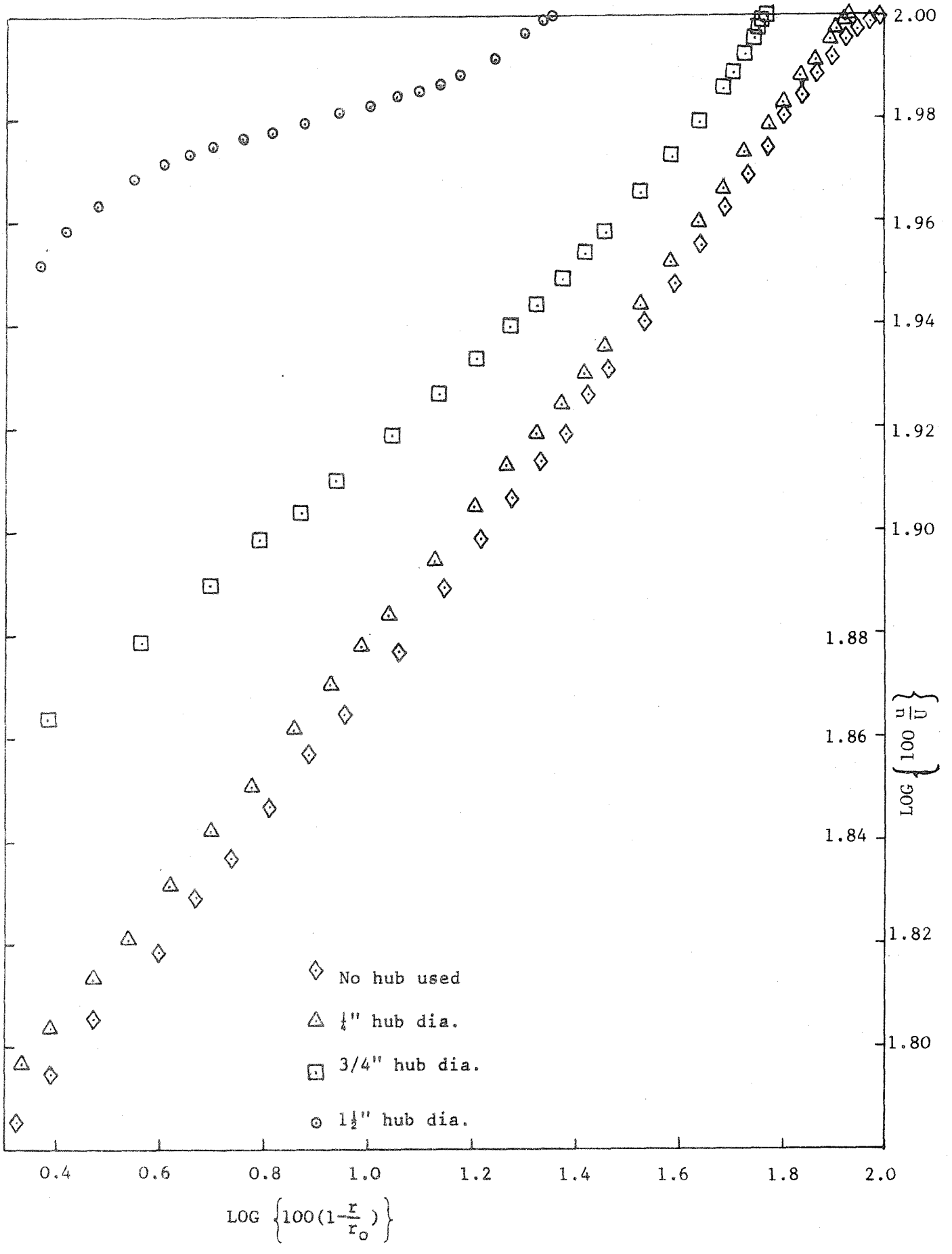

Fig. 4.8 RADIAL POSITION WHERE THE LINEAR PART OF ANNULUS VELOCITY PROFILE TERMINATES

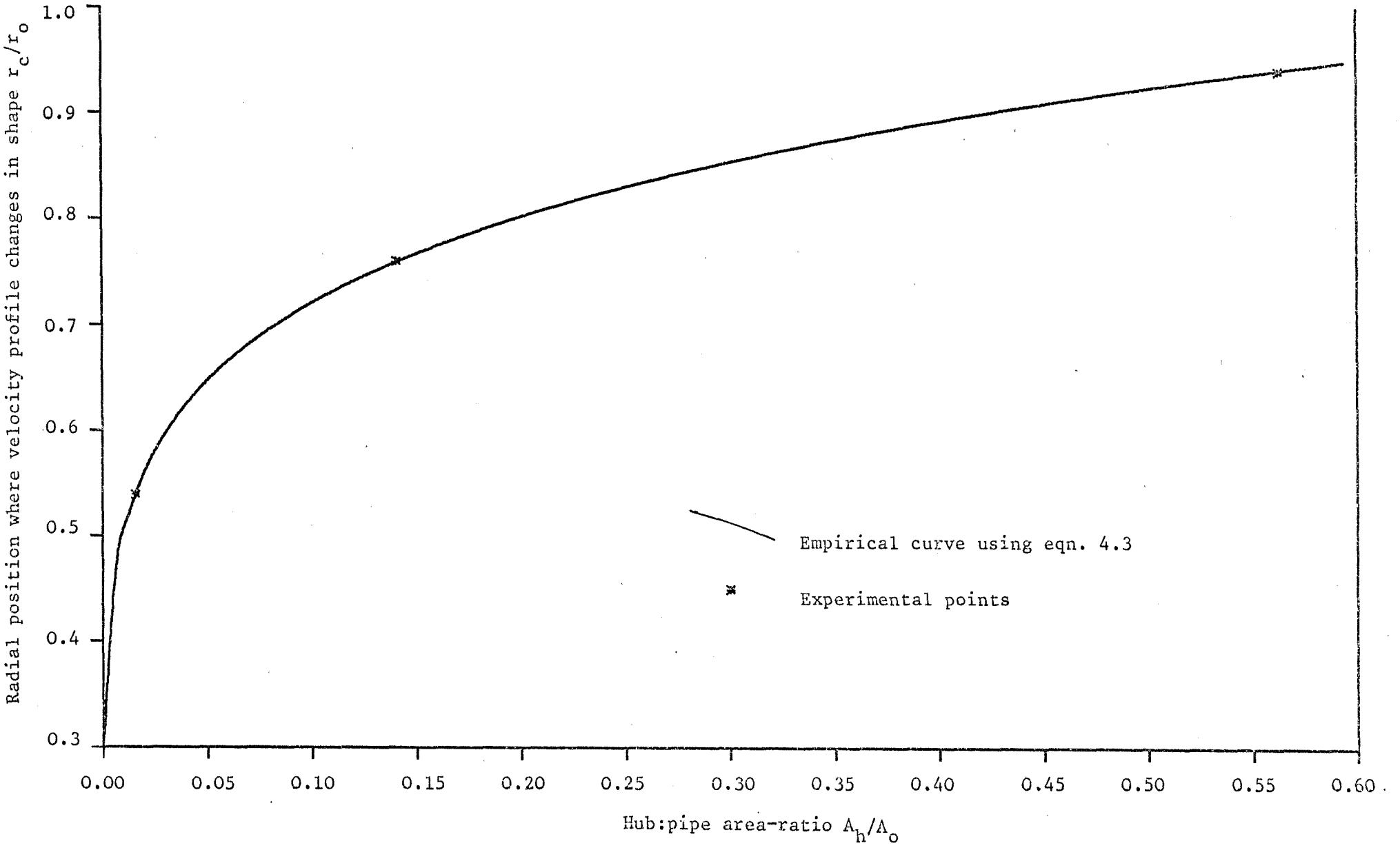

Fig. 4.9 GRADIENT OF LINEAR PART OF VELOCITY PROFILE IN METER ANNULUS

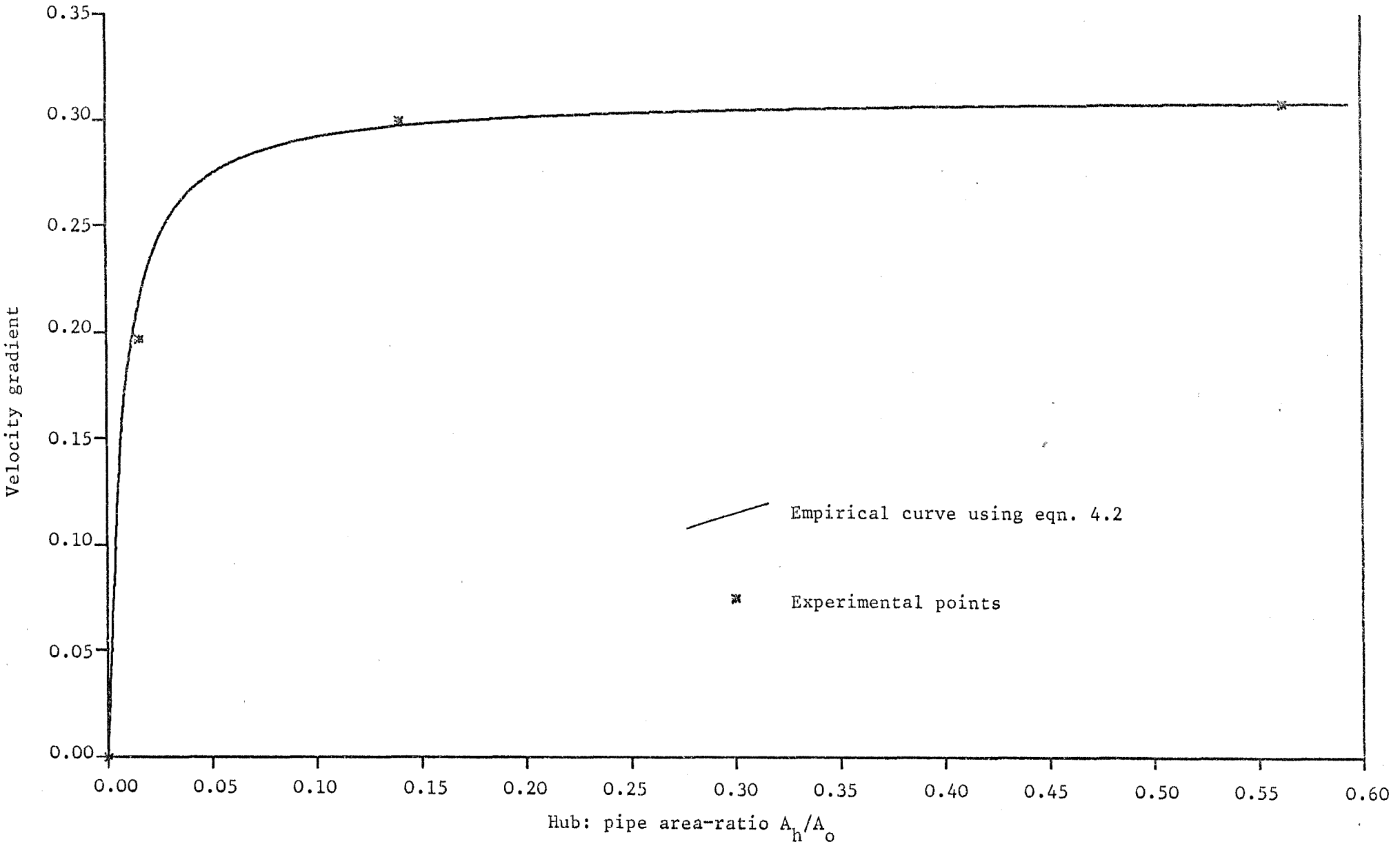

Fig. 4.10 RECIPROCAL OF EXPONENT OF POWER LAW THAT FITS THE NON-LINEAR PART OF ANNULUS VELOCITY PROFILE

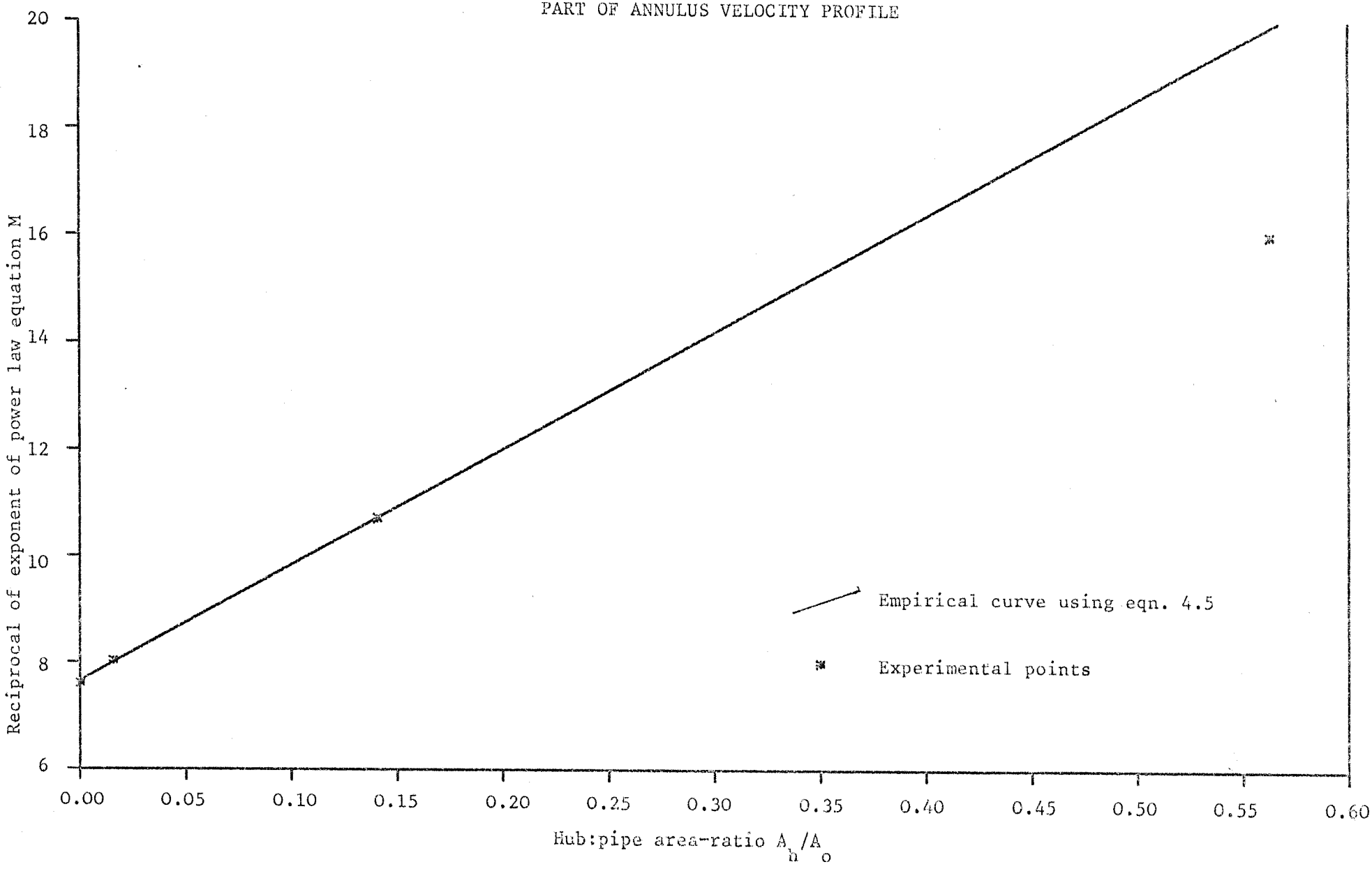

Fig. 4.11 COMPARISON BETWEEN THE TWO ASSUMED PROFILES AND PREDICTED PROFILE FOR 0.125 HUB-RATIO

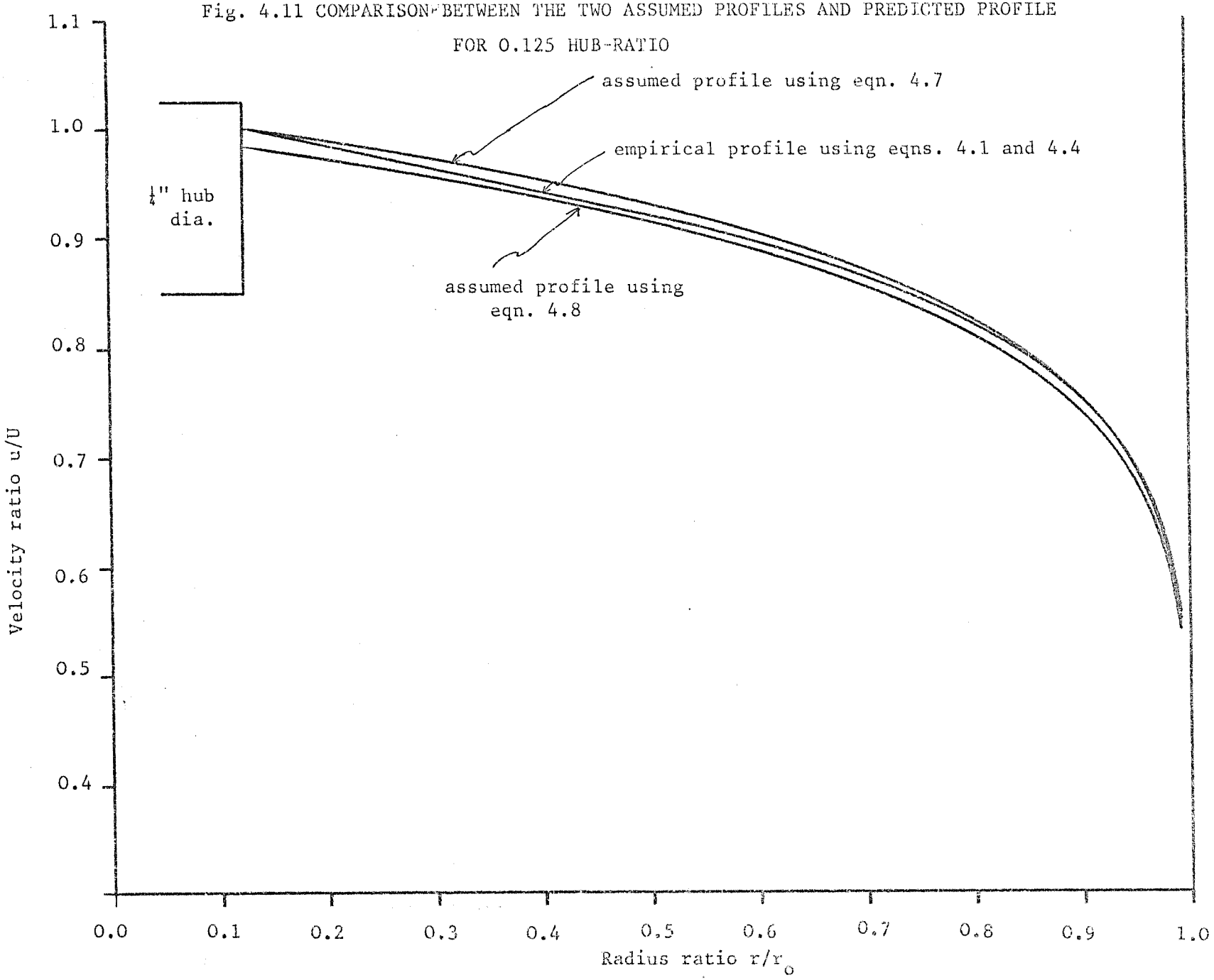

Fig 4.12 COMPARISON BETWEEN ASSUMED PROFILES AND PREDICTED PROFILE FOR 0.375 HUB-RATIO

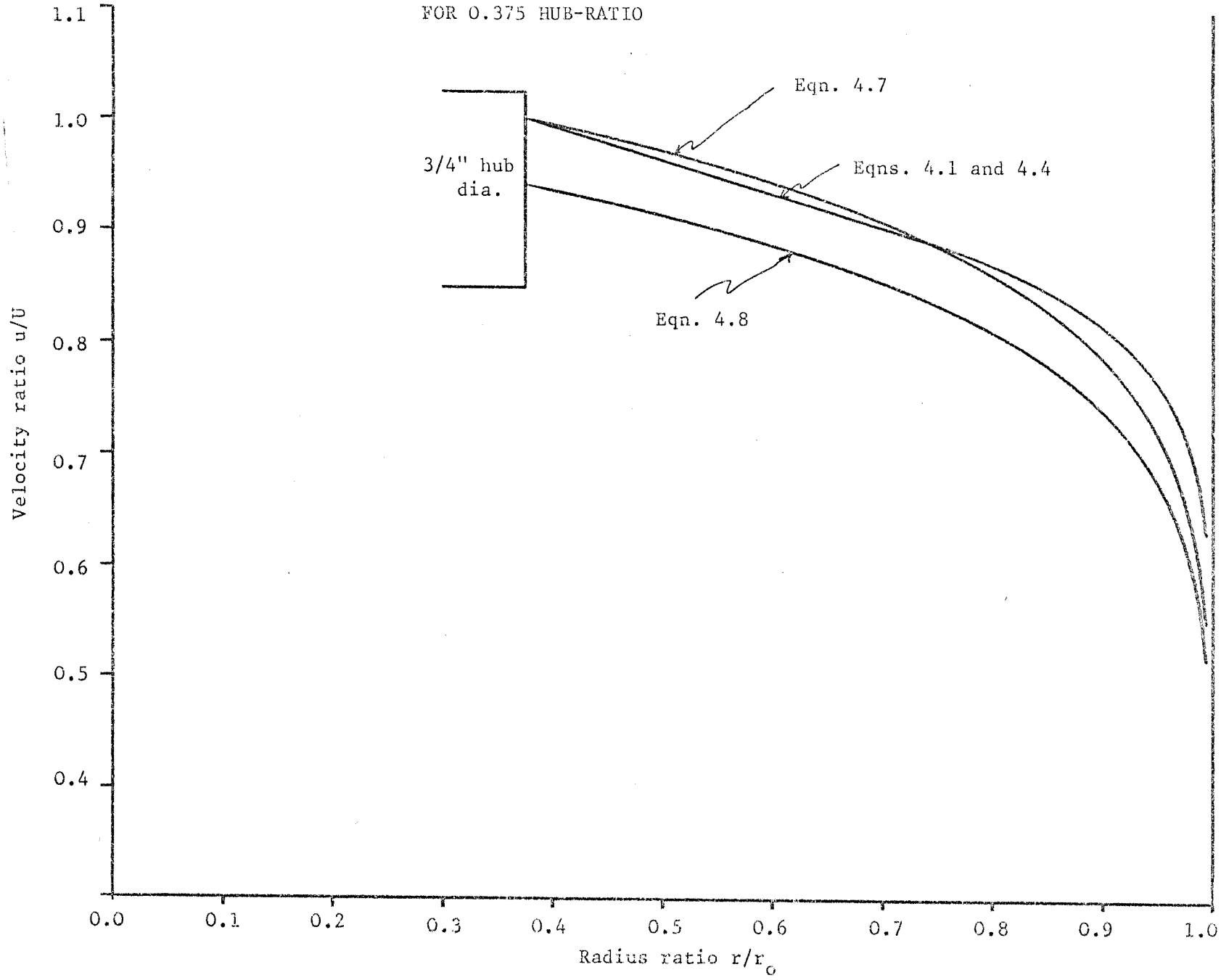

Fig. 4.13 COMPARISON BETWEEN ASSUMED PROFILES AND PREDICTED PROFILE FOR 0.75 HUB-RATIO

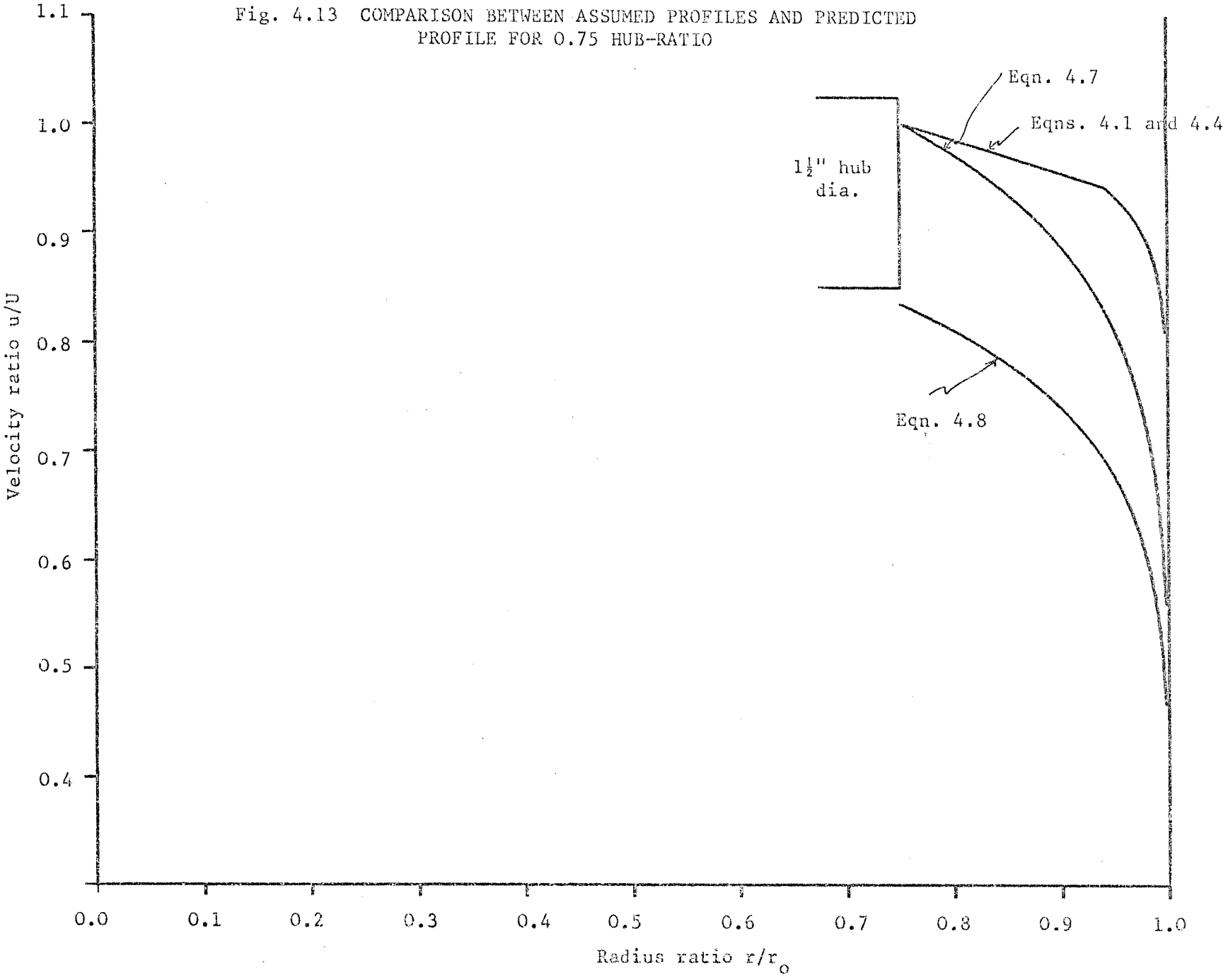

Fig. 4.14 Error in meter coefficient using assumed profiles

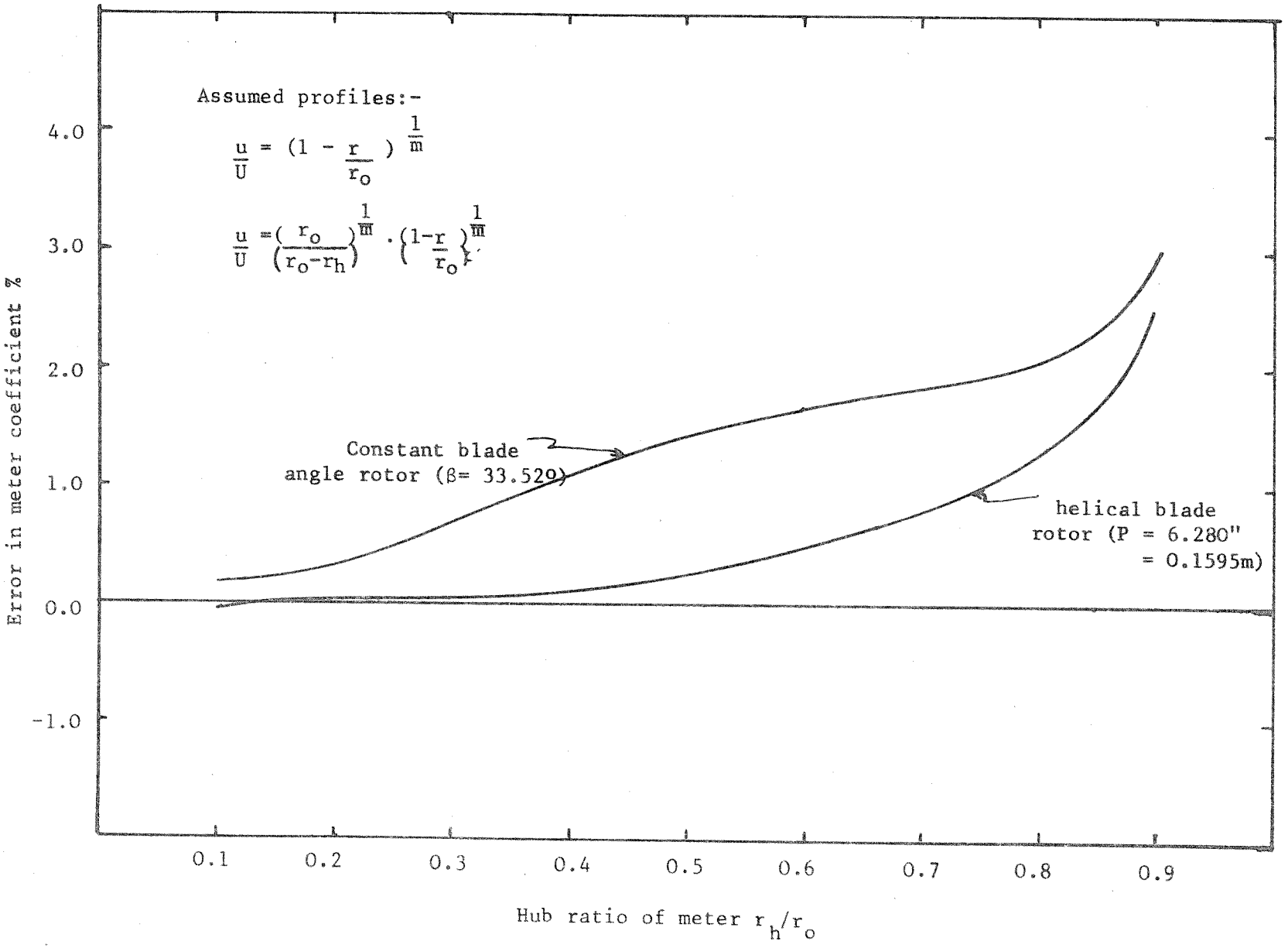

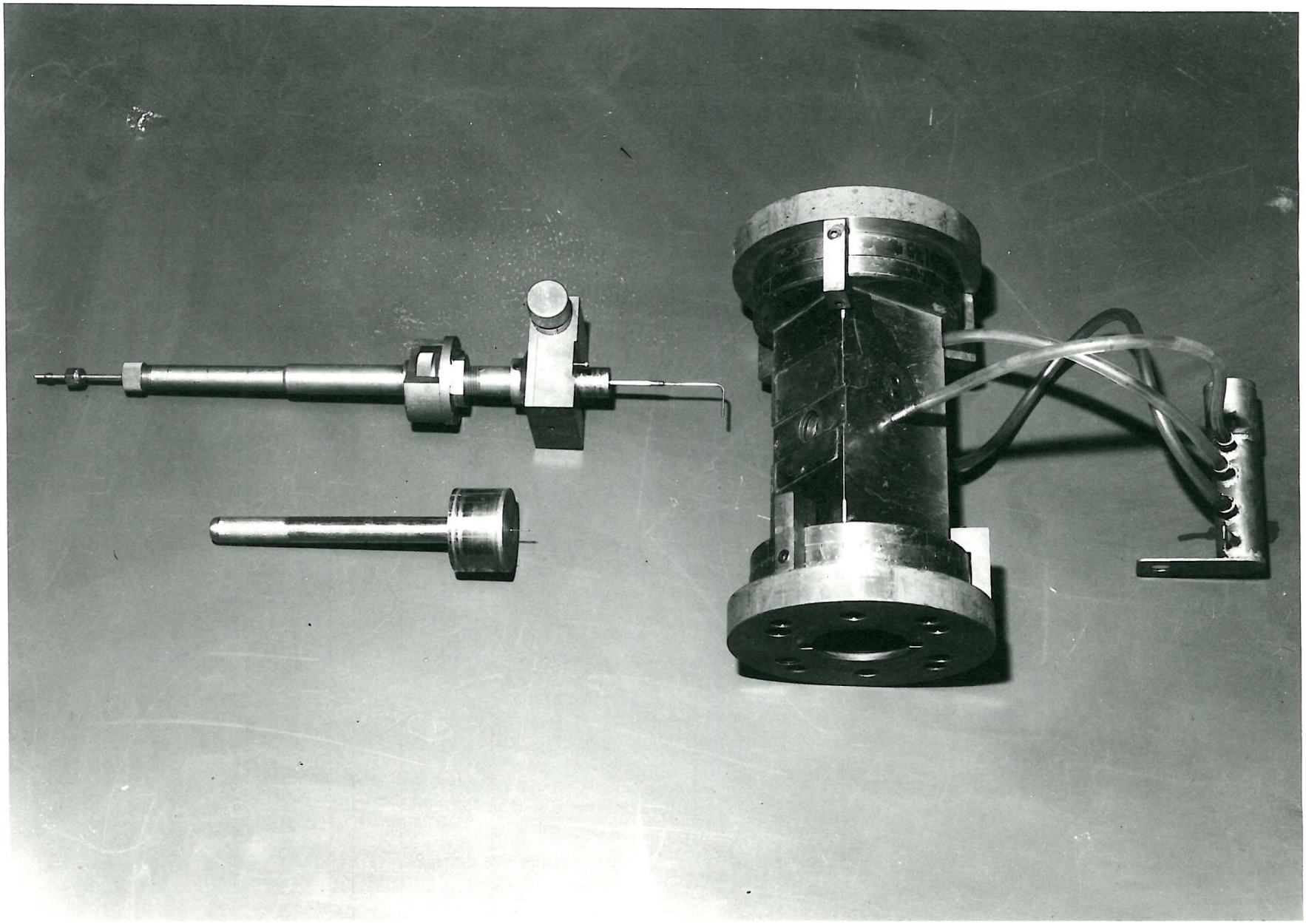

Fig. 4.15 Pitot Traversing Gear with Centering Plunger

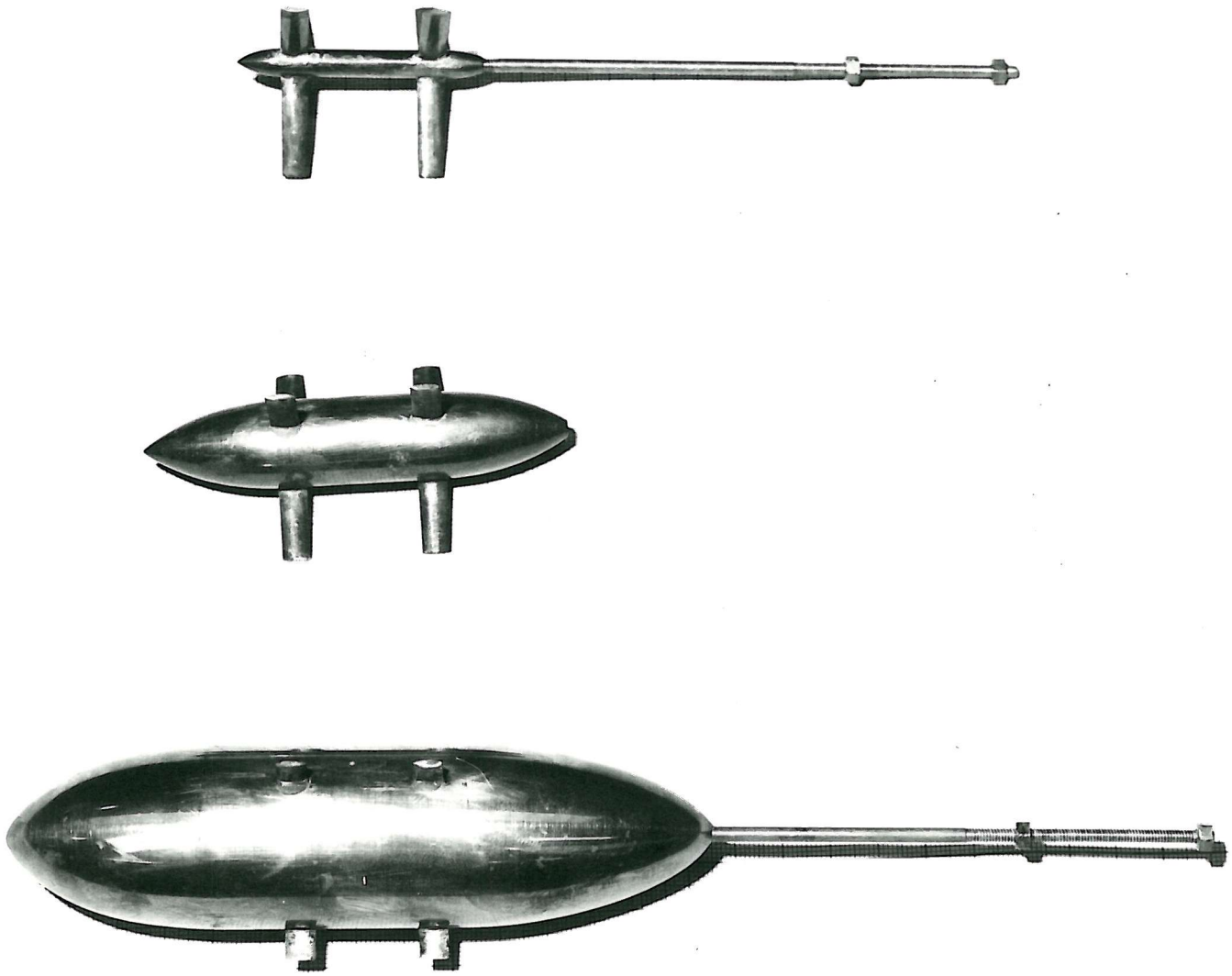

Fig. 4.16 $\frac{1}{4}$", $\frac{3}{4}$" and $1\frac{1}{2}$" Simulation Hubs

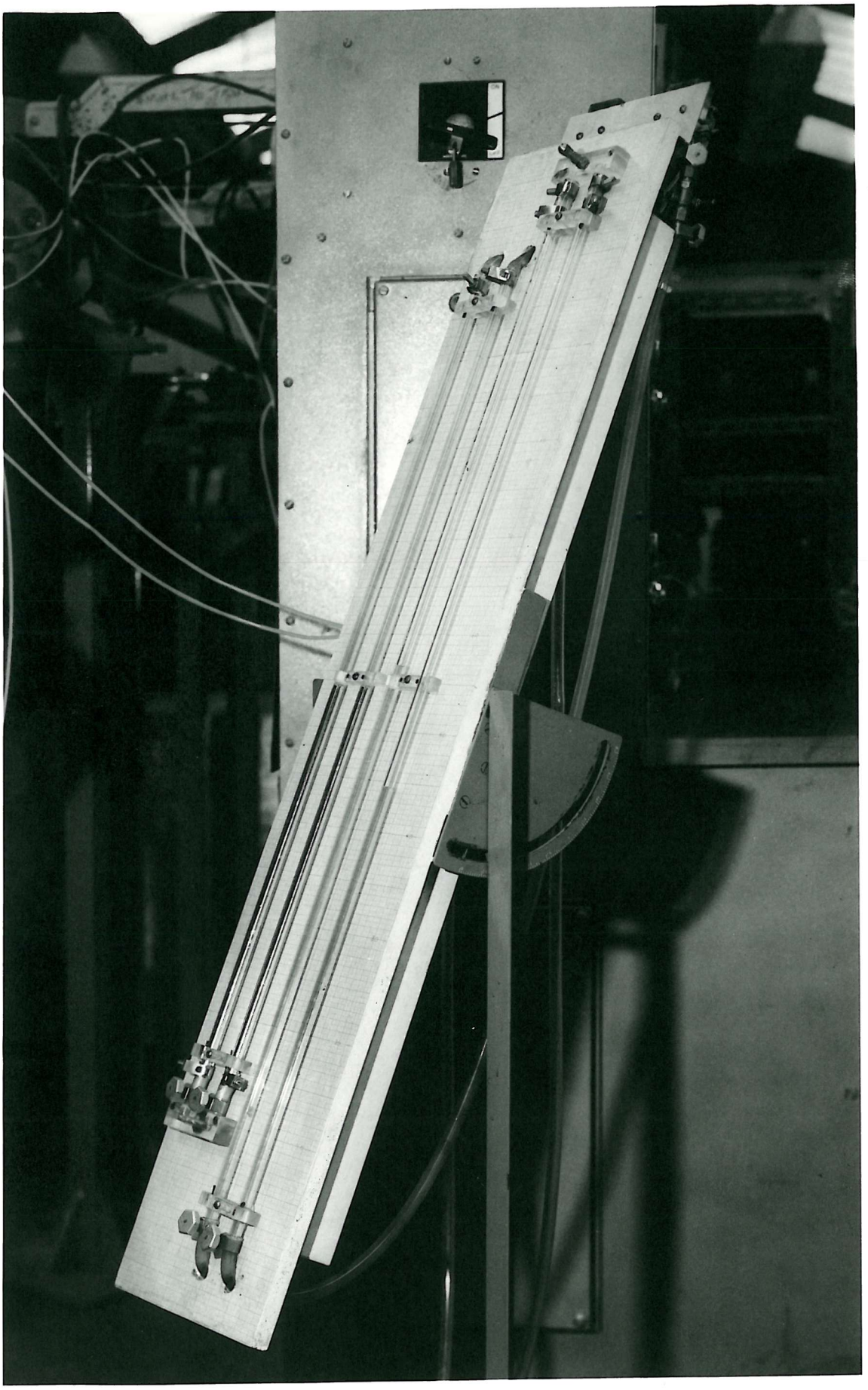

Fig. 4.17 COMBINED MERCURY AND WATER MANOMETER

Fig. 5.1 Effect of tip-clearance on the upstream calibration curves of the 0.125 hub-ratio constant blade angle research rotor

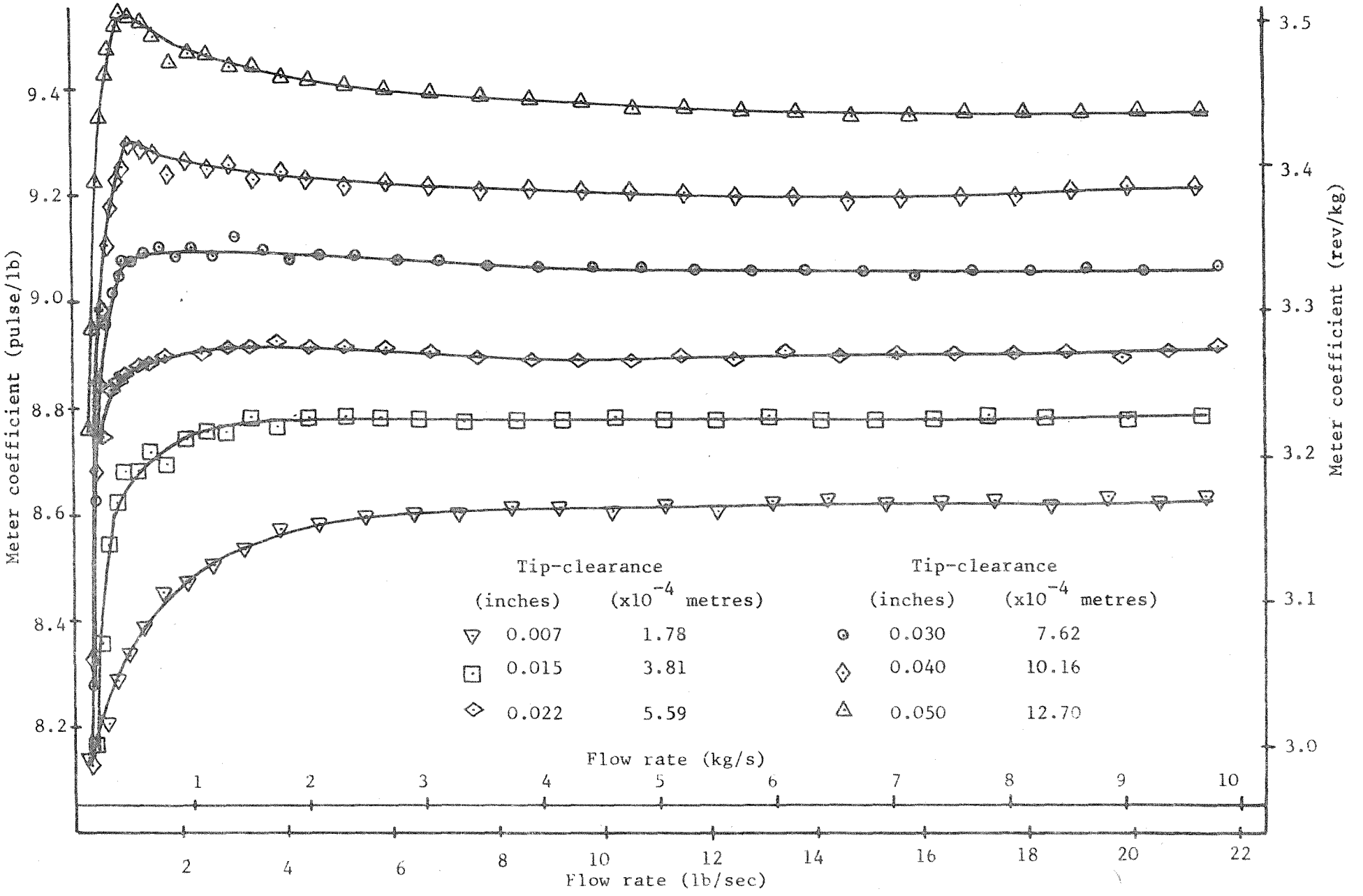

Fig. 5.2 Effect of tip-clearance on the downstream calibration curves of the 0.125 hub-ratio constant blade angle research rotor

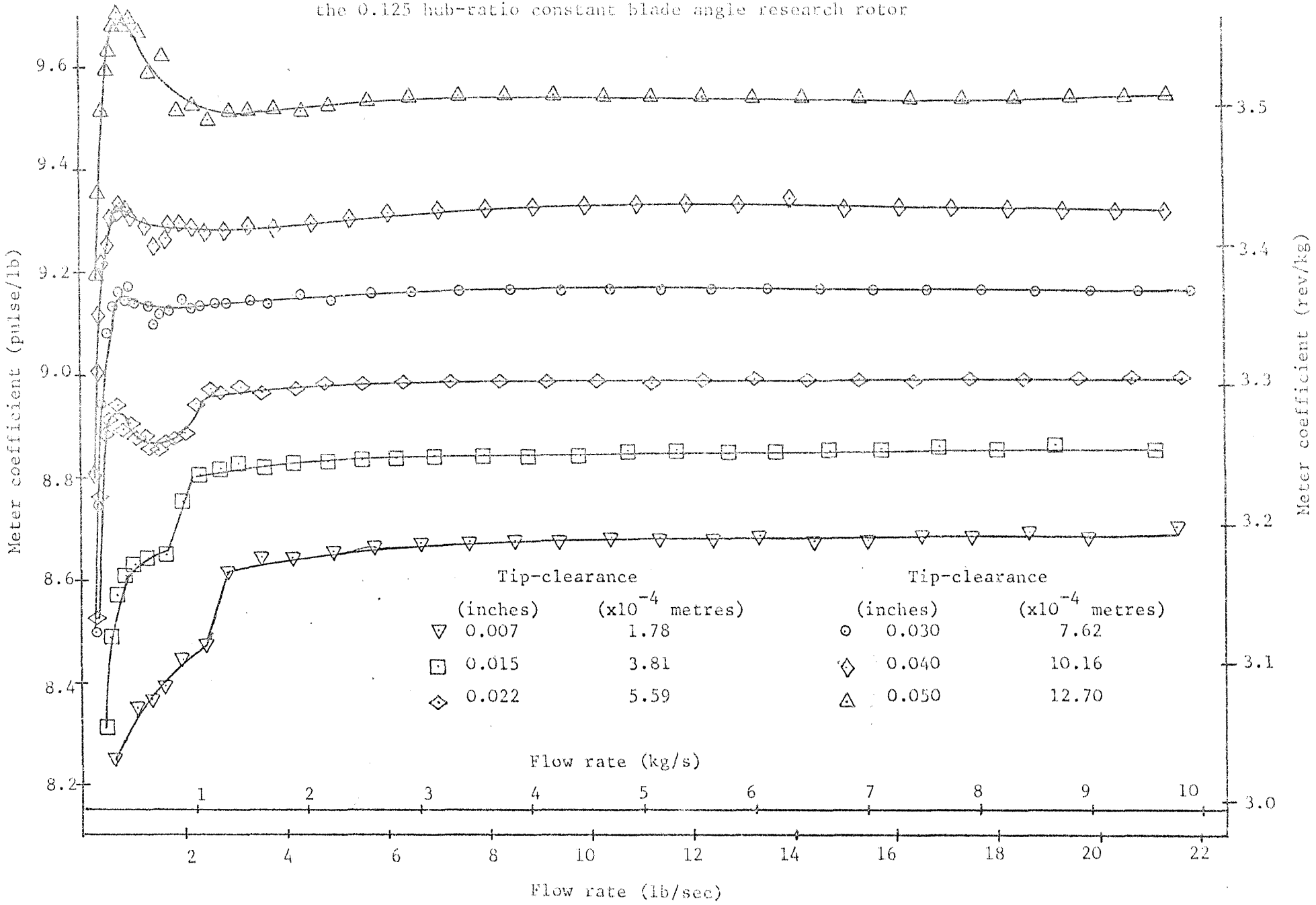

Fig. 5.3 Effect of tip-clearance on the upstream calibration curves of the 0.375 hub-ratio constant blade angle research rotor

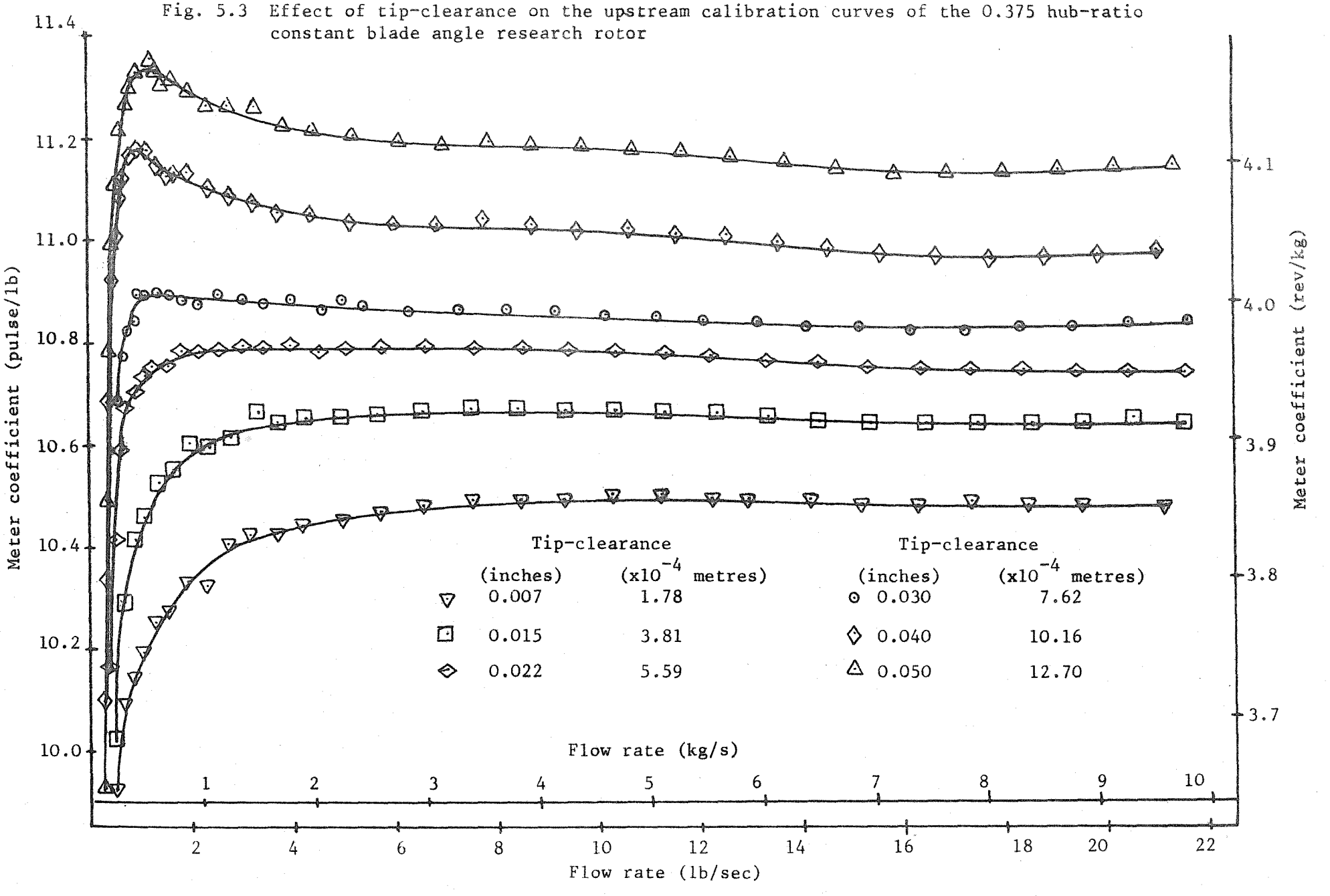

Fig. 5.4 Effect of tip-clearance on the downstream calibration curves of the 0.375 hub-ratio constant blade angle research rotor

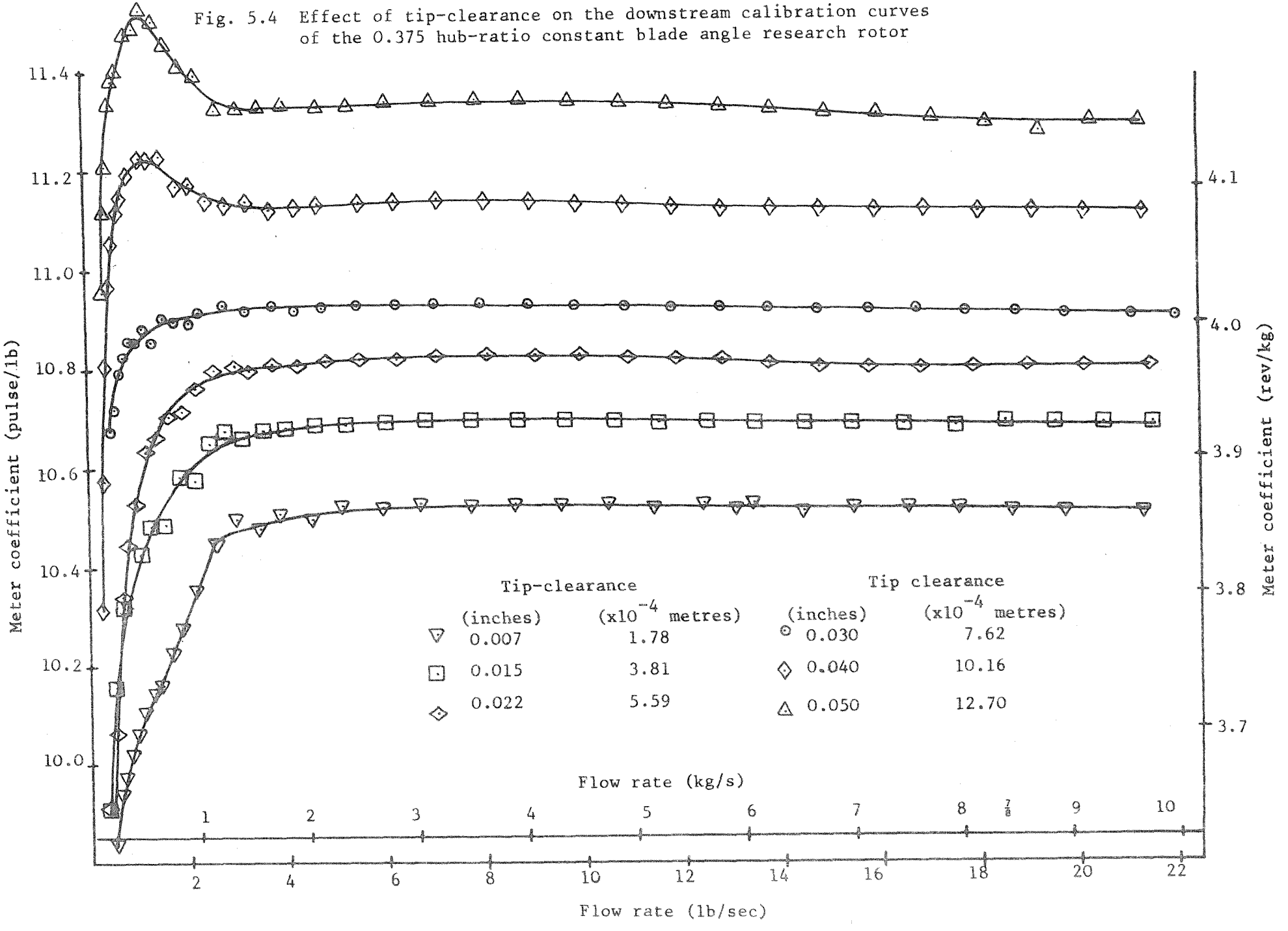

Fig. 5.5 Effect of tip-clearance on the upstream calibration curves of the 0.381 hub-ratio helical-blade research rotor (Part 1)

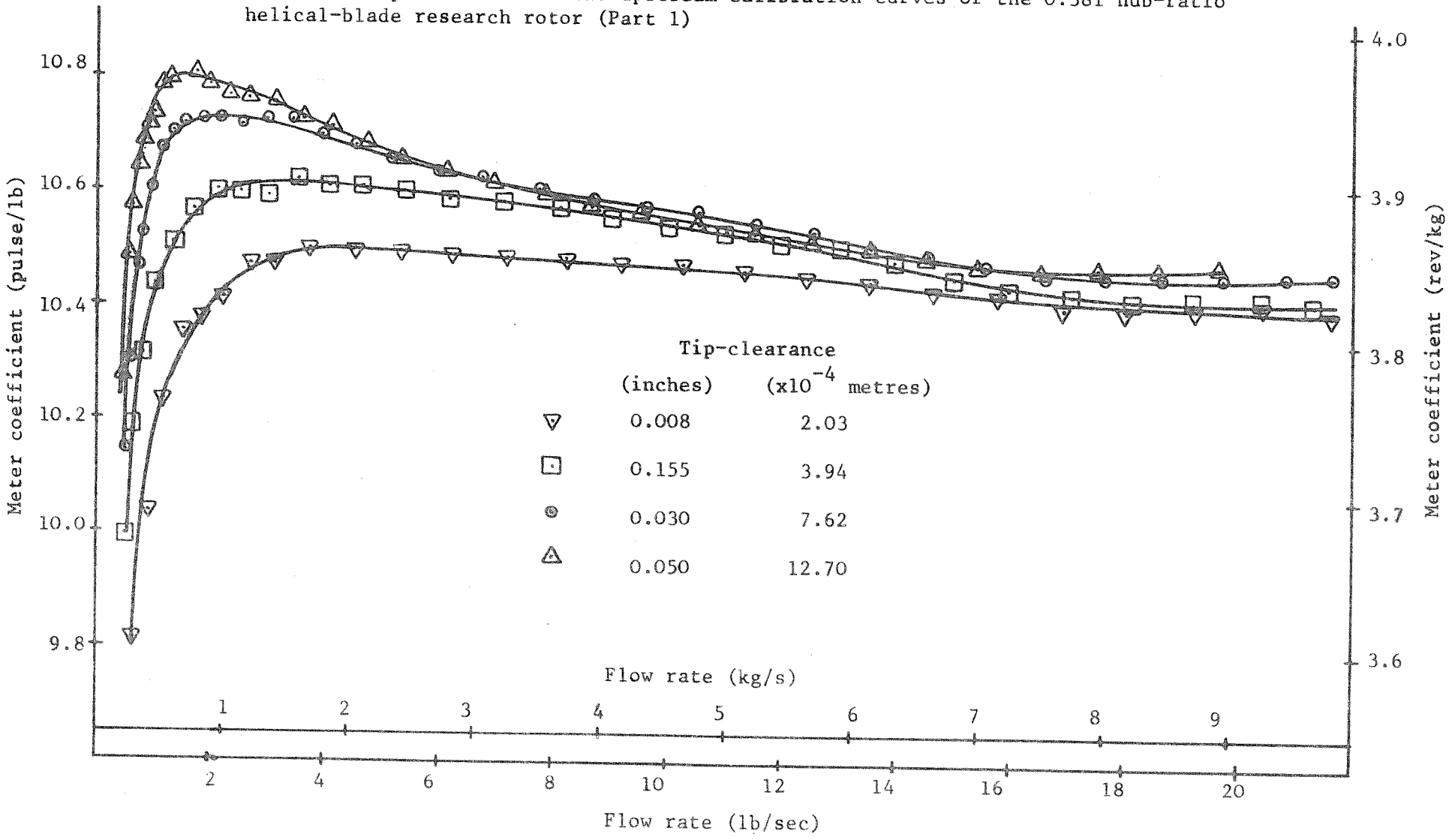

Fig. 5.6 Effect of tip-clearance on the upstream calibration curves of the 0.381 hub-ratio helical-blade research rotor (Part 2)

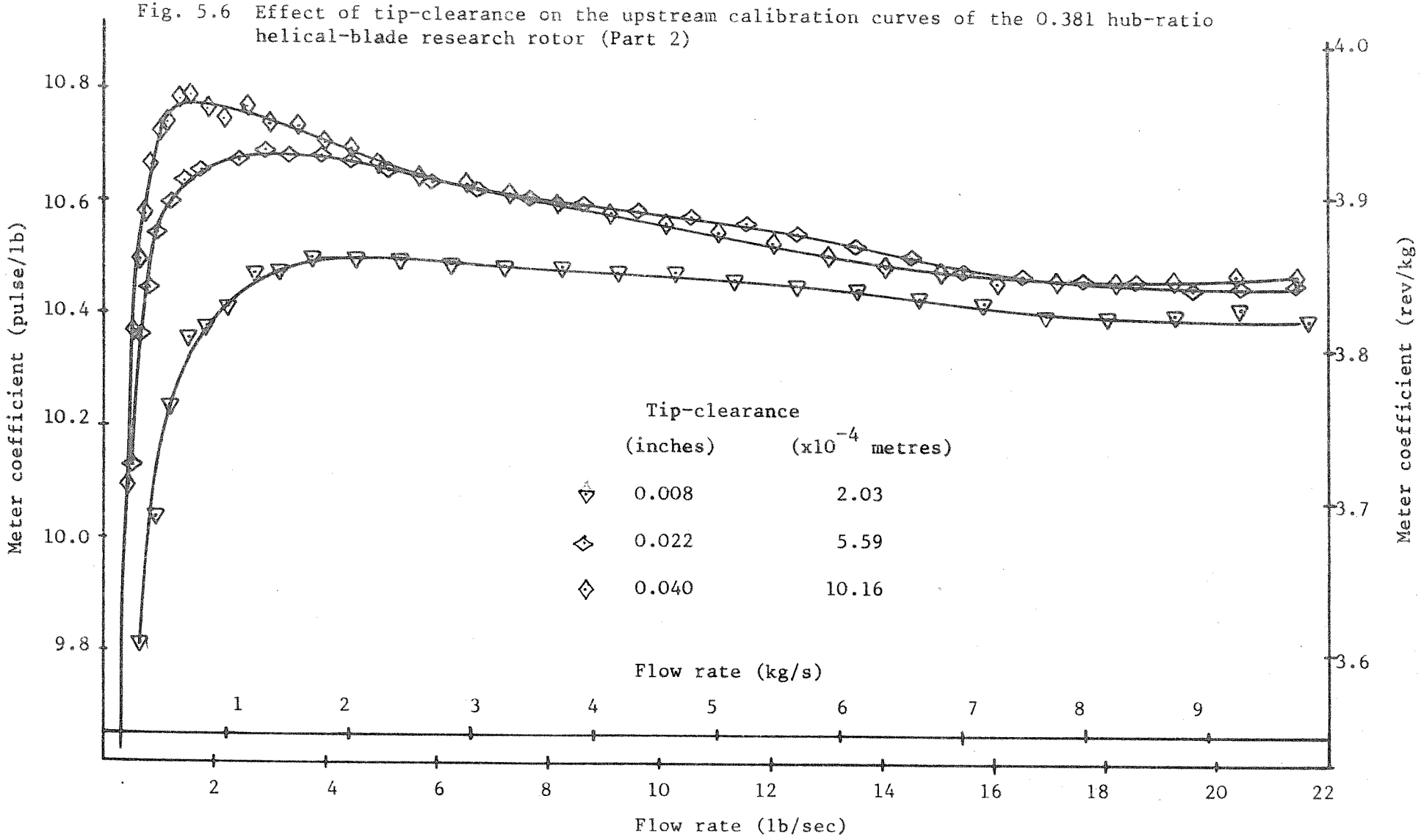

Fig. 5.7 Effect of tip-clearance on the downstream calibration curves of the 0.381 hub-ratio helical-blade research rotor

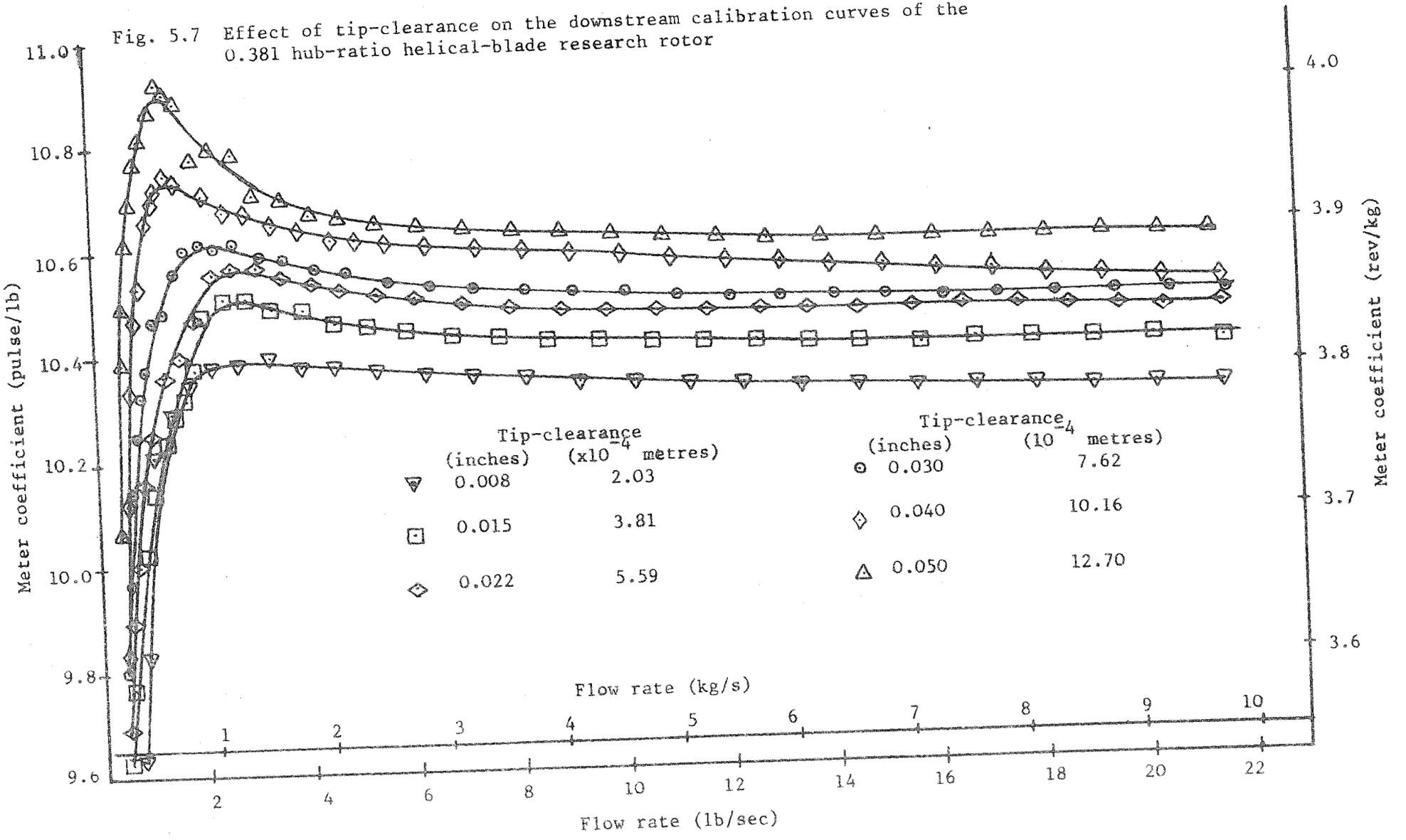

Fig. 5.8 Effect of tip-clearance on the upstream calibration curves of the 0.753 hub-ratio helical-blade research rotor

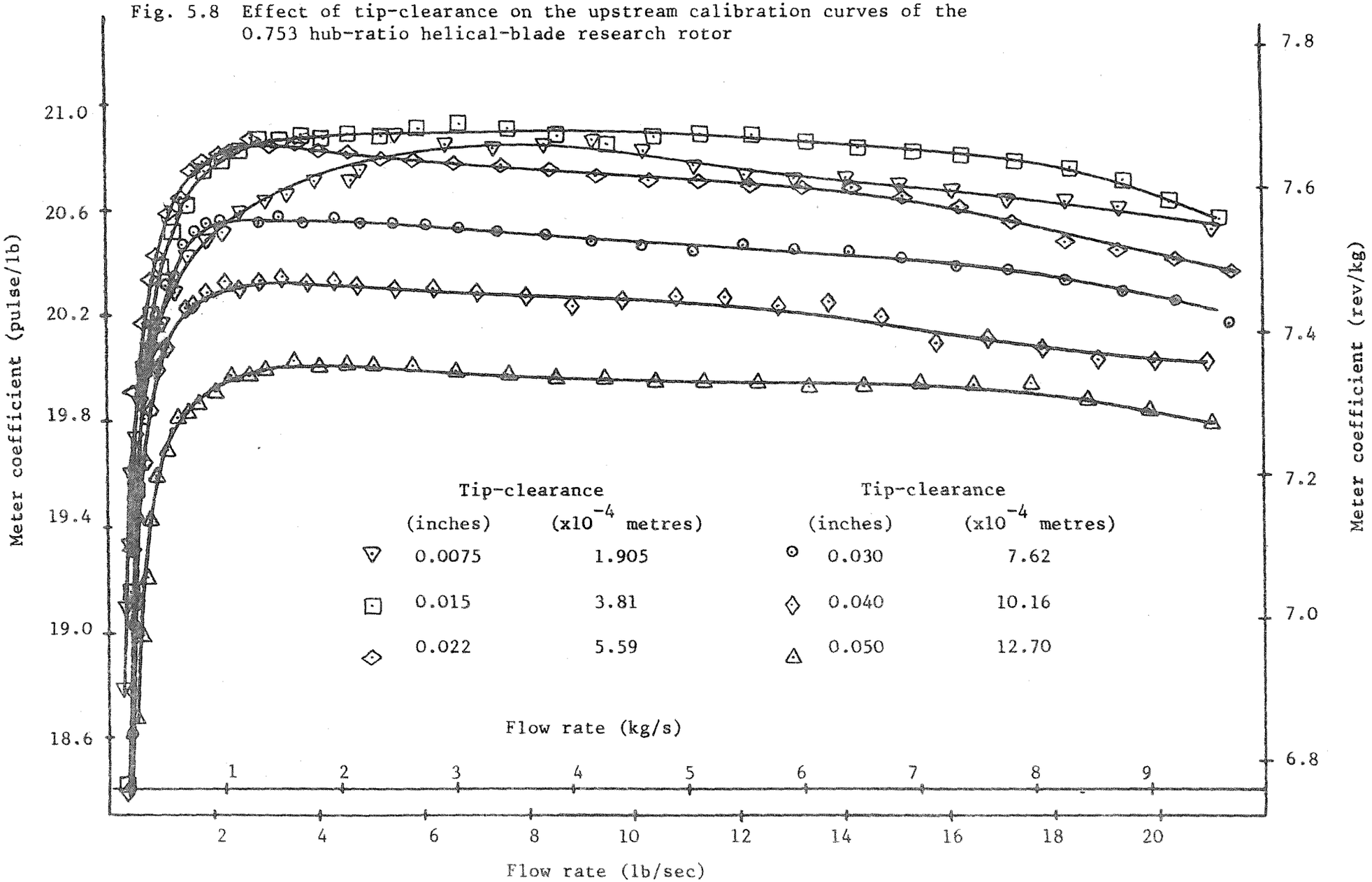

Fig. 5.9 Effect of tip-clearance on the downstream calibration curves of the 0.753 hub-ratio helical-blade research rotor

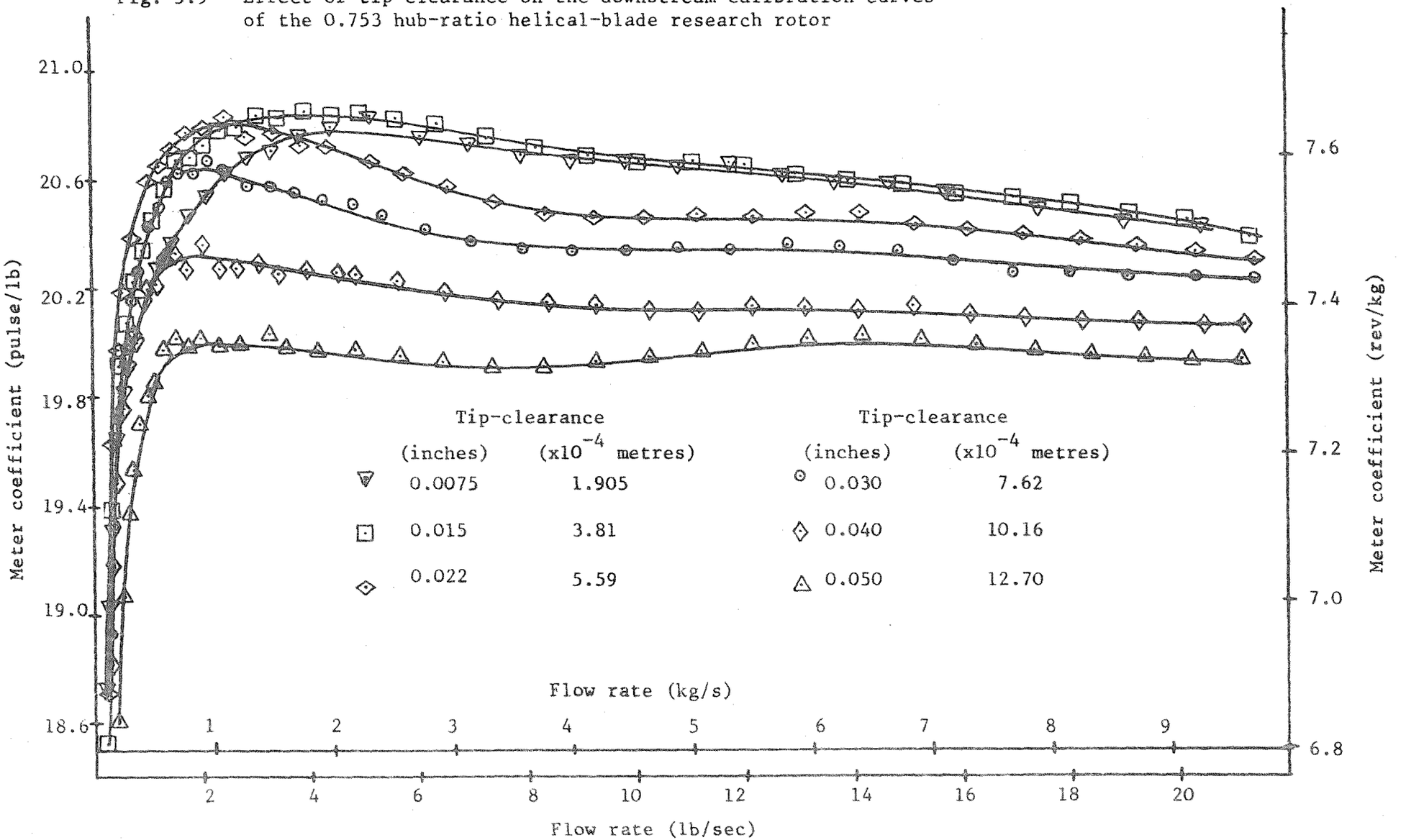

Fig. 5.10 Variation of meter coefficient with tip-clearance for constant blade angle rotors (at 15 lb/sec.)

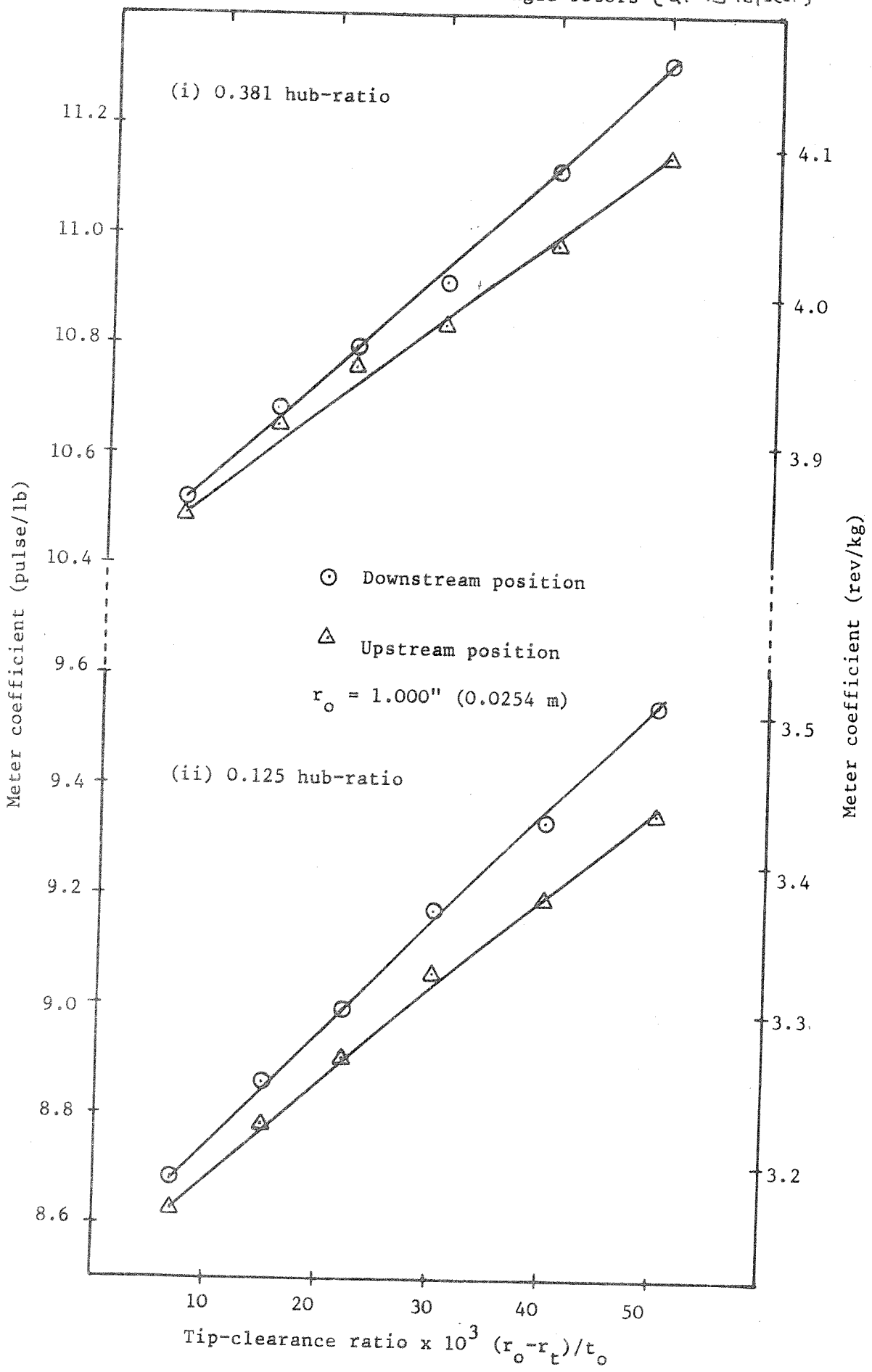

Fig. 5.11 Variation of meter coefficient with tip-clearance for helical-blade rotors (at 15 lb/sec)

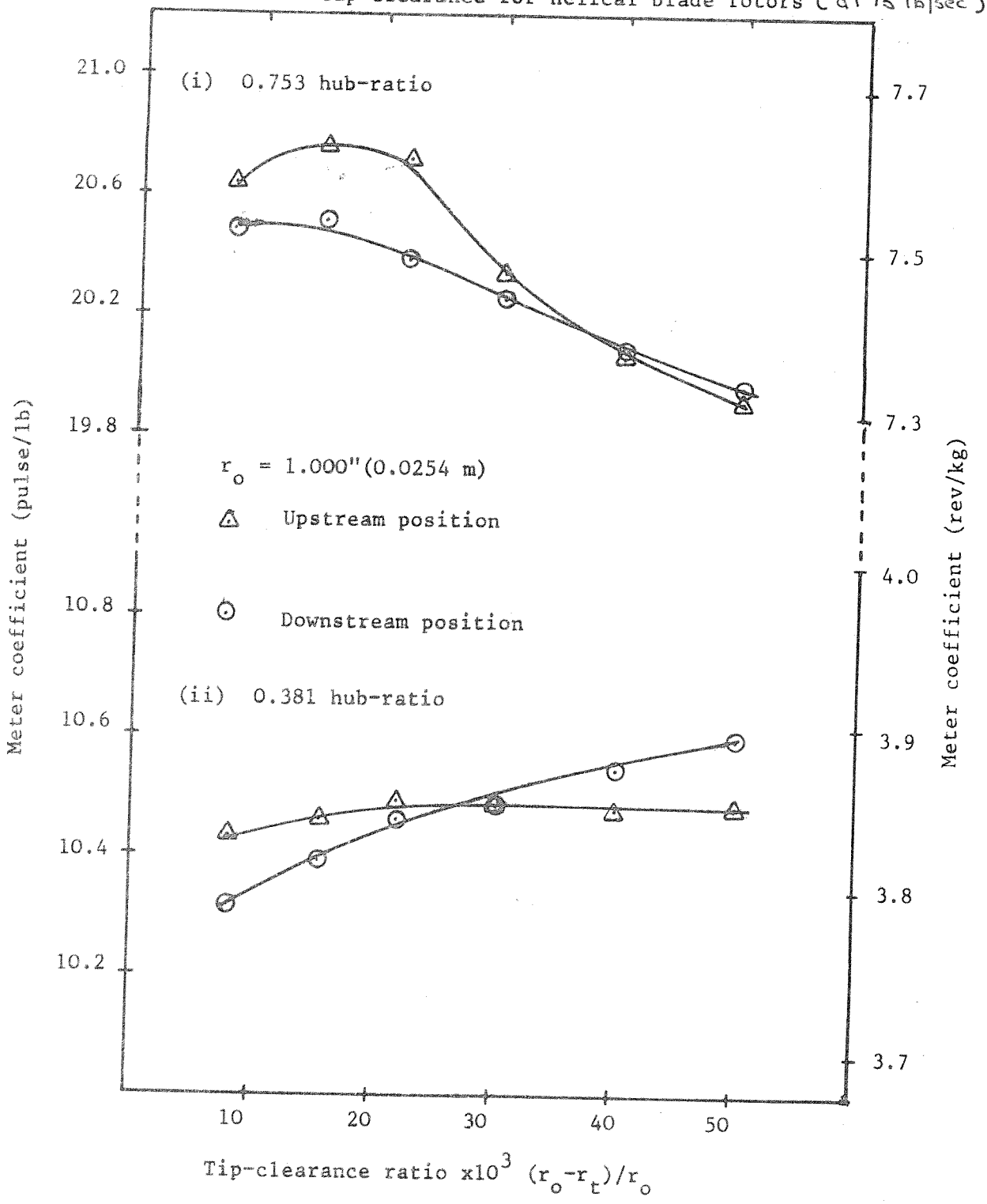

Fig. 5.12 Leakage ratio of helical-blade rotors

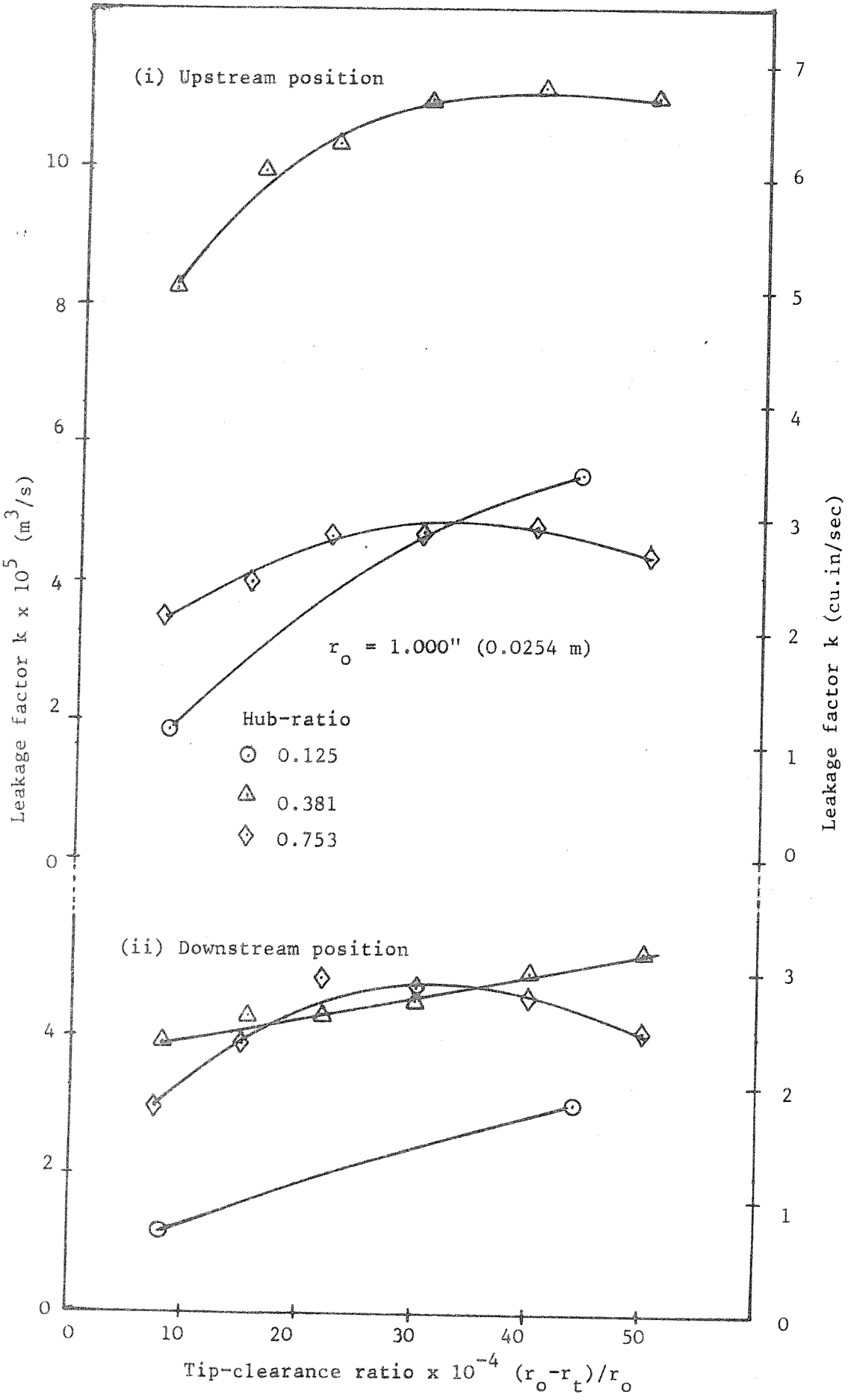

Fig. 5.13 Leakage factors of research rotors at upstream position

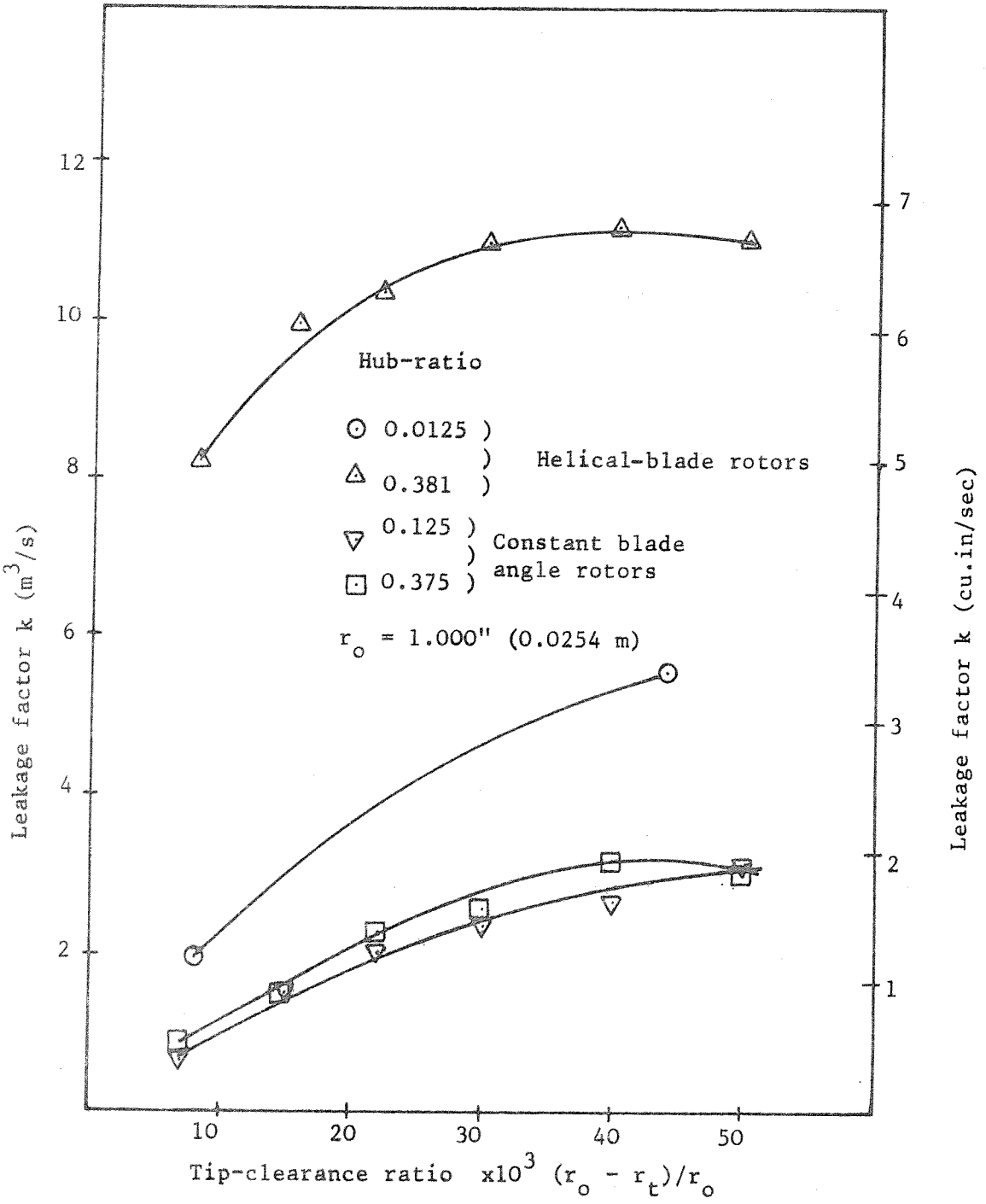

Fig. 5.14 Variation of leakage factor with tip-clearance area-ratio for helical-blade rotors

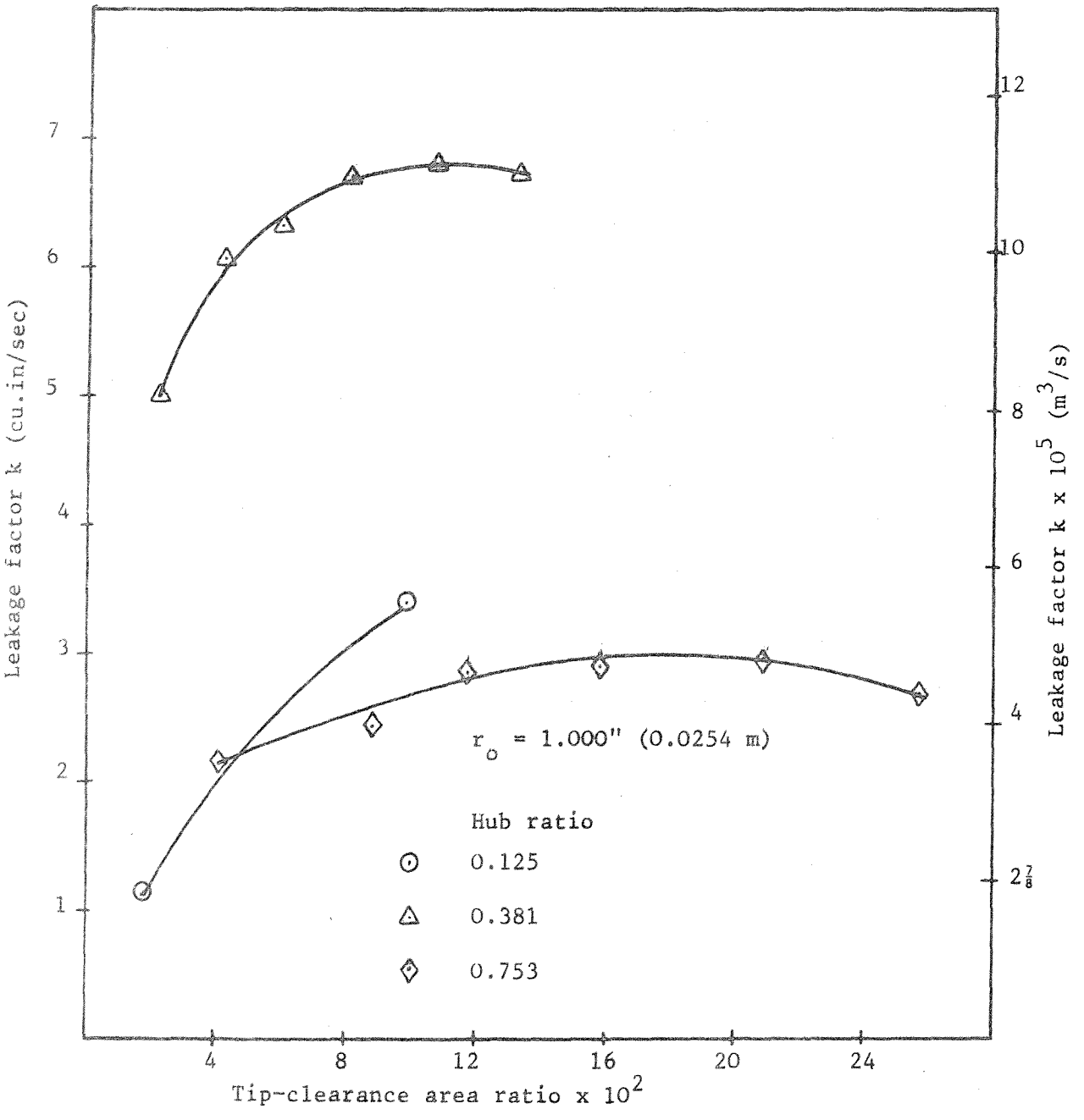

Fig. 5.15 Comparison of meter coefficient equations using different sets of assumptions

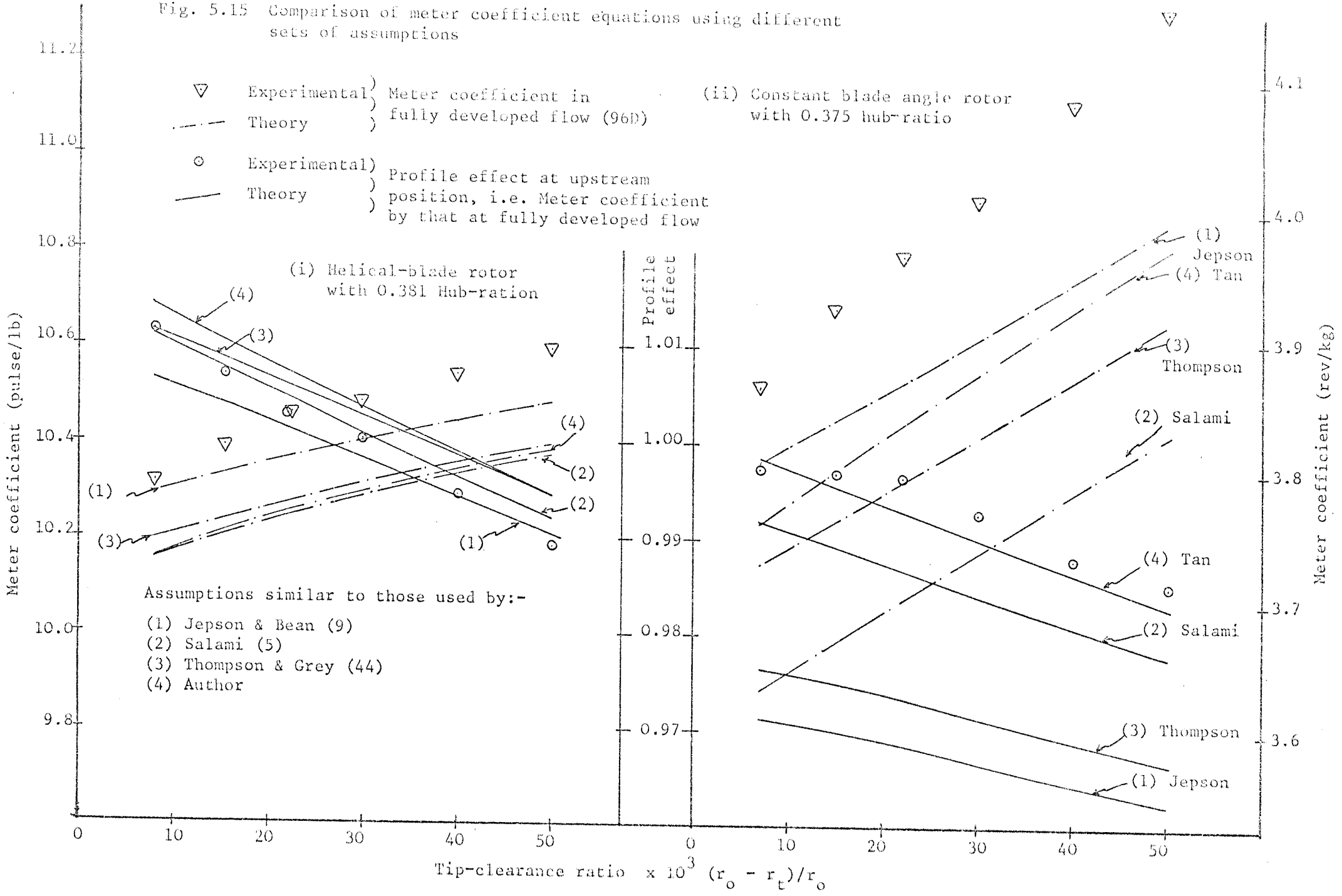

Fig. 5.16 Meter coefficient equation using effective blade angle β' and blade angle β

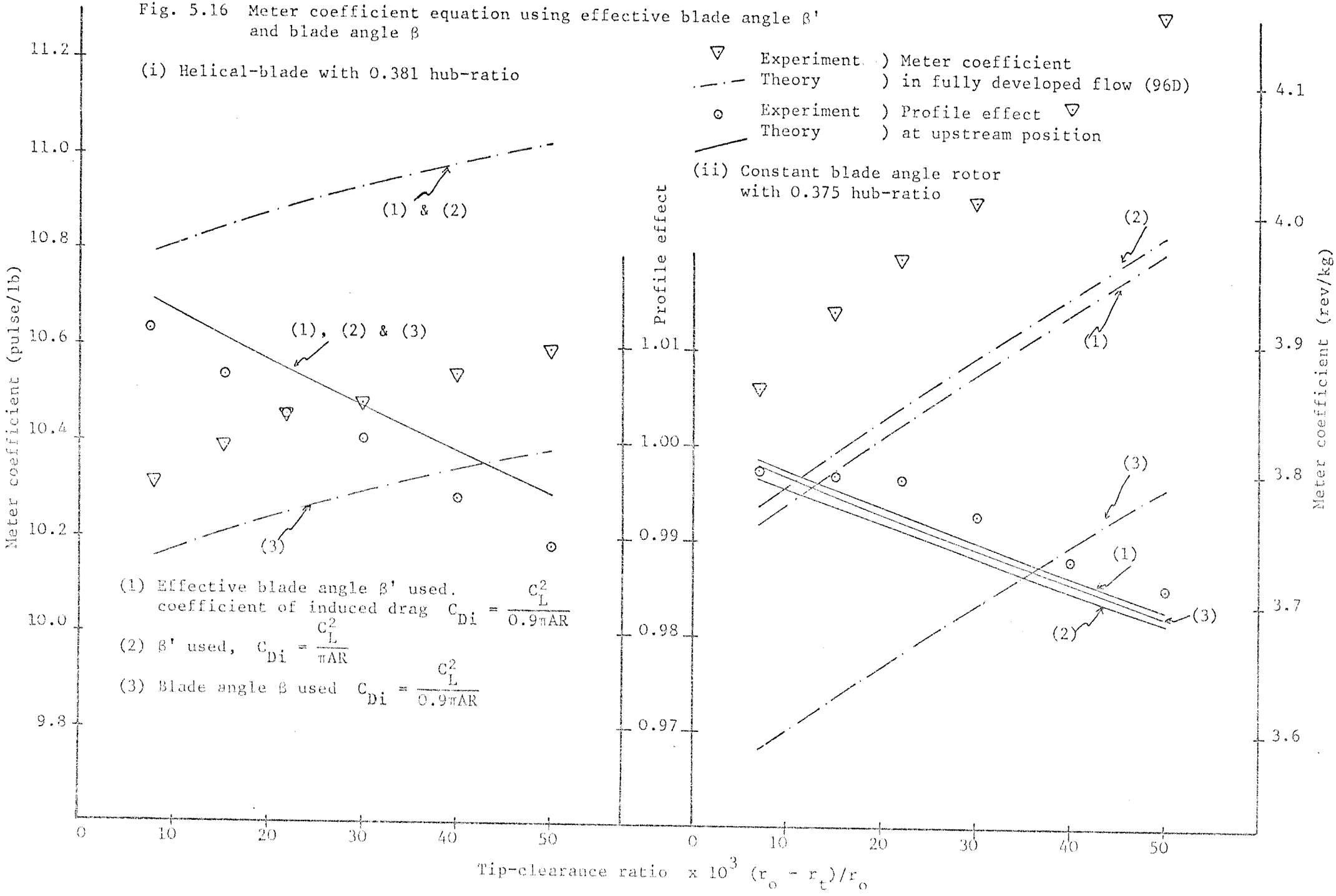

(1) Effective blade angle β' used. coefficient of induced drag $C_{Di} = \frac{C_L^2}{0.9\pi AR}$

(2) β' used, $C_{Di} = \frac{C_L^2}{\pi AR}$

(3) Blade angle β used $C_{Di} = \frac{C_L^2}{0.9\pi AR}$

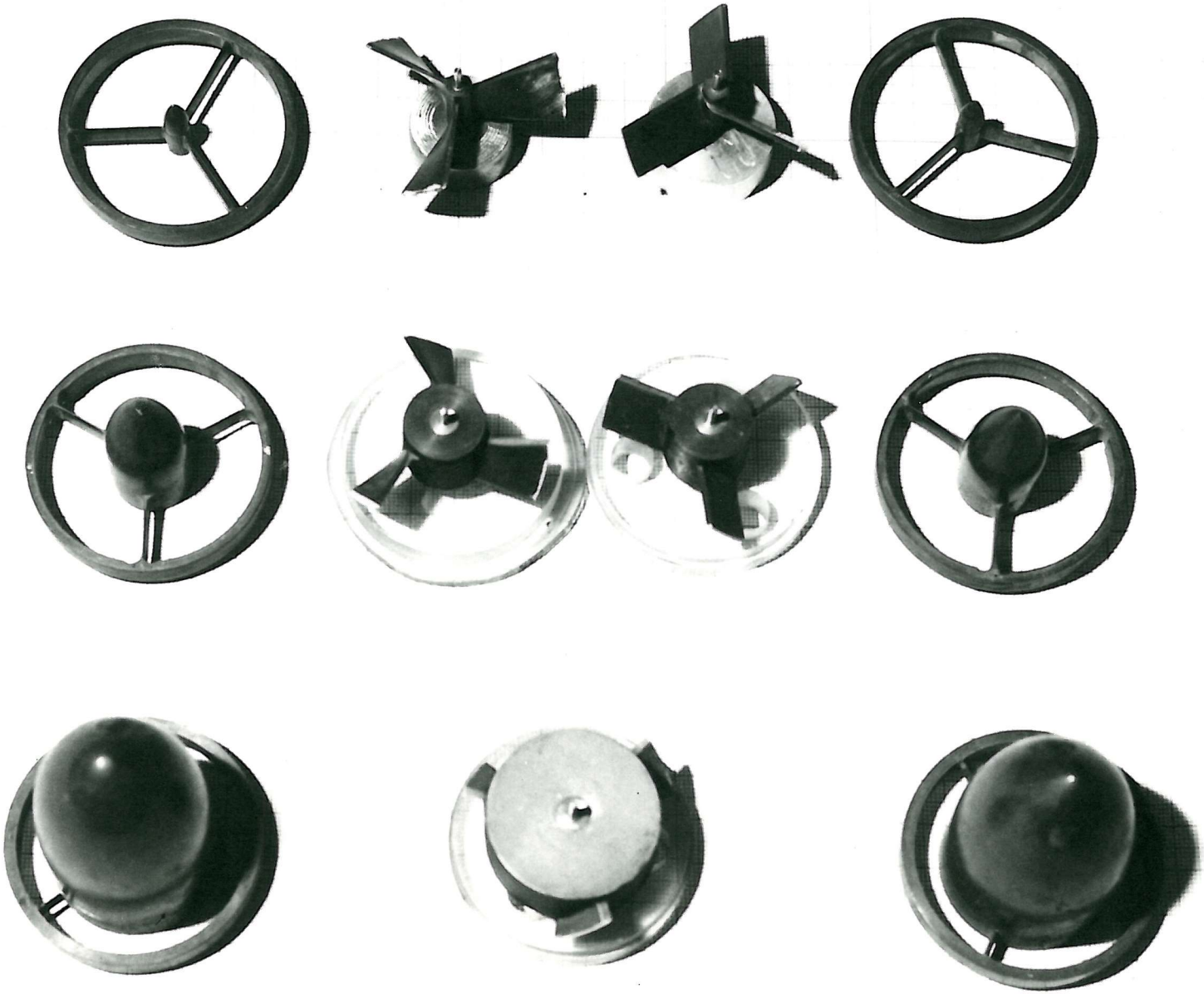

Fig. 5.17 $\frac{1}{4}$", $\frac{3}{4}$" and $1\frac{1}{2}$" Hub dia. Research Rotors with Bearing Housings

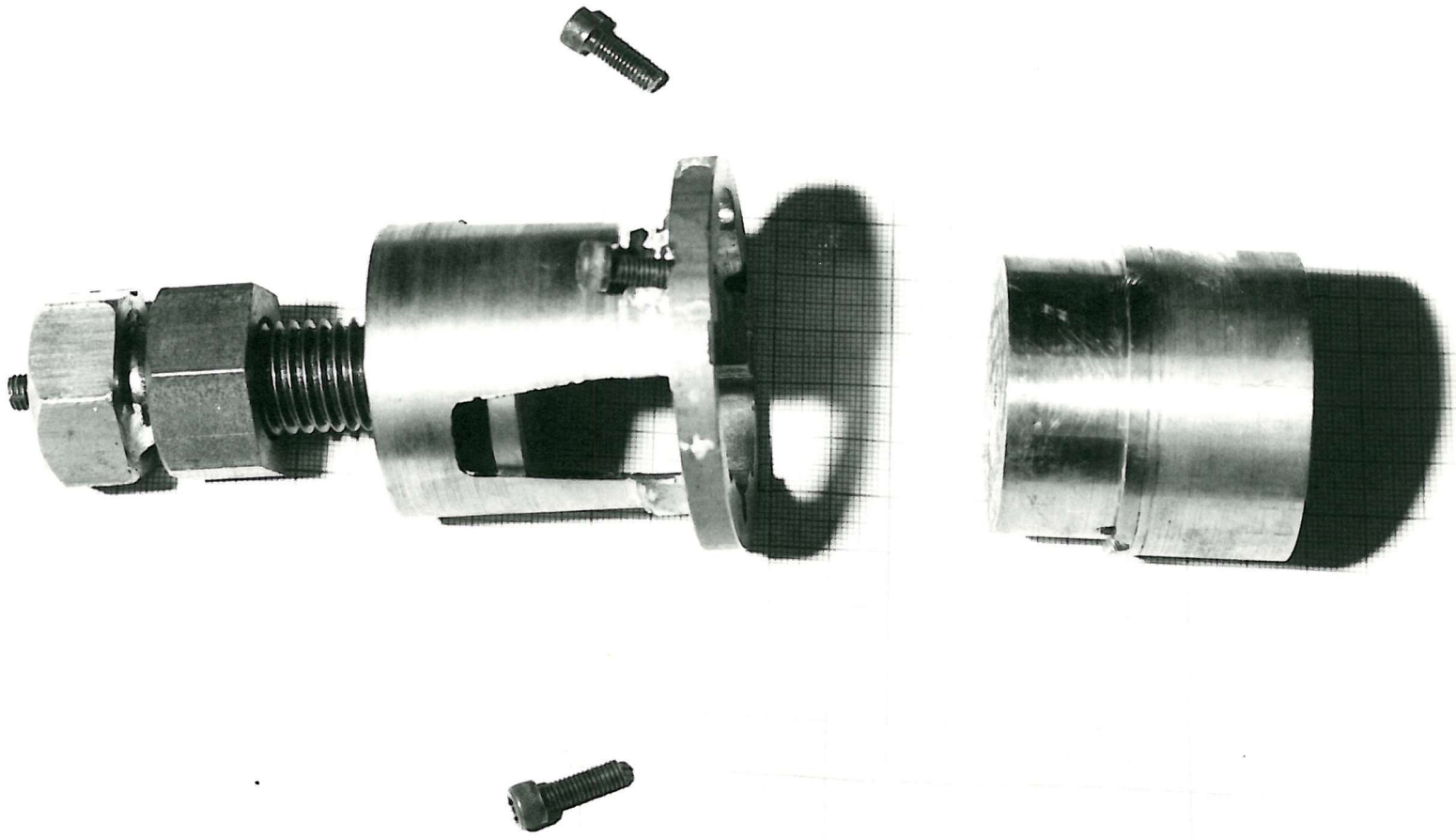

Fig. 5.18 Turbine Rotor Holder Used when Machining Down Blade Tip Radius

Fig. 6.1 Variation of boundary layer thickness downstream of pipe inlet

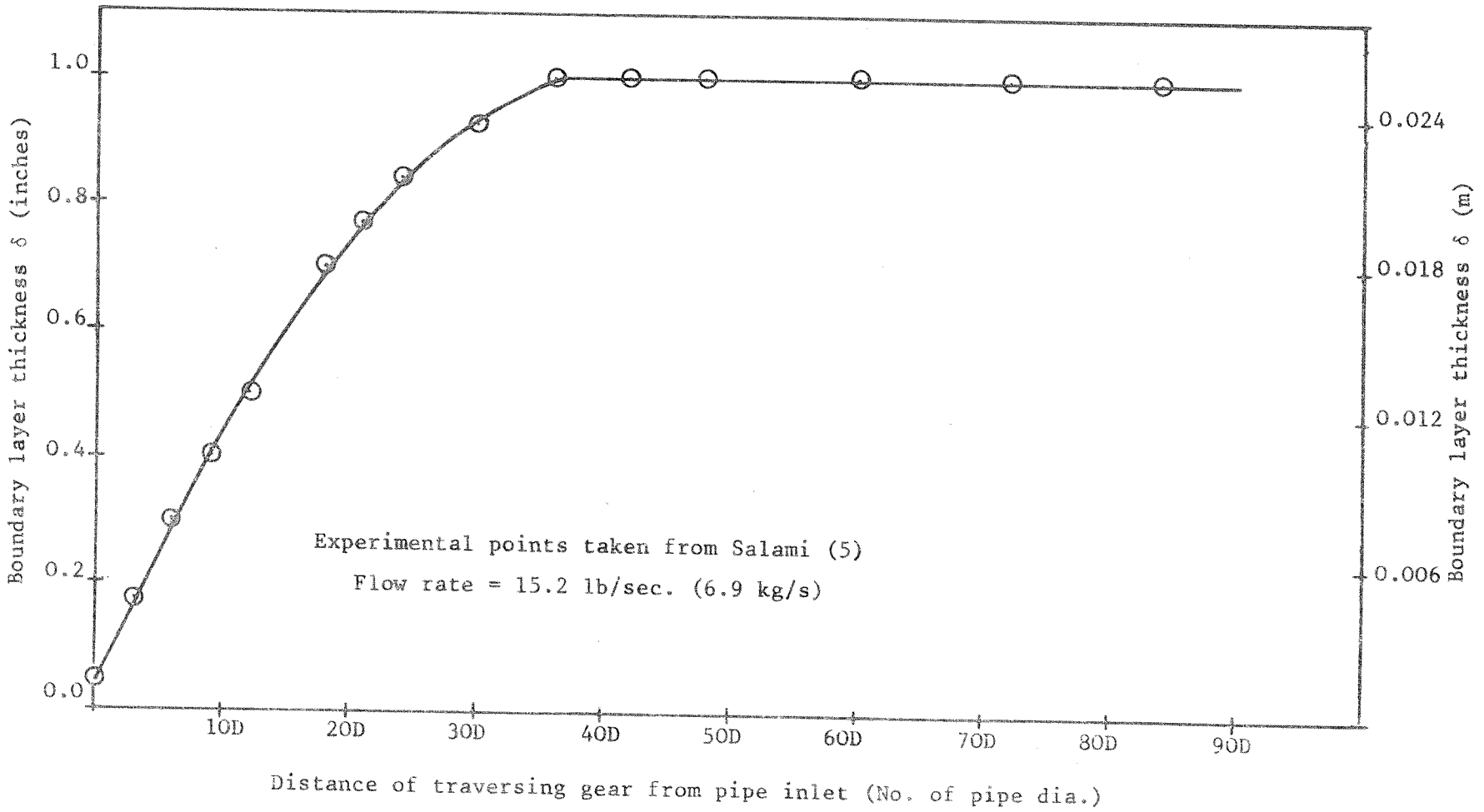

Fig. 6.2 Variation of m with distance downstream of pipe inlet

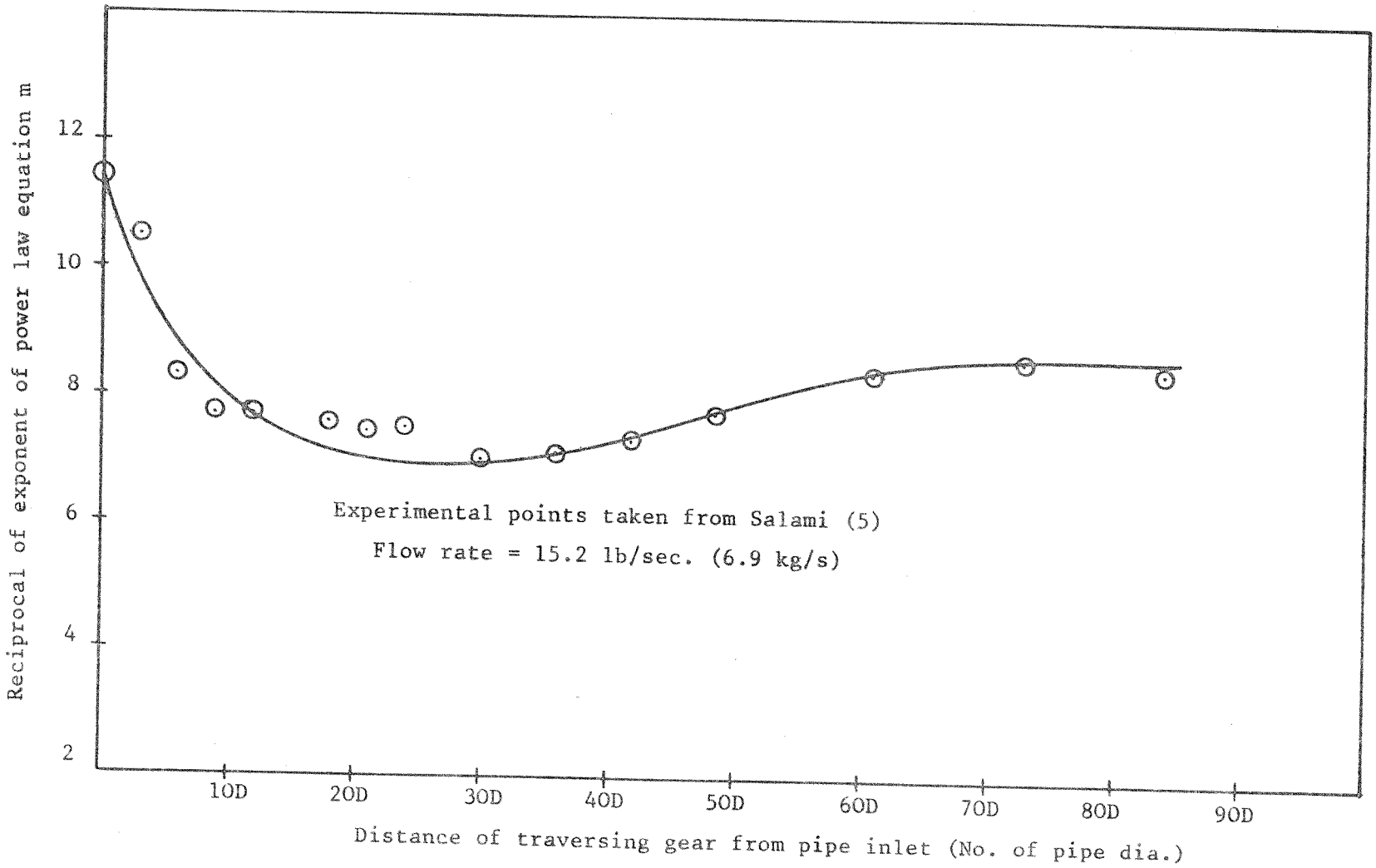

Fig. 6.3 Profile effect on the 0.38 hub-ratio helical-blade rotor subdivided into its constituent effects (at 151b/sec)

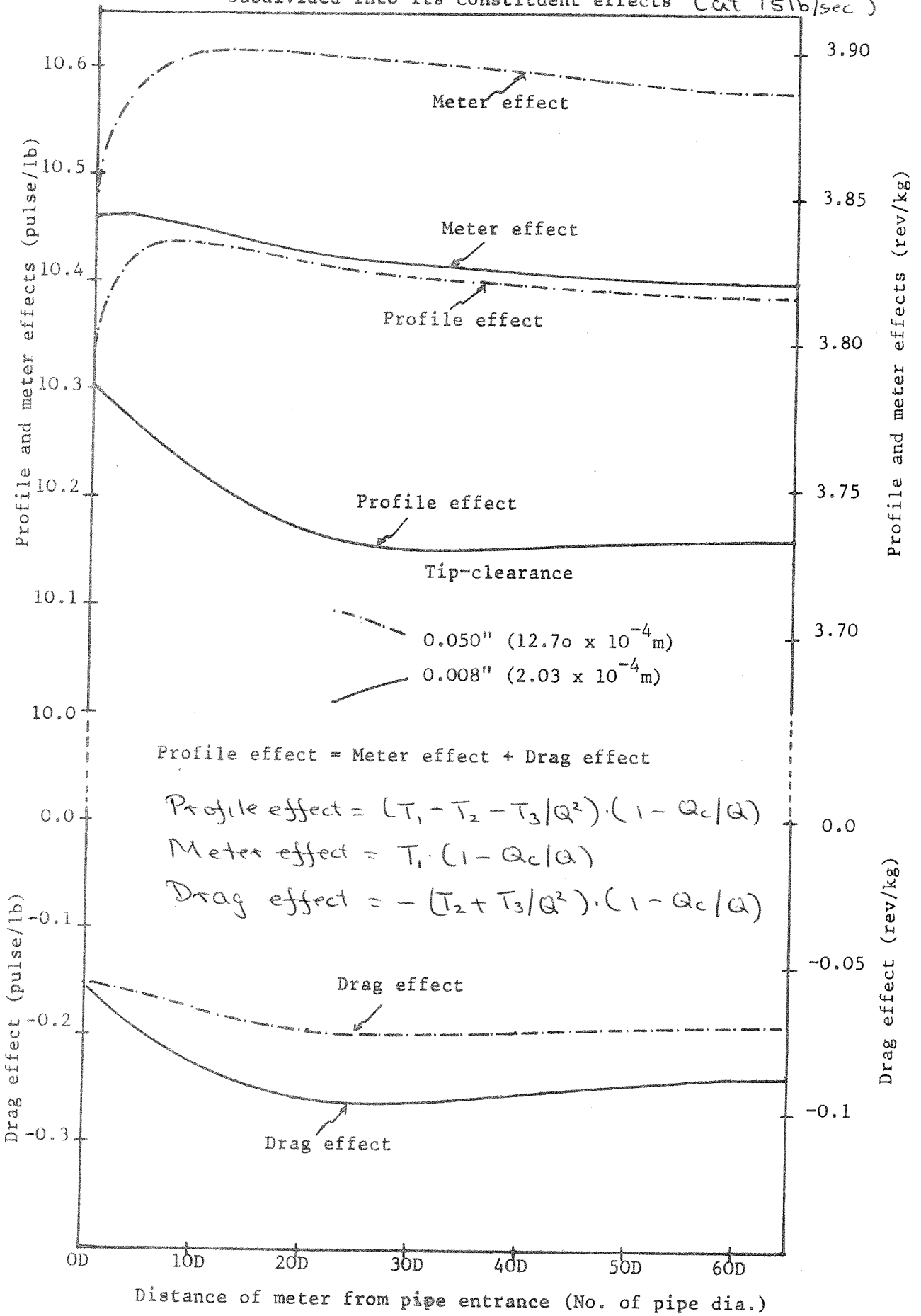

Fig. 6.4 Meter effect for the 0.38 hub-ratio helical-blade rotor subdivided further into its constituent effects (at 15 lb/sec)

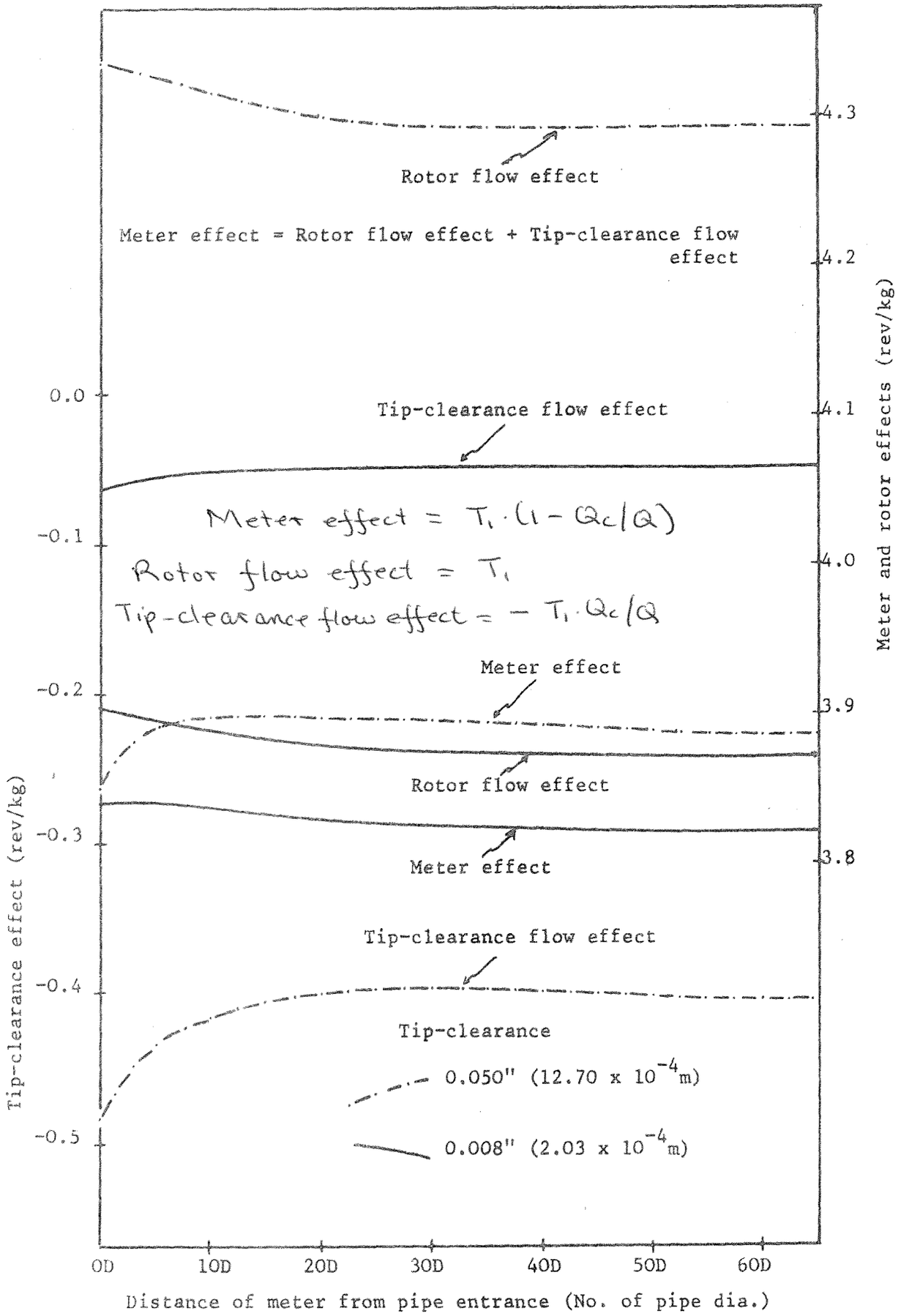

Fig. 6.5 Profile effect on the 0.375 hub-ratio constant blade angle rotor subdivided into its constituent effects (at 15 lb/sec)

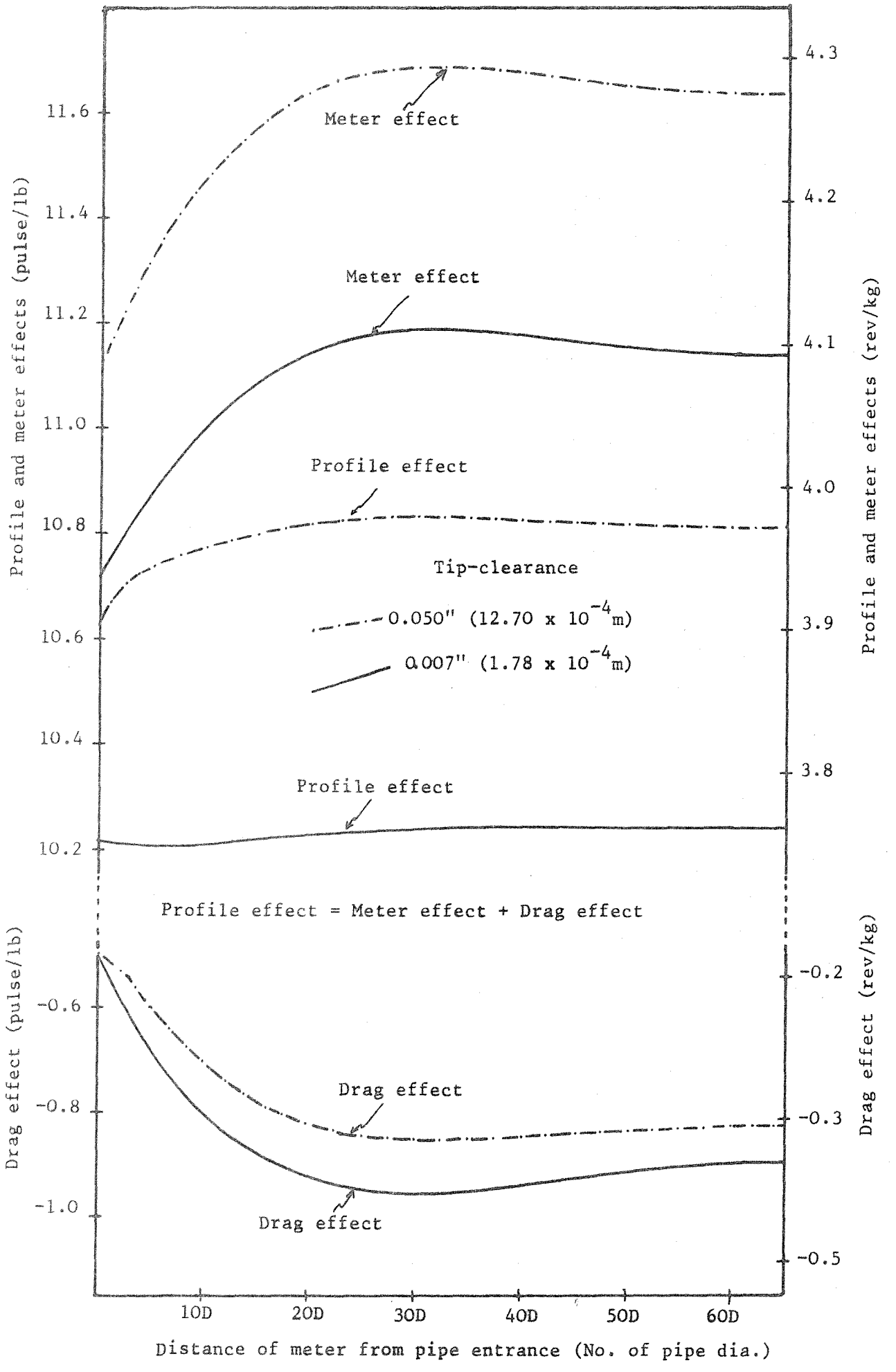

Fig. 6.6 Meter effect on the 0.375 hub-ratio constant blade angle rotor subdivided further into its constituent effects (at 15 lb/sec)

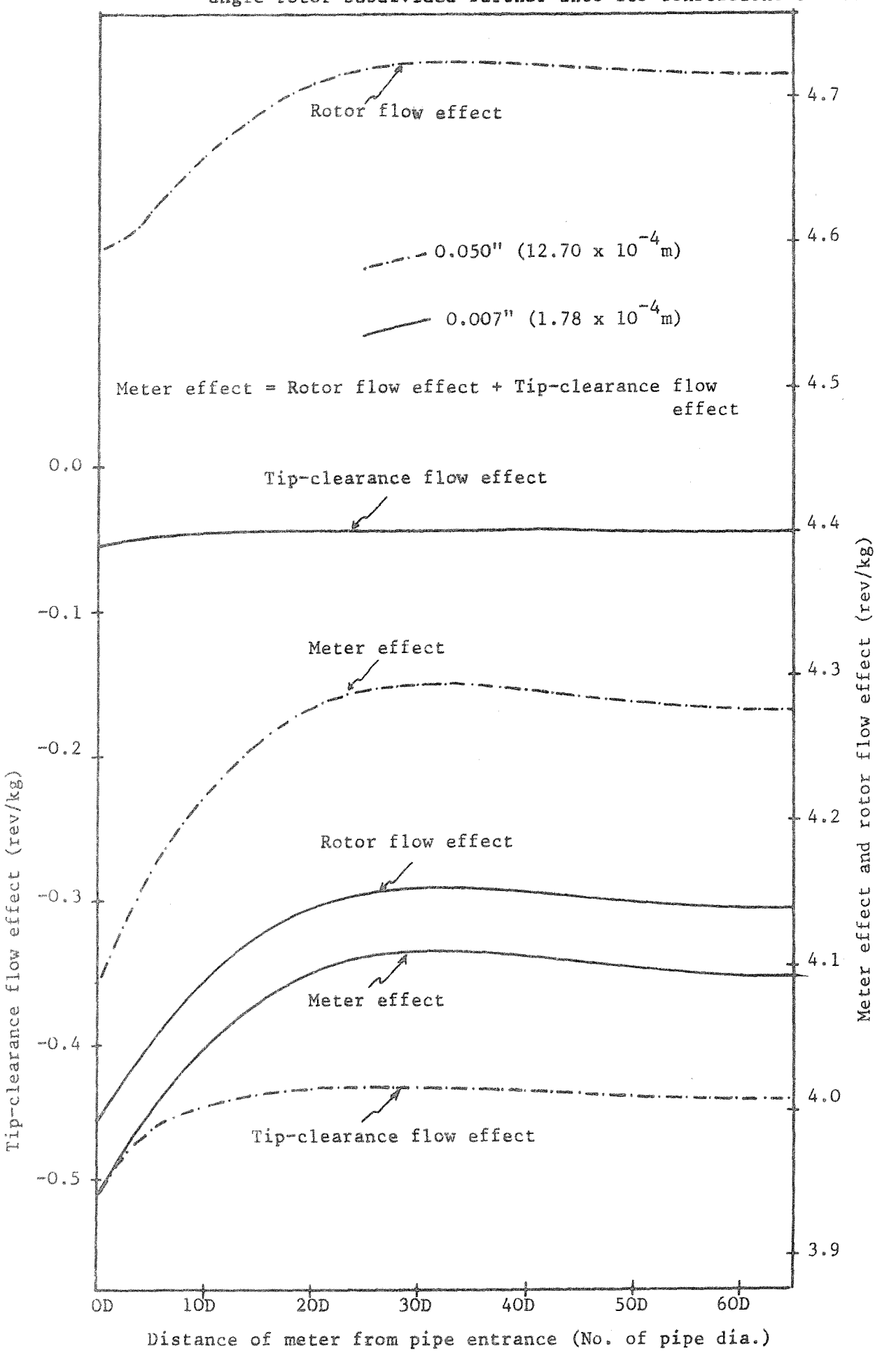

Fig. 6.7 Profile effect on turbine meters with helical-blade rotors

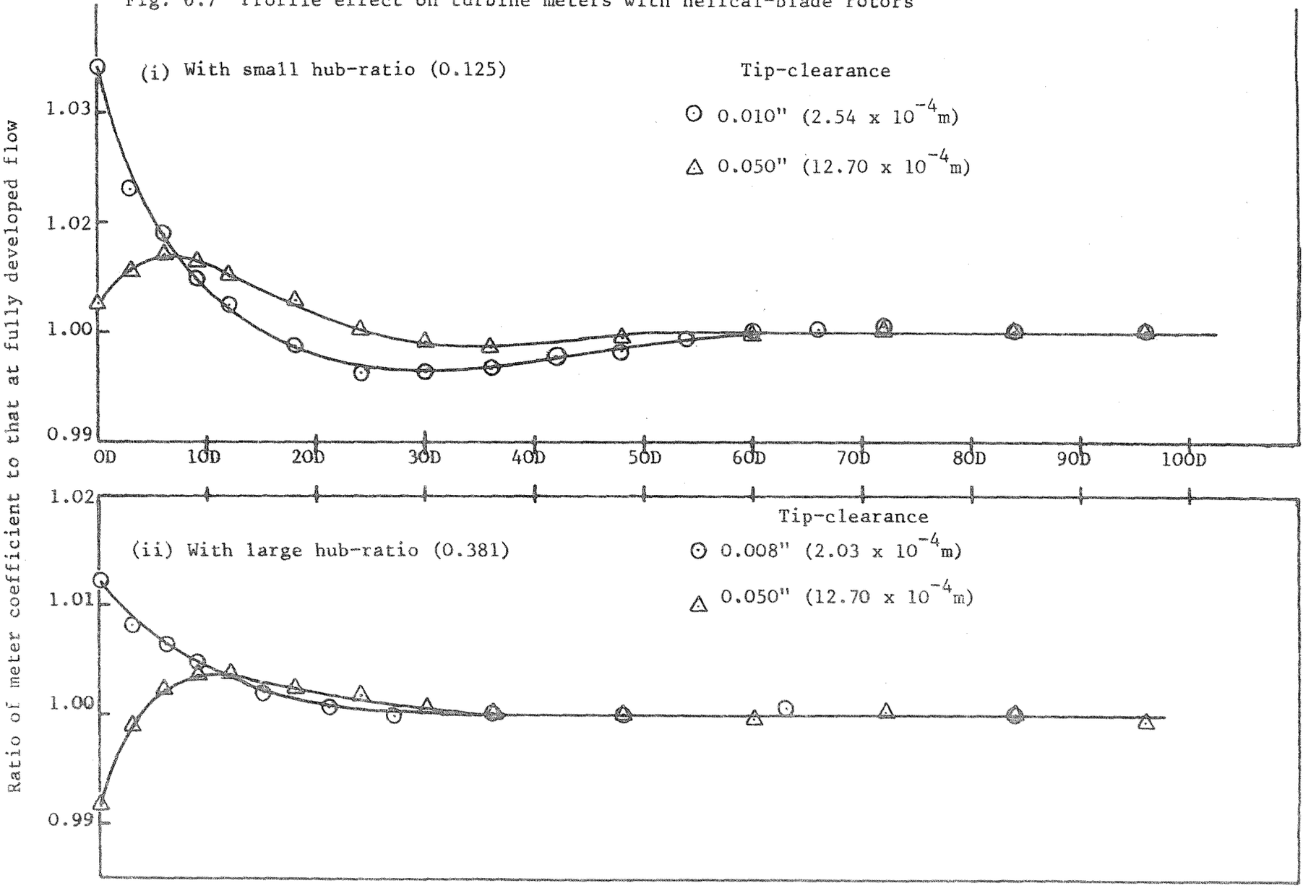

Fig. 6.8 Profile effect on different types of turbine meters with different tip-clearances

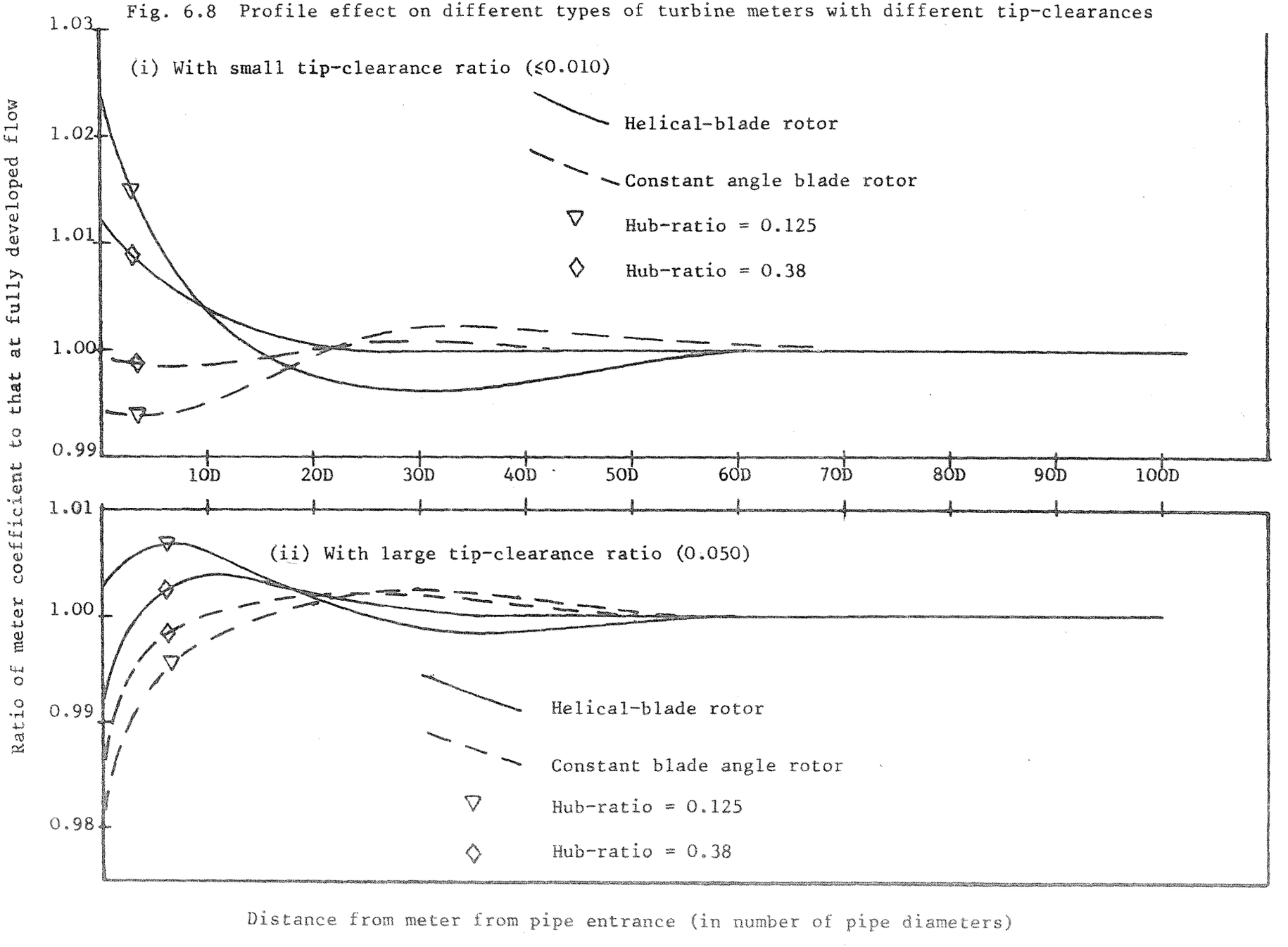

Fig. 6.9 Profile effect on turbine meters with constant blade angle rotors

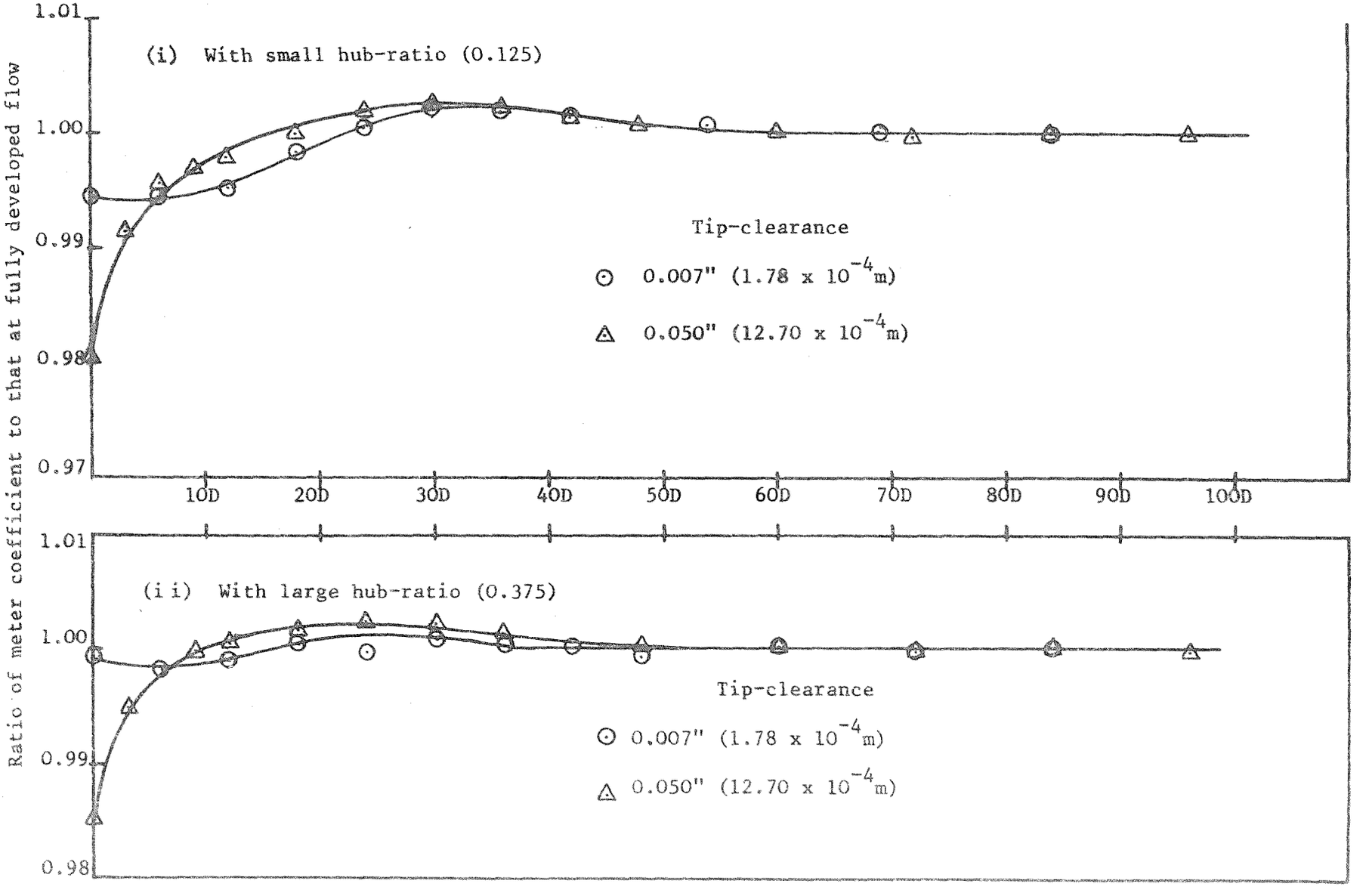

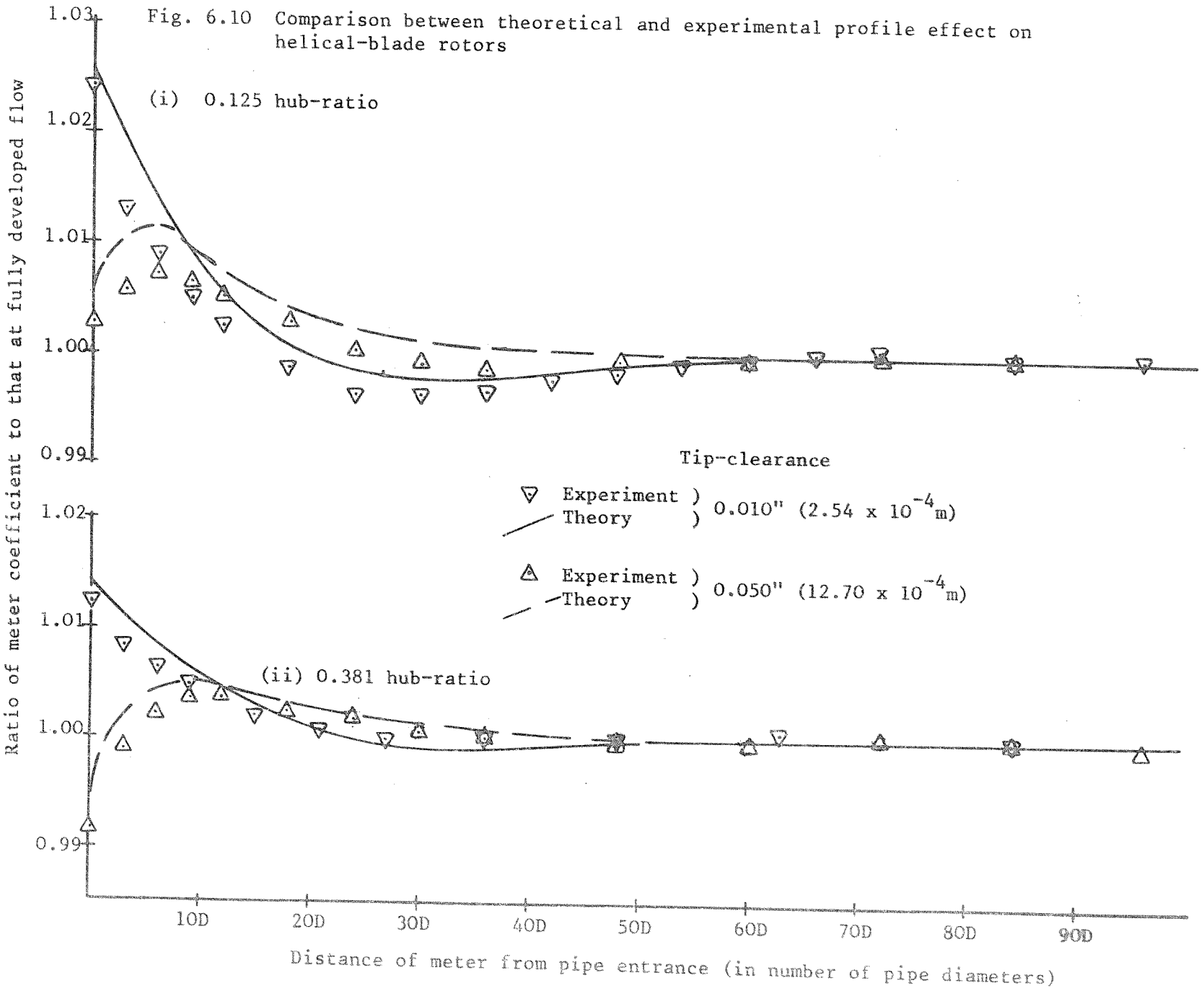
Fig. 6.10 Comparison between theoretical and experimental profile effect on helical-blade rotors
(i) 0.125 hub-ratio
(ii) 0.381 hub-ratio
Tip-clearance
Experiment
Theory
0.010" (2.54 x 10^-4 m)
Experiment
Theory
0.050" (12.70 x 10^-4 m)
Ratio of meter coefficient to that at fully developed flow
1.03
1.02
1.01
1.00
0.99
1.02
1.01
1.00
0.99
10D
20D
30D
40D
50D
60D
70D
80D
90D
Distance of meter from pipe entrance (in number of pipe diameters)

Fig. 6.11 Comparison between theoretical and experimental profile effect on constant blade angle rotors

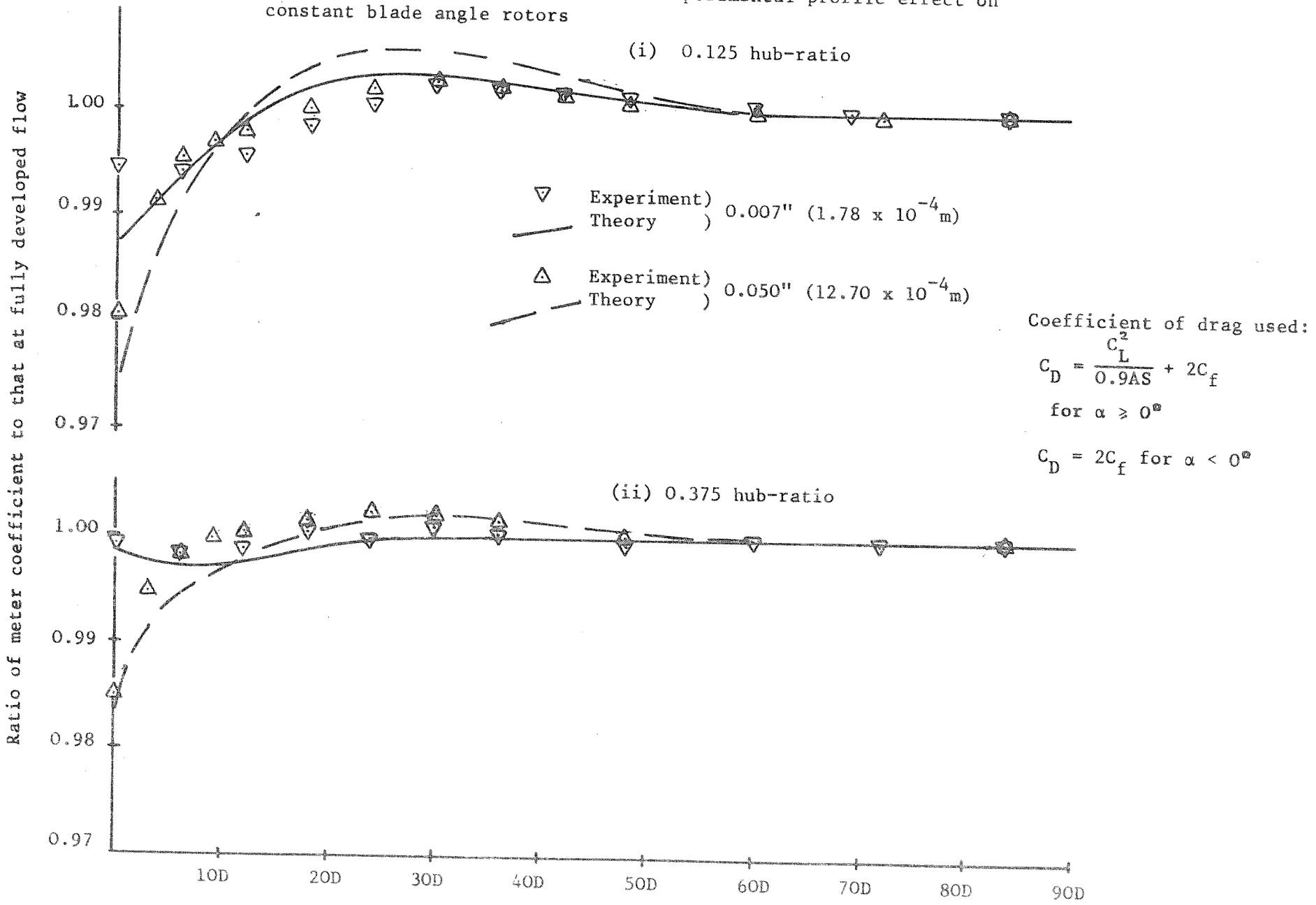

Fig.7.1 Effect of Gate Valve on $\frac{1}{4}$" Hub dia. Helical-Blade Rotor without Flow Straightener.

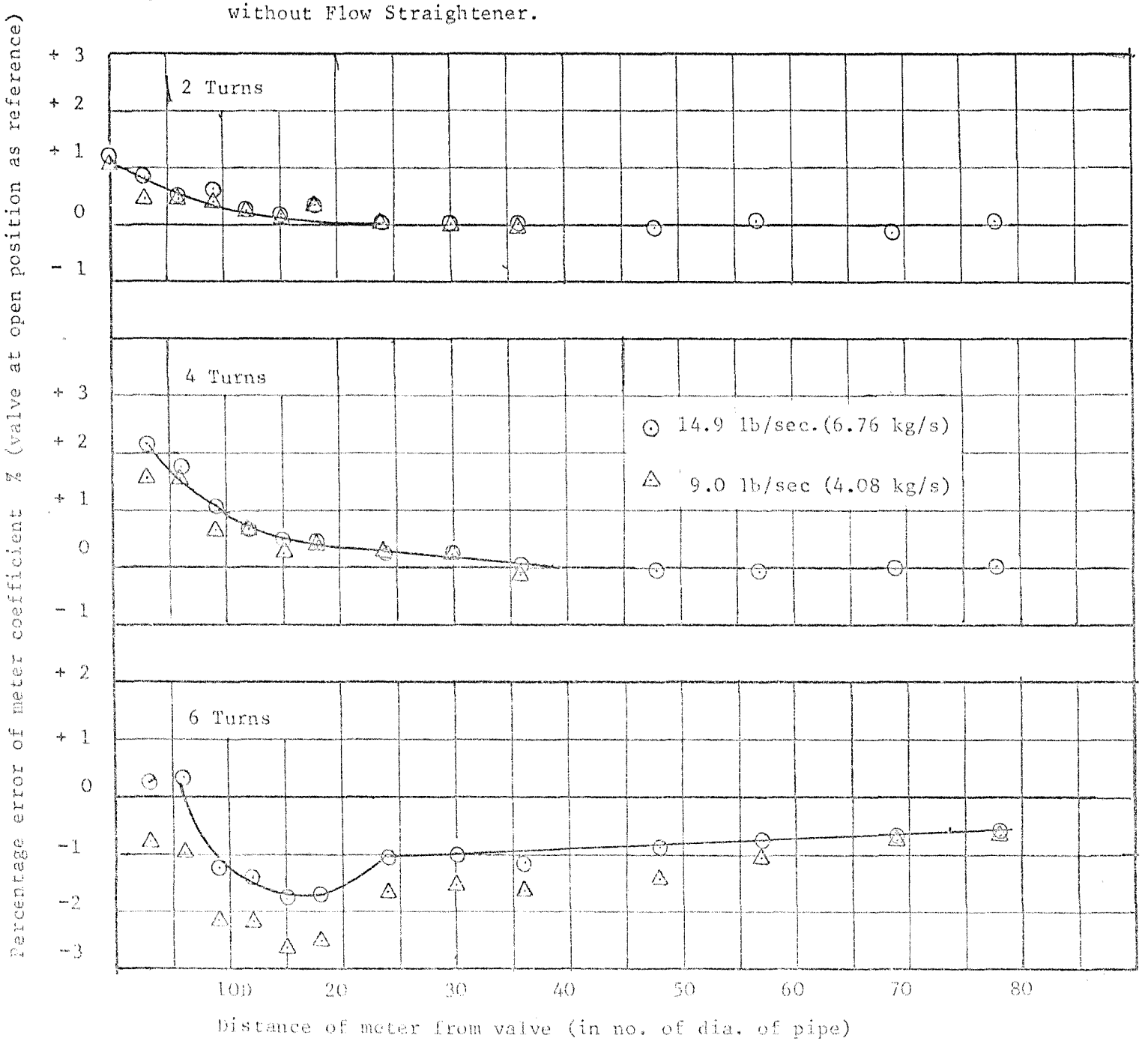

For 2, 4 and 6 turns from open positions

Valve closed at 8 turns

Fig. 7.2 Variation of Meter Coefficient with Different Positions of Valve Closure without Flow Straighteners

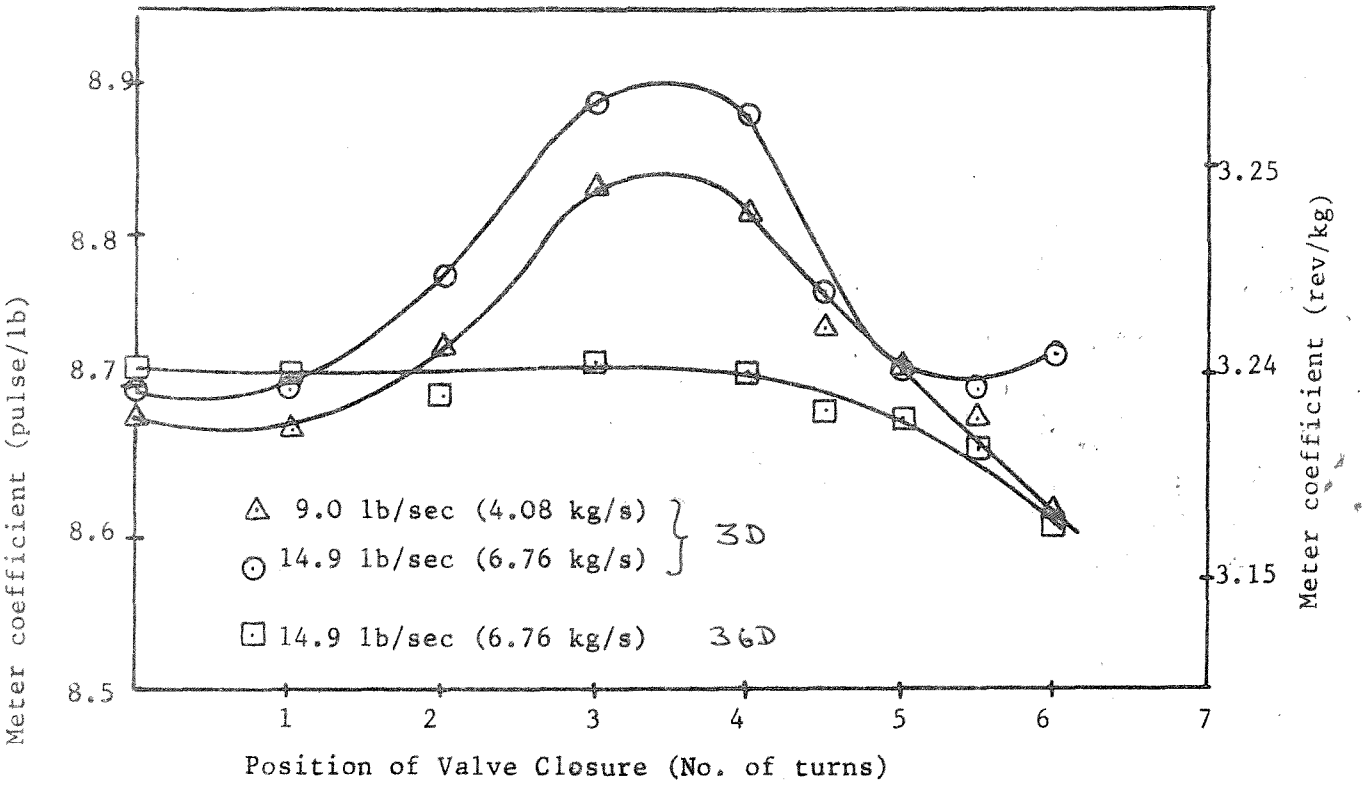

Fig. 7.3 Steadiness of Rotor Rotation at Different Position of Valve Closure without Flow Straighteners

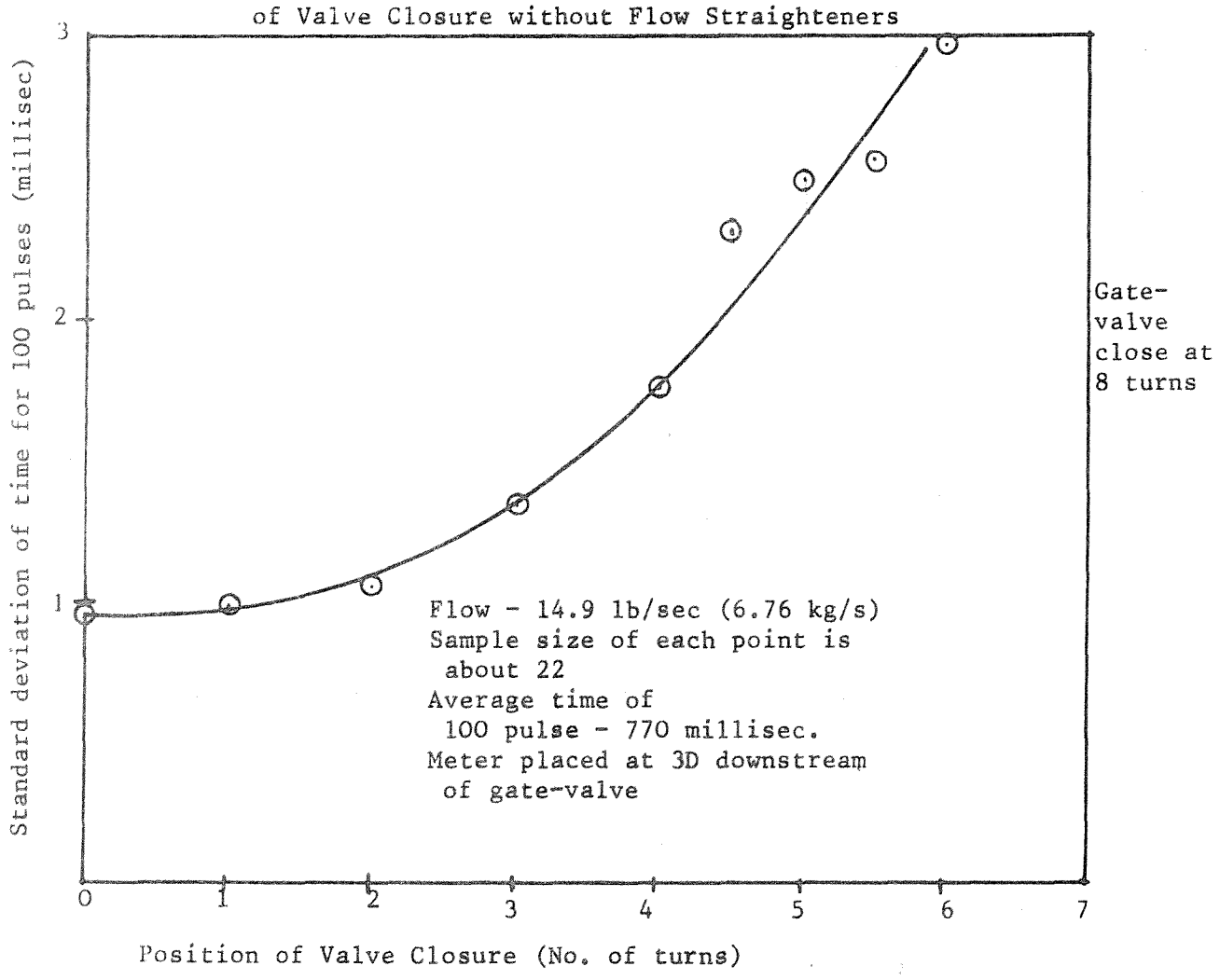

Fig.7.4- EFFECT OF VALVE ON ¼" HUB DIAMETER HELICAL-BLADE ROTOR WITH AND WITHOUT FLOW STRAIGHTENER

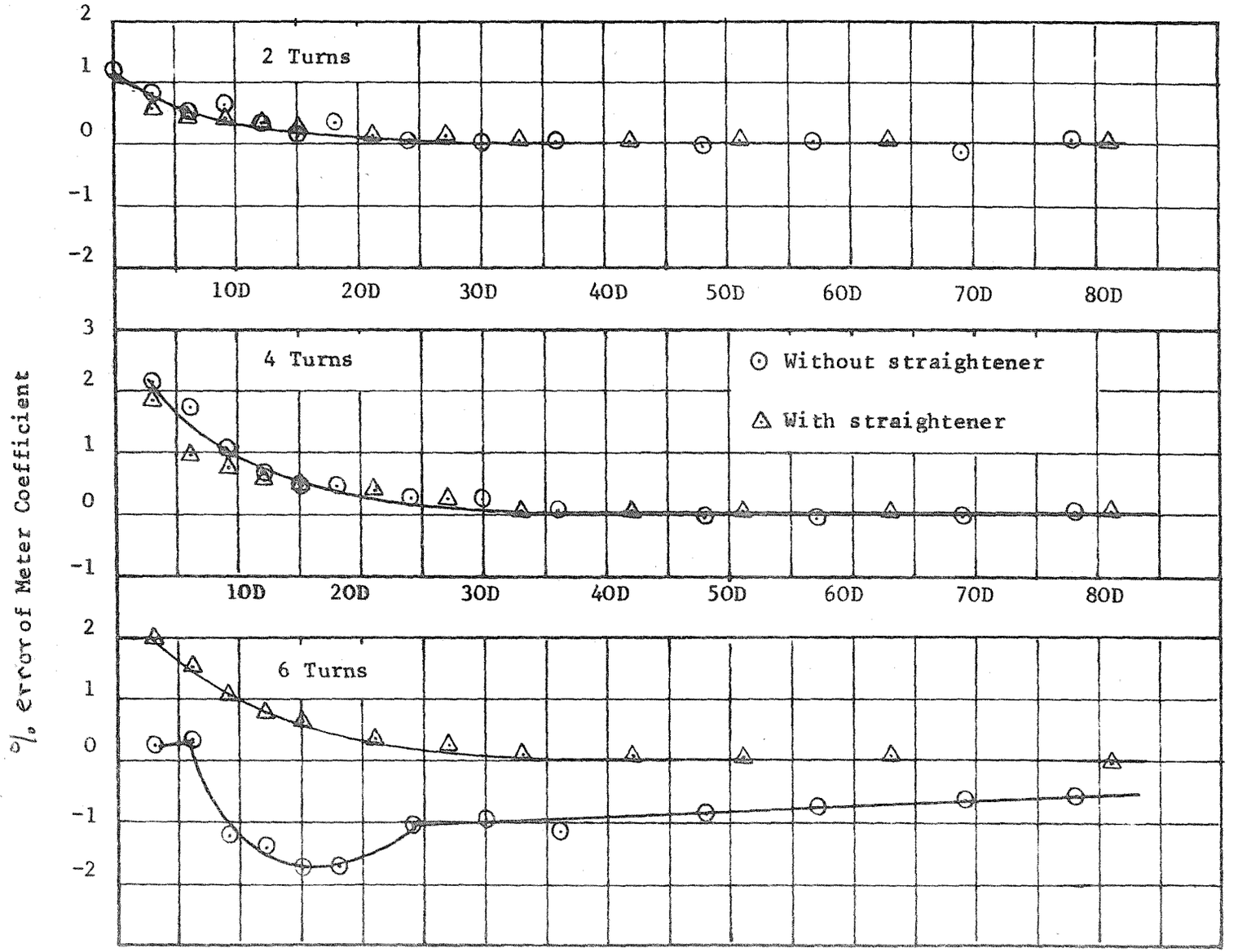

Fig.7.5 Effect of gate valve on turbine meters without flow straightener

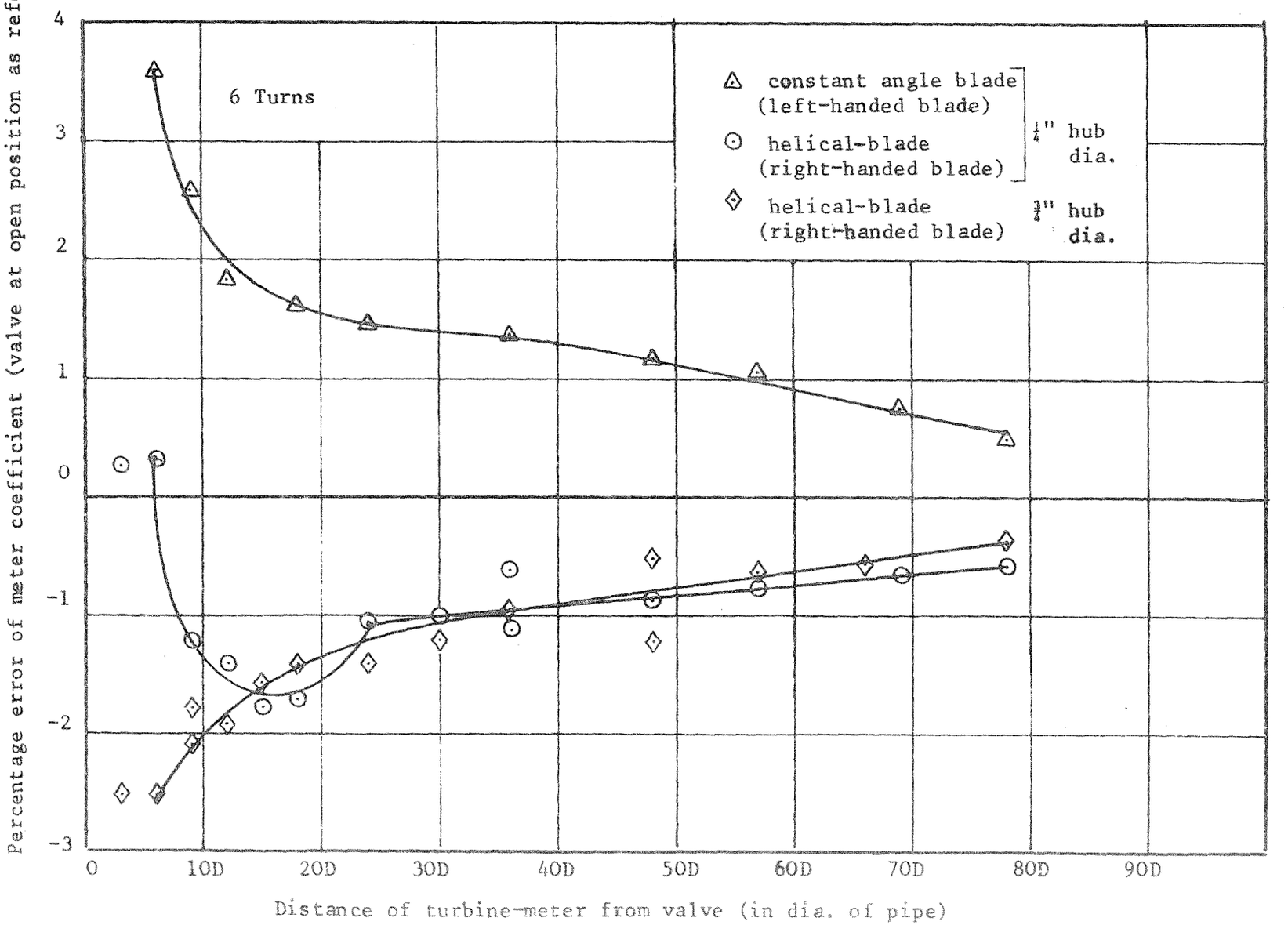

Fig. 7.6 Effect of gate valve on $\frac{1}{4}$" hub dia. rotors with different types of blades. (with flow straightener)

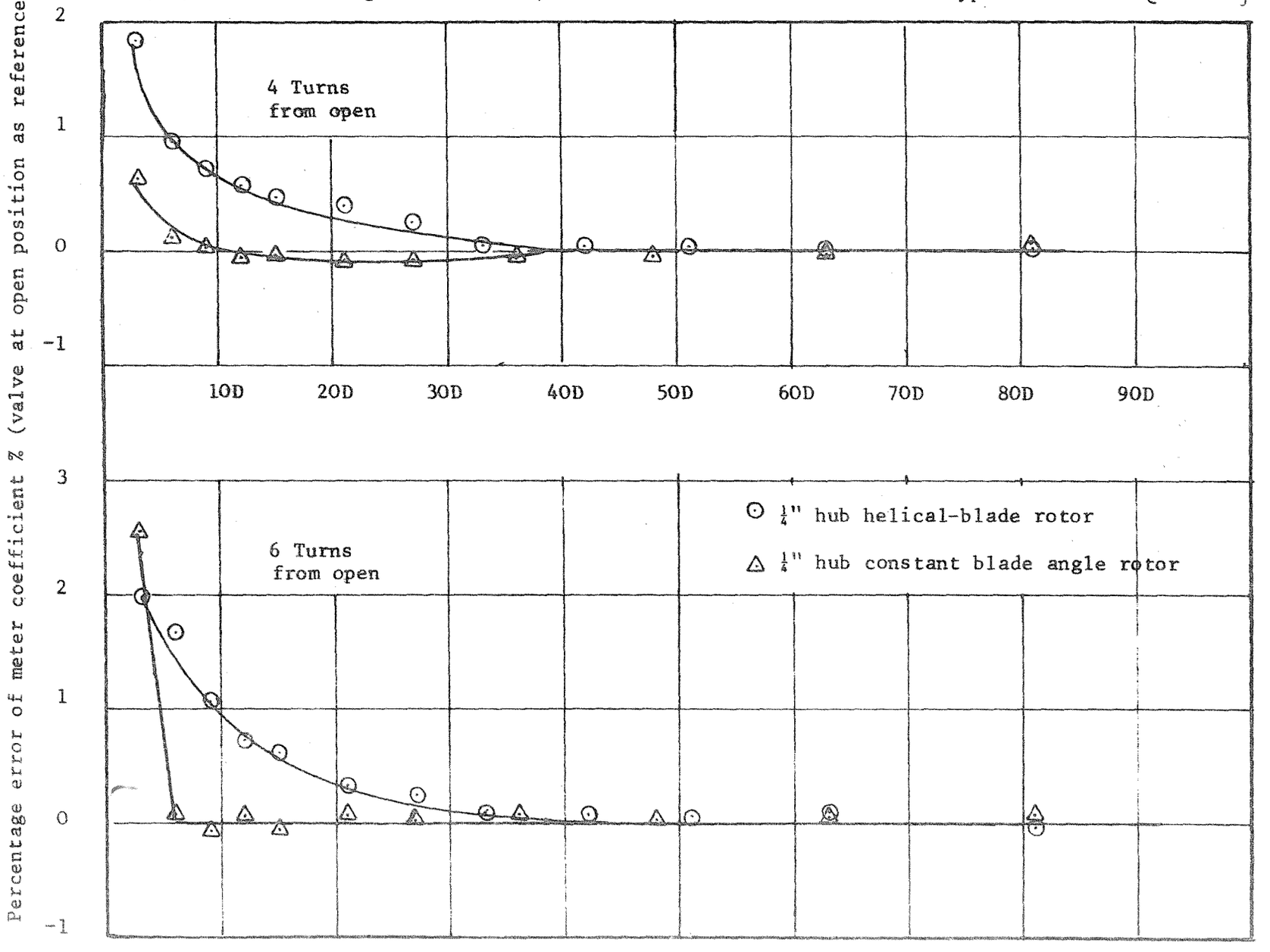

Meter casing dia. = 2.000"

Internal diameter of pipe = 2.000"

Fig. 7.7 Effect of valve on helical-blade rotors with flow straighteners

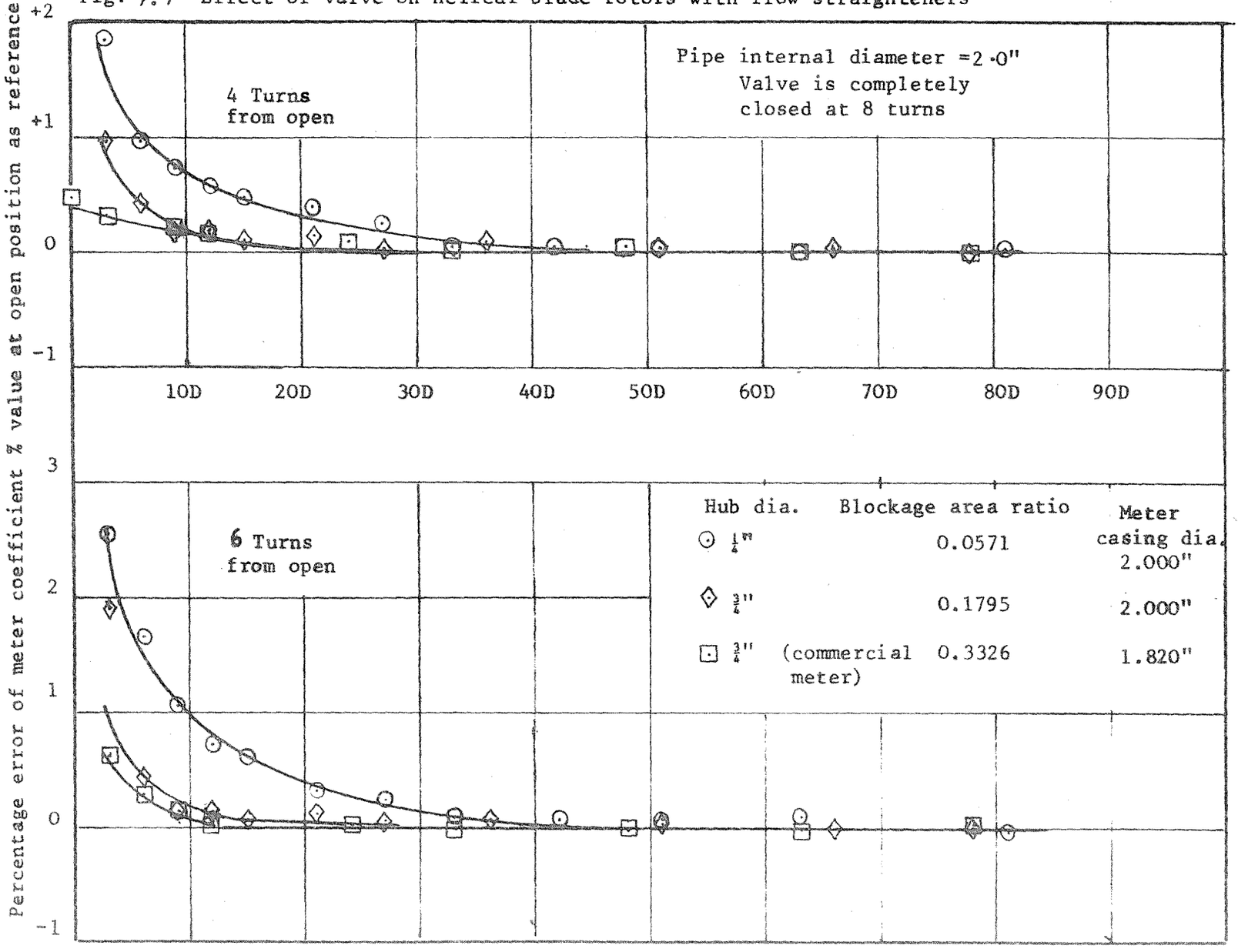

Distance of meter from valve (in no. of dia. of pipe)

Meter	¼" hub dia. right handed helical-blade rotor	¼" hub dia. left handed constant blade angle rotor
Meter coefficient without flow straightener (pulse/lb)	8.72	8.68
Meter coefficient with flow straightener (pulse/lb)	8.57	8.87
Difference in meter coefficient (pulse/lb)	-0.15	+0.19
Percentage difference in meter coefficient	-1.7%	+2.2%

TABLE 7.1 - Effect of flow straightener

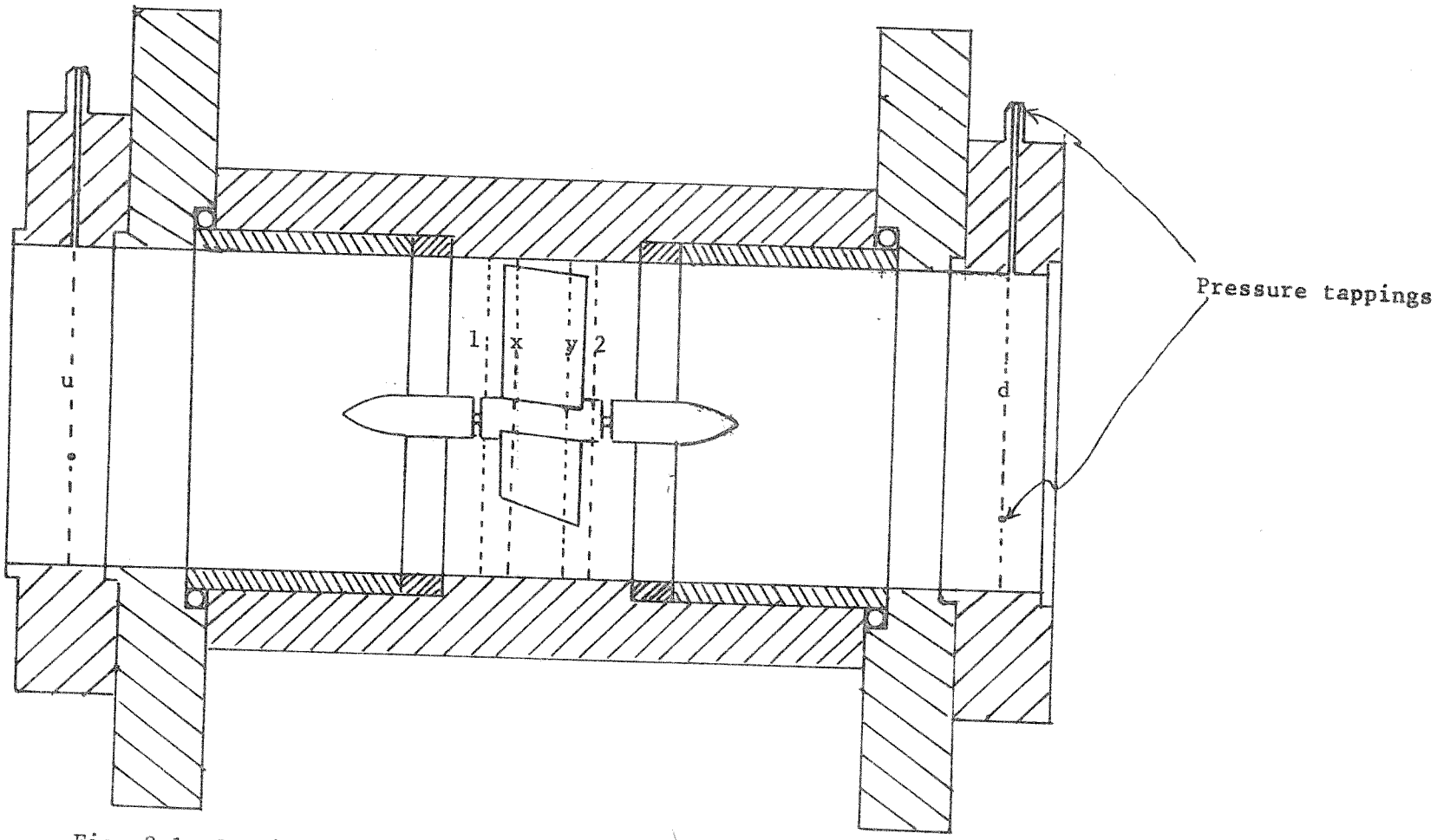

Fig. 8.1 Section of Turbine Meter Showing Positions of Pressure Tappings

Fig. 8.2

Head loss across 2" research turbine meters in fully developed flow

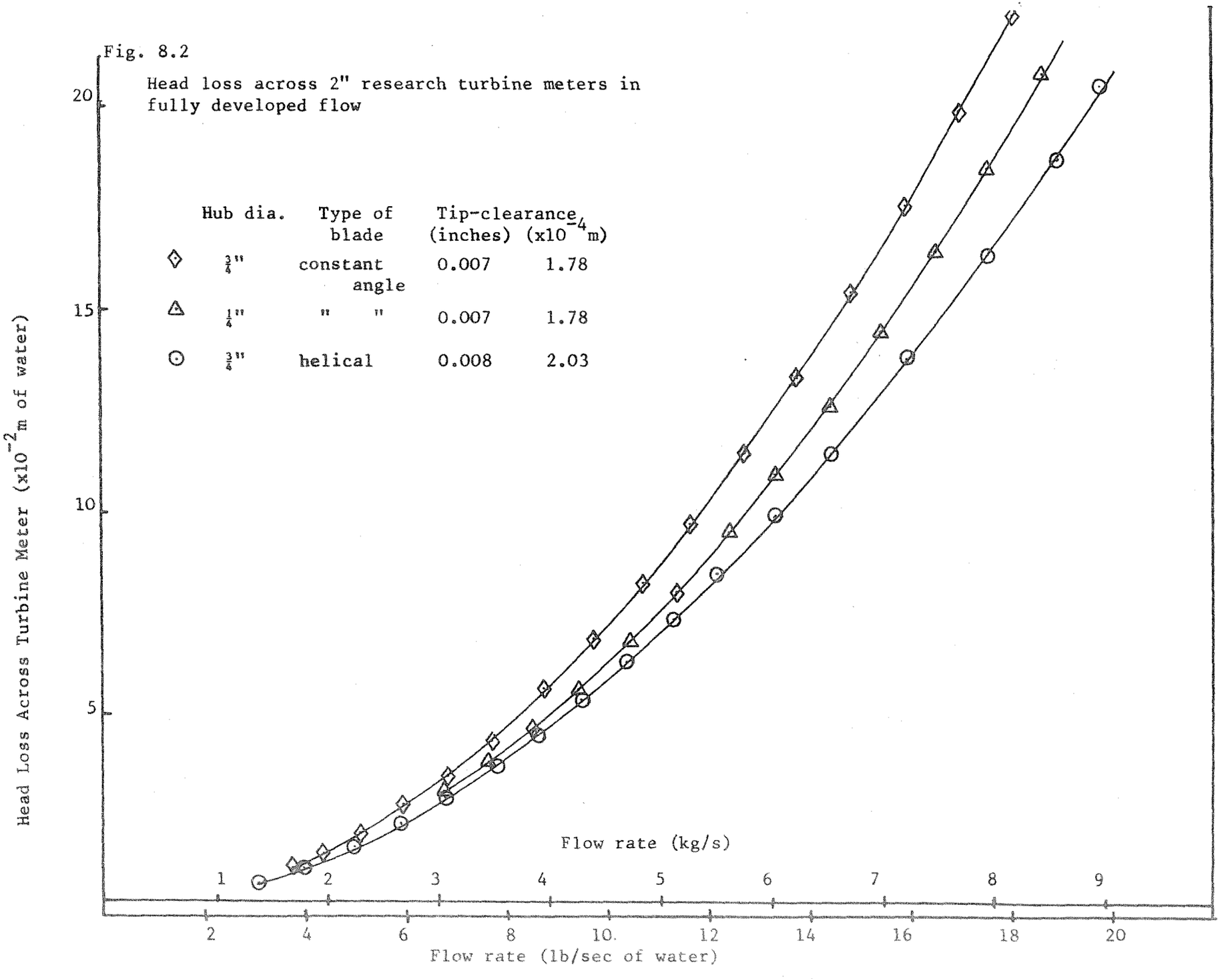

Fig. 8.3 Head Loss Across 2" Research Meters with $\frac{3}{4}$" Hub Diameter

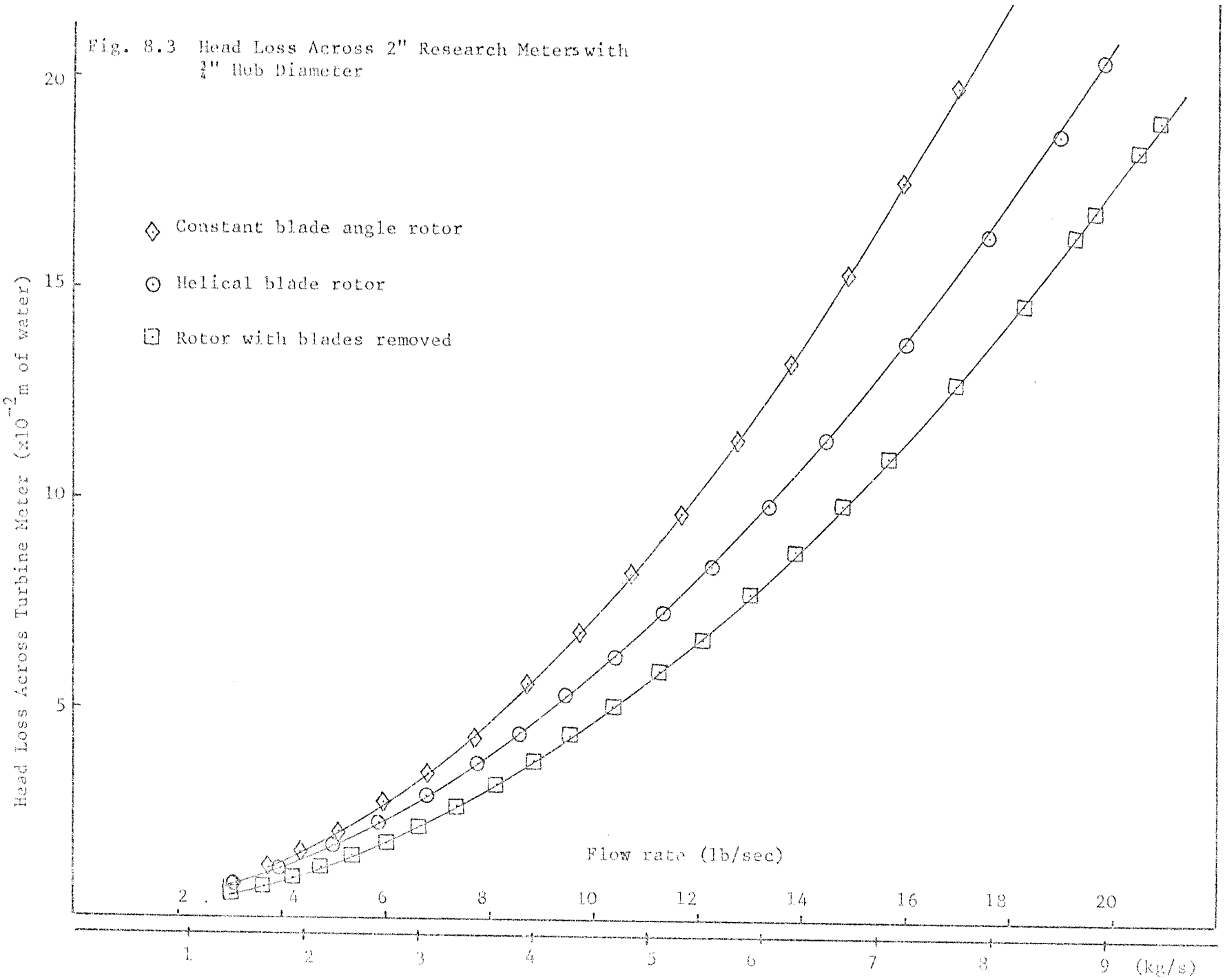

Fig. 8.4 Comparison between the head loss of a 2" commercial meter and a 2" research meter both with $\frac{3}{4}$" hub diameter

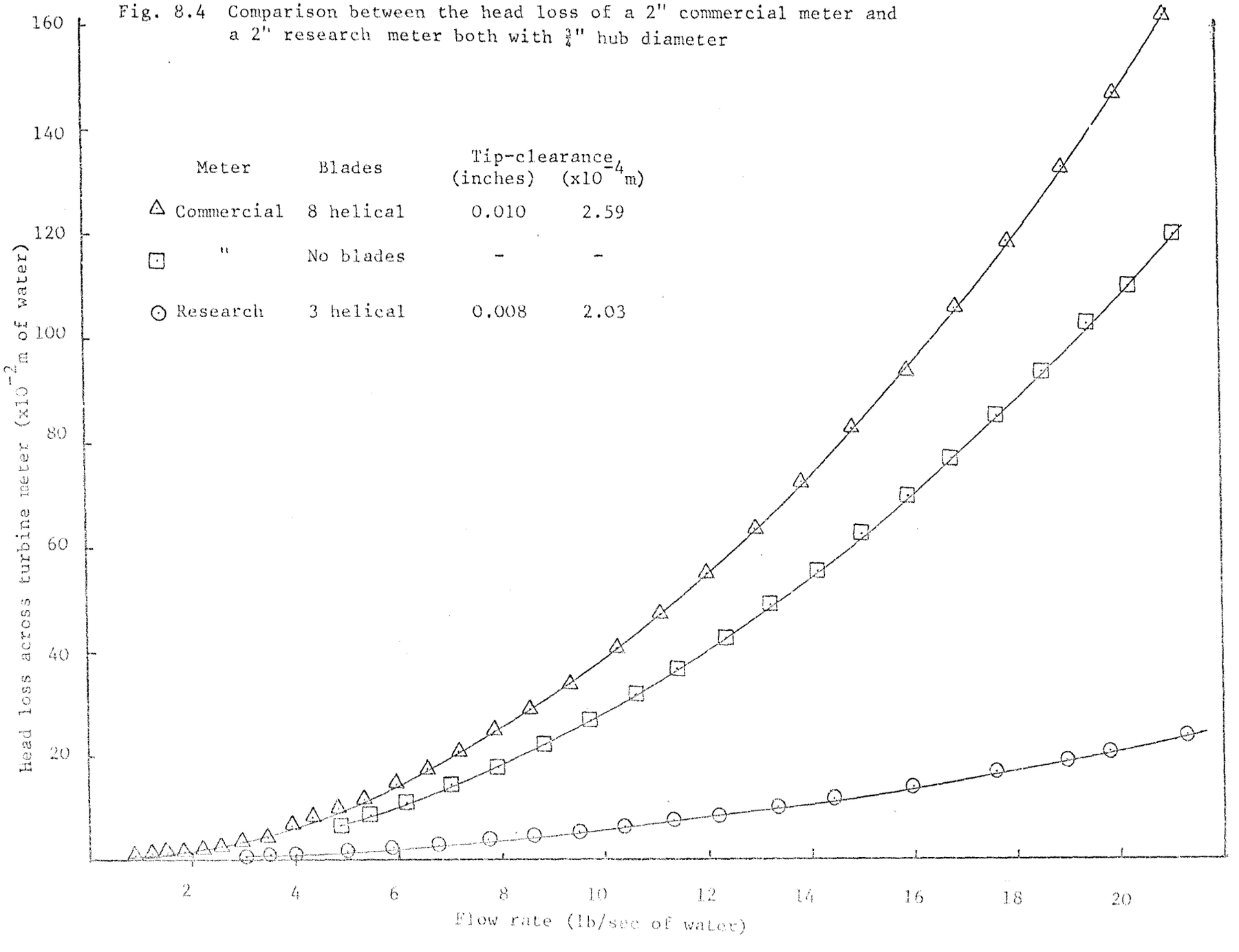

Fig. 8.5 Comparison of head losses across research meters with commercial meters

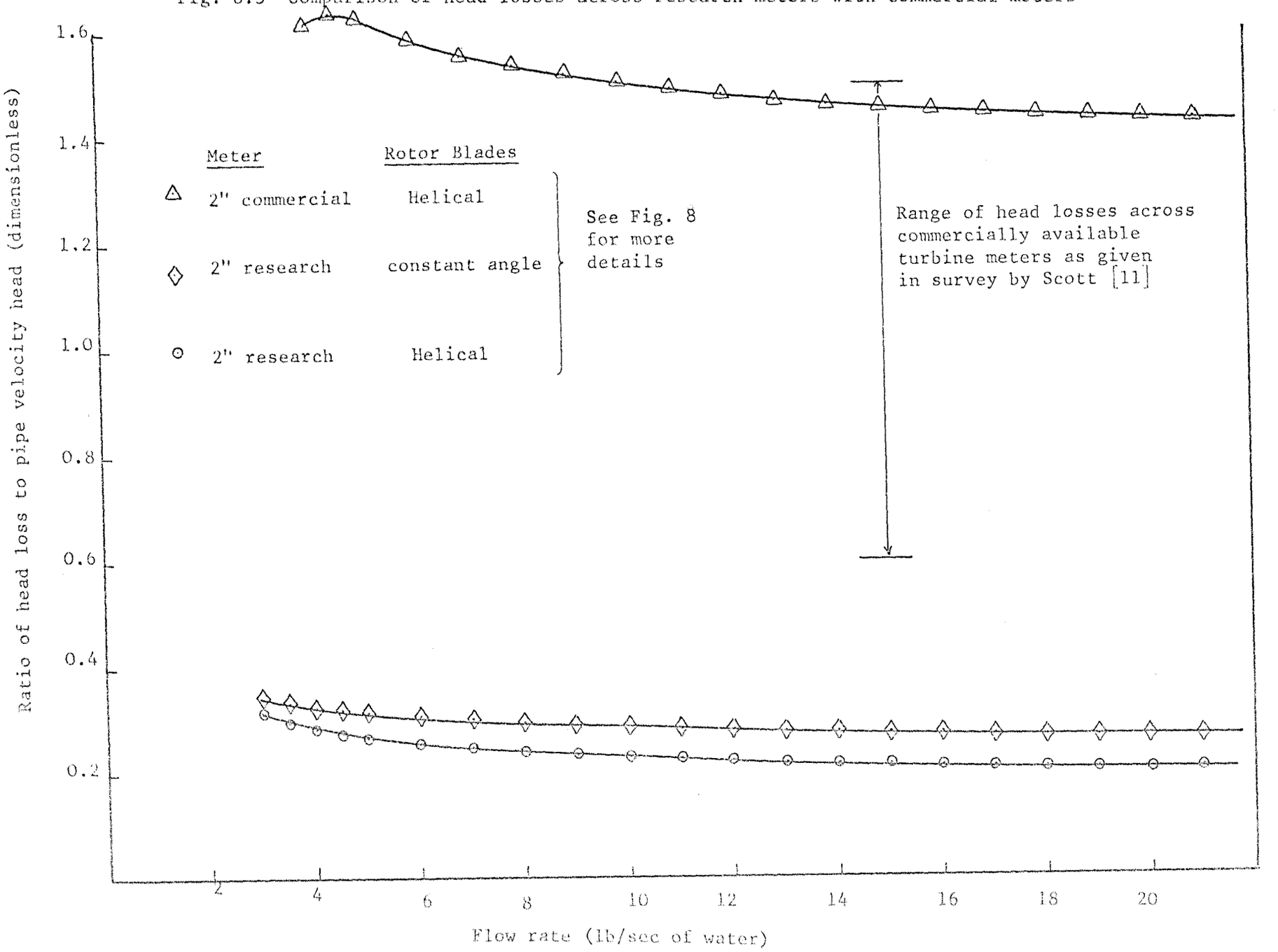

Fig. 8.6 Pressure recovery in flow deceleration due to the hub (as defined in Eqn. 8.15) for 2" turbine meter

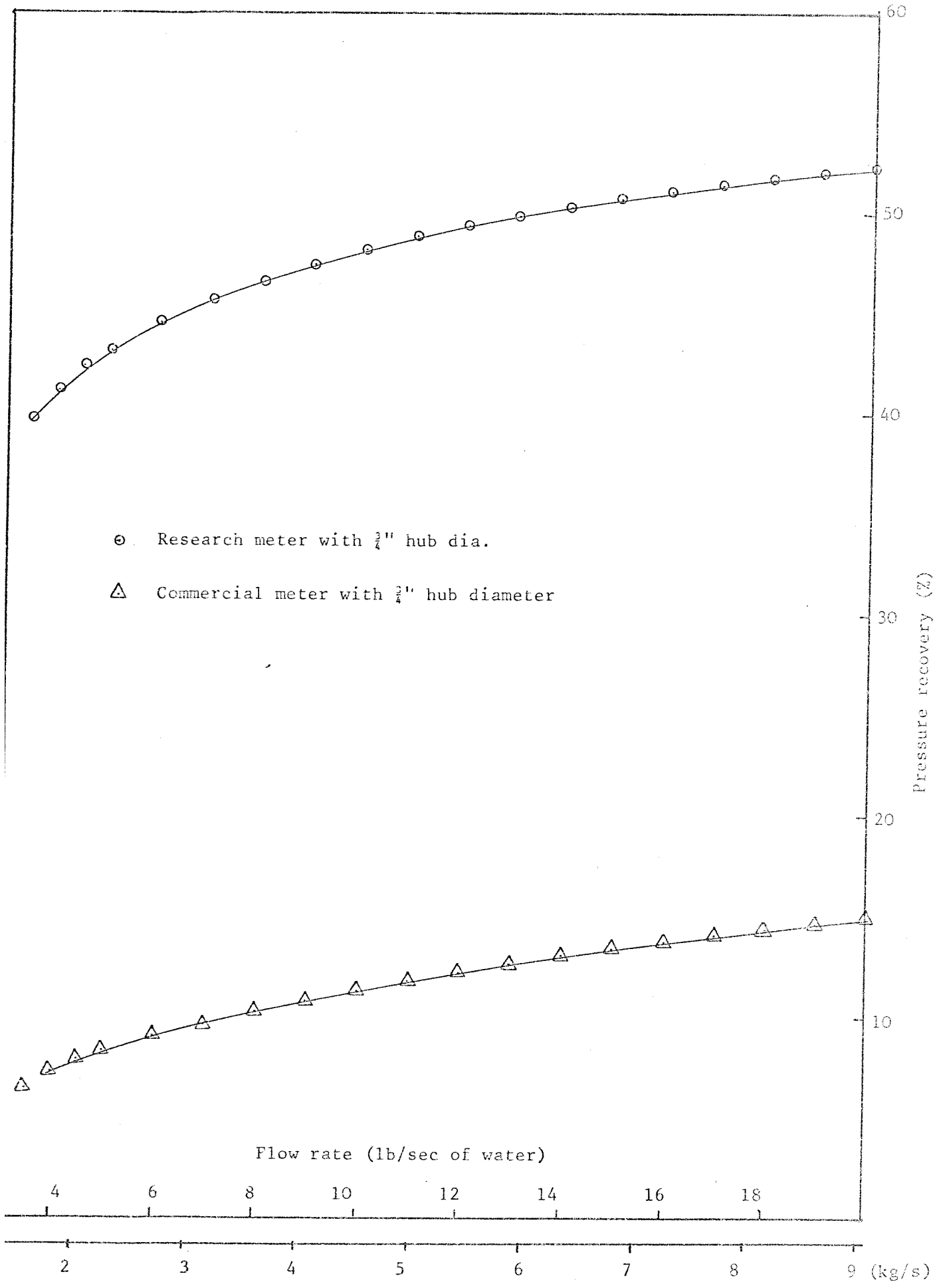

Fig. 8.7 Comparison of blade losses across research meters with a commercial meter

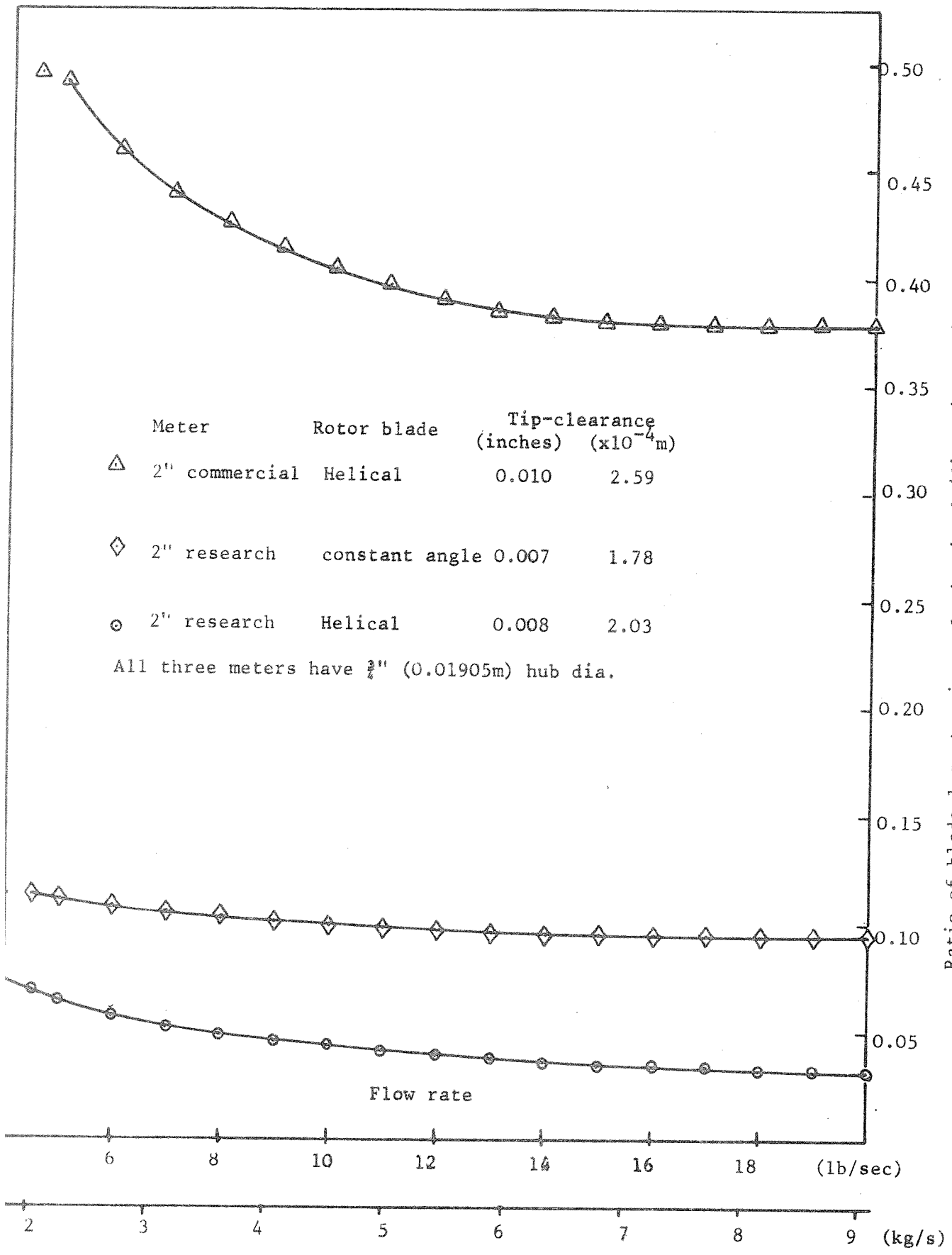

Fig. 8.8 Comparison of different types of losses of different turbine meters

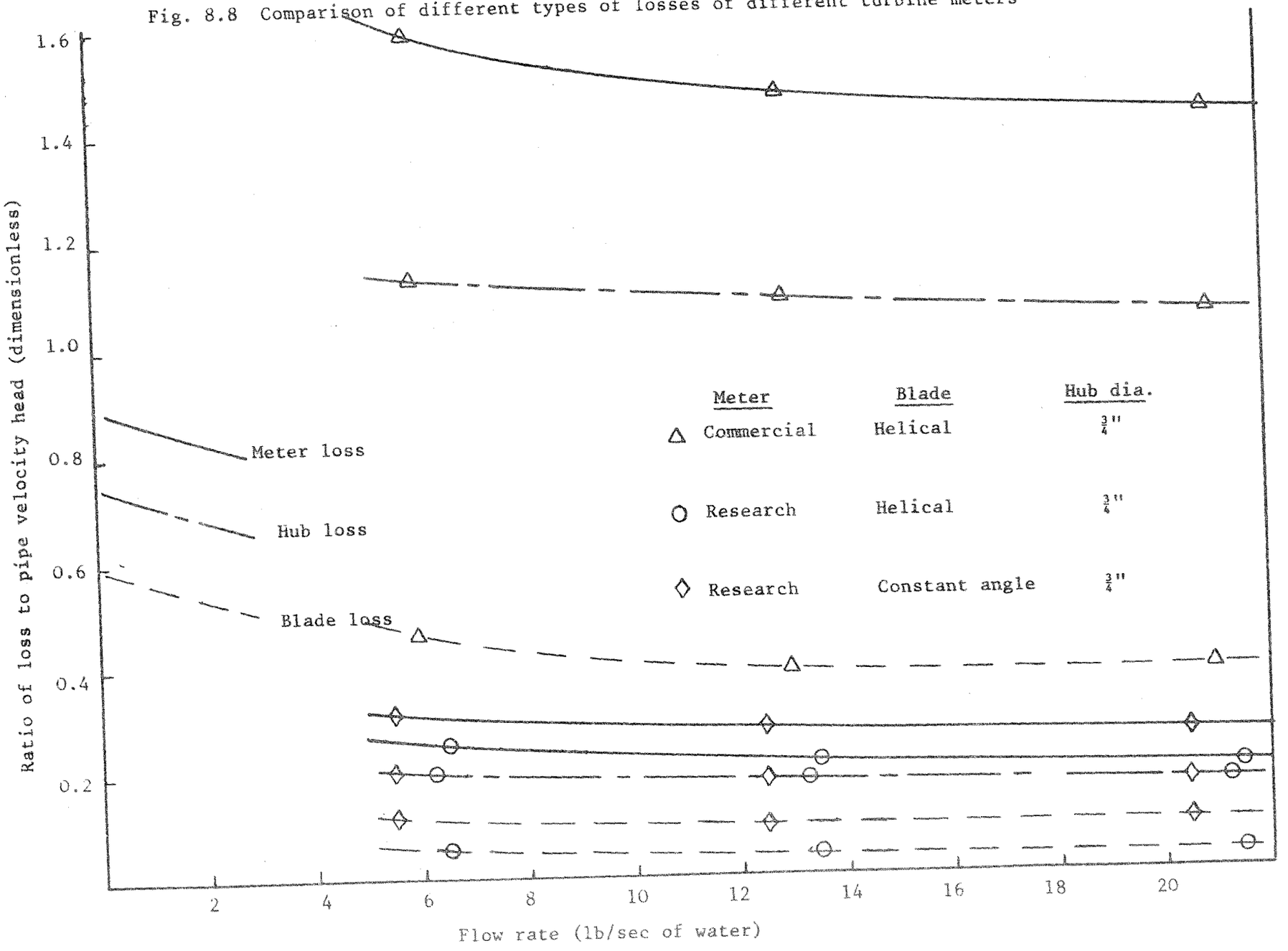

Fig. 8.9 Comparison between theoretical and experimental head loss of helical-blade rotor

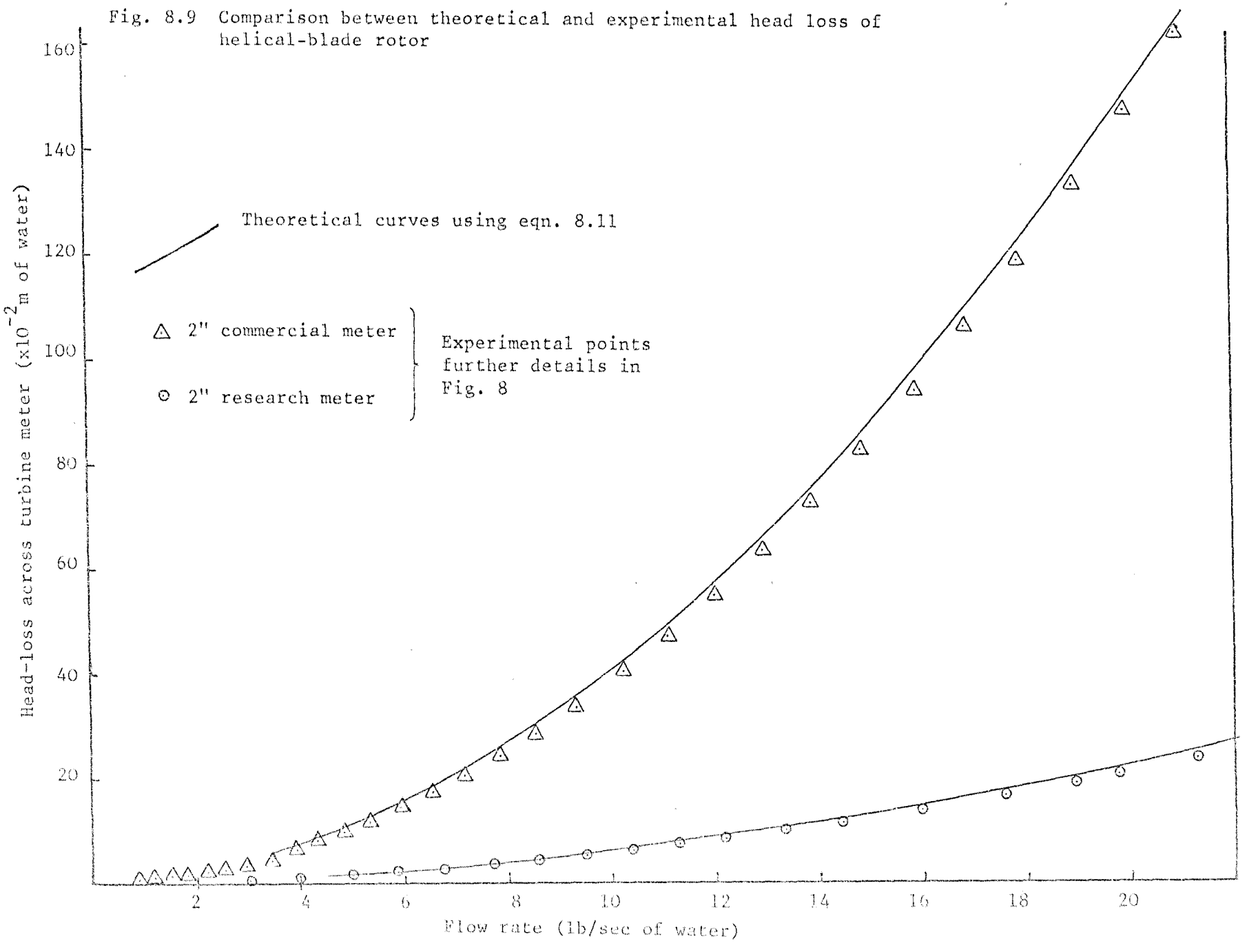

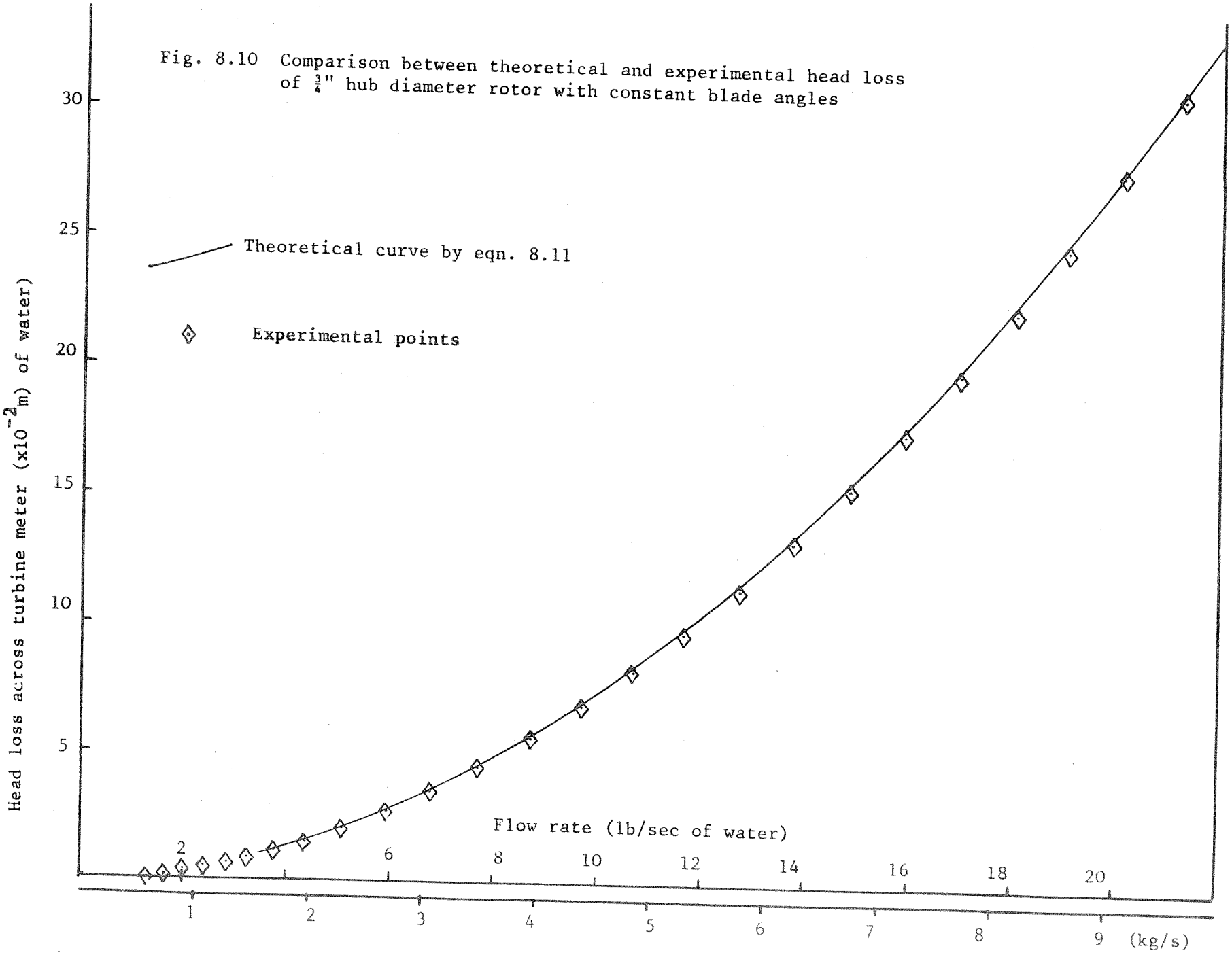
Fig. 8.10 Comparison between theoretical and experimental head loss of ¾" hub diameter rotor with constant blade angles
Theoretical curve by eqn. 8.11
Experimental points
Head loss across turbine meter (x10⁻²m) of water)
30
25
20
15
10
5
Flow rate (lb/sec of water)
2
6
8
10
12
14
16
18
20
1
2
3
4
5
6
7
8
9
(kg/s)

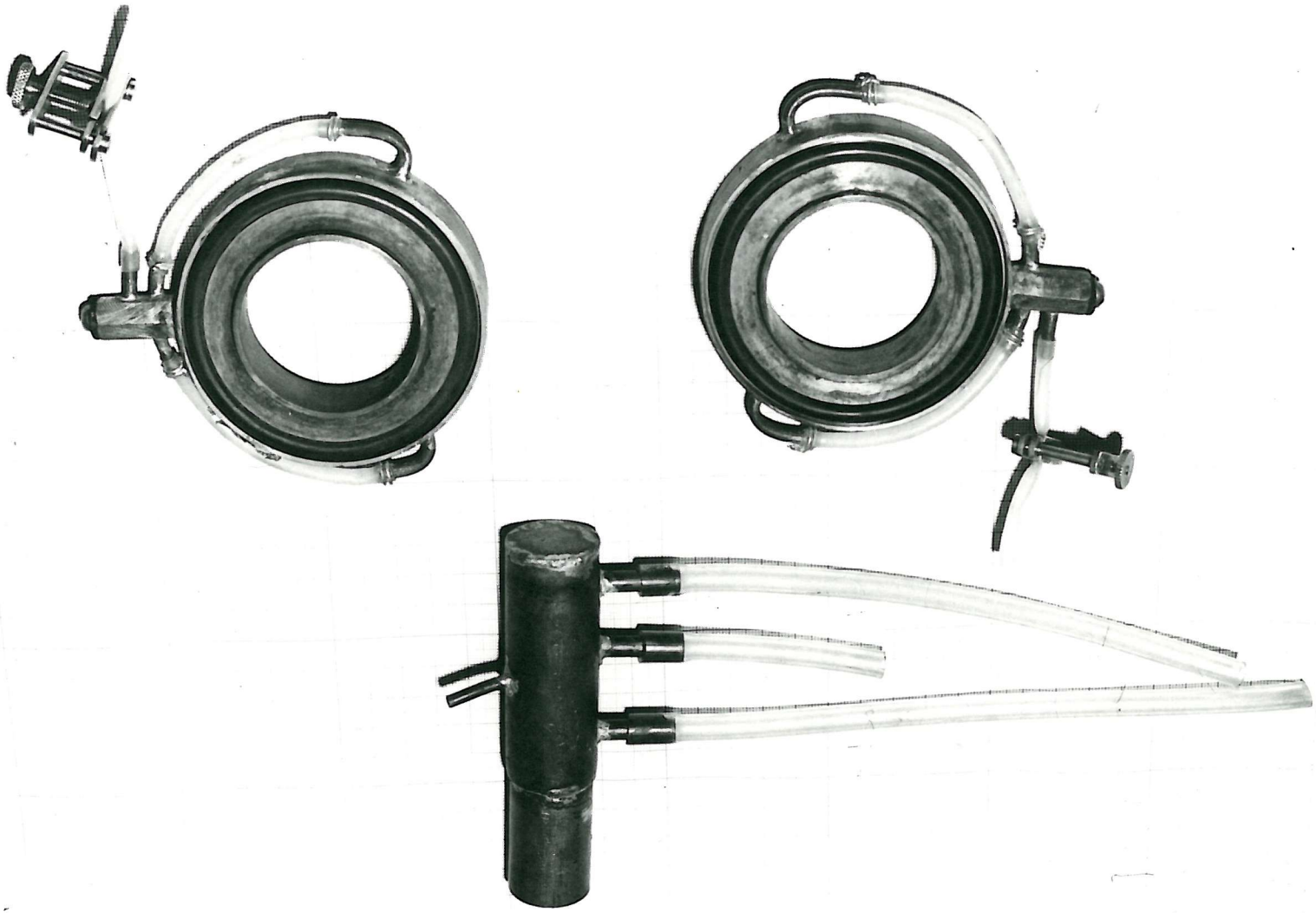

Fig. 8.11 Pressure Tapping Flanges with Pressure Averaging Chamber

Fig. 9.1 Repeatability test for full-diameter rotor using open bearings at downstream position (84D)

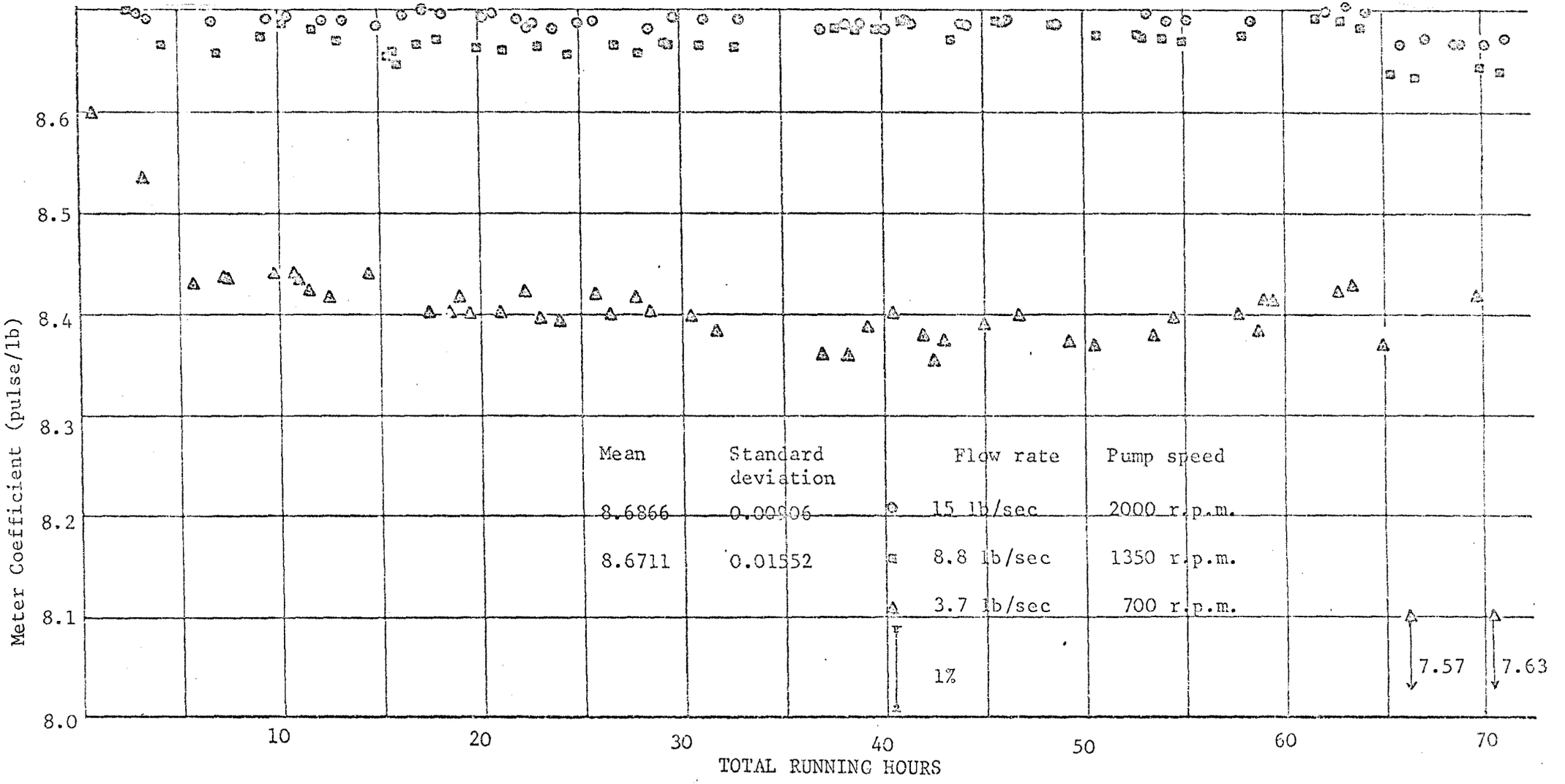

Fig. 9.2 Repeatability test for full-diameter rotor using shielded bearings at downstream position (84D)

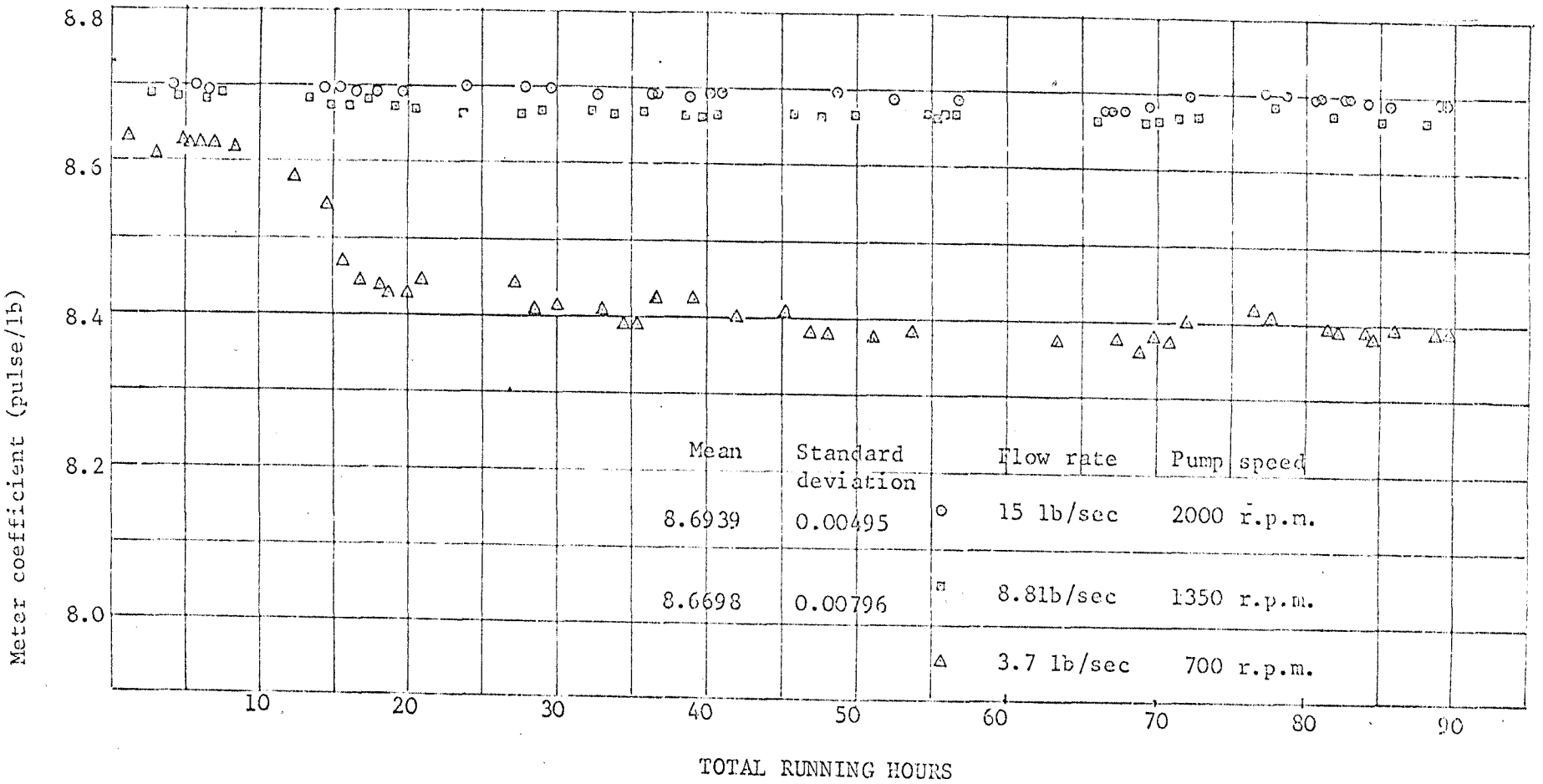

Fig. 9.3 Repeatability test for turned-down rotor using shielded bearings at downstream position

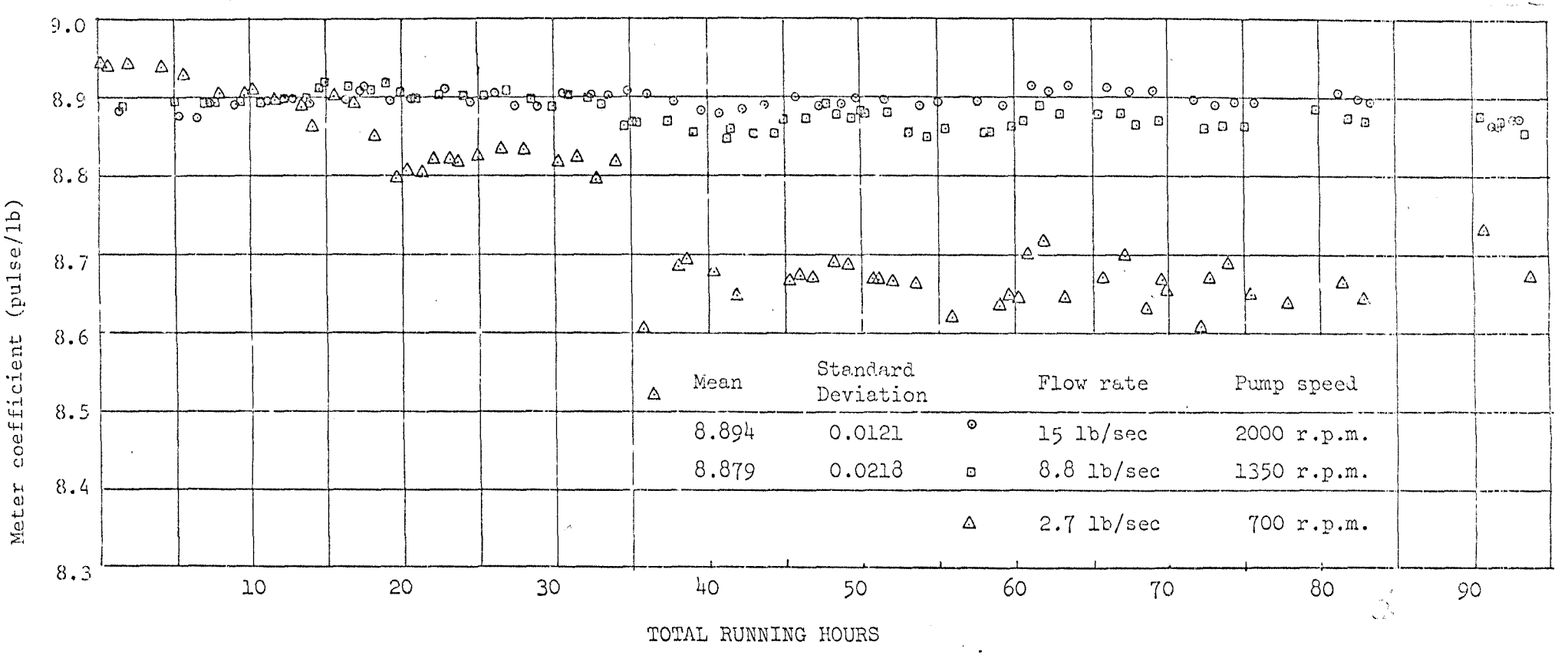

Fig. 9.4 Experimental and Theoretical Calibrations for Turned-Down Rotor with New and with "Run-in" Bearings

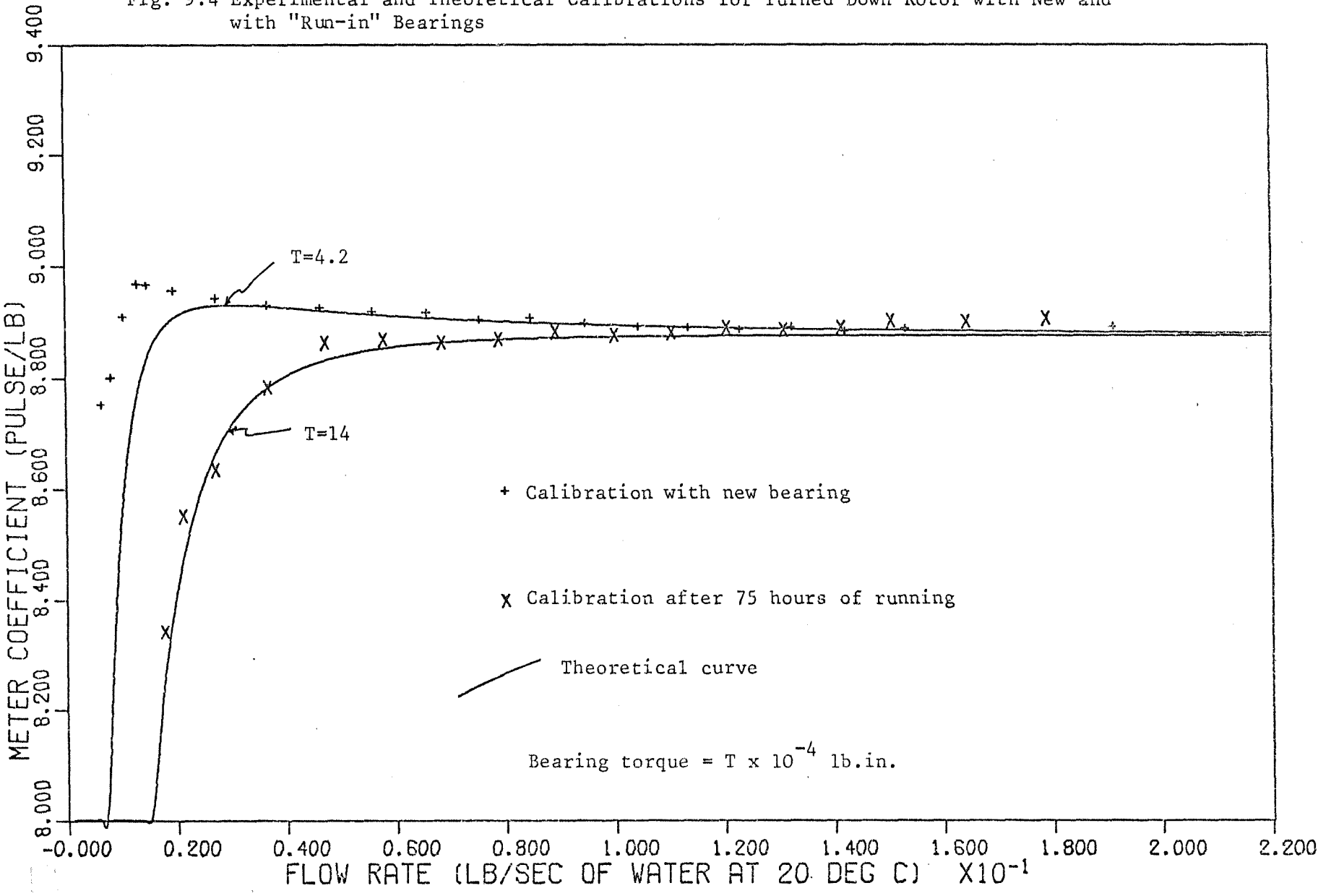

Fig. 9.5 Sensitivity of Meters to Increase in Friction Torque

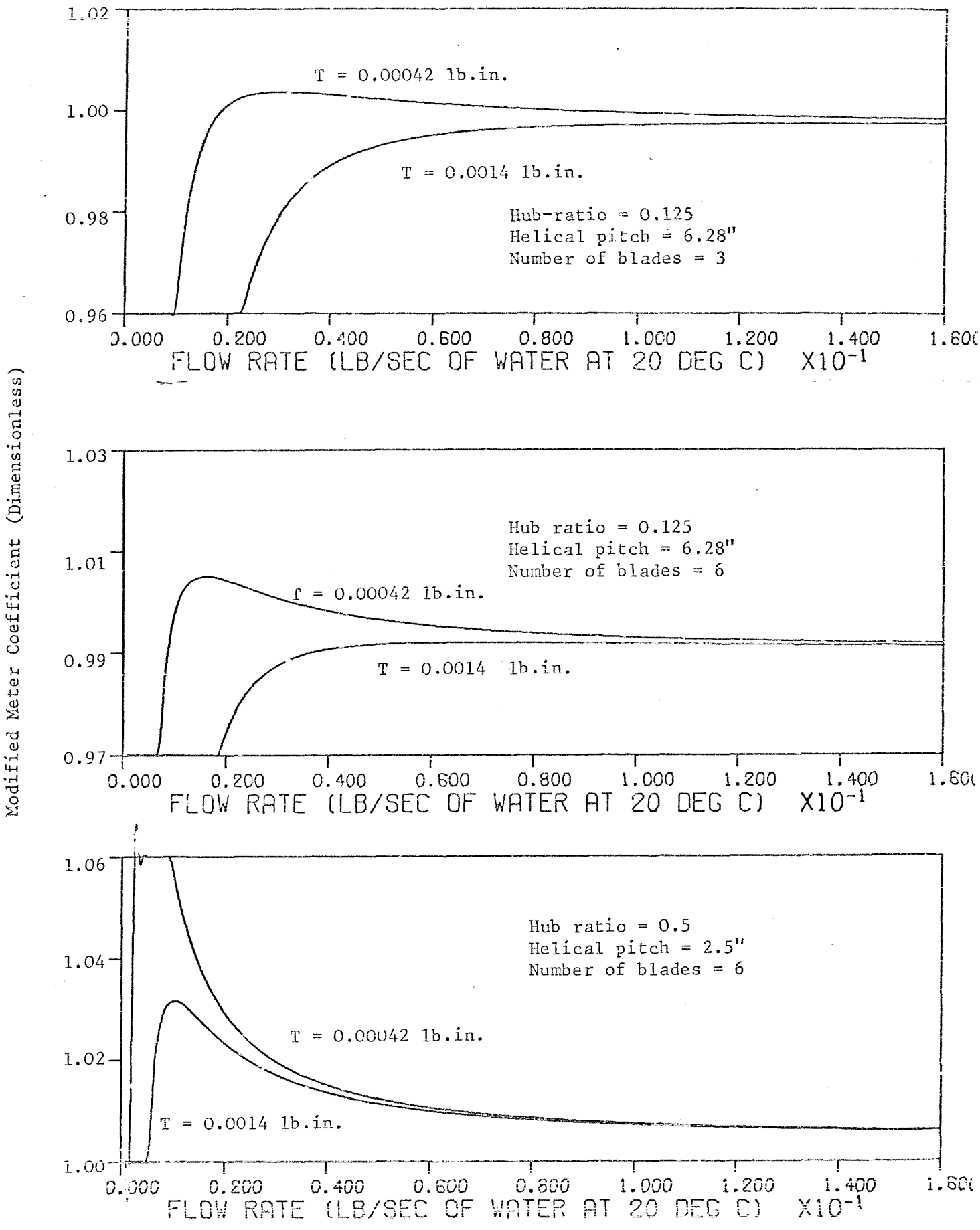

Fig. 9.6 Variation of meter calibration curve with resisting torque for full-diameter rotor in a uniform velocity profile

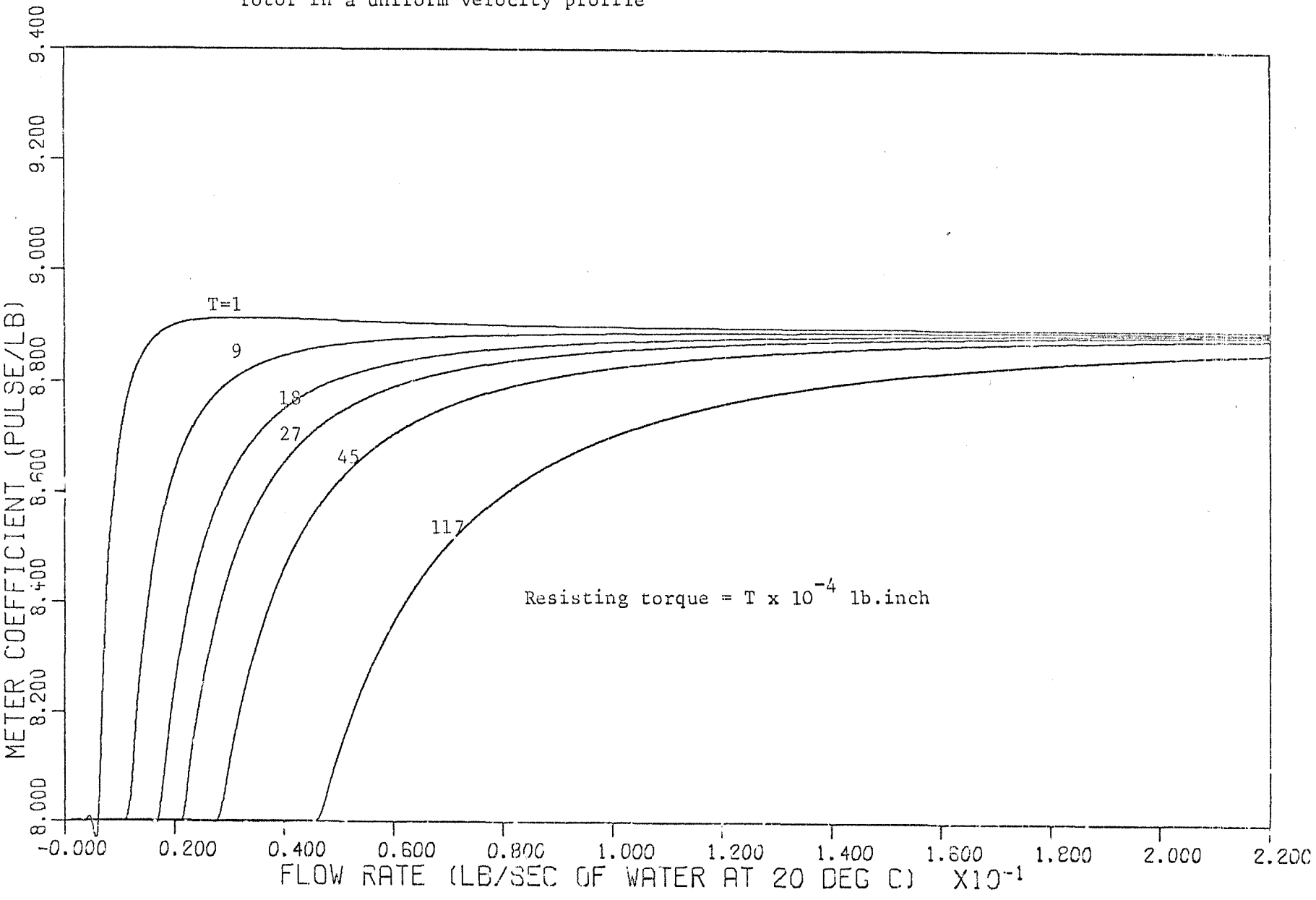

Fig. 9.7 Variation of meter calibration curve with resisting torque for turned down rotor in a uniform velocity profile

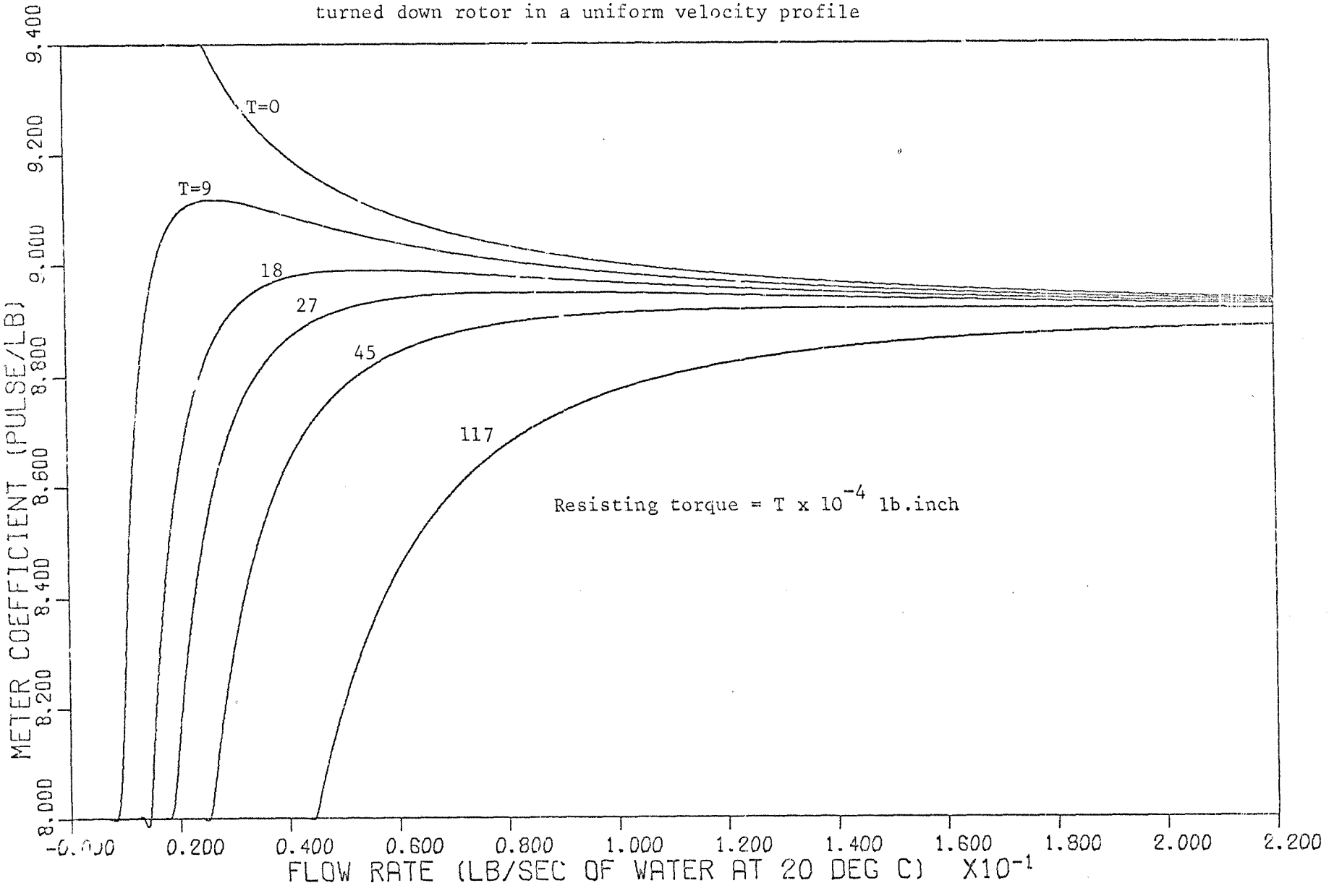

TABLE 9.1 Mean Meter Coefficient and Standard Deviation of Repeatability Test on Full Diameter Rotor Using Open Bearings

Flow Rate	15.0 lb/sec		8.8 lb/sec	
Total Running Hours	Mean Meter Coefficient	Standard Deviation	Mean Meter Coefficient	Standard Deviation
10	8.6912	0.00359	8.6742	0.01887
20	8.6916	0.00453	8.6705	0.01571
30	8.6896	0.00515	8.6678	0.01347
40	8.6890	0.00506	8.6695	0.01360
50	8.6884	0.00480	8.6718	0.01372
60	8.6887	0.00479	8.6724	0.01278
70	8.6874	0.00841	8.6711	0.01552
80	8.6866	0.00906	8.6704	0.01605

Table 9.2 Mean Meter Coefficient and Standard Deviation of Repeatability Test on Full Diameter Rotor Using Shielded Bearings

Flow Rate	15.0 lb/sec		8.8 lb/sec	
Total Running Hours	Mean Meter Coefficient	Standard Deviation	Mean Meter Coefficient	Standard Deviation
10	8.6973	0.00352	8.6855	0.00420
20	8.6949	0.00365	8.6802	0.00676
30	8.6960	0.00370	8.6752	0.00934
40	8.6938	0.00473	8.6728	0.00914
50	8.6939	0.00441	8.6712	0.00877
60	8.6937	0.00444	8.6705	0.00820
70	8.6931	0.00501	8.6696	0.00823
80	8.6941	0.00544	8.6699	0.00830
90	8.6939	0.00495	8.6698	0.06796

Meter coefficient and standard deviation expressed in pulse/lb

1 pulse/lb = 0.36744 rev/kg

Table 9.3 Mean Meter Coefficient and Standard Deviation of Repeatability Test on Turned-Down Rotor Using Shielded Bearings

Flow Rate	15.0 lb/sec		8.8 lb/sec	
Total Running Hours	Mean Meter Coefficient	Standard Deviation	Mean Meter Coefficient	Standard Deviation
10	8.8835	0.00866	8.9052	0.03221
20	8.8923	0.01238	8.9019	0.02443
30	8.8939	0.01133	8.9007	0.02005
40	8.8952	0.01070	8.8936	0.02234
50	8.8939	0.01033	8.8868	0.02356
60	8.8936	0.00965	8.8824	0.02425
70	8.8959	0.01065	8.8810	0.02273
80	8.8956	0.01023	8.8800	0.02238
90	8.8959	0.00997	8.8797	0.02205
100	8.8939	0.01208	8.8791	0.02178

Meter coefficient and standard deviation expressed in pulse/lb

1 pulse/lb = 0.36744 rev/kg
15.0 lb/sec = 6.80 kg/sec
8.8 lb/sec = 3.99 kg/sec

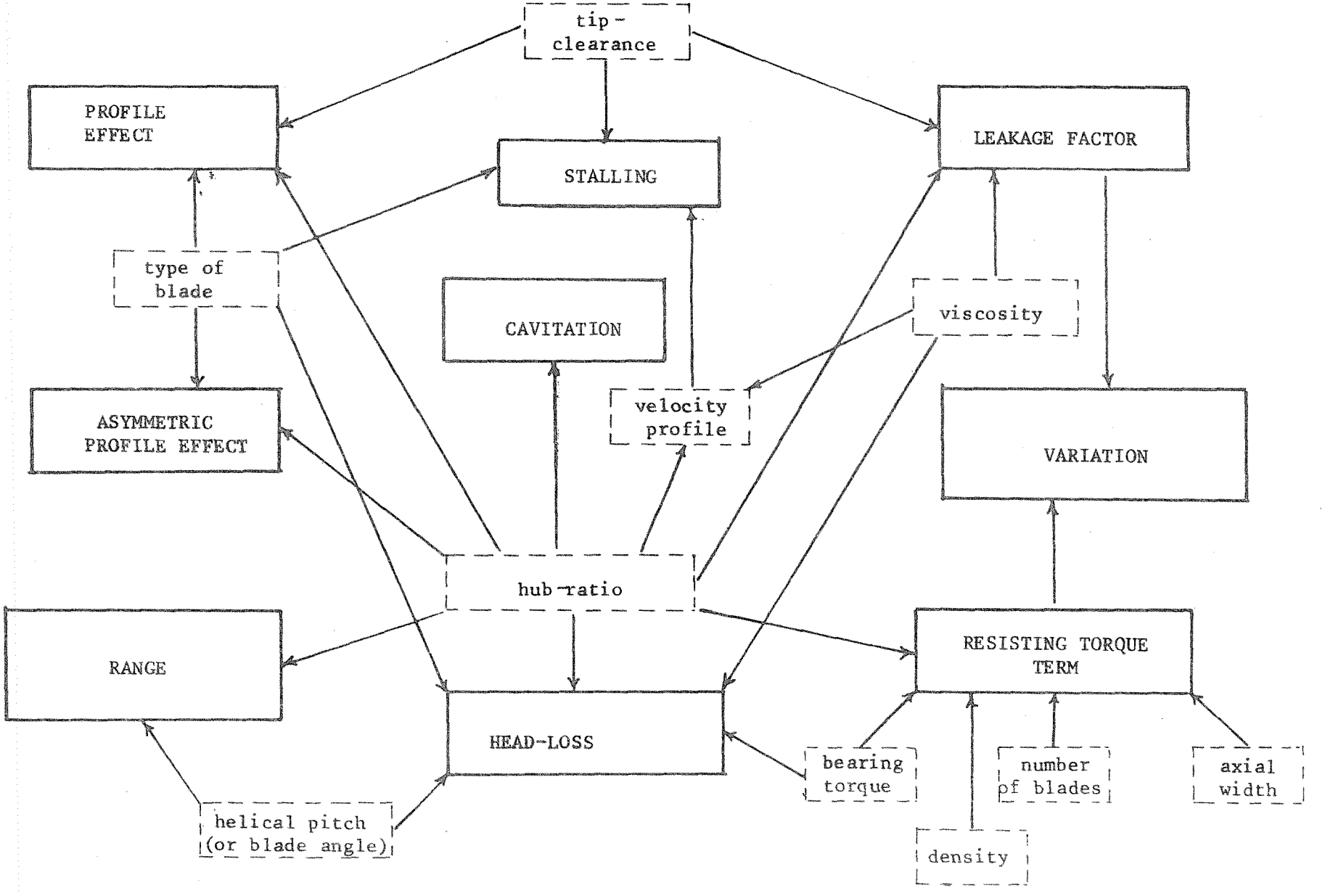

Fig. 10.1 - FACTORS AFFECTING CHARACTERISTICS OF TURBINE-TYPE FLOWMETER.

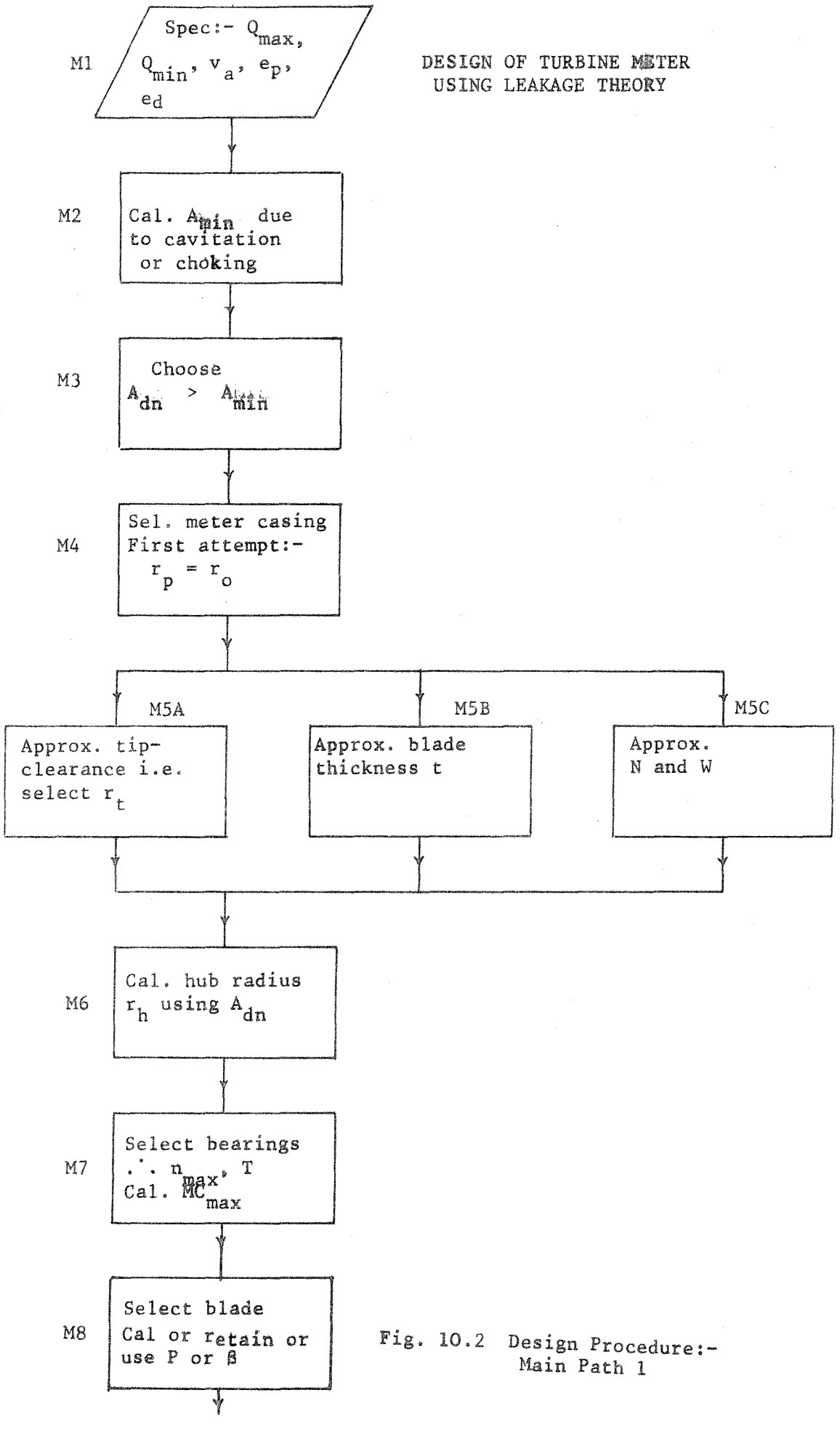

Fig. 10.2 Design Procedure:- Main Path 1

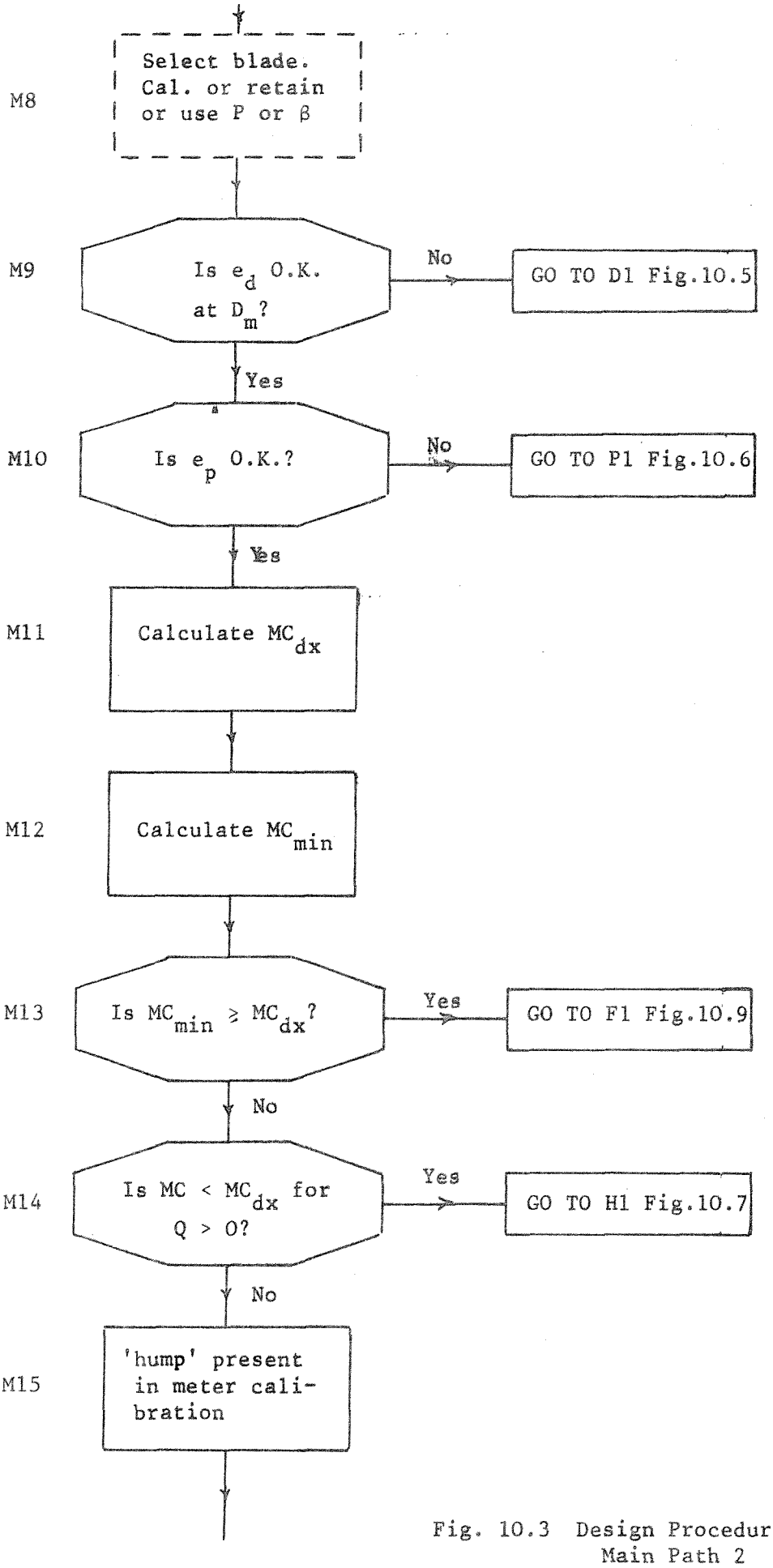

Fig. 10.3 Design Procedure:- Main Path 2

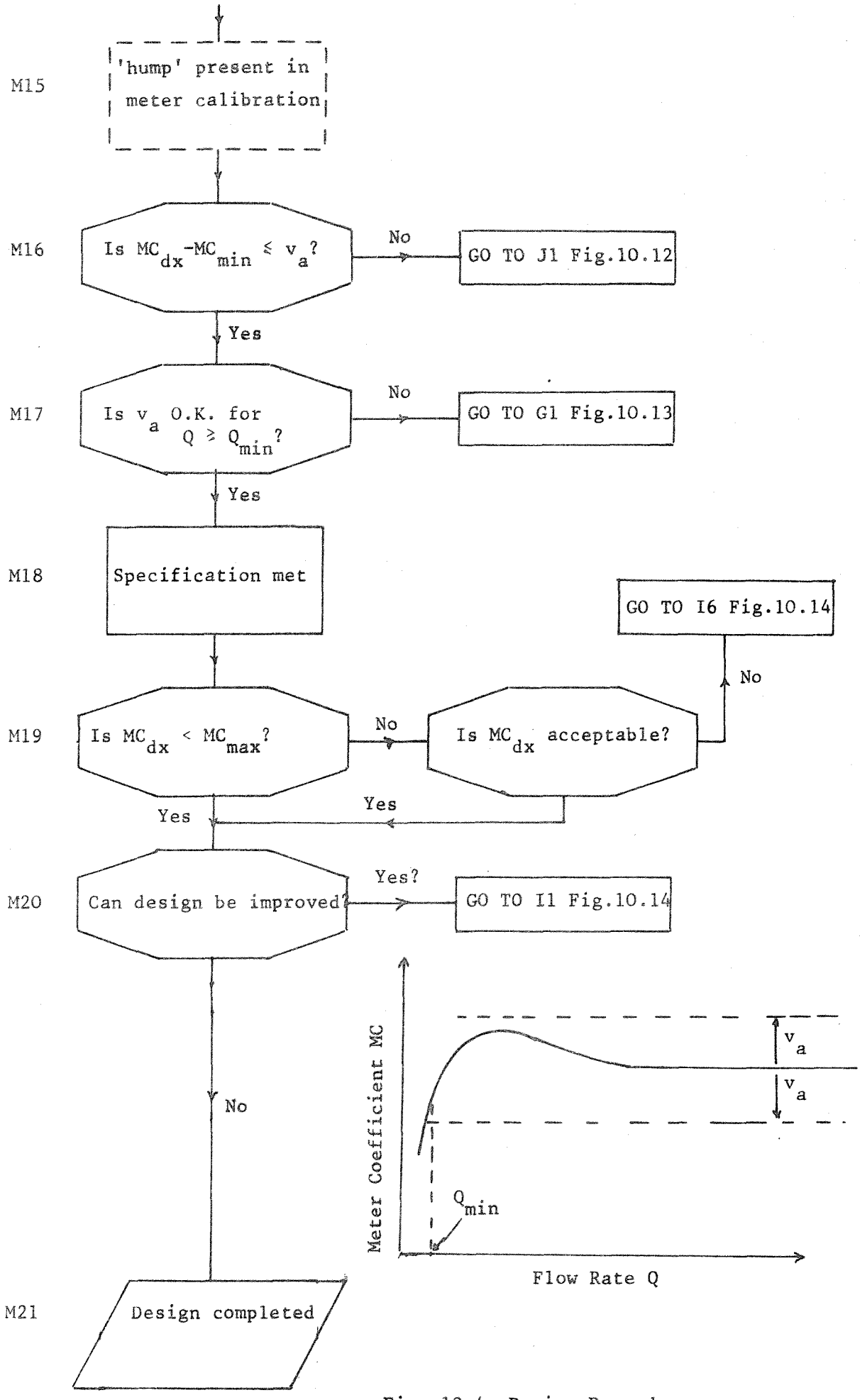

Fig. 10.4 Design Procedure:-
Main Path 3

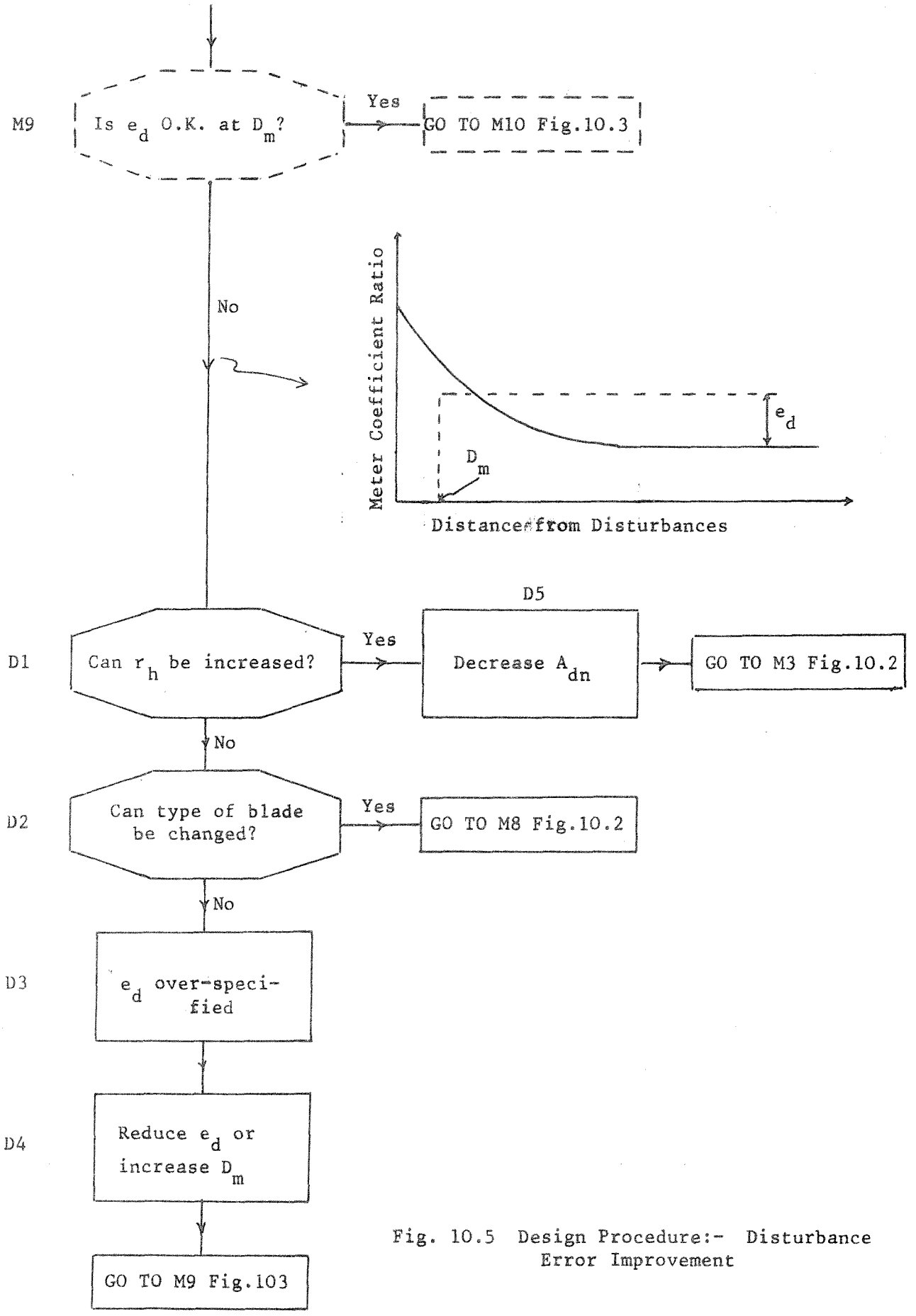

Fig. 10.5 Design Procedure:- Disturbance Error Improvement

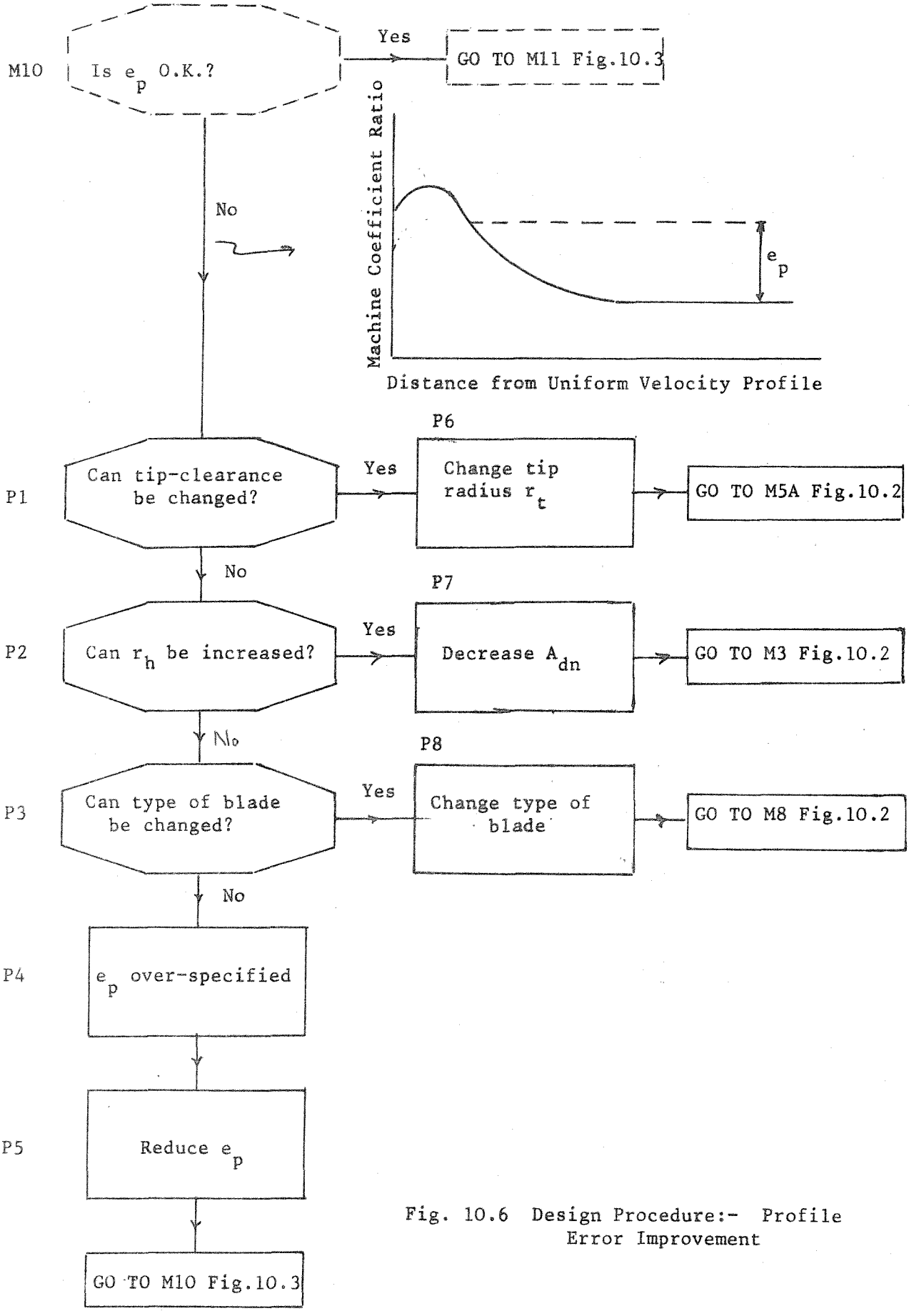

Fig. 10.6 Design Procedure:- Profile Error Improvement

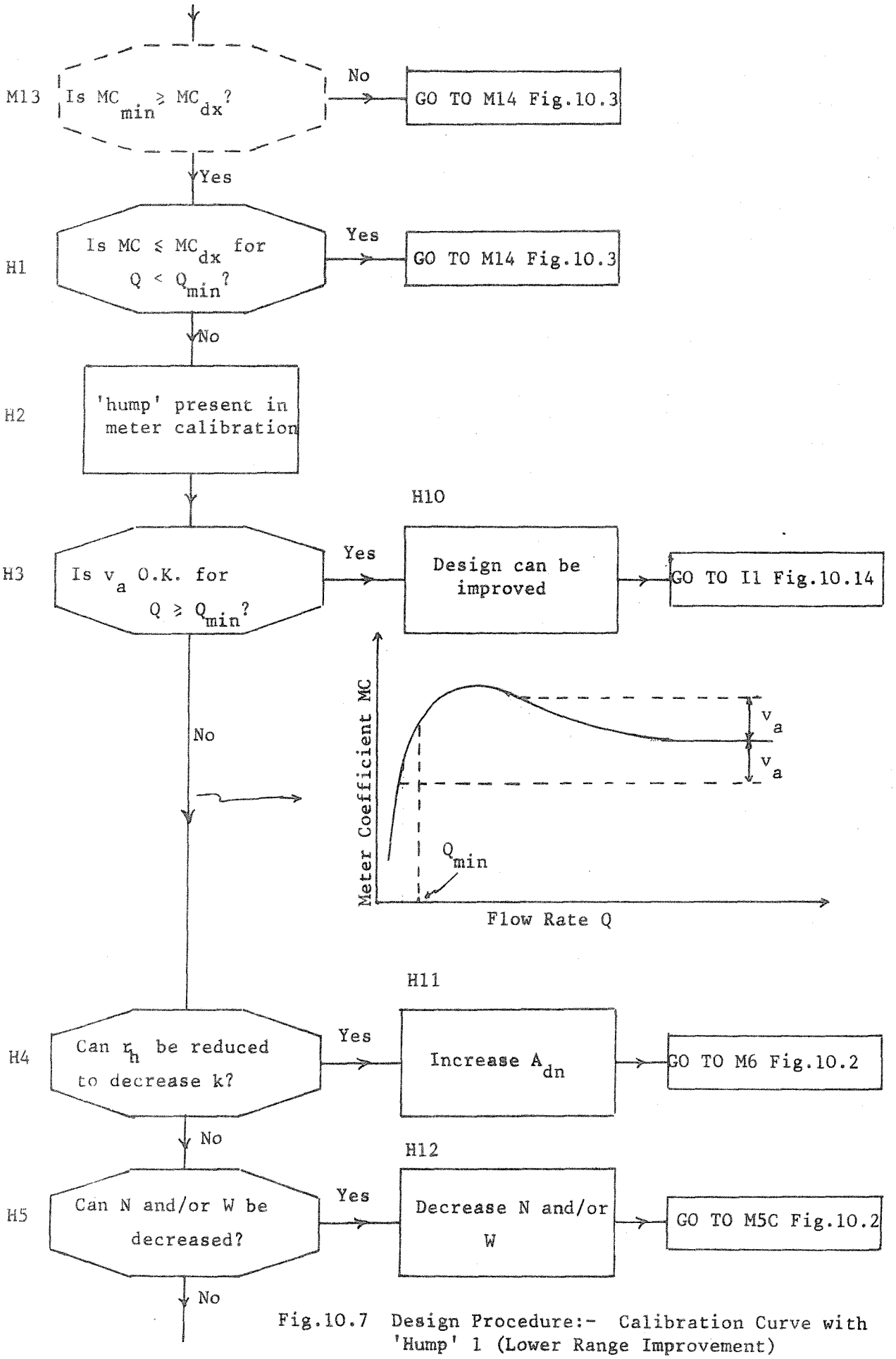

Fig.10.7 Design Procedure:- Calibration Curve with 'Hump' 1 (Lower Range Improvement)

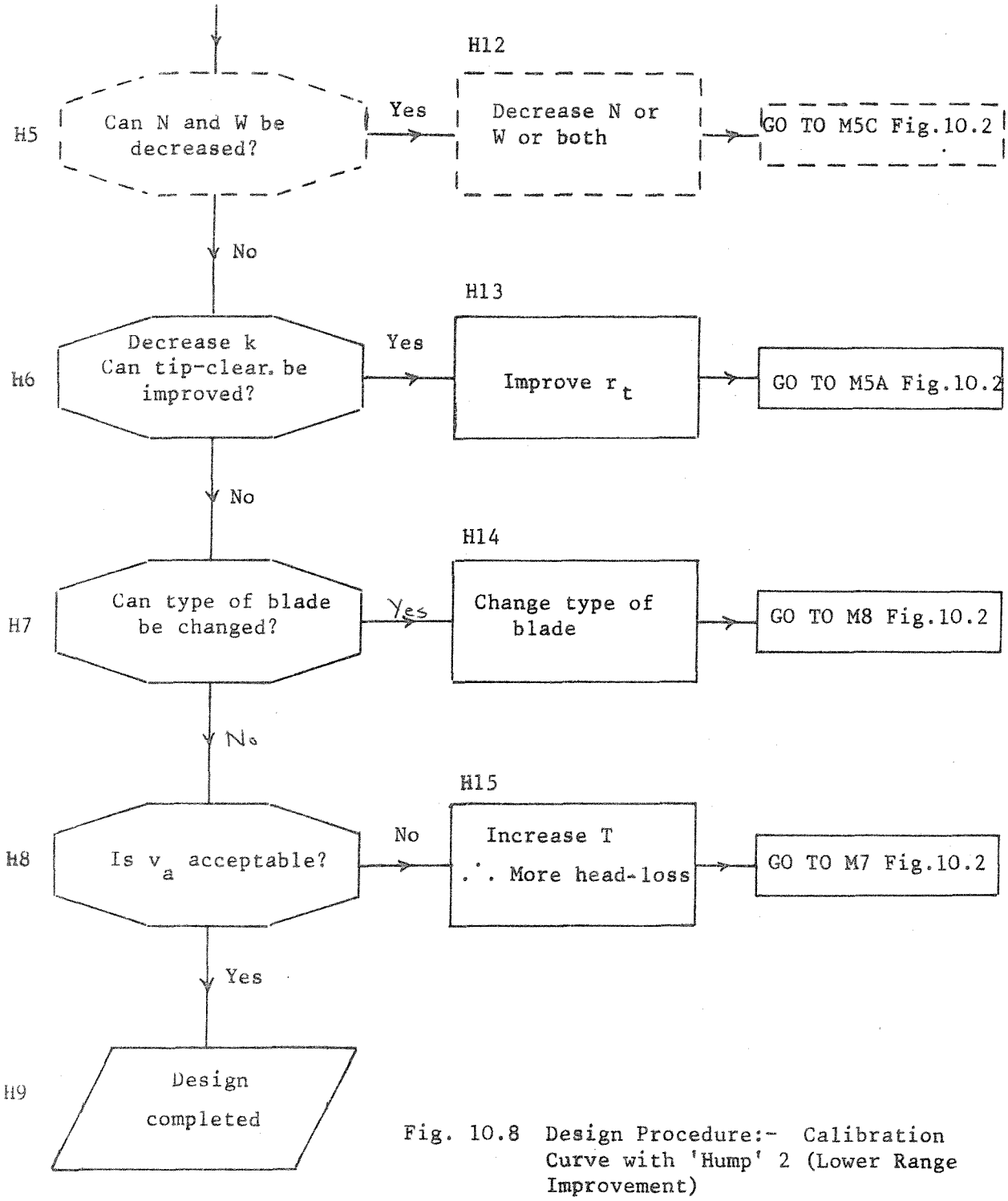

Fig. 10.8 Design Procedure:- Calibration Curve with 'Hump' 2 (Lower Range Improvement)

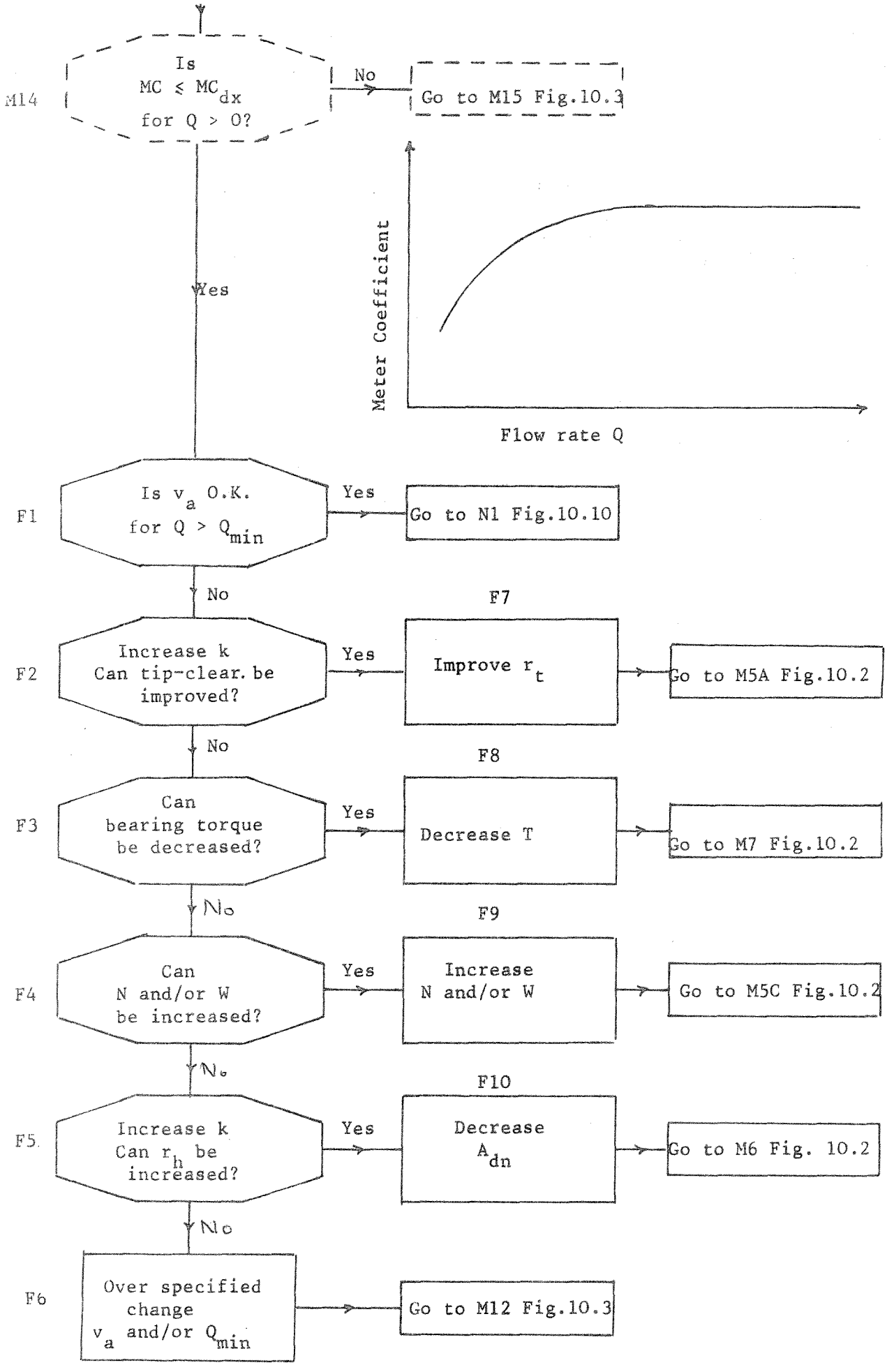

Fig. 10.9 Design Procedure:- Calibration Curve without 'Hump" 1 (Variation Improvement)

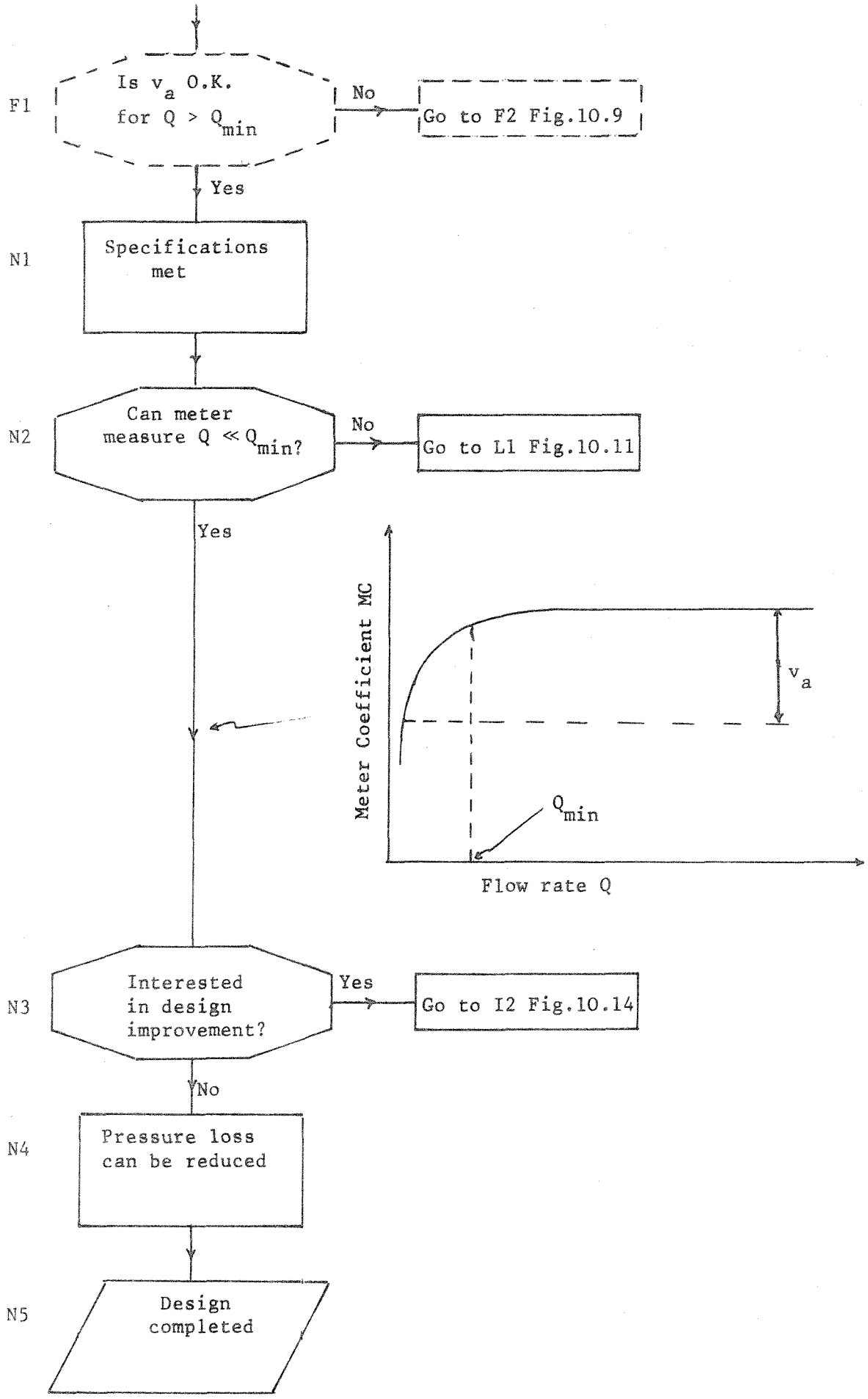

Fig. 10.10 Design Procedure:- Calibration Curve without 'Hump' 2
(Minimum Flow Rate Improvement)

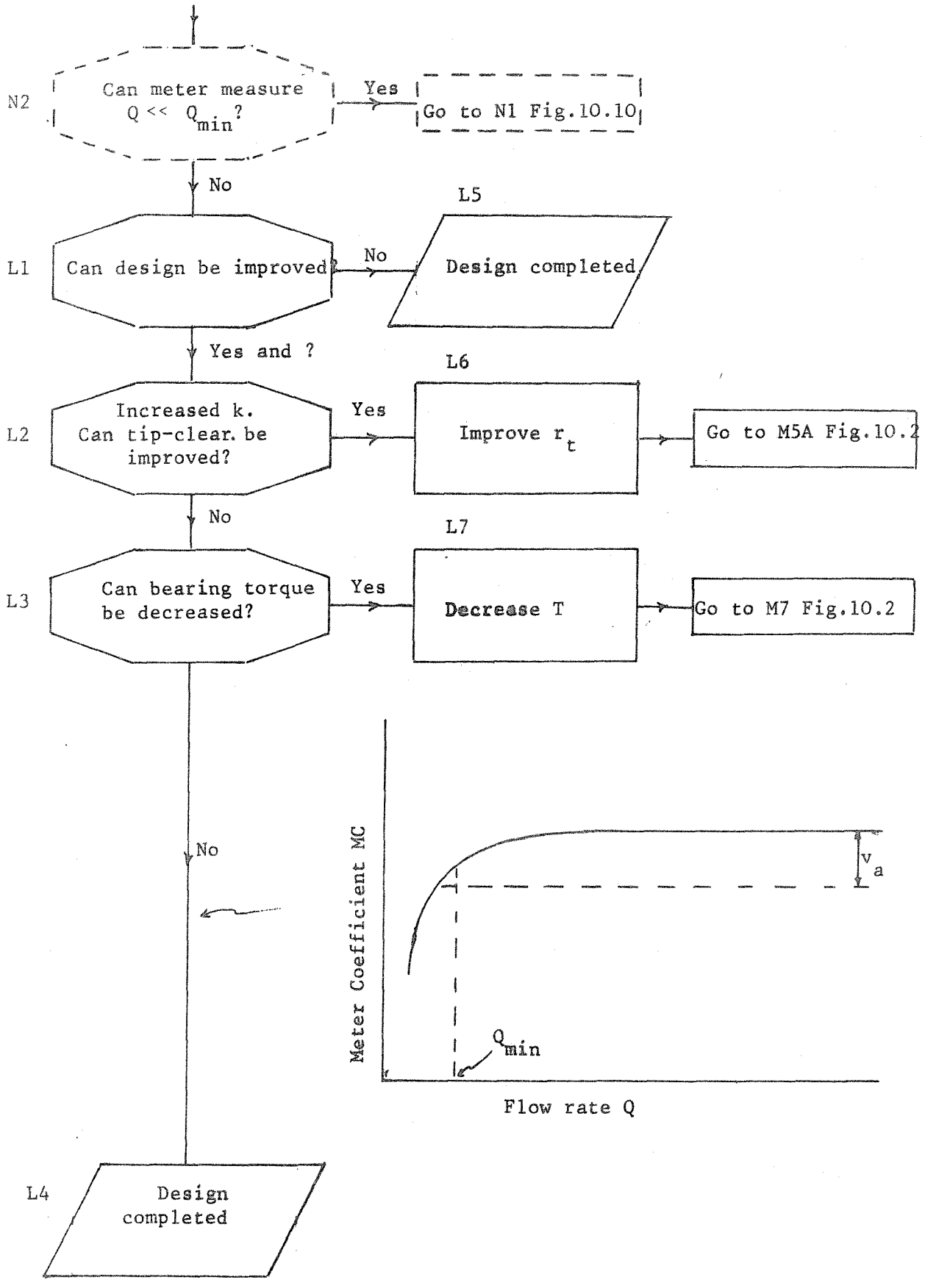

Fig. 10.11 Design Procedure:- Calibration Curve without 'Hump' 3 (Final Stage)

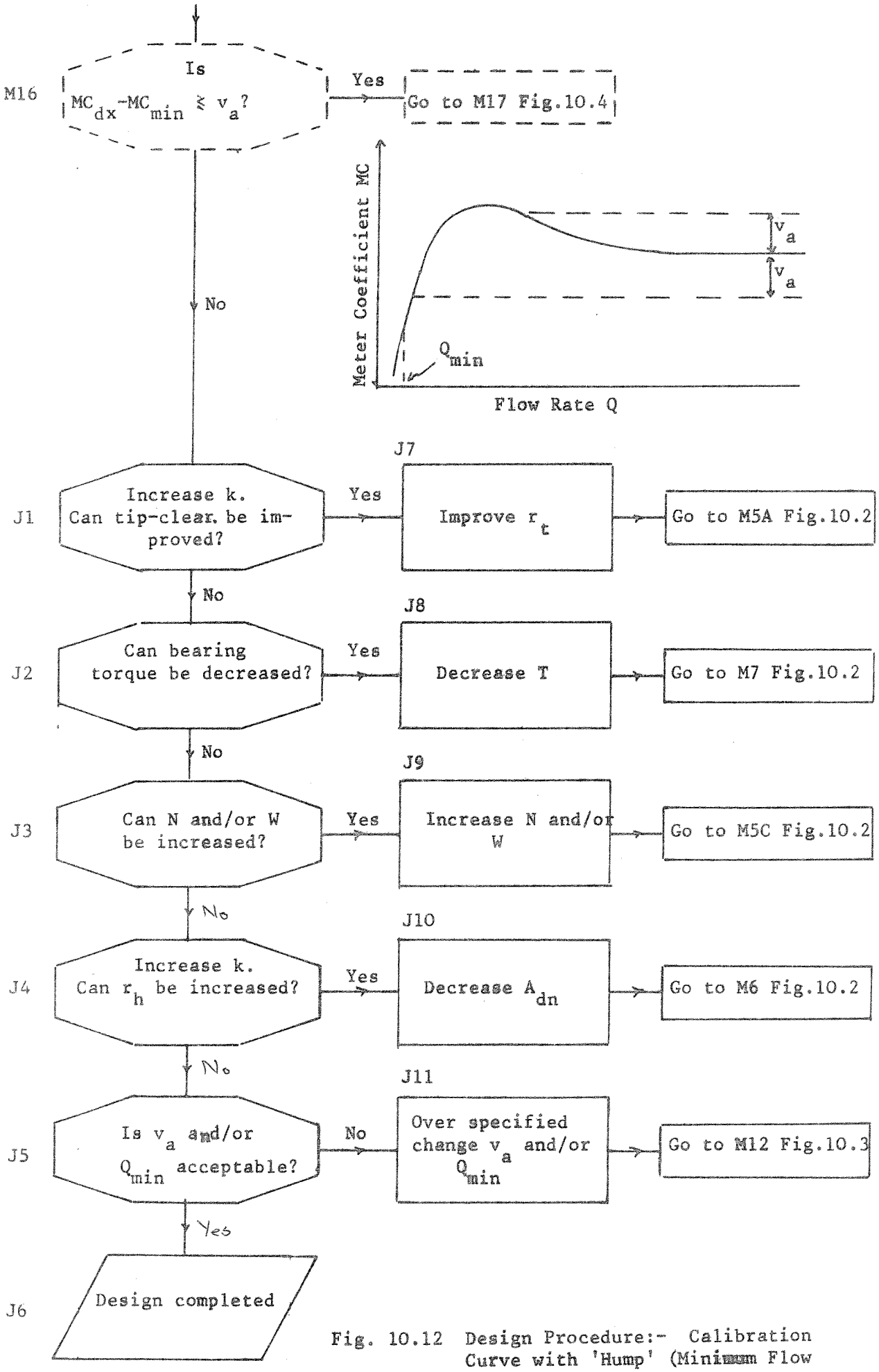

Fig. 10.12 Design Procedure:- Calibration Curve with 'Hump' (Minimum Flow Rate Improvement)

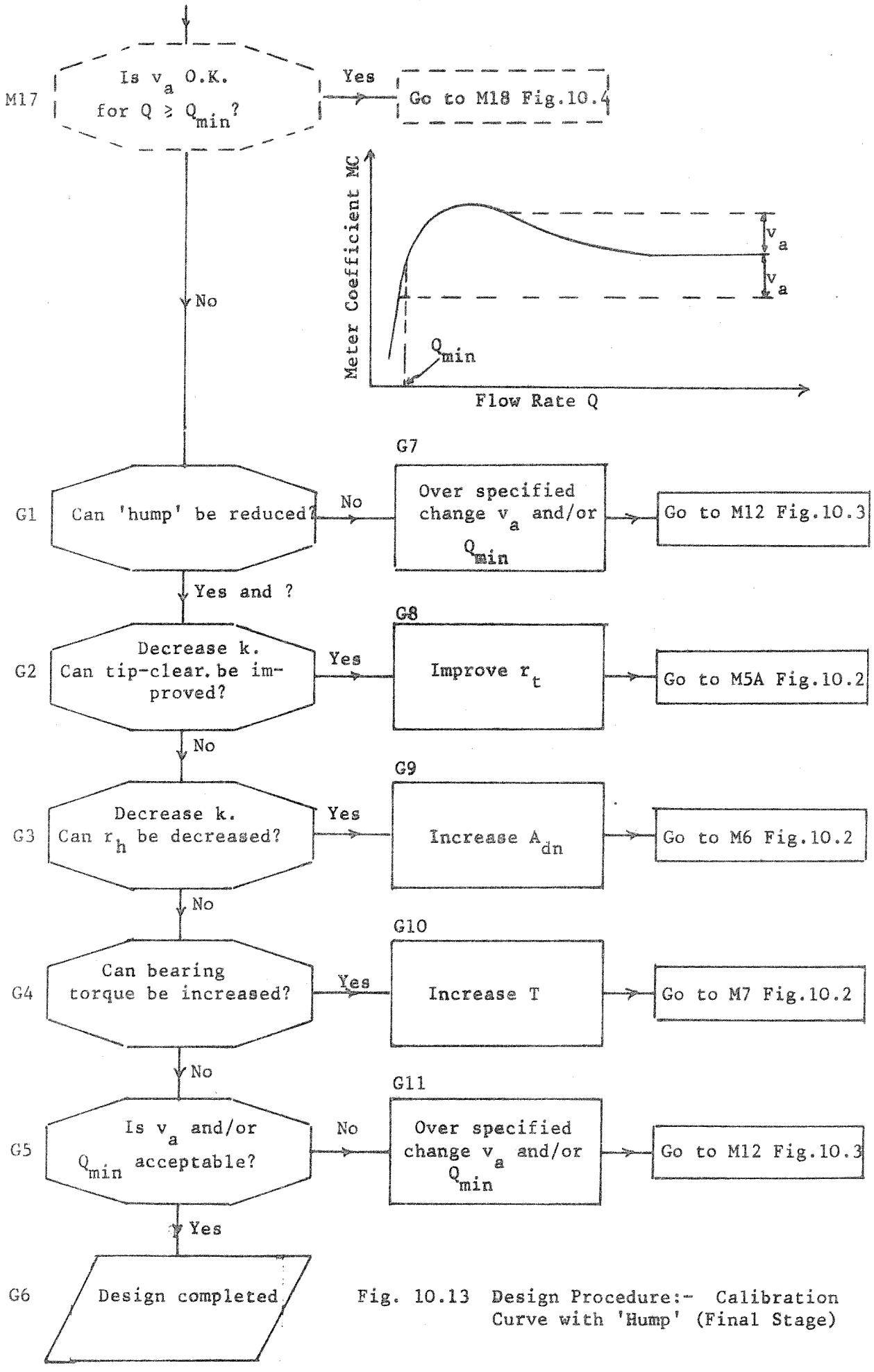

Fig. 10.13 Design Procedure:- Calibration Curve with 'Hump' (Final Stage)

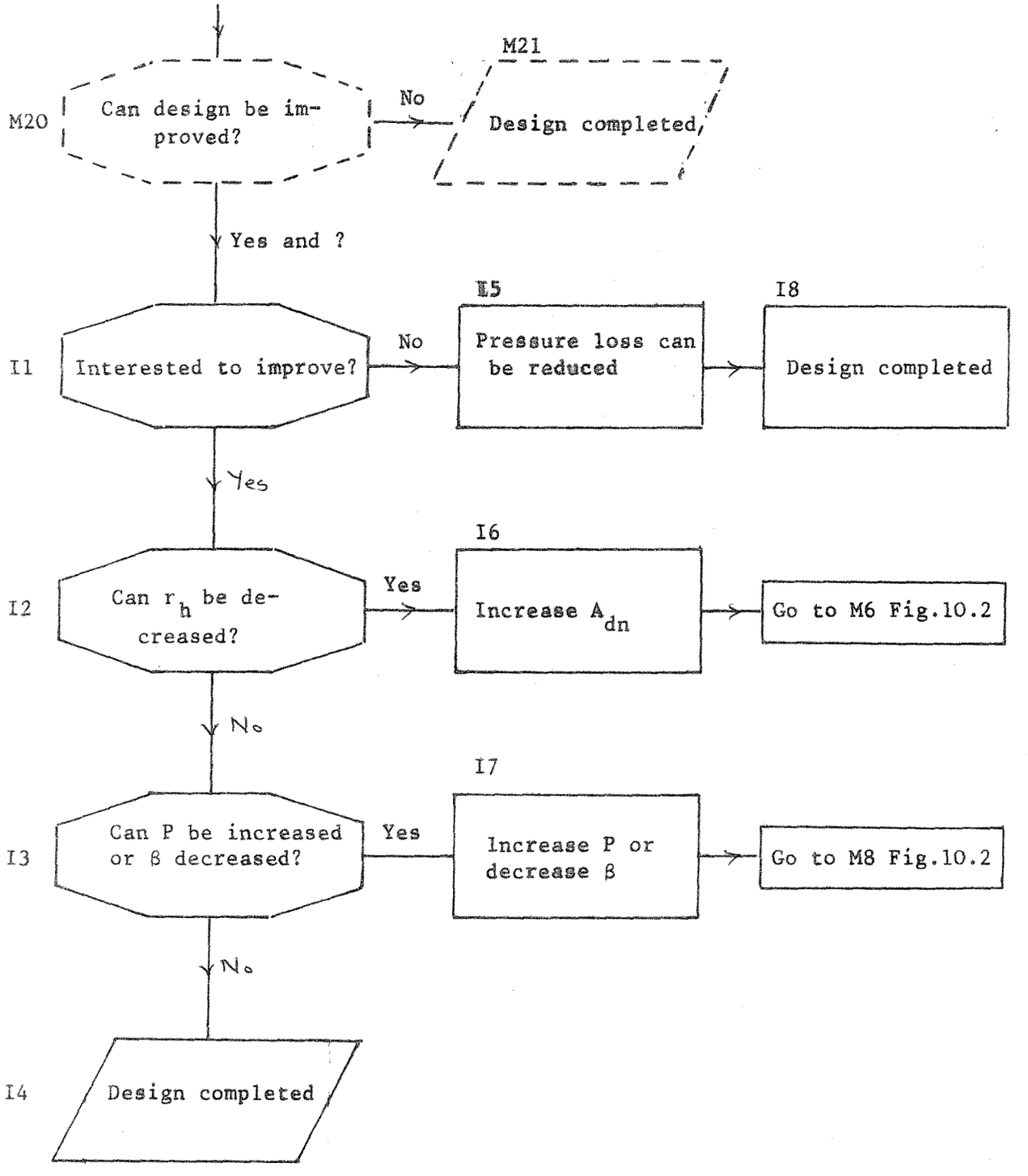

Fig. 10.14 Design Procedure:- Improvement in Design